Peptides as Therapeutics

Aimé López Aguilar

Balliol College, Department of Biochemistry
University of Oxford

Thesis submitted in partial fulfilment

of the requirements for the degree of Doctor of Philosophy

Trinity 2011

Peptides as Therapeutics

Aimé López Aguilar, Balliol College, D.Phil Thesis, 2011.

Abstract

Peptides have attracted increasing attention as therapeutics in recent years, at least partially as a consequence of the widespread acceptance of protein therapeutics; but also as possible solutions to problems such as short half-life and delivery of molecules, and as therapeutics in their own right. The current work presents three projects that involve applications of peptides in a therapeutic environment.

The first project studies the use of ER retaining peptides and CPPs (Cell penetrating peptides) in enhancing the effective concentration of DNJ (1-deoxynojirimycin), an α-glucosidase inhibitor, in cells. DNJ constructs with ER retaining peptides (6-[*N*-(1-deoxynojirimycino)]-hexanoyl-KDEL and 6-[*N*-(1-deoxynojirimycino)]-hexanoyl-KKAA) and CPPs (6-[*N*-(1-deoxynojirimycino)]-hexanoyl-TAT and 6-[*N*-(1-deoxynojirimycino)]-hexanoyl-MAP) were synthesised and analysed for their inhibitory activity against α-glucosidase I and II *in vitro*. The constructs were then analysed in a cell-based assay to determine their inhibitory activity on α-glucosidase-mediated hydrolysis of *N*-linked oligosaccharides. FITC-labelled ER retaining peptides were also synthesised to determine the internalisation and trafficking of the constructs by FACS and IF-microscopy. While none of the DNJ-constructs showed higher cellular inhibition than *N*B-DNJ (*N*-butyl DNJ; Miglustat), the CPP construct 6-[*N*-(1-deoxynojirimycino)]-hexanoyl-TAT showed comparable activity and the ER retaining construct 6-[*N*-(1-deoxynojirimycino)]-hexanoyl-KDEL showed a small but significant increase in activity following long-term administration.

The second project focuses on beauveriolides, a cyclic depsipeptide family shown to have activity as ACAT inhibitors and thus a possible treatment for Alzheimer's disease by the decrease in the production of Amyloid β (Aβ). A published total synthetic method was improved by the use of a cross-metathesis to reduce the total synthesis by 5 steps and increase its flexibility to allow the production of analogues. The synthesised beauveriolide III was used in attempts to develop an IF-FACS-based assay to measure the intracellular concentrations of Aβ. However, the location of γ-secretase in the used cell-line meant that levels of intracellular Aβ were not sufficient to track any decrease caused by ACAT inhibition.

The third project involves the design of a cyclic peptide that could block the binding site for the influenza virus in the host cell. The cyclic peptide (cGSGRGYGRGWGVGA) was developed from a comparative study of four different sialic acid-binding proteins and synthesised by solution cyclisation of the linear peptide synthesised by traditional solid phase peptide synthesis (SPPS). An *in silico* study showed that the cyclic peptide allowed overlap with the binding site of Hemagglutinin. A ^{1}H NMR titration determined the dissociation constant of the cyclic peptide to sialic acid. The K_D corresponded to a low binding affinity, however the observed binding seemed to be specific and caused by a single bound conformation.

Acknowledgements

Antes que nada, quisiera agradecer a mis padres Carlos y Silvia, y a mis hermanos Daniel y Carlos Alberto, por su apoyo constante. Su ejemplo de trabajo, dedicación y compromiso me ha guiado a lo largo de este proceso, y su cariño me ha ayudado a superar los retos y momentos difíciles que he encontrado en mi camino.

I would like to thank my supervisor, Dr. Terry Butters, for welcoming me to his lab and for his continuous support and advice. The Butters' lab has been a great environment to learn and grow as a person and as a scientist.

I am also grateful to my supervisor, Prof. Paul Wentworth, for giving me a place at the Scripps-Oxford lab as well as for his advice and supervision throughout the past years.

I am very grateful to CONACYT Mexico for the funding that allowed me to undertake this research.

My thanks go out to all the past and present members of the Oxford-Scripps Laboratory: Jason Chang, Dr. Michael Cole and Dr. Grant Boldt, to Dr. Daniel Witter for his coaching and answers to my many emails, Natalie Cygan, Dr. Johanna Scheinost, Kavitha Baruah and Kanlaya "Yaya" Prapainop for their continuous friendship and the many fun times shared, Joseph Rogel for being a great friend and an exemplary person, and Dr. Jaime Escribano for all his help, all the scientific discussions and all the time he dedicated to proofread this thesis.

My thanks are also due to all the past and present members of the Butter's Laboratory: Katy Patzel, Iona Easthope, Laura Pritchard, Johnny Howe, Gabrielle Twigg, Andreas Glawar, Charlotte Heads, Jalal Thompson, Omodele Ashiru, Sebastian Loscher, Pawel Link-Lenczowski, and Marvin Lee for their invaluable friendship, special thanks to Nikolay Kukushkin and Dominic Alonzi for their mentorship on biological techniques and their infinite patience when answering questions, particular thanks to Sarah Allman for sharing all her wisdom, humor and Haribo with me.

I would like to thank Balliol College from providing me with a home and for all the support I've encountered from friends and staff there.

Finally, I would like to thank Jenn Reuer, Michael Urban, Maya Bahoshy, José Basutto, Sara Silverstein, Héctor Pérez Urbina, and the many friends that have filled my time in Oxford with such wonderful memories ☺.

Abbreviations

2-AA	2-Anthranilic acid
A	Alanine
Aβ	Amyloid β
ACAT	Acetyl-CoA cholesteryl acyl transferase
ACE	Angiotensin converting enzyme
AChE	Acetylcholinesterase
ACTH	Adrenocorticotropic hormone
AD	Alzheimer's disease
AIDS	Acquired immune deficiency syndrome
Ala	Alanine
AMS	Aminomethylpoly(styrene)
ApoE	Apoliprotein E
ApoE-ε4	Apoliprotein E-type 4
APP	Amyloid precursor protein
Arg	Arginine
Asn	Aspargine
a.u.	Absolute units
BCA	Bicinchoninic acid
Bn	Benzyl
Boc	*tert*-Butoxycarbonyl protecting group
br	Broad
BSA	Bovine serum albumin
BVDV	Bovine viral diarrhoea virus
CALX	Calnexin
CALN	Calreticulin
cAMP	Cyclic adenosine monophosphate
Cat.	Catalyst
Cbz	Carboxybenzyl
CE	Cholesteryl esters
CFTR	Cystic fibrosis transmembrane receptor
CMT	Chaperone mediated therapy

CNS	Central nervous system
ConA	Concanavalin A
Conc.	Concentration
COPS	Cytosolic coat proteins
COSY	Correlation spectroscopy
CP	Cyclic peptide
CPP	Cell-penetrating peptide
CsA	Cyclosporin A
D	Aspartic acid
d	Doublet
DANA	2,4-dideoxy-2,3-dehydro-*N*-acetylneuraminic acid
DAPI	4',6-diamidino-2-phenylindole
DCM	Dichloromethane
dd	Doublet of doublets
ddd	Doublet of doublet of doublets
DEA	Diethylamine
DIAD	Diisopropyl azodicarboxylate
DIC	*N,N'*-Diisopropylcarbodiimide
DIPEA	Diisopropylethylamine
DMAP	Dimethylaminopyridine
DMF	Dimethylformamide
DMSO	Dimethylsulfoxide
DNJ	1-Deoxynojirimycin
DNPH	Dinitrophenylhydrazine
Dol	Dolichol
dt	Doublet of triplets
E	Glutamic acid
EDAC	1-Ethyl-3-(3-dimethylaminopropyl)carbodiimide
EDTA	Ethylenediaminetetraacetic acid
ELISA	Enzyme-linked immunosorbent assay
ENGase	Endo-β-*N*-acetylglycosaminidase
equiv.	Equivalents
ER	Endoplasmic reticulum

ERAD	ER-associated degradation
ERAD-C	Cytosolic ER-associated degradation
ERAD-L	Luminal ER-associated degradation
ERAD-M	Intra-membrane ER-associated degradation
ERGIC	ER-Golgi intermediate complex
ESI	Electrospray ionisation
FACS	Fluorescence-activated cell sorting
FC	Free cholesterol
FCS	Foetal calf serum
FDA	Food and drug administration
FITC	Fluorescein isothiocyanate
FL1-H	Fluorescence channel 1
Fmoc	9-Fluorenylmethyloxycarbonyl
FOS	Free oligosaccharides
FSC	Forward scatter
FSH	Follicle stimulating hormone
Gal	Galactose
GDP	Guanosine diphosphate
GHRH	Growth hormone releasing hormone
Glc	Glucose
GlcNAc	*N*-Acetyl glucosamine
Gln	Glutamine
GLP-1	Glucagon-like peptide-1
Glu	Glutamic acid
Gly	Glycine
GnRH	Gonadotropin-releasing hormone
GSL	Glycosphingolipids
h	Hour
HA	Hemagglutinin
HATU	2-(7-Aza-1H- benzotriazole-1-yl)-1,1,3,3-tetramethyluronium hexafluorophosphate
HIV	Human immunodeficiency virus
HMG-CoA	3-Hydroxy-3-methyl-glutaryl-coenzyme A

HMPA	4-Hydroxymethyl phenoxyacetic acid
HMQC	Heteronuclear multiple-quantum correlation
HOAt	1-Hydroxy-7-azabenzotriazole
HOBt	1-Hydroxybenzotriazole
HPLC	High performance liquid chromatography
HR-MS	High resolution mass spectrometry
Hz	Hertz
ICAH-1	Intracellular adhesion molecule-1
IF	Immunofluorescence
Ile	Isoleucine
IMP	Integral membrane protein
J	Coupling constant
K	Lysine
L	Leucine
LDL	Low density lipoproteins
Leu	Leucine
LH	Luteinising hormone
LR-MS	Low resolution mass spectrometry
Lys	Lysine
M	Molar
m	Multiplet
MA1A1	α-1,2-Mannosidase
Man	Mannose
+MDCPB	(+)-B-Methoxydiisopinocampheylboron
MHz	Megahertz
min	Minute
m.p.	Melting point
MRH	Mannose-6-phosphate homology domain
MS	Mass spectrometry
MTS	3-(4,5-Dimethylthiazol-2-yl)-5-(3-carboxymethoxyphenyl)-2-(4-sulfophenyl)-2H-tetrazolium
m/z	Mass to charge ratio
NA	Neuraminidase

*N*B-DGJ	*N*-Butyldeoxygalactonojirimycin
*N*B-DNJ	*N*-Butyldeoxynojirimycin
NEP	Nuclear export protein
NJ	Nojirimycin
*N*N-DNJ	*N*-Nonyldeoxynojirimycin
NMDA	*N*-Methyl-D-aspartate
NMO	*N*-Methylmorpholine-*N*-oxide
NMP	*N*-Methyl-2-pyrrolidone
NMR	Nuclear magnetic resonance
NP	Nuclear protein
NP-HPLC	Normal phase HPLC
ns	Not significant
OST	Oligosaccharyltransferase
pAntp	Antennapedia transcription factor - Penetratin
Pbf	2,2,4,6,7-Pentamethyldihydrobenzofurane
PBS	Phosphate buffer saline
PDB	Protein data bank
PDI	Protein disulphide isomerase
PI	Propidium iodide
PMB	Paramethoxybenzyl ether
PMS	Phenazine methosulfate
PNGase	Peptide:*N*-Glycanase
PP	Pyrophosphate
ppm	Parts per million
Pro	Proline
PyBrop	Bromo-tris-pyrrolidino phosphoniumhexafluorophosphate
q	Quartet
RCSB	Research collaboratory for structural bioinformatics
R_f	Retardation factor
RNA	Ribonucleic acid
ROESY	Rotating frame nuclear Overhauser effect spectroscopy
rpm	Revolutions per minute
RT	Room temperature

SA	Sialic acid (*N*-acetylneuraminic acid)
SEM	Standard error of the mean
Ser	Serine
siRNA	Small interfering RNA
SPPS	Solid phase peptide synthesis
SRT	Substrate reduction therapy
t	Time
t	Triplet
TBAF	Tetra *n*-butylammonium fluoride
TBS	*tert*-Butylsilyl
TBTU	*O*-(Benzotriazol-1-yl)-*N,N,N',N'*-tetramethyluronium tetrafluoroborate
TFA	Trifluoroacetic acid
TGN	Trans Golgi network
Thr	Threonine
THF	Tetrahydrofuran
TIS	Triisopropylsilane
TLC	Thin layer chromatography
TPAP	Tetrapropylammonium perruthenate
Trp	Tryptophan
Tyr	Tyrosine
UGGG1	UDP-glucose:glycoprotein-glucosyltransferase
UDP	Uridine diphosphate
UV	Ultraviolet
Val	Valine
Vis	Visible
vRNP	Viral ribonucleoproteins
WHO	World health organization
WHV	Woodchuck hepatitis virus

Acknowledgement of assistance

I am indebted to the following people for their help and assistance throughout the course of these projects.

Isolation of α-glucosidase II – Dr. Terry Butters, University of Oxford.

Large scale synthesis completion of Beauveriolide III – Dr. Jaime Escribano Cabeza, University of Oxford.

Docking of minimized cyclic peptide model to heamagglutinin crystal structure, production of Figure 4.16 – Dr. Kia Balali Mood, University of Oxford.

FOS analysis mentoring – Dr. Dominic Alonzi, University of Oxford.

FACS tutoring – Gabrielle Twigg, University of Oxford.

NMR setup and processing – Dr. Mark Wormald, University of Oxford.

Instruction and supervision for Fluorescence Microscopy – Dr. Ian Dobbie and Dr. Eva Wegel, University of Oxford.

Investigating DNA double-strand break repair in *Dictyostelium discoideum*

Claudia Anne-Marie Couto – Merton College

Submitted for the degree of Doctor of Philosophy, Trinity term, 2011

DNA double-strand breaks (DSBs) are toxic lesions that can be repaired by numerous mechanistically distinct pathways. However, regulation of DSB repair pathway utilisation is also essential for maintaining genomic integrity, and eukaryotes have evolved several mechanisms to achieve this. This includes post-translational modifications of DSB repair proteins to modulate their activity at DNA DSB ends. One example of a post-translational modification with a role in DNA repair is Poly-ADP ribosylation (PARylation), which in mammals is mediated by Poly-ADP ribose Polymerase 1 and 2 (PARP1 and 2). The best characterised roles of PARP1 and 2 is in single-strand break repair (SSBR) and base-excision repair (BER). However, their roles in DSB repair remain unclear, and to address this, the eukaryotic model *Dictyostelium discoideum* has been utilised. Several putative repair PARPs are conserved in the *Dictyostelium* genome, and the induction of PARylation following DNA SSBs and base-damage has been observed. Using a genetic approach, multiple *Dictyostelium* PARPs have been implicated in SSBR/BER, as is the case in mammals. PARylation is also induced following DNA DSBs, with the major contributor being Adprt1a. This work has demonstrated the regulatory role of Adprt1a in DSB repair by promoting non-homologous end joining (NHEJ), at the expense of homologous recombination (HR). This may be achieved by the enhanced association of the Ku70/Ku80 heterodimer, the DSB sensor that initiates NHEJ, with chromatin following DNA damage in a PAR-dependent manner. Consistent with this, a PAR binding zinc-finger, the PBZ domain, has been identified in *Dictyostelium* Ku70,

which is involved in the enhanced chromatin-association of Ku post-DSB induction. This work therefore highlights a mechanism by which Adprt1a-induced PARylation post-DSBs promotes NHEJ via Ku recruitment. The enhanced Ku association at damaged chromatin reduces engagement of other DSB repair pathways, placing Adprt1a at the crossroads of DSB repair pathway choice.

Acknowledgements

Many people deserve recognition for their contribution to the production of this thesis. Firstly, I am grateful to my supervisors Nick and Catherine for their advice, patience and encouragement over the course of my DPhil. It is with their help that I have developed as a scientist over the past four years. I would also like to thank members of the Lakin, Pears, Cox and Mahadevan lab, past and present, for lively discussions (scientific or otherwise), use of equipment, and general sustenance. In particular, I would like to mention Rhian and Annette, who were with me from start to finish, and who always offered support and much entertainment through the medium of song and interpretive dance.

I would like to thank Nick Crump, Amanda, Stella, Penny and DW for friendship, and especially their reassurance when I was at the end of my tether. My friends from Oxford and elsewhere have been constant sources of support and fun, especially Gabriela, Yi, Susie, Cherryl, Topaz, Sean and Lawrence – you have all been there for me, in good times and bad, and I am very grateful. I am also indebted to Esther and Noreen, without whom I would never have made the journey to Bristol and Oxford, and to Merton College and the Clarendon fund, for supporting my DPhil research.

I would like express sincere gratitude to my family: my brother, Jonathan, my aunts, Frances, Averil, Mimi, my father, Clement, and my grandmother, Claudia, who offered much needed support from afar. Finally, I am forever indebted to my mother, Teresa, who worked so very hard and sacrificed so much; it is due to her constant support and patience that I am who I am, and where I am, and it is to her that I dedicate my thesis.

Abbreviations

3’ PUA	3’ phospho-α,β unsaturated aldehyde
5’ dRP	5’deoxyribose phosphate
ADPRT	ADP-ribosyl transferase
Agg^-	Aggregation-deficient
Agg^+	Aggregation-proficient
AID	Activation-induced cytidine deaminase
AMD	Automodification domain
APE	AP-endonuclease
APLF	Aprataxin and PNKP-like factor
AP-site	Apurinic/Apyrimidinic site
APTX	Aprataxin
ARH	ADP-ribosylhydrolase
BER	Base excision repair
BIR	Break induced replication
Brca1	Breast cancer 1
Brca2	Breast cancer 2
BRCT	Carboxyl-terminal domain of breast cancer susceptibility protein
BsR	Blasticidin resistance
cAMP	Cyclic adenosine monophosphate
CDK	Cyclin dependent kinase
CO	Crossover
CPD	Cyclobutane pyrimidine dimer
CPT	Camptothecin

CSR	Class switch recombination
CtIP	CtBP interacting protein
DBD	DNA binding domain
DDR	DNA damage response
dHJ	Double Holliday junction
D-loop	Displacement-loop
DNAPKcs	DNA Protein Kinase catalytic subunit
DSB	Double strand break
FA	Fanconi Anaemia
Fen1	Flap Endonuclease 1
GFP	Green fluorescent protein
HR	Homologous recombination
ICL	Intra-strand crosslink
IR	Ionising radiation
Ka	*Klebsiella aerogenes*
LP-repair	Long-patch repair
mAR	Mono-ADP ribose
mART	Mono-ADP ribose transferase
MEF	Mouse embryonic fibroblast
MMS	Methyl methanesulfonate
MRN	Mre11/Rad50/Nbs1
MRX	Mre11/Rad50/Xrs2
NAD^+	Nicotinamide adenine dinucleotide
NCO	Non-crossover
NER	Nucleotide excision repair

NHEJ	Non-homologous end joining
PAR	Poly ADP-ribose
PARG	Poly ADP-ribose Glycohydrolase
PARP	Poly ADP-ribose Polymerase
PBZ	PAR binding zinc finger
PCNA	Proliferating cell nuclear antigen
PCR	Polymerase chain reaction
PNKP	Polynucleotide kinase phosphatase
Polβ/δ/ε	DNA Polymerase β/δ/ε
RAG	Recombination activating gene
RC-BER	Replication-coupled BER
REMI	Restriction enzyme mediated integration
ROS	Reactive Oxygen Species
RPA	Replication Protein A
SAM	S-adenosylmethionine
SCE	Sister chromatid exchange
SDSA	Synthesis dependent strand annealing
SP-repair	Short-patch repair
SSA	Single strand annealing
SSBR	Single strand break repair
TC-BER	Transcription coupled BER
TDP1	Tyrosyl-DNA phosphodiesterase 1
UNG2	Uracil DNA glycosylase 2
UV	Ultraviolet
ZF	Zinc finger

CHAPTER 1

General Introduction

1. Overview

This thesis presents three very different experimental areas where peptides have been evaluated for biological activity. Chapter two is aimed at the improvement of the cellular activity of the α–glucosidase inhibitor 1-deoxynojirimycin (DNJ) by the design and preparation of novel chemical structures comprising the iminosugar and either an ER-retaining signalling peptide or a cell penetrating peptide (CPP). The inhibitor-peptide constructs were tested *in vitro* for their inhibitory activity against α-glucosidases I and II, and in a cell-based assay to determine their activity on α-glucosidase-mediated hydrolysis of *N*-linked oligosaccharides. Fluorescently labelled ER-retaining peptides were also prepared to help determine the internalisation and trafficking of the constructs by FACS and IF-microscopy.

Chapter three presents a project with the double objective of improving the synthesis of the depsipeptide beauveriolide III and developing an IF-FACS-based method for the evaluation of Amyloid-β (Aβ) reduction as an effect of beauveriolide III's inhibitory activity on Acetyl CoA: cholesterol acyl transferase (ACAT). Chapter four is aimed at the development of a molecule that could target the host receptor for influenza virus entry. The design, synthesis and a simple evaluation by an NMR titration of a rationally designed cyclic peptide targeting sialic acid (SA) as the point of entry for the influenza virus are described.

Regardless of the different areas of application, these three experimental areas have one common feature: the use of peptides as key components of the active molecules tested. Whether as tools for targeting a small molecule to its desired cellular localisation as is the case in chapter two, as modified natural depsipeptides as presented in chapter three, or as completely novel sequences such as the cyclic peptide developed in chapter four, peptides are the unifying feature of the work presented here. Each chapter includes its own introduction with the background information of the clinical area involved, as well as a specific description of the peptides or techniques used in each project. After the

results, discussion and experimental methods are presented, each chapter contains a section establishing the conclusions reached in each project and a section on the future work that could be derived from the completed research. Chapter five sums the conclusions reached in each chapter and highlights the impact of the current work on the field of peptide therapeutics. The rest of this chapter merely aims to provide a brief review on the characteristics of peptides and some examples of their application as therapeutics.

2. Peptides as therapeutics

The distinction between peptide therapeutics and protein therapeutics can sometimes be ambiguous, however it is generally accepted that the term peptides refers to any sequence consisting of <100 amino acids used within a therapeutic environment.[1]

2.1. Limitations

Peptides have often been considered unsuitable candidates for drug development due to their inherent pharmacokinetic profiles. They are sensitive to proteases, have often low stability in plasma, and are liable to be rapidly removed from circulation by filtration in the kidneys due to their small size. Peptides also tend to be hydrophilic molecules, thus having limited ability to cross membranes. Their size and nature often limits their solubility and difficult the means of delivery. Until recently, intravenous delivery was considered the only reliable delivery method for peptide therapeutics, thus making this type of compounds unpopular with the medical research community.[1-3]

Another characteristic of peptides that has limited their use in therapeutics is their inherent flexibility. This trait often allows them to reach multiple conformations, resulting in a lack of selectivity for their target. In addition, the risk of generating an immune response is always present with this type of therapeutics. Finally, the high production cost of peptide therapeutics is a significant limiting factor for the research and development of peptide therapeutics.[2,3]

2.2. Advantages

Regardless of their many limitations, research for peptide therapeutics has continued, and many techniques have been developed to overcome the limitations mentioned above. The main justifications behind the continued support for peptide therapeutic are their overall low toxicity and potential for high specificity.[2] Their small size gives them advantage over proteins in terms of delivery, stability and ease of manipulation. Compared to small molecule drugs, they also offer the advantage of little drug-to-drug interactions, as well as few complications due to intermediate metabolites, and in most cases, little accumulation in the system.[2,3] Though perhaps their principal advantage is the vast potential for diversity inherent to their nature.

Peptide therapeutics have the added characteristic that they can be produced synthetically and thus can also be chemically modified. In general, small peptides have rapid clearance rates, which can prevent their accumulation to toxic levels. While they are also liable to protease degradation, some small peptides (up to 12 amino acids) have been shown to be structured in solution, thus increasing their resistance to proteases.[4,5] Nevertheless, the by-products of their degradation are natural amino acids which show significantly less toxicity than degradation products from common small-molecule drugs. It is also worth mentioning that a significant proportion of the peptide therapeutics isolated or developed from naturally occurring peptides act as agonists, and thus low doses are usually required for treatment.[6-9]

2.3. Supporting scientific advances

As mentioned before, several scientific advances have contributed to the continued interest in peptide therapeutics. Improved methodologies for Solid Phase Peptide Synthesis (SPPS) have significantly reduced the cost and effort required for the production of synthetic peptides.[3] Advancements in chemical techniques have allowed the introduction of modifications with aims to reducing their sensitivity to proteases, improving their stability and solubility, and/or limiting their flexibility to improve their specificity. Introduction of non-natural amino acids is often used to decrease the degradation of peptides by making them unrecognisable by proteases.[3] The same purpose is fulfilled by the use of

cyclisation, methylation or masking of the peptide terminus by esterification.[10] Cyclisation of the peptide has the added benefit of reducing its flexibility, thus limiting the number of conformations it can achieve and consequently increasing its specificity. Cyclisations can be done between the peptide terminus or among side chains.[11] Disulfide bonds are common methods for peptide cyclisation as well. Some other modifications involve the substitution of the amide backbone by alkyl chains or other functional groups, with the retention of the amino acid side chains that are required for the interaction with the target.[3] Glycosylation and pegylation are chemical modifications often used to improve the solubility of the peptide and its stability in plasma. [1,10]

In addition to chemical modifications, several routes for delivery have emerged. At present, peptide-based drugs can be administered orally, transdermally, or by mucosal or parenteral routes.[1] It is common procedure for newly developed therapeutics to be subjected to one or several chemical modifications during the optimization process to improve the limitations of the original peptide, as well as determining the optimal means of administration.[3]

2.4. Current applications

Due to the immense variability of peptides and peptide derivatives, few generalisations can be made regarding their properties. For example, highly immunogenic peptides have been used to increase immune responses in vaccines,[12] other peptide sequences have found therapeutic applications requiring them not to raise an immune response when administered,[13] yet other peptides are used for their immunosuppressant abilities (such as Cyclosporin A).[14] Nevertheless, areas that have benefited from peptide therapeutics include their use in vaccination,[12] as antimicrobials,[15] tools for drug targeting or for drug delivery,[16] cancer treatment and structure disruption.[17]

One use of peptides in vaccination is their application in cancer treatments. Anti-cancer peptide-based vaccines include several epitopes expressed by cancer-cells with the objective of raising an immune response against tumours.[12] Unfortunately, while some of these peptides have shown no toxicity and complete tumour eradication in mice, human trials remain largely ineffective.[18] Another interesting use of peptides as cancer therapeutics involve their action

against proliferating cells in tumors.[19] These particular peptides are identified *in vivo* from panels of combinatorial phage libraries in mice against characteristic antigens in tumour cells. They serve to target proliferating cells, block integrins and/or inhibit metalloproteases, either action leading to apoptosis.[20] Moreover, these peptides can be coupled to previously identified cytotoxic reagents, which can lead to increased drug efficacy and lower systemic toxicity.[21]

Yet another application of peptide therapeutics as anticancer treatments is as ACTH (Adrenocorticotropic hormone) releasing agents. Peptides such as corticorelin acetate (trademark Xerecept) or cosyntropin (trademark Cortrosyn) stimulate the pituitary gland to enhance the release of ACTH, which in turn increases the production and release of corticosteroids.[22] The overall effect for the treatment with these compounds is the reduction of permeability of the blood vessel walls, which leads to the reduction of inflammation associated with tumours. Corticorelin acetate (Xerecept) has been approved for the treatment of brain edema associated with cerebral tumours.[22]

Another well established use of a therapeutic peptide is the angiotensin II analogue saralasin acetate (trademark Sarenin). It is a competitive inhibitor of angiotensin II, an octapeptide whose main role is as part of the renin-angiotensin system. This peptide elicits vasoconstriction and release of aldosterone from the adrenal cortex. Aldosterone also promotes retention of sodium in the kidneys. The combined effect of angiotensin II is an increase in blood pressure, therefore Serinin is used mainly in the treatment of hypertension.[23,24] ACE inhibitors (angiotensin converting enzyme inhibitors) are a family of drugs that achieve a similar effect and that also include peptide-based therapeutics. ACE inhibitors stop the transformation of angiotensin I into angiotensin II, thereby preventing the increase in blood pressure induced by it.[25] FDA approved peptide ACE inhibitors include enalpril maleate (trademark Vasotec) and lisinopril (trademark Zestril), both of which are tripeptides rationally designed from a naturally occurring inhibitor, the bradykinin potentiating factor.[26]

Regarding the activity of peptides as antimicrobial agents, several sequences have been identified in nature.[15] Many of these are amphipathic in nature, with a cationic phase that attracts them to the lipid bilayer in their target's membrane, and a hydrophobic phase that, upon binding, interacts with the lipids to further

disrupt the membrane.[27] Based on the isolated sequences and their mode of action, several antimicrobial peptides have been developed *de novo*.[19] Some of these have found further applications in therapeutics, such as the linking of these sequences to peptides isolated from phage libraries against cancer epitopes. These constructs allowed targeting of the newly designed sequences to oncogenic cells, which upon internalisation, disrupt mitochondrial membranes and cause apotosis.[17, 28]

Peptides have also been used as antidiabetic agents. Exenatide (trademark Byetta) and liraglutide (trademark Victoza) are examples of peptide incretin mimetics that are used in the treatment of diabetes mellitus II. Incretins are hormones that stimulate the release of insulin and inhibit glucagon release in the pancreas.[29] Byetta is an analogue of glucagon-like peptide-1 (GLP-1). It was designed to increase the natural short half-life of the native 39-amino acid-peptide that is produced following food ingestion, and causes insulin secretion even in a diabetic state.[30]

Peptide therapeutics are also present as antithrombotic agents. Bivalirudin trifluoroacetate hydrate (trademark Angiomax) is a synthetic peptide which is a potent, highly specific and reversible inhibitor of thrombin. This enzyme is a serine proteinase that cleaves fibrinogen, stimulating the release of platelets and the thrombotic process. Therefore, this peptide is commonly used in the treatment of angina.[31] Eptifibatid (trademark Integrilin) is a similar antiplatelet agent. It is a cyclic heptapeptide that inhibits glycoprotein IIb/IIIa, binding reversibly to platelets and therefore used to reduce the risk of acute myocardial infarction in patients with angina.[32]

Another peptide drug used for the treatment of a cardiovascular disease is icatibant (trademark Firazyr). This decapeptide mimics bradykinin, and therefore acts as a specific antagonist for bradykinin B2 receptors. The natural peptide is produced in response to trauma, increasing vessel permeability and dilating blood vessels causing inflammation. Firazyr has been FDA approved for the treatment of acute attacks of hereditary angioedema.[33, 34]

A different application that has been found for short peptides is the ability of some sequences to disrupt β-sheet conformations.[35] This ability holds particular interest for diseases such as Alzheimer's disease or Creutzfeldt-Jakob disease,

which are linked to the aggregation of misfolded proteins/peptides (Aβ and prion protein respectively) in a β-sheet conformation. For example, a five-amino acid peptide, iAβ5p, was able to disrupt β-sheets in Aβ fibrils, and due to its small size, it has also shown ability to cross the blood-brain barrier, making it a promising therapeutic for these kind of diseases.[17]

An interesting application of peptides is also found in the efforts to prevent malaria. A 12-mer (SM1) that specifically binds to the salivary gland and midgut epithelia of the mosquitoes responsible for malaria transmission (*Anopheles gambiae*) was isolated from a phage library.[36] The peptide binds at the locations where *Plasmodium*, the causative agent of malaria, enters those tissues to complete its life cycle, thus effectively blocking invasion.[37] Furthermore, transgenic mosquitoes expressing SM1 are unable to transmit the parasite to mice.[37] Peptide therapeutics have also been used in the treatment of viral infections. For example, enfuvirtide (trademark Fuzeon) is an HIV fusion inhibitor used in combination therapy in the treatment of HIV-1.[38] It is a 37-amino acid competitive inhibitor that mimics the HIV-1 fusion peptide, binding gp41 and preventing the pore formation that would allow entry of the virus to the host cell.[39]

Many of the peptide therapeutics that have been approved for treatment of various diseases are hormone analogues. An example of this is ceruletide diethylamine (trademark Takus), which is a cholecystokinin analogue. This decapeptide is a hormone involved in the digestion of protein and fat. Cholecystokinin stimulates secretions from the pancreas and gallbladder, by upregulating pancreatic acinar cell intercellular adhesion molecule-1 (ICAM-1) to enhance pancreatic inflammation.[40] In addition, as a neuropeptide, cholecystokinin induces a satiating effect.[41] Nevertheless, Takus has been approved as a diagnostic tool and to help re-establish pancreas homeostasis. It has also been considered for the treatment of psoriasis.[42] Sincalide (trademark Kinevac) is a similar analogue of cholecystokinin, however it comprises only the eight final amino acides from the C-terminus.[43]

Several GHRH (Growth hormone releasing hormone) analogues are peptides such as Sermorelin acetate (trademark Groliberin) or somatorelin acetate (trademark Ferring). These peptides are designed to test for growth hormone

secretion. This hormone is a 44-amino acid-peptide produced in the hypothalamus with the function of stimulating the release of growth hormone. This type of drugs is often used to reduce cognitive decline in older people, to treat growth hormone insufficiency, and is often exploited in sports for doping purposes.[44,45]

A significant number of peptide therapeutics are agonists or antagonists of GnRH (gonadotropin-realising hormone receptor). A few example of these are Buserelin acetate (trademark Bigonist), gonadorelin acetate (trademark Factrel), goserelin acetate (Zoladex), histrelin acetate (trademark Supprelin), and leuprolide acetate (trademark Enantone).[46] GnRH is a hormone secreted by the pituitary gland, and it stimulates the secretion of luteinizing hormone (LH) and follicle stimulating hormone (FSH).[47] The aforementioned agonist peptides mimic GnRH (10 amino acids) and thus are used for the treatment of some cancers (such as prostate or breast cancer), some oestrogen-dependent conditions, and as treatments to assist reproduction.[46] Some GnRH antagonists are also peptides that instead of stimulating the release of LH and FSH, bind to the GnRH receptors and suppress any further hormone release. Some examples of FDA-approved GnRH antagonists are abarelix acetate (trademark Plenaxis), cetrorelix acetate (trademark Cetrotide), and degarelix acetate (trademark Firmagon).[48]

A different example of hormone-related peptide therapeutics are the oxytocin analogues that act as inhibitors for the oxytocin receptors. Native oxytocin is a peptide hormone that acts as a neuromodulator and whose main effect is the facilitation of labour and breastfeeding during mammalian reproduction.[49] Atosiban acetate (trademark Antocin) and carbetocin acetate (trademark Duratocin) are examples of FDA-approved oxytocin mimetics.[50] While Antocin acts as an inhibitor and thus is used to stop premature labour,[51] Duratocin is an oxytocin analogue that is used instead to promote contractions.[52]

Somatostatin is another peptide hormone that has been identified as a therapeutic target. Its natural role is the regulation of the endocrine system, affecting neurotransmission and cell proliferation. When it is released in the pituitary glad, its main role is to inhibit the release of growth hormone and thyroid stimulating hormone, as well as the inhibition of adenylyl cyclase. When

somatostatin is involved in the gastrointestinal system, it inhibits the release of hormones such as secretin, cholecystokinin, insulin, glucagon and gastrin, with an overall effect of decreasing the rate of digestion.[53] Due to the multiple functions of the hormone, several somatostatin analogues have been approved for various applications. For example, octreotide acetate (trademark Sandostatin), edotreotide (trademark Onalta) and lanreotide acetate (trademark Somatuline) are all used for treatment of carcinoid syndrome and polycystic diseases in the liver and kidney.[54,55]

Another common peptide that is well established in the market is calcitonin. This 32-amino acid linear peptide is a hormone produced in the thyroid with the purpose of reducing blood calcium. Calcitonin isolated from salmon (trademark Salco) or synthetically produced (trademark Carbocalcitonin) are used for the treatment of hypercalcemia or osteoporosis.[56]

2.5. Market

Novel peptide therapeutics are constantly being developed for clinical applications and many peptides are already being marketed successfully.[57] The peptide market started in the 1970s when Novartis launched Lypressin, a vasopressin analogue.[58] Since then, many peptides have been approved for commercialisation.[3] They often fall into one of three categories: naturally occurring peptides (such as hormones) or protein fragments and their analogues, peptides isolated from library screenings, and rationally designed peptides. As can be observed from the examples presented in Section 2.3 , the vast majority of approved peptides belong to the first category. This is understandable, since naturally occurring peptides and their analogues are less likely to elicit side-effects or generate immune responses.

Nevertheless, the vast improvement in the development, design and cost of combinatorial libraries, particularly by phage display, has led to several discoveries of peptides with therapeutic applications.[59] It seems likely that with this continuous advance in technology, more and more peptides belonging to this category will reach the market in the coming years. Rationally designed peptides are by their very nature more time and resource-consuming. Nevertheless, while their appearance in the market might be slower than peptides from the other

categories, their intrinsic promise for specificity ensures that research will continue in this area.

At the moment, there are just over 65 peptide-based drugs approved in the European, American and/or Japanese markets. In addition, there are over 140 peptide candidates undergoing clinical trials.[60,3]

3. Conclusion

The examples of therapeutic peptides mentioned previously are only a few of the possible applications of peptides as therapeutics. As can be appreciated from this brief review, the areas and methods of application for therapeutic peptides vary widely, reflecting the flexibility of these molecules and their vast potential for therapeutic use. Nevertheless, the problems faced by peptide therapeutics are many. As in all drug development areas, while peptide therapeutics can be promising *in vitro,* they often have little efficacy when tested *in vivo.*[2] In this case, interactions with proteases and immune responses are the main concerns in the development of peptide therapeutics. Additionally, delivery methods have to be analysed individually for each peptide, since their nature varies considerably depending on their constitutive sequences.[1] Despite the technical difficulties, the continued emergence of new peptide therapeutics and the rapid advancement of peptide research seem to indicate that peptides will become a significant branch of drug discovery in the near future.[57]

4. References

1. Lien, S. and Lowman, H.B. Therapeutic peptides. *Trends in Biotechnology*. 2003;21(12):556-62.

2. Pichereau, C. and Allary, C. Therapeutic peptides under the spotlight. *Bionest Publications*. 2004.

3. Vlieghe, P.; Lisowski, V.; Martinez, J. and Khrestchatisky, M. Synthetic therapeutic peptides: science and market. *Drug Discovery Today*. 2010;15(1-2):40-56.

4. Nakamura, G.R.; Reynolds, M.E.; Chen, Y.M.; Starovasnik, M.A. and Lowman, H.B. Stable "zeta" peptides that act as potent antagonists of the high-affinity IgE receptor. *Proceedings of the National Academy of Sciences of the United States of America*. 2002;99(3):1303-8.

5. Cochran, A.G.; Skelton, N.J. and Starovasnik, M.A. Tryptophan zippers: stable, monomeric beta-hairpins. *Proceedings of the National Academy of Sciences of the United States of America*. 2001;98(10):5578-83.

6. Chidgey, A. and Boyd, R. Agonist peptide modulates T cell selection thresholds through qualitative and quantitative shifts in CD8 co-receptor expression. *International Immunology*. 1997;9(10):1527-36.

7. Cwirla, S.E. Peptide agonist of the thrombopoietin receptor as potent as the natural cytokine. *Science*. 1997;276(5319):1696-9.

8. Doorbar, J. and Winter, G. Isolation of a peptide antagonist to the thrombin receptor using phage display. *Journal of Molecular Biology*. 1994;244:361-9.

9. Zhou, N.; Luo, Z.; Luo, J.; Hall, J.W. and Huang, Z. A novel peptide antagonist of CXCR4 derived from the *N*-terminus of viral chemokine vMIP-II. *Biochemistry*. 2000;39(13):3782-7.

10. Shechter, Y.; Mironchik, M.; Saul, A.; Gershonov, E.; Precido-Patt, L.; Sasson, K.; Tsubery, H.; Mester, B.; Kapitkovsky, A.; Rubinraut, S.; Vachutinski, Y.; Fridkin, G. and Fridkin, M. New technologies to prolong life-time of peptide and protein drugs *in vivo*. *International Journal of Peptide Research and Therapeutics*. 2006;13(1-2):105-17.

11. Davies, J.S. The cyclization of peptides and depsipeptides. *Journal of Peptide Science*. 2003;9(8):471-501.

12. Rosenberg, S.A.; Yang, J.C. and Schwartzentruber, D.J.; Hwu, P.; Marincola, M.; Topalia, S.L.; Restifo, N.P.; Dudley, M.E.; Schwarz, S.L.; Spiess, P.J.; Wunderlich, J.R.; Parkhurst, M.R.; Kawakami, Y.; Claudia, A.; Einhorn, J.H. and White, D.E. Immunologic and therapeutic evaluation of a synthetic peptide vaccine for the treatment of patients with metastatic melanoma. *Nature Medicine*. 1998;4(3):321-7.

13. Schnabel, C.A.; Fineberg, S.E. and Kim, D.D. Immunogenicity of xenopeptide hormone therapies. *Peptides*. 2006;27(7):1902-10.

14. Borel, J.F. History of the discovery of cyclosporin and of its early pharmacological development. *Wiener Klinische Wocheschrift*. 2002;114(12):433-7.

15. Jenssen, H.; Hamill, P. and Hancock, R.E.W. Peptide antimicrobial agents. *Clinical Microbiology Reviews*. 2006;19(3):491-511.

16. Dharap, S.S.; Wang, Y.; Chandna, P.; Khandare, J.J.; Qiu, B.; Gunaseelan, S.; Sinko, P.J.; Stein, S.; Farmanfarmaian, A. and Minko, R.. Tumor-specific targeting of an anticancer drug delivery system by LHRH peptide. *Proceedings of the National Academy of Sciences of the United States of America*. 2005;102(36):12962-7.

17. Soto, C.; Kascsak, R.J.; Saborío, G.P.; Aucouturier, P.; Wisniewski, T.; Prelli, F.; Kascsak, R.; Mendez, E.; Harris, D.A.; Ironside, J.; Tagliavini, F.; Carp, R.I. and Frangione, B. Reversion of prion protein conformational changes by synthetic β-sheet breaker peptides. *The Lancet*. 2000;355(9199):192-7.

18. Klinik, A.M, Sahin, U. and Pfreundschuh, M. Serological identification of human tumour antigens. *Cancer*. 1997:709-16.

19. Ellerby, H.M.; Arap, W.; Ellerby, L.M.; Kain, R.; Andrusiak, R.; Rio, G.D., Krajewski, S.; Lombardo, C.R.; Rao, R.; Ruoslahti, E.; Bredesen, D.E. and Pasqualini, R. Anti-cancer activity of targeted pro-apoptotic peptides. *Nature Medicine*. 1999;5(9):1032-8.

20. Koivunen, E.; Arap, W.; Valtanen, H.; Rainisalo, A.; Medina, O.P.; Heikkila, P.; Kantor, C.; Gahmberg, C.G.; Salo, T.; Konttinen, Y.T.; Sorsa, T.; Ruoslahti, E. and Pasqualini, R. Tumor targeting with a selective gelatinase inhibitor. *Nature Biotechnology*. 1999;17(8):768-74.

21. Curnis, F.; Sacchi, A.; Borgna, L.; Magni, F.; Gasparri, A. and Corti, A. Enhancement of tumour necrosis factor alpha antitumor immunotherapeutic

properties by targeted delivery to aminopeptidase N (CD13). *Nature Biotechnology*. 2000;18(11):1185-90.

22. Celtic Pharma. XERECEPT®. *The Portafolio*. 2006. Available at: http://www.celticpharma.com/theportfolio/xerecept.html. Accessed January 27, 2012.

23. Solomon, T.A. and Buckley, J.P. Inhibitory effects of central hypertensive activity of angiotensin I and II by 1-sar-8-ala-angiotensin II (saralasin acetate). *Journal of pharmaceutical sciences*. 1974;63(7):1109-13.

24. Weir, M.R. and Dzau, V.J. The renin-angiotensin-aldosterone system: a specific target for hypertension management. *American Journal of Hypertension*. 1999;12:205S-213S.

25. Barone, J.A.; Byerly, W.G. and Lacy, C.R. Angiotensin-converting enzyme inhibitors: a comparative review . *The Annals of Pharmacotherapy* . 1990;24 (5):506-25.

26. Lancaster, S.G. and Todd, P.A. Lisinopril. A preliminary review of its pharmacodynamic and pharmacokinetic properties, and therapeutic use in hypertension and congestive heart failure. *Drugs*. 1988;35(6):646-69.

27. Ganz, T. and Lehrer, R.I. Antimicrobial peptides of vertebrates. *Current Opinion in Immunology*. 1998;10(1):41-4.

28. Permanne, B.; Dorpe, J.; Dewachter, I. and Banks, W.A. Reduction of amyloid load and cerebral damage in a transgenic mouse model of Alzheimer ' s disease by treatment with a β-sheet breaker peptide. *The FASEB Journal*. 2002;16(8):860-2.

29. Nielsen, L.L. Incretin mimetics and DPP-IV inhibitors for the treatment of type 2 diabetes. *Drug discovery today*. 2005;10(10):703-25.

30. Amylin Pharmaceuticals Inc. Byetta - Exenatide. 2012. Available at: http://www.byetta.com/Pages/index.aspx. Accessed January 27, 2012.

31. Bertrand, M.E.; Lincoff, A.M.; Moses, J.W.; White, H.D.; Pocock, S.J.; Ware, J.H.; Feit, J.H.; Feit, F.; Colombo, A.; Aylward, P.E.; Cequier, A.R.; Darius, H.; Desmet, W.; Rupprecht, H.; Hoekstra, J. and Mehran R. Bivalirudin for patients with acute coronary syndromes. *The New England Journal of Medicine*. 2006;355(21):2203-16.

32. Phillips, D.R.P. and Scarborough R.M.P. Clinical pharmacology of eptifibatide. *The American Journal of Cardiology*. 1997;80(4, Supplement 1):11B-20B.

33. Bork, K.; Frank, J.; Grundt, B.; Schlattmann, P.; Nussberger, J. and Kreuz, W. Treatment of acute edema attacks in hereditary angioedema with a bradykinin receptor-2 antagonist (Icatibant). *Journal of Allergy and Clinical Immunology*. 2007;119(6):1497-503.

34. Cicardi, M.; Banerji, A.; Bracho, F.; Malbran, A.; Rosenkranz, B.; Riedl, M.; Bork, K.; Lumry, W.; Aberer, W.; Bier, H.; Bas, M.; Greve, J.; Hoffmann, T.K.; Farkas, H.; Reshef, A.; Ritchie, B.; Yang, W.; Grabbe, J.; Kivity, S.; Breuz, W.; Levy, R.J.; Luger, T.; Obtulowics, K.; Schmid-Grendelmeier, P.; Bull, C.; Sitkauskiene, B.; Smith, W.B.; Toubi, E.; Werner, S.; Anne, S.; Bjorkander, J.; Bouillet, L.; Cillari, E.; Hurewitz, D.; Jacobson, K.W.; Katelaris, C.H.; Maurer, M.; Merk, H.; Bernstein, J.A.; Feighery, C.; Floccard, B.; Gleich, G.; Herbert, J.; Kaatz, M.; Keith, P.; Kirkpatrick, C.H.; Langton, D.; Martin, L.; Pichler, C.; Resnick, D.; Wombolt, D.; Fernandez Romero, D.S.; Zanichelli, A.; Arcoleo, F.; Knolle, J.; Kravec, I.; Dong, L.; Zimmermann, J.; Rosen, K. and Fan, W. Icatibant, a new bradykinin-receptor antagonist, in hereditary angioedema. *The New England Journal of Medicine*. 2010;363(6):532-41.

35. Rocha, S.; Cardoso, I.; Börner, H.; Pereira, M.C.; Saraiva, M.J. and Coelho, M. Design and biological activity of beta-sheet breaker peptide conjugates. *Biochemical and Biophysical Research Communications*. 2009;380(2):397-401.

36. Ghosh, A.K.; Ribolla, P.E. and Jacobs-Lorena, M. Targeting *Plasmodium* ligands on mosquito salivary glands and midgut with a phage display peptide library. *Proceedings of the National Academy of Sciences of the United States of America*. 2001;98(23):13278-81.

37. Ito, J.; Ghosh, A.; Moreira, L.A.; Wimmer, E.A. and Jacobs-Lorena, M. Transgenic anopheline mosquitoes impaired in transmission of a malaria parasite. *Nature*. 2002;417(6887):452-5.

38. Klein, R. FDA approves Fuzeon. *Food and Drug Administration*. 2003. Available at: http://www.fda.gov/ForConsumers/ByAudience/ForPatientAdvocates/HIVandAIDSActivities/ucm125088.htm. Accessed January 28, 2012.

39. Bewley, C.A.; Louis, J.M.; Ghirlando, R. and Clore, G.M. Design of a novel peptide inhibitor of HIV fusion that disrupts the internal trimeric coiled-coil of gp41. *The Journal of biological chemistry*. 2002;277(16):14238-45.

40. Munro, S. and Pelham, H.R. A C-terminal signal prevents secretion of luminal ER proteins. *Cell*. 1987;48(5):899-907.

41. Moroji, T.; Itoh, K. and Itoh K. Antipsychotic effects of ceruletide in chronic schizophrenia. *Annals of the New York Academy of Sciences*. 1985;448(1):518-34.

42. Kelesheva, Lamara F. Use of ceruletide diethyl amine salt in the treatment of psoriasis. 1995022346. 1995.

43. Smith, G.P. The therapeutic potential of cholecystokinin. *International Journal of Obesity*. 1984;8(1):35-8.

44. Walker, R.F. Editorial foreword. *Aging*. 2006;1(4):307-8.

45. Carlsson, L.; Christiansen, J.S.; Clemmons, D.; Hintz, R.; Ho, K.; Laron, Z.; Tanaka, T.; Thorner, M.; Sizonenko, P. and So, P.H. Growth hormone deficiency in adulthood and the effects of growth hormone replacement : a review. *Endocrinology And Metabolism*. 1998;83(2):382-95.

46. Fedele, L. and Berlanda, N. Emerging drugs for endometriosis. *Expert Opin Emerg Drugs.* 2004;9(1):167-77.

47. Schneider, F.; Tomek, W. and Gründker, C. Gonadotropin-releasing hormone (GnRH) and its natural analogues: a review. *Theriogenology*. 2006;66(4):691-709.

48. Al-Inany, H. and Aboulghar, M. GnRH antagonist in assisted reproduction: a Cochrane review . *Human Reproduction* . 2002;17 (4):874-85.

49. Am, C.; Ness, A. and Je, T. Prophylactic oxytocin for the third stage of labour (Review). *The Cochrane Library*. 2010;(2).

50. Goodwin, T.M.; Paul, R.; Silver, H.; Spellacy, W.; Parsons, M.; Chez, R.; Hayashi, R.; Valenzuela, G.; Creasy, G.W. and Merriman, R. The effect of the oxytocin antagonist atosiban on preterm uterine activity in the human. *American Journal of Obstetrics and Gynecology*. 1994;170(2):474-8.

51. Borthwick, A.D. Oxytocin antagonists and agonists. *Annual Reports on Medicinal Chemistry*. 2006;41(06):41028.

52. Rath, W. Prevention of postpartum haemorrhage with the oxytocin analogue carbetocin. *EuropeanJjournal of Obstetrics, Gynecology, and Reproductive Biology*. 2009;147(1):15-20.

53. Weckbecker, G.; Lewis, I.; Albert, R.; Schmid, H.A.; Hoyer, D. and Bruns, C. Opportunities in somatostatin research: biological, chemical and therapeutic aspects. *Nature reviews. Drug discovery*. 2003;2(12):999-1017.

54 de Herder, W.W. and Lamberts, S.W.J. Somatostatin and somatostatin analogues: diagnostic and therapeutic uses. *Current Opinion in Oncology*. 2002;14(1).

55. Modlin, I.M.; Pavel, M.; Kidd, M. and Gustafsson, B.I. Review article: somatostatin analogues in the treatment of gastroenteropancreatic neuroendocrine (carcinoid) tumours. *Alimentary Pharmacology & Therapeutics*. 2010;31(2):169-88.

56. Findlay, D.M. and Sexton, P.M. Calcitonin. *Growth Factors*. 2005;22(4):217-24.

57. Reichert, J. Development trends for peptide therapeutics. *Peptide Therapeutics Foundation Review*. 2010:46.

58. Dakters, J.G.; Yashon, D.; Purnell, E.W.; Volk, M. and White, R.J. Ultrasonography for diagnosis of orbital tumors. *JAMA : The journal of the American Medical Association*. 1968;203(9):803-5.

59. Szardenings, M. Phage display of random peptide libraries: applications, limits, and potential. *Journal of Receptors and Signal Transduction*. 2003;23(4):307-49.

60. Thayer, A.M. Improving peptides. *Chemical & Engineering News*. 2011;89(22):13-20.

CHAPTER 2

Enhancing iminosugar glucosidase inhibition using synthetic peptide constructs which increase ER targeting and retention

1. Project objective

The aim of this project is to improve the activity of the α-glucosidase inhibitor 1-deoxynojirimycin (DNJ), by the design and preparation of novel chemical structures comprising the iminosugar and either an ER-retaining signalling peptide or a cell penetrating peptide (CPP). This approach, if successful, could be a general tool to improve the effective concentration of any iminosugar whose site of action resides within the lumen of the ER.

2. Introduction

The Butters' research group has long been involved in the study of the therapeutic applications of iminosugars as inhibitors for glucosidases.[1-3] The project presented in this chapter expands upon this line of research and introduces the use of peptides as tools for improvement of the biological activity and ultimately the medicinal chemistry of iminosugars.

This introductory section is divided into three main parts. The first part provides a brief introduction to *N*-linked glycosylation and its connection to the quality control of newly synthesised glycoproteins and ER-associated degradation (ERAD) of proteins. A description of the appearance and fate of free oligosaccharides is also provided, as well as the effect of α-glucosidase inhibition. The second part focuses on iminosugars, highlighting their main properties and current therapeutic applications. The final section reviews the delivery peptides involved in this project, ER-retaining signalling peptides and cell-penetrating peptides (CPPs).

The results and discussion section is divided into three subsections. The first one is focused on the synthesis of DNJ (**1**) and the DNJ-peptide constructs. The second one describes the experimental assays involving DNJ-ER retaining peptide constructs, including *in vitro* and *in cellulo* assays as well as fluorescence

based experiments of ER retaining peptides. The final section focuses on the study of DNJ-CPP constructs.

The conclusions section provides a summary of the results obtained as well as the key conclusions that could be drawn from these results. The future work section highlights the next experiments that need to be performed to build upon the results obtained and explore the avenues of research opened by the current work. Finally, the experimental section provides detailed procedures for the synthesis and assays completed, as well as characterisation of the synthetic products generated. References for this project are provided at the end of the chapter.

2.1. *N*-linked glycosylation

Protein glycosylation occurs through one of two pathways, *O*-glycosylation or *N*-glycosylation. While *O*-glycosylation is a continuous process involving the elongation of complex glycans in both the ER and the Golgi from potentially any Thr or Ser in a growing polypeptide, *N*-glycosylation has a concerted, well-established origin.[4]

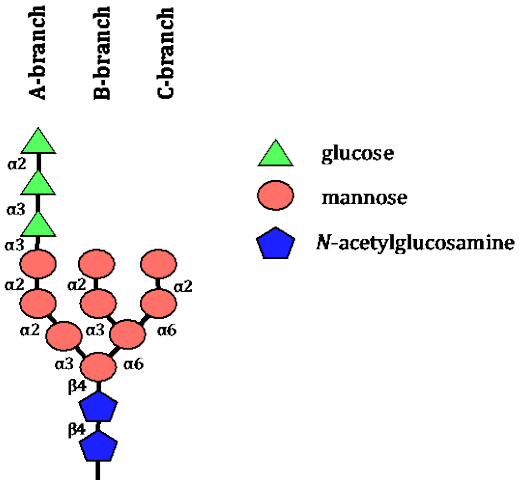

Figure 2.1 - Symbolic representation of $Glc_3Man_9GlcNAc_2$ with intercarbohydrate linkages indicated.

N-Glycosylation starts with a fully mature glycan ($Glc_3Man_9GlcNAc_2$ – Figure 2.1) being transferred from a dolichyl pyrophosphate carrier to a growing

polypeptide. Synthesis of the dolichyl linked oligosaccharide starts on the cytosolic side of the ER membrane, where dolichol is anchored, from nucleotide-activated monosaccharides as sugar donors.[5] After Dol-PP-$GlcNAc_2Man_5$ is assembled, the construct flips to finish glycan assembly on the lumenal side of the ER membrane (Figure 2.2).[6]

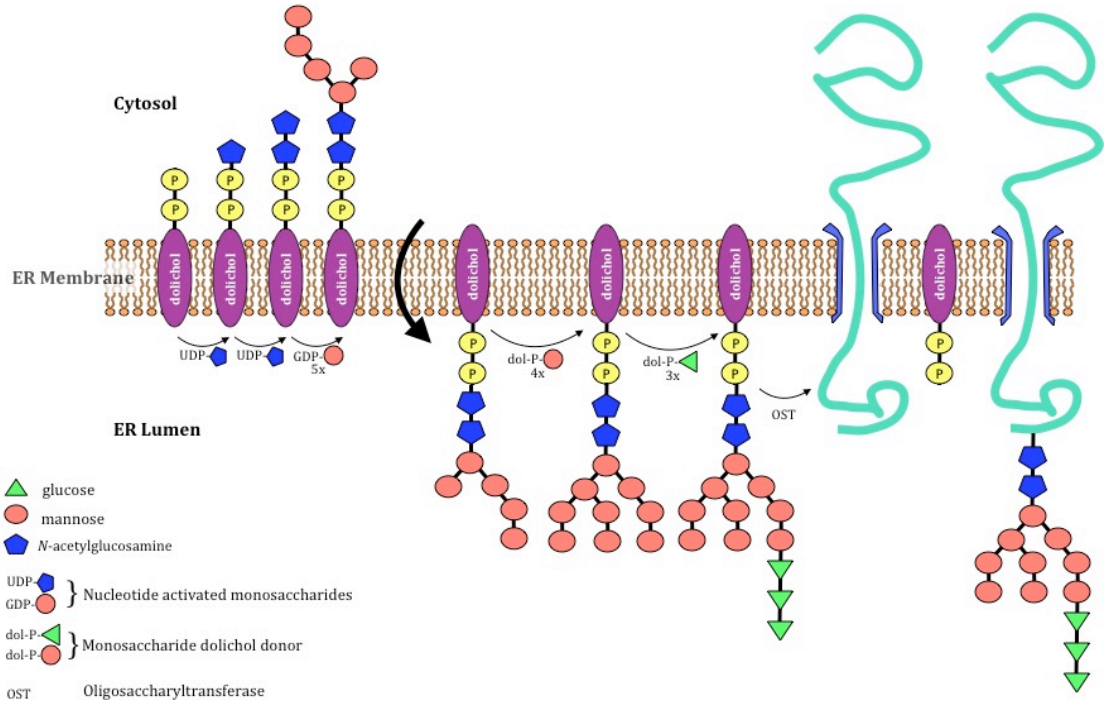

Figure 2.2 - Assembly of dolichol-linked $Glc_3Man_9GlcNAc_2$ and transfer to nascent polypeptide.

While *N*-glycosylation is often referred to as a post-translational modification, in reality it is a co-translational event, with glycosylation occurring as soon as the growing polypeptide is translocated into the ER lumen. The glycosylation site is identified by the sequence Asn-X-Ser/Thr (Asn sequon), where X can be any amino acid except proline. The glycan transfer from the dolichol donor to the peptide is done by oligosaccharyltransferase (OST),[7,8] a multisubunit enzyme complex located in close proximity to the entry pore (Sec61) of the nascent polypeptide.[9] The location of OST guarantees its action on unfolded glycoproteins, which allows the flexibility needed in the Asn sequon to bring close the guanidyl moiety of Asn to the OH group in Thr or Ser.[10,11]

Although *N*-glycosylation requires the addition of $Glc_3Man_9GlcNAc_2$, the final complex glycans are generated after multiple trimming and elongation reactions

that occur throughout the secretory pathway. Regardless, the first reaction is the hydrolysis of the outermost α-1,2-linked glucose by mannosyl-oligosaccharide α-glucosidase-I (glucosidase I) as seen in Figure 2.3.[12] This enzyme is a homotetramer that resides in the ER and is part of the OST complex.[4]

The diglucosylated *N*-glycans quickly bind to the ER-resident glucan α1,2-glucosidase complex (α-glucosidase II), which acts on the remaining two glycosidic linkages, albeit with different kinetics.[13] Glucosidase II is a heterotetramer formed from 2 subunits; the α-subunit is responsible for its hydrolytic activity, while the β-subunit is responsible for substrate specificity *in vivo*.[14] The diglucosylated *N*-glycans bind to the α-subunit of Glucosidase II, however hydrolysis does not occur until the β-subunit binds through its mannose-6-phosphate receptor homology domain (MRH) to the next glycan presented. This trans-glycan binding starts the hydrolysis to generate a monoglucosylated *N*-glycan. The last glucose is protected from hydrolysis because it stays topologically inaccessible due to the association of the second glycan to the β-subunit.[15]

The resulting mono-glucosylated glycan is free to bind to the calnexin/calreticulin (CALX/CALN) complex.[16] CALX/CALN form a complex with protein disulfide isomerase (PDI). This set-up acts as a chaperone that allows correct folding (and disulfide bond formation) for the nascent polypeptide. [17,18] After the nascent protein is released from the Sec61 pore and it dissociates from the calnexin complex, the monoglucosylated *N*-glycans are fully deglucosylated by Glucosidase II and can continue their trafficking along the secretory pathway.[15]

2.2. Calnexin/calreticulin cycle

At this point only a few glycoproteins are correctly folded. To prevent misfolded proteins from leaving the ER, UDP-glucose:glycoprotein-glucosyltransferase (UGGG1) reglucosylates the A-branch on some *N*-glycans.[19] UGGG1 is the main element on the quality control mechanism in the ER. It functions both as a folding sensor and a glucosyltransferase, localised in the ER by its KDEL ER-retention signal.[20] UGGG1 recognises substrates that have their core GlcNAc-Asn exposed and have surrounding hydrophobic amino acid patches. The glycan core

is usually buried in a protein grove in native conformations, thus its exposed presence indicates an immature glycoprotein. The hydrophobic patches are consistent with the molten-globule stage of near native conformations, which excludes the action of UGGG1 on terminally misfolded or aggregated proteins with exposed GlcNAc-Asn. The monoglucosylated species are then free to bind to the CALX/CALR complex again.[21] Most glycoproteins undergo several cycles of reglucosylation to allow more exposure to ER-mediated protein folding.[22,23]

After some time, the new glycoproteins can either be targeted for degradation or approved for export. *N*-glycans can directly target glycoproteins to the Golgi, however in other cases, mature protein conformation dependent mechanisms are triggered for transport. Another alternative is the cleavage of Mannose residues from the A-branch of *N*-glycans by α-1,2-mannosidase (MA1A1) to yield $Man_{6\text{-}8}GlcNAc_2$, which effectively depletes the substrate for UGGG1 and acts as an ER export signal.[24,18]

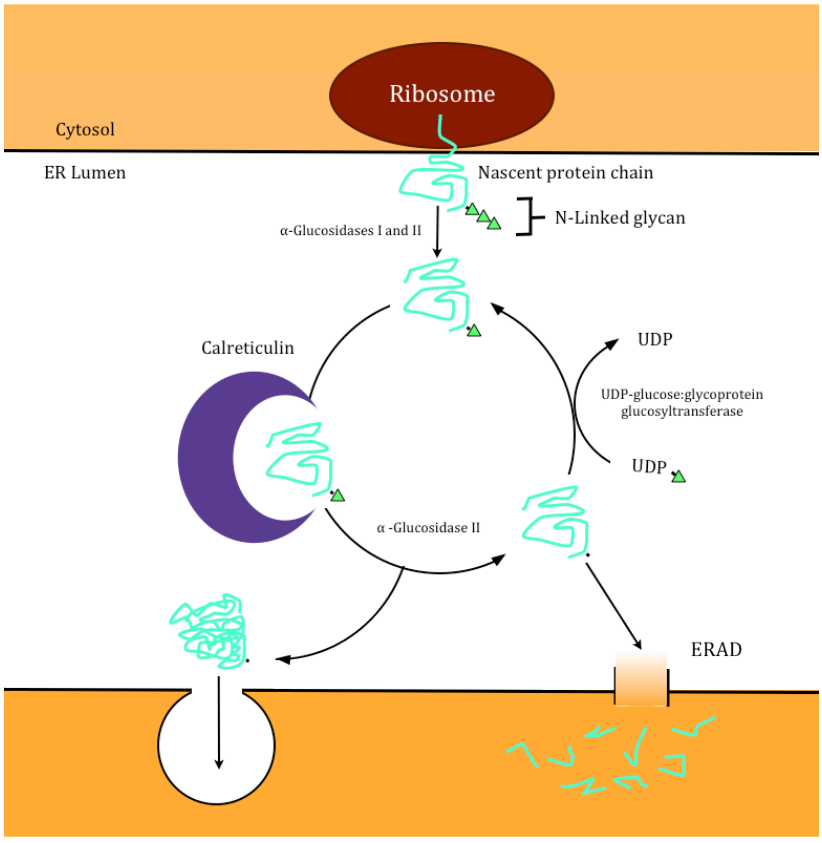

Figure 2.3 - The calnexin and calreticulin cycle.

Most proteins entering the secretory pathway have similar mannose-trimmed glycans when entering the Golgi, but the glycoproteins leaving exhibit a wide

variety of glycans. Four types of enzymes are responsible for this diversification: trimming α-mannosidases, nucleotide sugar transporters, glycosyltransferases, sulfotransferases and *O*-acetylases. The diversification starts with α-1,3/6 mannosidases trimming the B and C branches of the *N*-glycans. This trimming allows the elongation of the chain by glycosyltransferases to generate complex glycans using the activated donors carried by nucleotide sugar transporters.

Some of the glycosyltranferases involved in the branching and elongation of this complex glycans include mannosyl β-*N*-acetylglucosaminyltransferases, *N*-acetylglucosaminyl-β-galactosyltransferases, sialyltransferases, fucosyltransferases, glucoronyltransferases and sulfotransferases.[4]

2.3. ER-associated degradation (ERAD)

Regarding the proteins that are targeted for degradation instead of entering the secretory pathway, there are several possibilities for ER-associated degradation. ER mannosidase I acts as a timer for the quality control mechanism in the ER. Misfolded and immature proteins cycle through the CALX/CALR complex several times, but to prevent accumulation in the ER, if they are still misfolded after a number of cycles they are targeted for degradation.[22] Mannosidase I cleaves the α1,2-linkage to remove the last mannose in the B arm of the glycan, thus targeting the protein for degradation.[25] The slow reaction kinetics of mannosidase I provide the molecular clock required to prevent newly synthesised glycoproteins to be targeted for degradation.[26]

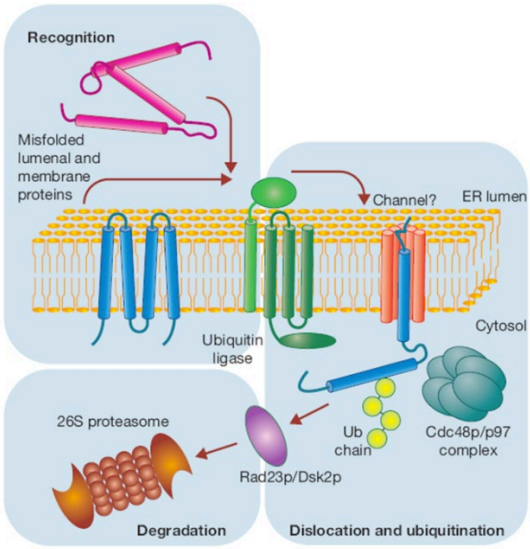

Figure 2.4 – ER-Associated Degradation.
Taken from Meusser, H., *et.al*. *Nature Cell Biology*, 2005, Vol. 7(8), pp 766-772.

ERAD uses the cytosolic proteasome as the main proteolytic pathway to remove misfolded glycoproteins from the ER (Figure 2.4). The misfolded proteins targeted for degradation are retrotranslocated to the cytosol, where they are polyubiquitinated. Proteins with misfolded ER-luminal domains use the ERAD-L (Luminal ER-associated degradation) pathway where ubiquitination is mediated by the association of the Hrd1p/Hrd3p complex to Yos9p, possibly requiring cycling through the cis-Golgi. Proteins misfolded in their cytosolic domains are ubiquitinated through the ERAD-C (Cytosolic ER-associated degradation) pathway that targets the proteins directly to the Doa10p ubiquitin ligase. Finally, proteins misfolded in their intra-membrane domain use the ERAD-M (Intra-Membrane ER-associated degradation) pathway which functions similarly to ERAD-L but doesn't require all the components of the Hrd1p complex. Regardless of how it has been polyubiquitinated, the polyubiquitin chain is recognised by a cytosolic ATPase complex, which finally allows proteins to be degraded by the proteasome.[27,28]

While ERAD is the most common degrading mechanism, there has been some evidence that not all proteins are degraded by it. Examples of which are the inability of proteasome inhibitors to completely inhibit degradation of ERAD substrates and the dual location of Peptide:*N*-Glycanase (PNGase).[29,30]

2.4. Free Oligosaccharides (FOS)

Once a misfolded glycoprotein has been retrotranslocated to the cytosol, the glycans are removed by PNGase.[31,32] This enzyme hydrolyses the amide bond between the Asn residue and the *N*-linked glycan (Figure 2.5). While this enzyme can be also found in microsomes and the ER,[33] in the cytosol it is part of the degradation complex including ubiquitin ligase and the proteasome. The FOS produced have a di-*N*-acetylglucosamine sequence (chitobase core $GlcNAc_2$) at the reducing terminus.[34,35]

It has been shown that deglycosylation is not required for retrotranslocation,[36] nor is it a requirement for protein degradation, however inhibition of PNGase causes ER stress. This indicates, that while deglycosylation is not essential for protein degradation, at least makes the degradation process more efficient.[37]

The glycan with the chitobase core is then cleaved by either the cytosolic endo-β-*N*-acetylglucosaminidase (ENGase) or chitobiase to generate a $Man_8GlcNAc_1$.[38] This glycan can then be acted on by α-mannosidase, which trims the remaining mannoses until $Man_5GlcNAc_1$ is obtained.[39] This structure is the same as the one present on the dolichol intermediate in the cytosol before it flips onto the ER lumen during glycoprotein synthesis. $Man_5GlcNAc_1$ is then transported to the lysosome for further degradation.

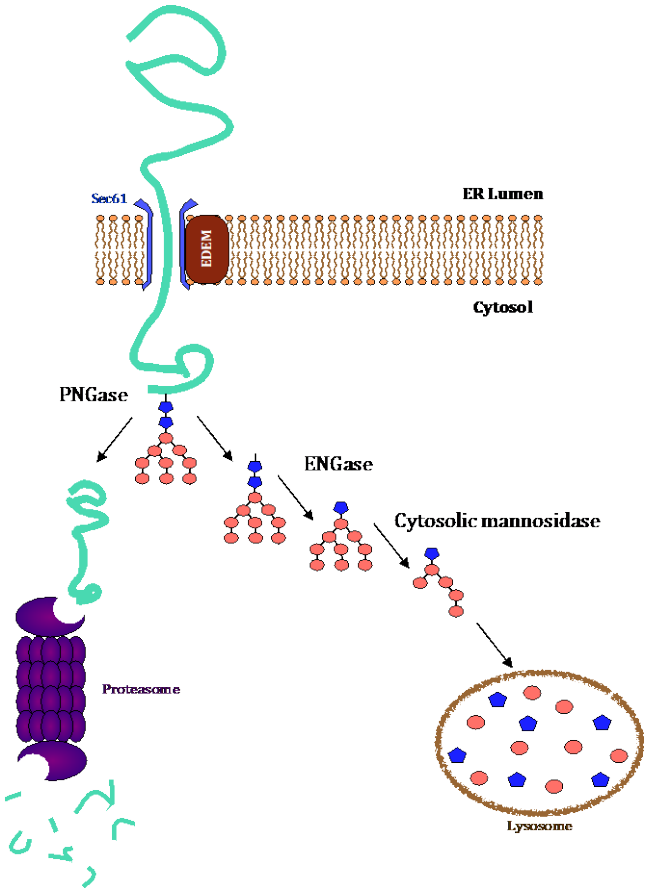

Figure 2.5 – Catabolism of Free Oligosaccharides (FOS) in the proteasomal degradation pathway.

2.5. α-Glucosidase I inhibition

α-Glucosidase inhibition prevents newly formed glycoproteins entering the CALX/CALR cycle of protein folding. Its inhibition also prevents deglucosylation of glycoproteins in the ER.[40] Under normal conditions, there is little accumulation of glucosylated free oligosaccharides in the cytosol. The major species that has been detected is $Glc_1Man_5GlcNAc_1$, as observed in HL60 and HepG2 cells.[41,42] However, following the addition of an α-glucosidase inhibitor, the levels of glucosylated species increase significantly.[43,40] $Glc_3Man_5GlcNAc_1$

seems to be the metabolic endpoint in the cytosol,[44] where cytosolic mannosidase is unable to digest the A arm due to the glucosyl cap. These glucoses also prevent the translocation of the glycan into the lysosome because the transporter is optimised for Man5GlcNAc1 or smaller glycans.[45] The addition of an α-glucosidase inhibitors also generates a small amount of $GlcNAc_2$ species. These species must be located in the ER lumen, since they have not been exposed to ENGase or chitobiase.[46]

α-Glucosidase inhibition can be relieved to a certain extent by endomannosidase.[47,48] This enzyme is located in post ER compartments, mostly in the cis Golgi,[49] and is able to remove the glucose cap by cleaving the last Man-α-1,2-Man linkage from the A arm of the glycan.[48] It appears some glucosylated glycoproteins can travel from the ER to the Golgi via either bulk flow or VIP36, a lectin that mediates transport.[50] This by-pass route seems to be increased when α-glucosidase is inhibited. Until recently, it was considered possible that endomannosidase had a role in quality control mechanism distal from the ER,[51,52] however recent research has made this an unlikely possibility.[53]

2.6. Iminosugars

Iminosugars are monocyclic heterocycle mimics of cyclic sugars where a nitrogen atom replaces the endocyclic ring oxygen. The replacement of this key atom prevents iminosugars from being metabolised as their counterpart sugar analogues. However, what makes iminosugars useful in medicinal chemistry is that their conformation is similar to their monosaccharide analogues. This structural simile is particularly true of the piperidine iminosugars, and thus these molecules bind to carbohydrate-processing enzymes, such as glucosidases, in a similar manner and with similar affinity as their counterparts.[54]

One such iminosugar is deoxynojirimycin (DNJ, **1**) (Figure 2.6). DNJ (**1**) is a 1-deoxy glucose mimic, which unlike the glucose mimic nojirimycin (**2**), is stable.[55] DNJ occurs naturally in mulberry plants, *Streptomyces* and *Bacillus*.[56]

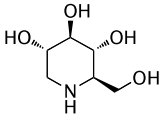

1

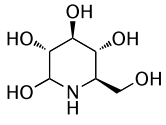

2

Figure 2.6 – 1-Deoxynojirimicin (DNJ, **1**) and nojirimycin (NJ, **2**).

DNJ has been shown to posses inhibitory activity against glucosidase enzymes,[57] and has thus received much attention to narrow its selectivity and increase its already good inhibitory activity (<1 μM, for inhibition of rat liver α-glucosidase I *in vitro*). The proposed model for α-glucosidase inhibition by DNJ (**1**) involves protonation of the endocyclic nitrogen atom forming an ammonium cation intermediate **1a** that is thought to mimic the oxocarbenium ion formed during both the acid and glucosidase catalysed hydrolysis of oligosaccharides (Figure 2.7-a).[58,59] A model superimposing *N*B-DNJ (**4**) with the terminal glucose cleaved by α-glucosidase I highlights the importance of the hydroxyls at C2, C3 and C4 for the activity of the iminosugar, when its endocyclic N is aligned with the endocyclic O of glucose for the inhibitor to mimic the oxocarbenium ion (Figure 2.7-b).[58]

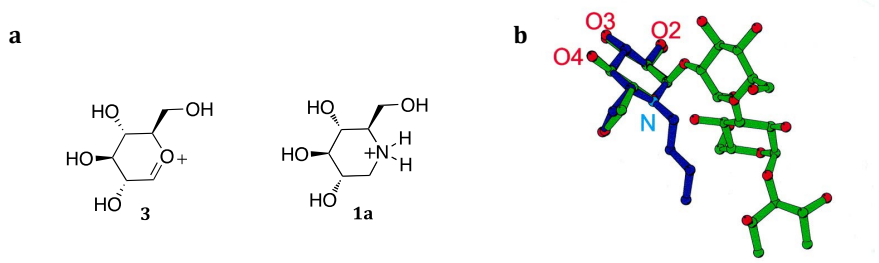

Figure 2.7 – Inhibition mechanism by DNJ (**1**). (a) Oxocarbenium ion intermediate (**3**) during the hydrolysis of the glycosidic bond catalysed by α-glucosidases and DNJ's ammonium cation (**1a**); (b) superposition of *N*B-DNJ (**9**) with the terminal glucose residue cleaved by α-glucosidase I. (b) Taken from Butters, T.D.; van der Broek L.A.G.M; Fleet, G.W.J.; *et.al*. *Tetrahedron: Asymmetry*. 2002. Vol. 11. pp. 113-24.

Several DNJ analogues have been prepared with the aim of improving specificity and cellular localisation.[43,60] One of the major modifications that has been used is *N*-alkylation (Figure 2.8). *N*-Butyldeoxynojirimycin (*N*B-DNJ, **4**) has been shown to be a better inhibitor of ER α-glucosidases than DNJ.[61,62] However its *in cellulo* activity is poor compared with its *in vitro* activity against purified α-glucosidase enzyme, requiring concentrations 2,000 fold greater than its *in vitro* K_i to obtain comparable levels of enzyme inhibition.[57,63] The current explanation for *N*B-DNJ's poor activity *in vitro* is either due to its low accessibility at the ER lumen or poor protonation (*N*B-DNJ's pK_a is 6.6 while the pH in the ER is 7.1). It has been shown that iminosugars cross the plasma membrane quickly and reach

equilibrium with the extracellular concentration within 30 min.[43] However, the concentration inside the ER is much lower than in the cytosol, based on α-glucosidase I inhibition measurements.[58]

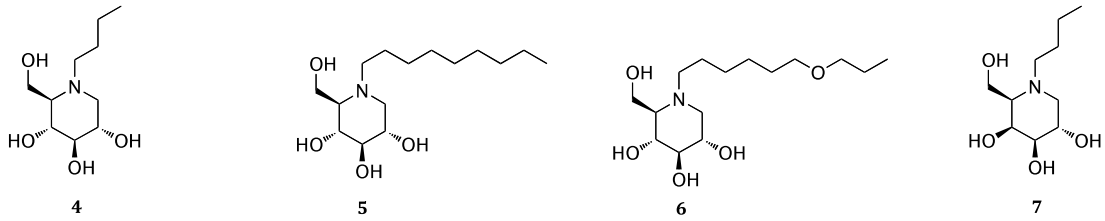

Figure 2.8 – DNJ derivatives: *N*-butyldeoxynojirimycin (*N*B-DNJ, **4**), *N*-nonyldeoxynojirimycin (*N*N-DNJ, **5**), *N*-7-oxadecyldeoxynojirimycin (**6**), and *N*-butyldeoxygalactonojirimycin (*N*B-DGJ,**7**).

2.6.1. Therapeutic applications

2.6.1.1. Substrate Reduction Therapy (SRT)

*N*B-DNJ (**4**) is an inhibitor of the enzymes α-glucosidase I and II, as well as the glucosyltransferase specific for ceramide formation. This last enzyme plays a key role in the biosynthesis of glycolipids. Thus, *N*B-DNJ (**4**) has found clinical application for the treatment of type I Gaucher's disease[64] and is presently marketed under the label of Zavesca. In this case, *N*B-DNJ (**4**) is thought to function *via* a process involving 'Substrate Reduction Therapy' (SRT). SRT is proposed to alleviate the cellular stress produced during the accumulation of the substrate of a deficient or defective enzyme. During Gaucher's disease treatment, *N*B-DNJ (**4**) blocks ceramide glucosyltransferase activity and thus prevents it from generating glucosylceramide, the substrate for the deficient enzyme in this disease.[65] *N*-Butyldeoxygalactonojirimycin (*N*B-DGJ, **7**) has also shown activity as a ceramide glucosyltransferase inhibitor and has a higher selectivity than *N*B-DNJ (**4**) because it exhibits reduced inhibition of α-glucosidases I and II.[66]

2.6.1.2. Antiviral

Iminosugars have also been studied for their antiviral capabilities.[2,67,68] α-Glucosidase inhibition has been shown to be a viable route for reducing the titre of HIV *in vitro,*[69,70] as confirmed by analysis of *N*-linked glycosylation of the HIV envelope glycoprotein gp120. It has been proposed that α-glucosidase inhibition changes the folding of the V1 and V2 loops of gp120, thus preventing the exposure of the peptide gp41 required for fusion with host cells.[2,1,71]

Unfortunately, *N*B-DNJ (**4**) was poorly tolerated in high doses by AIDS patients during clinical trials, and the drug concentration in plasma was insufficient for reduction of the viral titre.[72]

The antiviral effects of DNJ derivatives have also been studied against hepatitis viruses. For example, the use of *N*N-DNJ (**5**) against Woodchuck Hepatitis Virus (WHV) gave positive results showing a dose dependent decrease of secreted virus.[73] *N*B-DNJ (**4**) also showed antiviral effects against Bovine Viral Diarrhoea Virus (BVDV), the Hepatitis C model virus.[68] It is noteworthy to point out that this last study also identified a secondary mechanism for antiviral activity for long-chain alkylated iminosugars, possibly related to inhibition of a membrane protein channel leading to the increased formation of E2-E2 homodimers relative to E2-E1 heterodimers.[74] These BVDV envelope glycoproteins are known to interact with Calnexin to allow them to fold properly.[67,75]

2.6.1.3. Chaperone Mediated Therapy (CMT)

Another therapeutic mode of action of iminosugars has been termed 'Chaperone Mediated Therapy' (CMT), where the compound targets protein folding and trafficking pathways and modulates the activity of a lysosomal glycosidase.[76] CMT works on the premise that iminosugars bind with good affinities (10^{-6} M to 10^{-9} M) to the active sites of glycosidases and therefore may provide partial protection against misfolding or targeting for degradation, thus allowing more enzyme to reach the lysosome. In this case, a partial increase of enzyme activity by CMT may be sufficient to cross the critical threshold for enzyme activity to reach a non-pathological concentration of glycosphigolipids (GSL) in the lysosome.[77]

CMT with iminosugars has been shown to be an effective approach against Gaucher's β-glucosidase,[78] Fabry's α-glucosidases,[79-81] Tay'Sachs/Sandhoff's β-hexosaminidase,[82] and GM1 gangliosidosis.[83] CMT has also been applied to cystic fibrosis by improving the cell surface expression of functional cystic fibrosis transmembrane receptor (CFTR). In this case, *N*B-DNJ (**4**) prevents α-glucosidase hydrolysis of the CFTR glycans, thus preventing mutant delF508, the protein responsible for this disease, from binding CALX/CALR and eventually from entering ERAD. Given that the mutant protein still retains its cAMP

activated Cl^- channel activity, by-passing the ER quality control mechanism effectively increases the amount of CFTR that reaches the cell surface.[84]

2.7. Delivery Peptides

The process of delivering drugs to their target cells and to the specific organelle where they are required has been a long-standing challenge.[85,86] The cell membrane is a selectively permeable barrier, and so small molecules need to be generally lipophilic and small to cross this barrier.[87] Such limitations restrict the number and nature of possible compounds that can have an intracellular site of action, and have limited the general use of therapeutic methods that involve gene-targeting or protein/peptide-based approaches. Several methods have been developed to improve the intracellular delivery of drugs/small molecules that on their own do not meet the physiochemical requirements necessary for crossing the cell membrane. A few examples are viral vectors, liposomes, and membrane perturbation techniques.[85] However, these approaches all have their limitations and often have associated toxic effects, cause immunoreactivity or/and they have poor delivery yields. Cell penetrating peptides are a possible solution to the challenge of crossing the membrane.[87]

It has been known for some time that newly synthesised proteins are tagged with short peptide sequences that direct the tagged protein to a specific location within the cell.[88] This tagging has recently been applied to facilitate drug delivery to specific cellular organelles.[85] In this project, ER retaining peptide sequences are exploited because the enzymes targeted by the iminosugar focus of this study (DNJ, **1**) are located in the lumen of the ER.

2.7.1. Cell penetrating peptides (CPP)

The first CPP identified was the Tat peptide in 1988, an 86-amino acids-transcriptional activator coded by the HIV-1 genome, expressed upon HIV-1 infection of a host cell.[89] It was found that Tat could be taken up from the surrounding medium by HeLa cells *in vitro* and could activate its target, HIV LTR gene, in the nucleus. Later studies using mutagenesis identified a region between residues 48–60 as being responsible for its penetrating ability.[90] Since then, several other CPP have been identified, such as the Antennapedia transcription

factor or Penetratin (pAntp).[91] The analysis of the characteristics of these peptides has also led to the development of chimeric sequences such as the polyarginine peptides (mimicking Tat), Transportan (derived from Galanin-mastoparan) or MAP (an amphipathic α-helix).[92-94]

Polyarginine CPPs were derived from a study of the TAT peptide, which indicated that the positively charged arginine residues were crucial to its membrane penetrating properties.[95] It has also been determined that the guanidine moiety of Arg is the key to its translocational properties, because other positively charged amino acids such as lysine, ornithine or citrulline show no activity.[96] This was also confirmed by the generation of poly guanidyl peptoids which retain the cell penetrating activity of guanidine-containing peptides.[96] The MAP peptide is similarly derived from the peptide Transportan, both of these peptides form amphipathic α-helices, with one side presenting hydrophobic residues while the other presents hydrophilic ones. This conformation enables the peptides to interact and cross the plasma membrane.[97]

The method of internalisation of CPP has been a long-standing debate. Currently, it is generally accepted that each CPP has its own preferred method of entry (Figure 2.9). The majority of the evidence points to a major route of entry through endocytosis, with other approaches including direct translocation, the formation of inverted micelles, the formation of a transient β-barrel pore, and pinocytosis.[98,94,99]

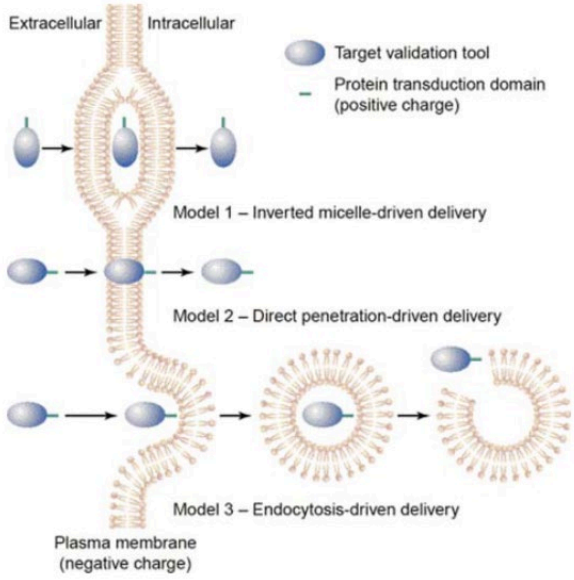

Figure 2.9 – Proposed methods for internalisation of CPPs.

Taken from Green, I., Christison, R., and Voyce C.,*Trends in Pharmacological Sciences*, 2003, Vol. 5 (24), pp.213-215.[94]

CPPs exhibit many benefits compared to other delivery methods. For example, unlike liposomes, CPPs have been successful in delivering cargoes to numerous cell types, including human Jurkat and HeLa cell lines.[101] They also exhibit low toxicity and it has been considered unlikely that conjugated CPPs would elicit an immune response, although this remains to be proven for each particular case.[87] There is also evidence of sustained presence and functionality of CPP-delivered protein cargoes.[102,103] And in contrast to the membrane rupturing techniques, such as electroporation or microinjection, there is no evidence of membrane perturbation caused by CPP-induced cell entry.[104,105]

It is known that CPPs have to resist degradation once internalised. Studies have shown that D-amino acid-containing peptides (so-called D-peptides) are more resistant to proteolysis than their L-amino acid analogues, however they often also lose their biological activity. An interesting study showed that pAntp prepared in reverse order using D-amino acids maintains the biological activity of the native CPP.[106]

Some examples of successful uses of CPPs include Tat delivery of β-galactosidase in a mouse model which even facilitated crossing of the blood brain barrier,[107] pAntp linked to a siRNA complementary to the reporter protein 'firefly luciferase[108] and VP22 used to deliver Gata4, a transcription factor into cardiac cells.[105] While most of the applications of CPPs have been with protein targets, some small molecules have also been coupled to CPPs to enhance their delivery.[106] One example is the coupling of cyclosporin A (CsA) with an arginine heptamer to facilitate drug delivery to epidermal cells *via* topical administration for the treatment of inflammatory skin disease.[109] At the last report, this conjugate had entered Phase II clinical trials under the trademark PsorBan.[110] Regardless of these successes, the primary focus still remains the delivery of oligonucleotides and proteins.

2.7.2. ER retaining peptides

Ground-breaking cell biology studies have established that newly synthesised proteins are tagged with short polypeptide sequences which then serve to direct

the protein to where they are required within the cell to complete their function,[88] whether that be a specific organelle or the cell membrane. ER retaining signals are a variant of these sequences, which allow proteins to be retained in the ER. One such sequence is the carboxy-terminal tetrapeptide sequence tag, KDEL.[111] A second consensus motif consists of two lysines located at positions 3 and either 4 or 5 from the cytoplasmic carboxyl terminus.[112]

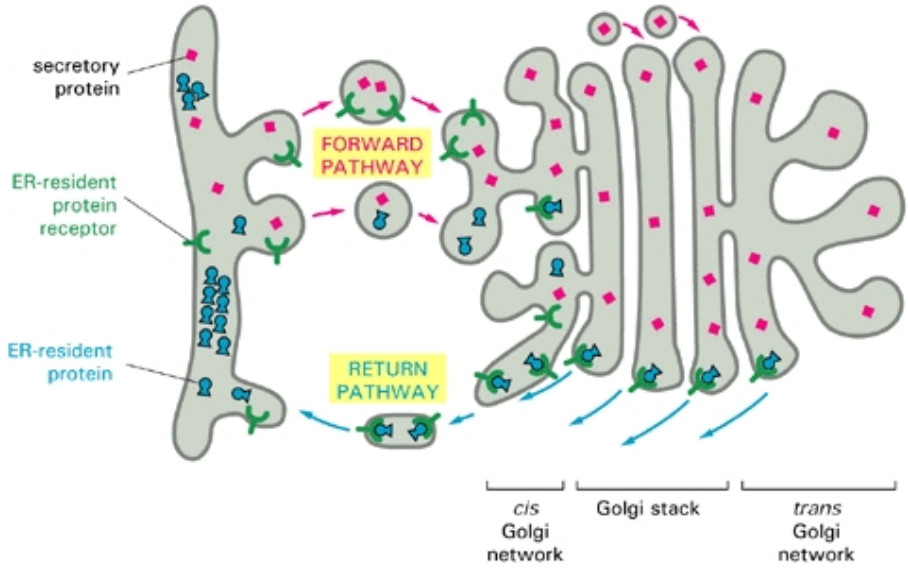

Figure 2.10 – Retrieval mechanism for soluble proteins residing in the ER.
Taken from Alberts, B., *et.al*. (1994) *Molecular Biology of the Cell*. New York: Garland Science, 3rd edition. [113]

Proteins containing the KDEL signal are soluble proteins that get retrieved form the Golgi complex to the ER lumen. The soluble proteins tend to exit the ER by bulk flow, and then get recognised by the KDEL receptor (ERD1 and ERD2)[114,115] in the ER-Golgi Intermediate Complex (ERGIC), which then activates a retrograde vesicular transport into the ER (Figure 2.10).[116]

Proteins containing the dilysine motif (such as KKAA) are often transmembrane proteins retrieved from post-ER compartments by cytosolic coat proteins (COPS) controlling retrograde vesicular transport to the ER. [117-118]

3. Results and Discussion

As described earlier, the primary aim of this project is to enhance the inhibitory activity of the α-glucosidase inhibitor DNJ (**1**) by improving its effective concentration at the ER. Two strategies were devised to achieve this objective, the first one involves the use of ER retaining peptide tags coupled to DNJ (**1**) to target the inhibitor to its place of action and maintain it there, thereby increasing its effective concentration and consequently its overall efficacy. KKAA and KDEL were selected as the tetrapeptide sequences to be used because they are among the most-studied ER retention signals.[111,112,117] The second strategy involved the use of CPPs coupled to DNJ in an attempt to help the inhibitor cross the cell membrane more efficiently and hence increase the intracellular concentration of DNJ (**1**), thereby also increasing its activity/administered drug ratio. MAP, R_7, TAT and Transportan were chosen as CPPs (Table 2.1), because they are representative of the major classes of CPPs, and have each been used with some success for delivery of protein cargoes. It is worth mentioning that while extensively studied as protein delivery/target peptides, none of these sequences have been studied for small molecule cargoes.

Table 2.1 – Peptide sequences of selected CPPs

Peptide	Sequence
MAP	Ala-Leu-Ala-Lys-Ala-Leu-Ala-Lys-Ala-Leu-Ala-Lys
R_7	Arg-Arg-Arg-Arg-Arg-Arg-Arg
TAT	Pro-Gly-Arg-Lys-Lys-Arg-Arg-Gln-Arg-Arg-Pro-Pro-Gln
TRANSPORTAN	Gly-Trp-Thr-Leu-Asn-Ser-Ala-Gly-Tyr-Leu-Leu-Gly-Lys-Ile-Asn-Leu-Lys-Ala-Leu-Ala-Ala-Leu-Ala-Lys-Lys-Ile-Leu

The initial challenge for this project was the synthesis of the specific DNJ peptide constructs. It was decided that the best strategy for the assembly of these constructs was an on-resin condensation between an *N*-alkylated carboxy DNJ moiety **8** with the amino-terminus of the desired peptide (Figure 2.11).

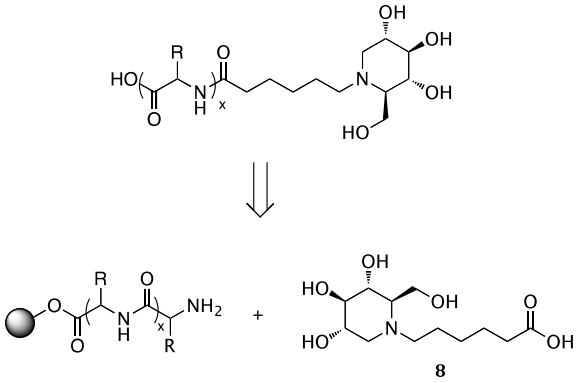

Figure 2.11 – Retrosynthetic scheme for the synthesis of DNJ-peptide constructs.

3.1. Synthesis of DNJ (**1**)

To be able to synthesise the DNJ-peptide constructs for biological testing in sufficient amounts, DNJ (**1**) needed to be synthesised in sufficient quantity to be first *N*-alkylated with an appropriate linker moiety, followed by coupling in excess of this *N*-alkylated DNJ derivative (**8**) to peptides on resin. Several total syntheses of DNJ have been reported,[119-122] however at the time when this study was initiated, none were suitable for large-scale, multigram, synthesis. After some consideration, it was decided to use the synthetic pathway developed by the Hollingsworth group, based on readily available reagents and a reported yield of 21% over 7 steps (Figure 2.12).[121] The synthesis starts from commercially-available D-mannono-1,4-lactone (**9**), which is easily transformed into 2,6-dibromo iditol (**11**) over two steps by bromination of the sugar with a solution of HBr in acetic acid to obtain compound **10** followed by reduction with $NaBH_4$. Regioselective acetonide formation to obtain ketal **12** (in 64% yield) with acetone and catalytic amounts of *p*-toluenesulfonic acid, was followed by selective protection of the primary hydroxyl group with *tert*-butyldimethylsilylchloride (1.1 equiv.) gave the monohydroxy TBS ether **13**. Regioselective aminolysis of the less-hindered primary alkylbromide gave the primary amine **14** in an 82% yield over two steps. The synthesis to this point followed with similar yields to the reported by the Hollingsworth group. However, the following step in the synthesis, a formal intramolecular nucleophilic substitution reaction between the primary amino group and the secondary alkyl bromide of **14** to yield the acetonide-protected DNJ **15** was frought with problems. Repeated attempts under different conditions of reaction

concentration and temperature, all failed to yield a single major product as reported, and the purification of both the protected and deprotected DNJ was neither trivial nor high yielding. The isolated yield for **15** could not be obtained in anything approximating the reported yield of 78%, in fact, only close to 10% yield was obtained from this reaction after multiple purification steps. NMR analysis of the crude reaction mixture indicated the formation of several side products, in particular the epoxide formed from TBS deprotection and Br elimination was observed as one of the main products. The desired compound **15** was observed as one of the minor reaction products. It was successfully isolated from the reaction mixture after multiple silica column chromatography purifications and subjected to acetonide deprotection using aqueous HCl in methanol to obtain DNJ (**1**). Such a low overall yield of DNJ (**1**) (1.1% for 7 steps) made the projected cost of the synthesis of DNJ at the multigram amounts required for this project, untenable.

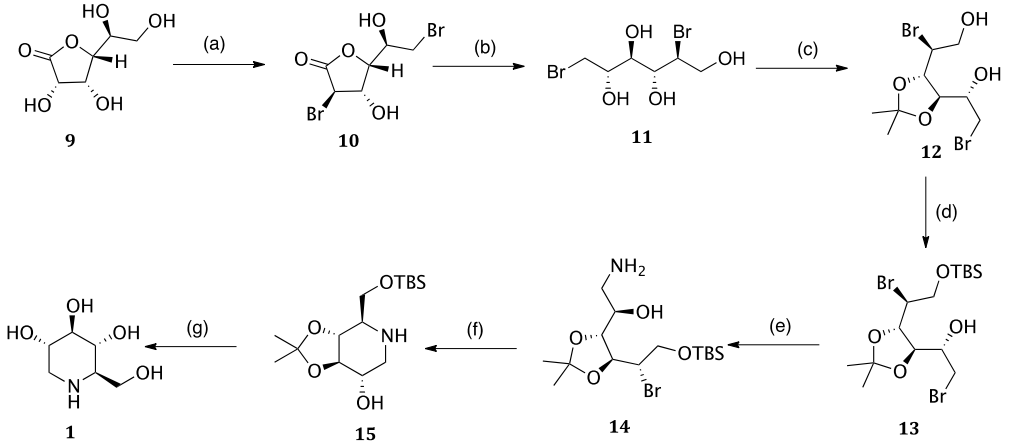

Figure 2.12 – Synthetic approach to DNJ (**1**) by Song, X, *et.al*.[121] *Reagents and conditions*: (a) HBr/AcOH; (b) $NaBH_4$; (c) Acetone/p-TsOH (72%); (d) TBS-Cl: (e) aq. NH_3 (81% over two steps); (f) NaOAc/$MeNO_2$ (68%); (g) HCl/MeOH (96%).

Fortunately, during the time Hollingworth's synthesis was being attempted, Fleet and co-workers published a synthesis of DNJ (**1**) optimised for large scale (Figure 2.13).[119] This synthesis was optimised for large-scale reactions with crystallisation as the purification method for most of the steps. Fleet's synthesis starts from D-glucoronolactone (**16**), which after protection to form the acetonide **17** in a 93% yield, has the stereochemistry of the C-5 alcohol inverted in two steps, *via* formation of an intermediary triflate ester, which is subjected to

nucleophilic displacement with the sodium salt of trifluoroacetic acid. The resultant trifluoroacetate ester is then saponified under aqueous work-up conditions to give the C-5 epimeric alcohol **18** in a 91% yield. The stereochemistry at C-5 is then returned to its original configuration *via* the displacement of an activated triflate ester with sodium azide in DMF to give the requisite azidolactone **19** (66% yield). These first steps were characterised by the product being isolated in high yield (93%, 91%, and 66% respectivey) in analytical purity by a fairly routine recrystallisation procedure.

The lactone **19** is then reduced in a two-step process, with the first step involving DIBAL-H reduction to the difuranose **20** (72% yield), followed by $NaBH_4$ reduction to diol **21** (93% yield). This two-step reduction process is a common procedure for effective reduction of lactones that have a propensity to be unstable to base. Acetonide deprotection of **21** under acidic conditions furnishes tetraol **22**. This compound is subjected to azide reduction under catalytic hydrogenation conditions, which leads to a spontaneous rearrangement of the intermediary aminofuranol into the thermodynamically more stable piperidine, DNJ (**1**). It is important to mention that while the published synthesis involves hydrogenation at 50 psi, the reaction was completed at 1 atm over 2 days with continuous H_2 flushing. Interestingly, after isolation of the acetonide protected azidodiol **22**, the subsequent reactions do not require further purification and DNJ is isolated in analytically pure form by recrystallisation from methanol.

DNJ (**1**) was synthesised through this route with an overall yield of 37% (7 reactions, published 31.9% overall yield) in sufficient multigram quantities (~5 g) to permit the synthesis of all the peptide constructs proposed in this study. The ^1H NMR spectrum of the obtained DNJ (**1**) is shown in Figure 2.14.

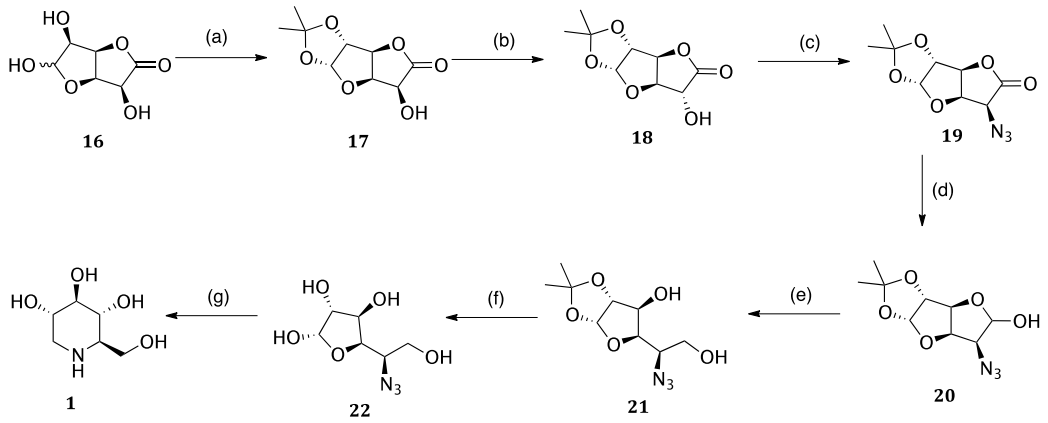

Figure 2.13 – Synthetic route for DNJ (**1**) by Best, D., *et.al*.[119] *Reagents and conditions*: (a) acetone/H_2SO_4 (79%); (b) triflic anhydride, sodium trifluoroacetate (73%); (c) triflic anhydride, NaN_3 (87%); (d) DIBAL-H, potassium sodium tartrate (92%); (e) $NaBH_4$ (96%); (f) Dowex 50Wx8 H^+ (98%); (g) Pd/C, H_2 (72%).

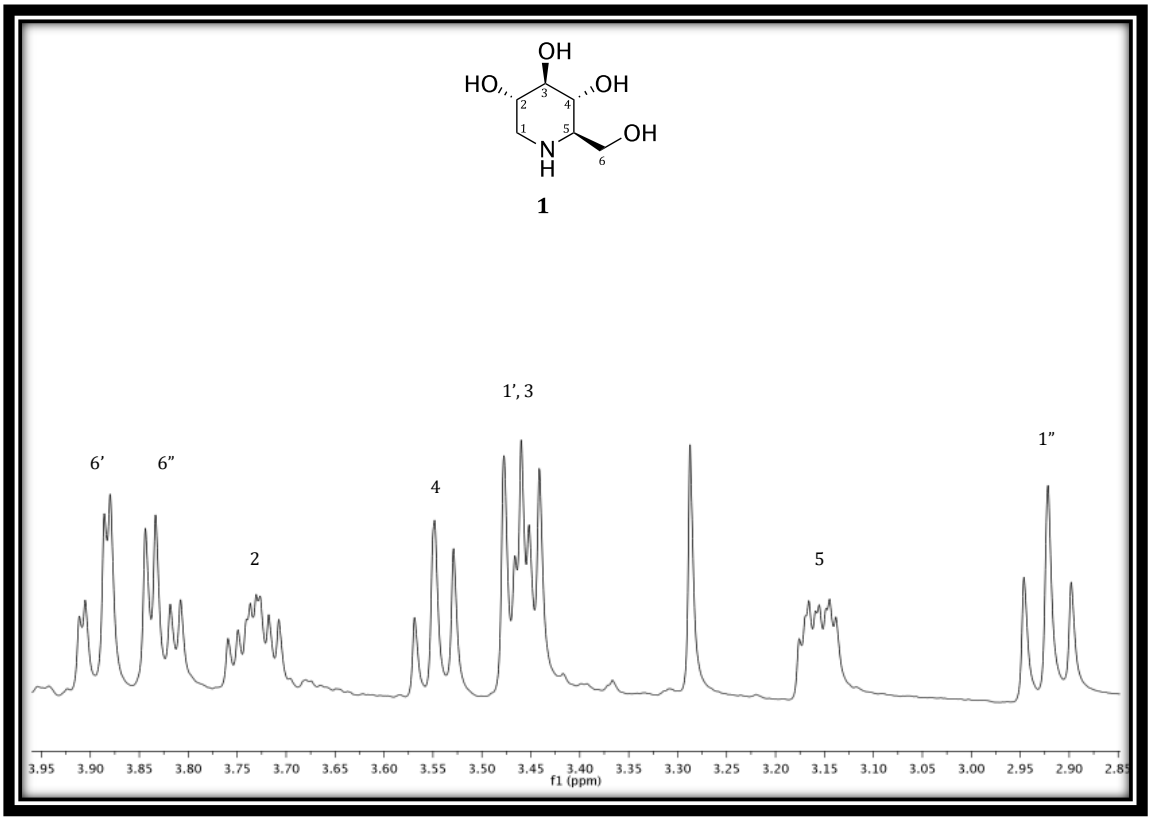

Figure 2.14 –^{1}H NMR spectrum (500 MHz, D_2O/TFA) of DNJ (**1**).

3.2. Synthesis of DNJ constructs

After the synthesis of DNJ (**1**) was completed, the next step was the preparation of the key intermediate *N*-(5-carboxypentyl)-DNJ (**8**), which, as described above, was to be used for coupling with all the peptide amines (Figure 2.11). Traditionally, alkylation of DNJ (**1**) is performed using reductive amination with

excess aldehyde with a fully deprotected iminosugar (Figure 2.15).[123] The main disadvantages with such a synthesis is the presence of the free alcohols, which makes purification by traditional silica gel chromatography problematic on large scale, and in the absence of a UV chromophore, purification by preparative-scale HPLC is also inefficient.

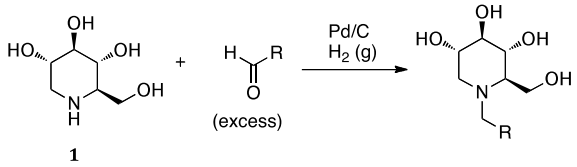

Figure 2.15 – Reductive amination of DNJ in the presence of excess aldehyde.

The choice of a six-carbon linker was guided by both the known improvement of α-glucosidase inhibition of *N*-alkylated DNJ derivatives with increasing alkyl chain length up to 9 carbons,[62,123] and the ready availability of the 6-carbon lactone **23** needed. Thus, methyl-6-oxohexanoate (**25**) was viewed as the aldehyde intermediate for the reductive amination.

There are many plausible synthetic routes to **25**, but the one traditionally used in the Butters' laboratory starts from acid catalysed ring opening of ε-caprolactone (**23**) in methanol to generate the methyl-6-hydroxyhexanoate **24** (Figure 2.16). The primary alcohol **24** is then oxidised to the corresponding aldehyde with SO_3 pyridine complex.[124] A few problems are typical for this short synthesis. First, the aldehyde **25** hydrated readily to the corresponding acetal (as observed by NMR), rendering it inactive in the following reductive amination reaction. In addition, the crude reaction mixture obtained after SO_3 oxidation of alcohol **24** was a complex mixture that could only be purified by an extended silica gel chromatography process. During this purification, aldehyde **25** appeared to degrade, resulting in poor yields (5-10%). Another problem was that after the reductive amination reaction was completed, the removal of aldehyde by silica gel chromatography was problematic because it was used in such excess, lastly product **26** contained several free hydroxyls requiring harsh conditions for elution.

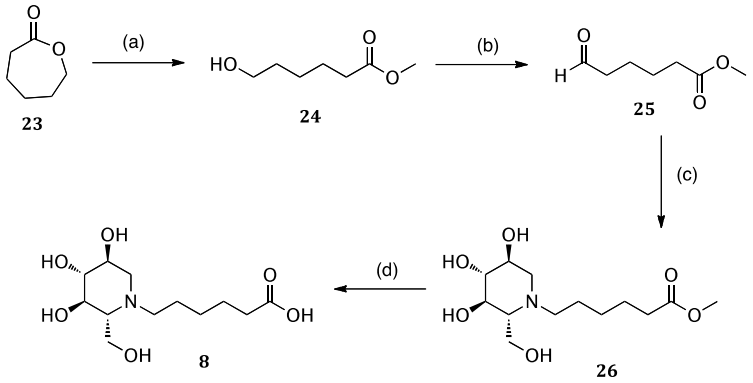

Figure 2.16 – Available synthetic scheme of *N*-(5-carboxypentyl)-DNJ **(5)** (unpublished). *Reagents and conditions*: (a) H_2SO_4, MeOH (95%); (b) SO_3·pyr (44%); (c) DNJ (**1**), Pd/C, H_2; (d) NaOH.

To circumvent these problems, it was decided to change the synthetic approach for the aldehyde-linker moiety (Figure 2.17). The new synthetic method commenced with a base-catalysed ring opening of ε-caprolactone (**23**) in aqueous NaOH to obtain, after neutralisation with an acidic resin, hydroxyacid **27**.

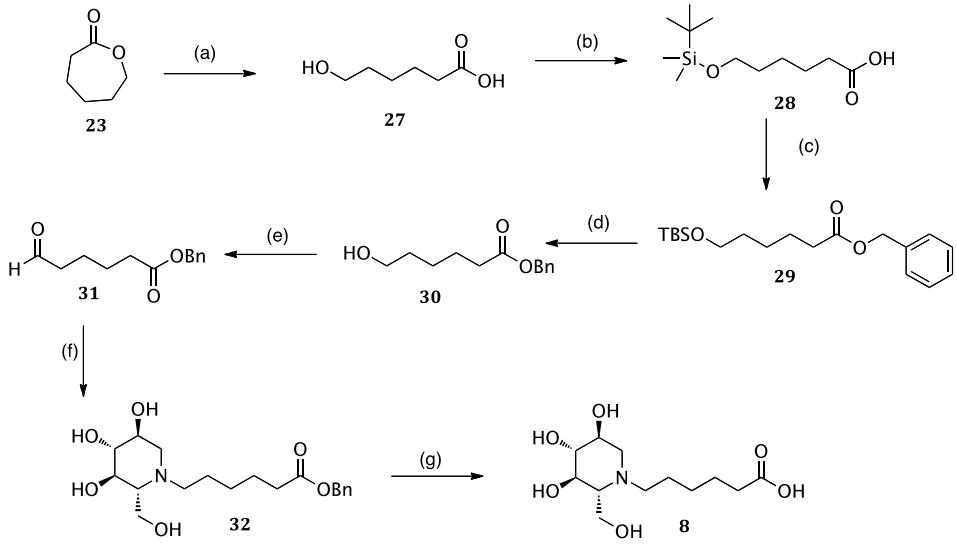

Figure 2.17 – Proposed synthetic scheme for *N*-(5-carboxypentyl)-DNJ (**8**). *Reagents and conditions*: (a) i. NaOH, ii. Dowex 50Wx8 H^+ (84%); b) TBS-Cl (quant.); (c) K_2CO_3, benzyl bromide (70%); (d) TBAF (89%); (e) Dess-Martin periodinane (45%); (f) DNJ (**1**), $NaCNBH_3$ on solid support (57%); (g) Pd/C, H_2 (quant.).

The alcohol was then treated with *tert*-butyldimethylsilyl chloride and imidazole in DMF to afford TBS ether **28** in quantitative yield.[125] The terminal carboxylate was then treated with BnBr and K_2CO_3 in anhydrous acetone, to give ester **29** in good yield (70%) after silica gel chromatography. Desilylation of **29** was

achieved smoothly using tetra *n*-butylammonium fluoride (TBAF). The resultant primary alcohol **30** was then oxidised using Dess-Martin periodinane to give the key aldehyde ester **31**.[126] The crude reaction mixture was readily purified by a flash silica gel column chromatography, reducing aldehyde loss on the column.

Reductive amination between DNJ (**1**) and the benzyl ester-protected **31** was performed using $NaCNBH_3$ on solid support, with activated molecular sieves in MeOH to prevent, in part, hydration of the aldehyde **31** during the reaction. These heterogeneous conditions, using the reducing agent on a macroporous resin, have been chosen to allow for facile separation of excess reagents by filtration. This approach reduced significantly the loss of aldehyde **31** during reductive amination reaction with DNJ (**1**).

The benzyl-protecting group that was built into this synthesis was more useful than the original methyl group used in the original approach because it is UV active and allows both, purification by preparative scale HPLC, and optimisation of the critical reductive amination reaction, which had been difficult to monitor before.

The optimisation of the reductive amination reaction between **1** and **31** was focused primarily on the determination of the best solvent mixture for the reaction. Typically, the *N*-alkylation of DNJ (**1**) is performed using the required aldehyde as the solvent for the reaction. In this case, it was settled to use 3 equivalents of aldehyde **31**, allowing for degradation during the reaction while also taking a green chemistry approach by using as low amount of **31** as possible. Additional components in all reactions were activated molecular sieves and in the case where acetic acid was included, this was standardised as 0.1% v/v. All reactions were monitored by HPLC at 1, 5 and 20 h (at λ260 nm) (Figure 2.18 and Table 2.2).

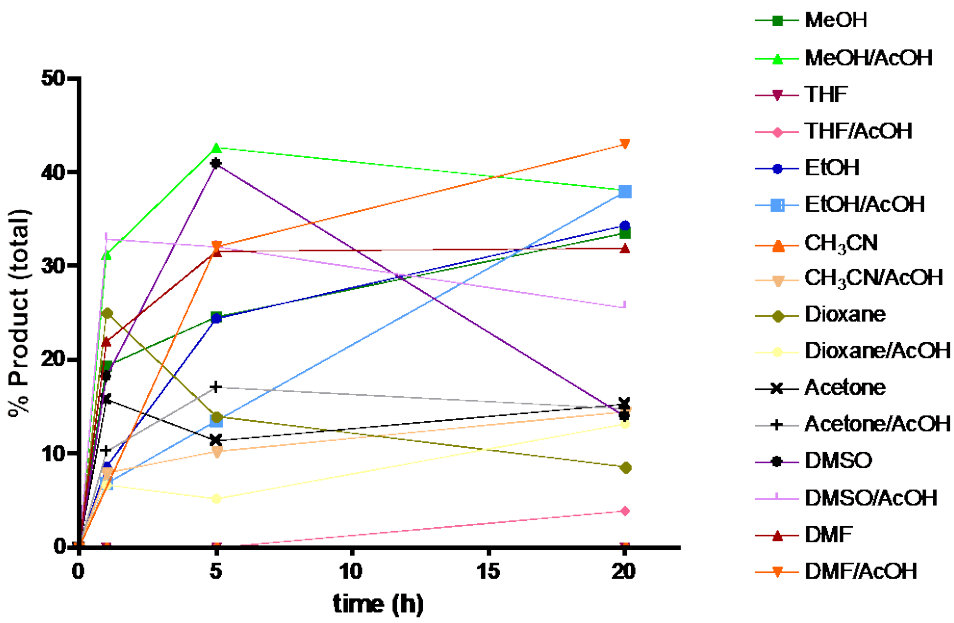

Figure 2.18 – Effect of solvent on the reductive amination of DNJ (**1**) by aldehyde **31** in different solvent systems. Product **32** formation is reported as the % of the total peak area (at λ260 nm, including starting material and other unknown peaks). If solvent was visible, its peak area was substracted from the total peak area.

The most clear observation from these direct reductive amination studies is that inclusion of acetic acid into the solvent improves the formation of *N*-alkylated product **32** regardless of solvent (Figure 2.18 and Table 2.2). Based on the well-established mechanism of the reductive amination reaction,[127] which proceeds *via* initial iminium ion formation, involving a specific catalysed dehydration of a carbinolamine intermediate, it is to be expected that product formation would be enhanced in the presence of acetic acid. That product **32** is observed, albeit in lower amounts, in the absence of AcOH is again in-line with the known reactivity of aldehydes in the reductive amination reaction.[127]

What is perhaps most surprising is the very low amount of product formed in the polar aprotic solvents THF and CH_3CN, in the presence of AcOH. These solvents are routinely used for reductive amination reactions and with poor solubility of both **1** and **31** not being the problem, it was surprising that **32** was not produced in higher yields. The poor yield is especially surprising considering the good formation of **32** in the other polar aprotic solvent, such as DMF and DMSO.

Table 2.2 – Optimisation of the reductive amination between DNJ (**1**) and aldehyde **31** in different solvent systems.

Solvent[a]	Product (32) formation[b]		
	1 h	5 h	20 h
Methanol	19.4	24.4	33.6
Methanol/Acetic acid	31.3	42.5	38.0
THF	0	0	0
THF/Acetic acid	0	0	3.9
Ethanol	8.6	24.3	34.3
Ethanol/Acetic acid	6.7	13.5	17.9
Acetonitrile	0	0	0
Acetonitrile/Acetic acid	7.9	10.2	14.5
Dioxane	25.0	14.0	8.5
Dioxane/Acetic acid	6.7	5.1	13.2
Acetone	15.7	11.3	15.3
Acetone/Acetic acid	10.2	17.0	14.8
DMSO	18.2	40.8	13.9
DMSO/Acetic acid	32.9	32.1	25.5
DMF	22.0	31.5	31.9
DMF/Acetic acid	nd[c]	32.0	42.9

[a]Standard experimental conditions used for this comparison were amine **1** (30 µmol) and aldehyde **31** (90 µmol) in a total reaction volume of 1.5 mL, with activated molecular sieves (3 mg), $NaCNBH_3$ on solid support (111 µmol) in the presence or absence of glacial acetic acid (0.1% v/v). The reaction mixture was shaken in a sealed glass vial at RT for the designated time period, at which time an aliquot (50 µL) was removed, passed through a syringe filter (0.2 µm) and evaporated to dryness under a stream of argon. The residue was then reconstituted in HPLC mobile phase and injected onto the HPLC system. [b]Data is reported as the % of the total peak area (at λ260 nm), and includes starting material and other unknown peaks. If solvent was visible, its peak area was substrated from the total peak area. [c]Not detected.

Furthermore, the polar protic solvents methanol and ethanol generated the higher yields, both in the presence and absence of AcOH. The use of MeOH and EtOH for such reactions would seem contraindicated because of the competing diacetal formation between the solvent and aldehyde. However, either acetal formation does not occur in the time frame of this study, or it occurs at a much lower rate than imine formation, because high levels of conversion to product are observed in these solvents.

Comparison of the solvent systems reveals that the mixture of DMF/AcOH produces comparable results, in terms of product yield, to MeOH/AcOH over 20 h, the lower boiling point of MeOH and the shorter reaction time with MeOH/AcOH led us to select the MeOH/AcOH mixture as the best solvent system for the reductive amination reaction. This reaction proved to be scalable, and on the mmol scale lead to the isolation of **32** in 57% yield after semi-preparative scale HPLC purification.

Catalytic hydrogenation (Pd/C, H_2, 1 atm) of **32** proceeded smoothly at RT, and the desired *N*-(5-carboxypentyl)-DNJ (**8**) was isolated in quantitative yield after filtration. Therefore, although this new synthetic route to **8** is more involved that the original route, the overall yield and ease of purification of the final product, as can be seen by the ^{1}H NMR spectrum of *N*-(5-carboxypentyl)-DNJ (**8**) recorded after just filtration of the catalyst following hydrogenation (Figure 2.19), makes the new route a much more useful system.

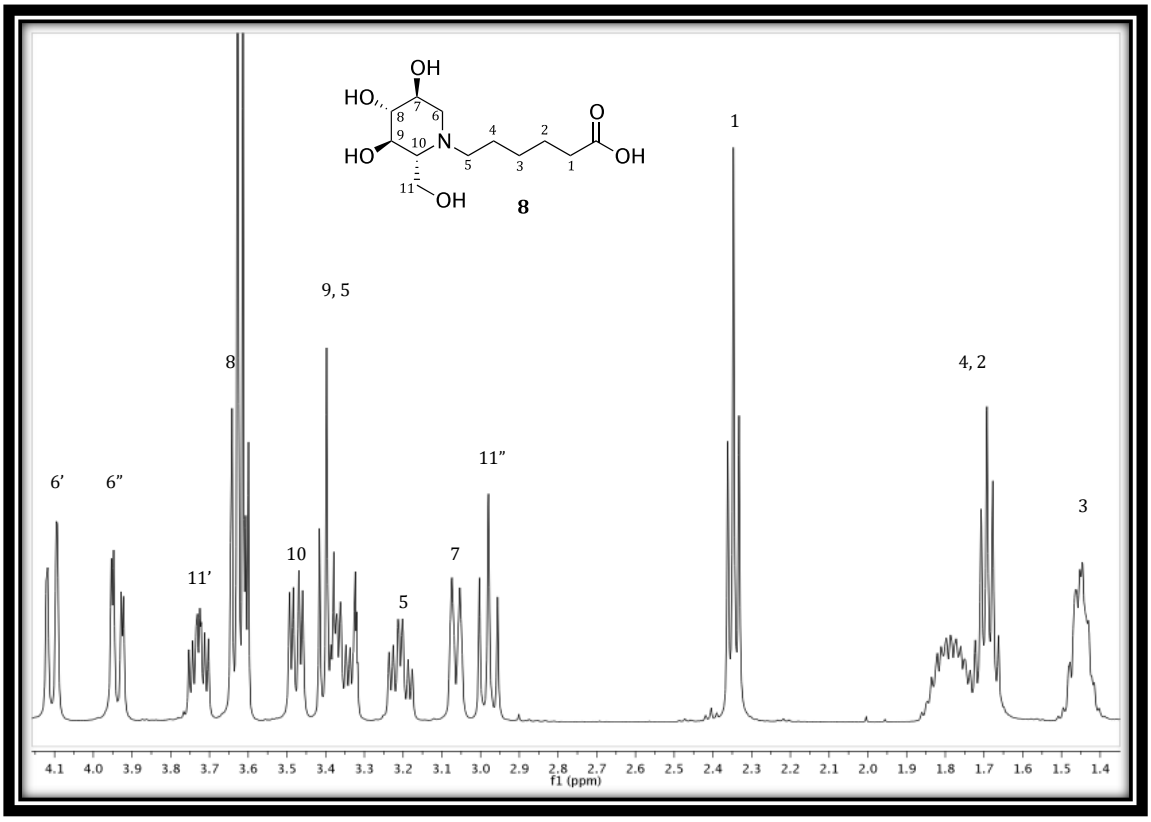

Figure 2.19 –^{1}H NMR spectrum (500 MHz, MeOD-d_4) of *N*-(5-carboxypentyl)-DNJ (**8**) prepared by the newly developed route.

Once the DNJ moiety with the free acid (**8**) was available, the next step was its coupling to the corresponding peptide sequences on resin. All peptides were

synthesised by traditional fluorenylmethyloxycarbonyl (Fmoc) solid phase peptide synthesis (SPPS).[128] On resin synthesis involves cycles of deprotection of the Fmoc-protected amine terminus of the first loaded amino acid, followed by coupling with the next Fmoc-protected amino acid's free acid (Figure 2.20). Each coupling involved the use of diisopropyl carbodiimide (DIC) as coupling reagent and hydroxybenzotriazole (HOBt) for ester activation of the added Fmoc-protected amino acid to minimise racemisation.[129]

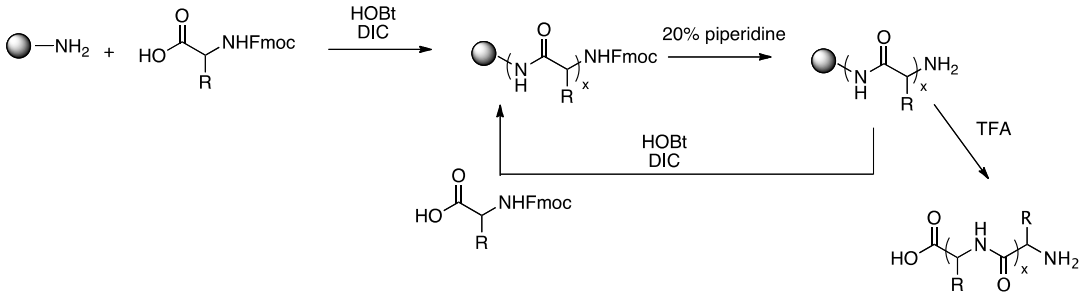

Figure 2.20 – General scheme for Fmoc-SPPS

KKAA, TAT, Transportan, and MAP peptides were synthesised directly onto commercially available Fmoc-Ala-Wang resin. However, KDEL and R_7 peptides required the preparation of a resin with Leu or Arg as the initial amino acid respectively. They were prepared by use of a Wang-like resin (**35**) formed by the addition of a 3-hydroxymethylphenylacetic acid (HMPA, **34**) linker to a commercially-available low-crosslinked aminomethyl poly(styrene) (AMS) resin (**33**). The first amino acid was loaded onto the prepared resin **35** *via* a 4-hydroxybenzyl ester bond formation as shown in Figure 2.21.

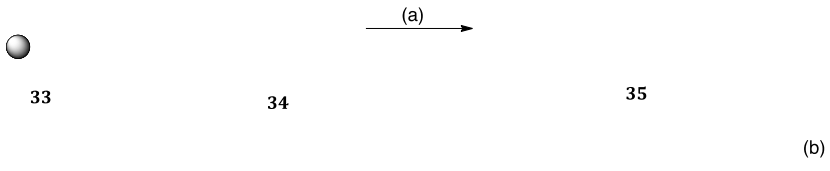

Figure 2.21 – General scheme for the loading of the first amino acid to a Wang-like resin **35** prepared on an AMS resin (**33**) with a HMPA linker (**34**) for Fmoc SPPS. (a) **34** (5 equiv.), HOBt (5 equiv.), DIC (5 equiv.), (b) DMAP (1 equiv.), DIC (1 equiv.).

The synthesis of these peptides was tested by HPLC and MS analysis of the crude cleavage mixture after treatment of a small resin sample with TFA. The correct mass, corresponding to the KKAA, KDEL, TAT, MAP and R_7 peptides was observed. However, MS analysis of the Transportan cleavage mixture revealed that only fragments of the required peptide were present. In addition, while some R_7 peptide was present in the cleavage mixture, HPLC analysis showed that the overall yield of the desired peptide was very low. The synthesis of both peptides, Transportan and R_7, required further optimisation since Transportan's length makes its synthesis non-trivial, and the synthesis of poly-arginine peptides is known to suffer from side-reactions. Ultimately, due to these reasons, both peptides were abandoned for this study and only TAT and MAP were used as representative CPPs.

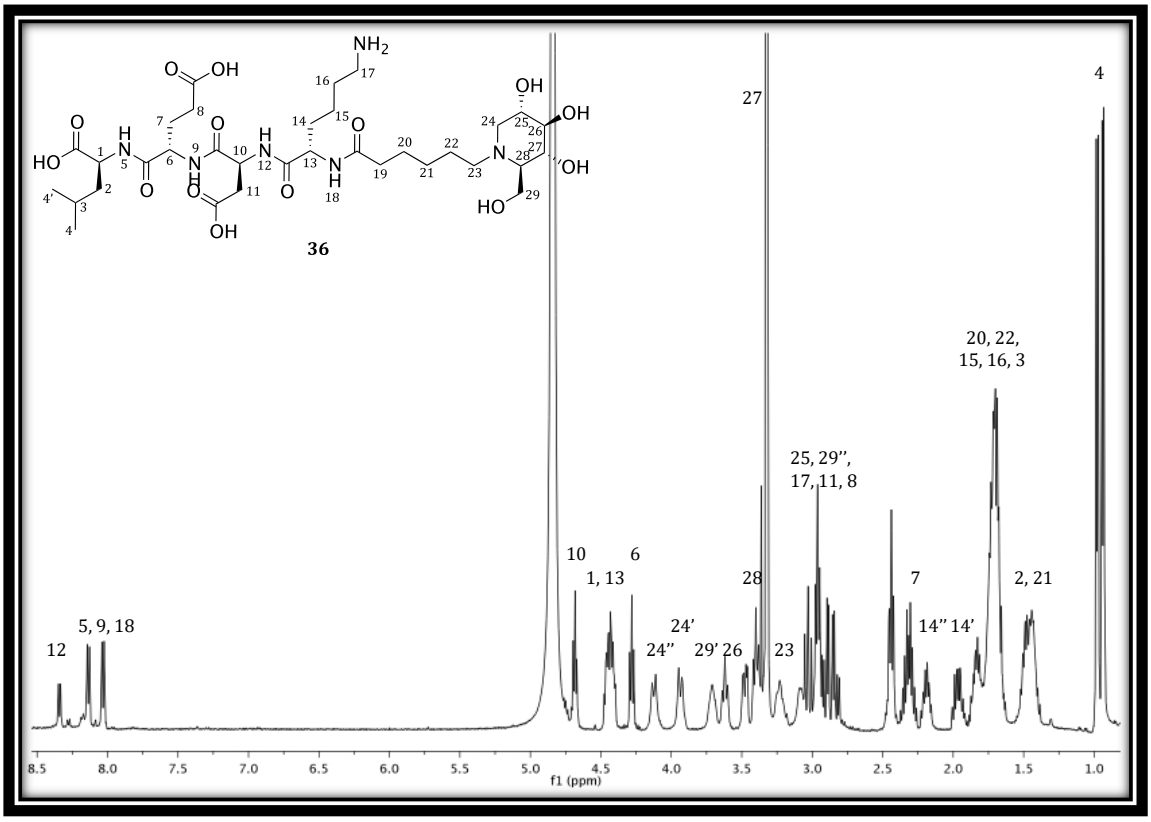

Figure 2.22 –^{1}H NMR spectrum (500 MHz, MeOD-d_4) from a DNJ-peptide contruct: DNJ-KDEL (**36**).

Once the peptides were synthesised, the DNJ linker **8** was coupled to the free amine of the peptides under the same conditions used for amino acid couplings.

Cleavage with a TFA/TIS/H_2O cocktail (97/2/1% v/v/v) followed by cold diethylether precipitation and purification by semi-preparative scale HPLC led to the desired peptide constructs DNJ-KKAA (**37**), DNJ-KDEL (**36**), DNJ-TAT (**38**) and DNJ-MAP (**39**). Figure 2.22 shows a representative ^{1}H NMR spectrum of the obtained DNJ-KDEL (**36**) in MeOD-d_4.

3.3. ER-retaining peptide DNJ constructs

3.3.1. *In vitro* inhibition

Having completed the synthesis of compounds **36**-**39**, it was necessary to isolate α-glucosidases I and II to determine the *in vitro* inhibitory activity of the compounds before testing them in cells. α-Glucosidase II is available in the Butters' laboratory from a previous isolation done by Dr. Butters (Glycobiology Institute, Oxford). α-Glucosidase I was isolated from rat livers as a Lubrol extract using an affinity gel prepared using *N*-(5-carboxypentyl)-DNJ (**8**) synthesised as described above. In a standard activity assay,[81] the purified α-glucosidase I hydrolysed $Glc_3Man_7GlcNAc_1$ substrate [labelled with 2-Anthranilic acid (2-AA) – see section on FOS analysis] with an activity of 0.27 pmol/min/mL (Figure 2.23).

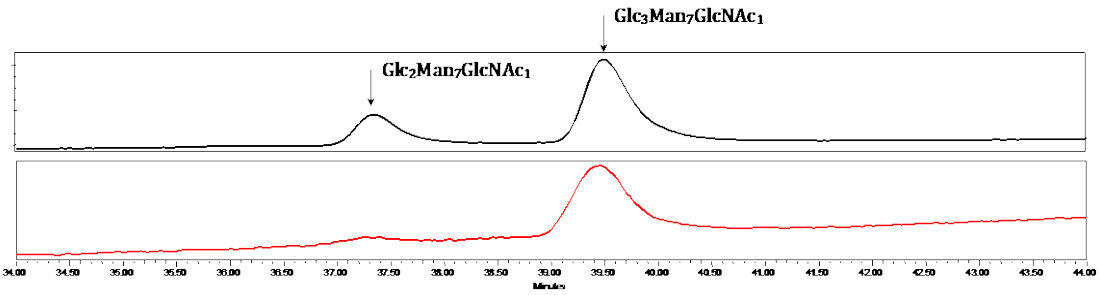

Figure 2.23 – NP-HPLC analysis of enzyme hydrolysis of $Glc_3Man_7GlcNAc_1$-2AA by purified α-glucosidase I, t= 2 h, in the presence (⊕) or absence (⊖) of 100 μM DNJ-KKAA (**37**).

An *in vitro* study (Figure 2.24) of α-glucosidase I and II hydrolysis inhibition with 2-AA labelled $Glc_3Man_7GlcNAc_1$ and $Glc_1Man_7GlcNAc_1$ as substrates respectively, after incubation with 0.1, 1, 5, 20, 50 and 100 μM DNJ-ER retaining peptide (DNJ-KKAA, **37** or DNJ-KDEL, **36**) allowed the assignment of the IC_{50} values summarised in Table 2.3, compared to the well studied *N*B-DNJ (**4**) and the precursor *N*-(5-carboxypentyl)-DNJ (**8**).

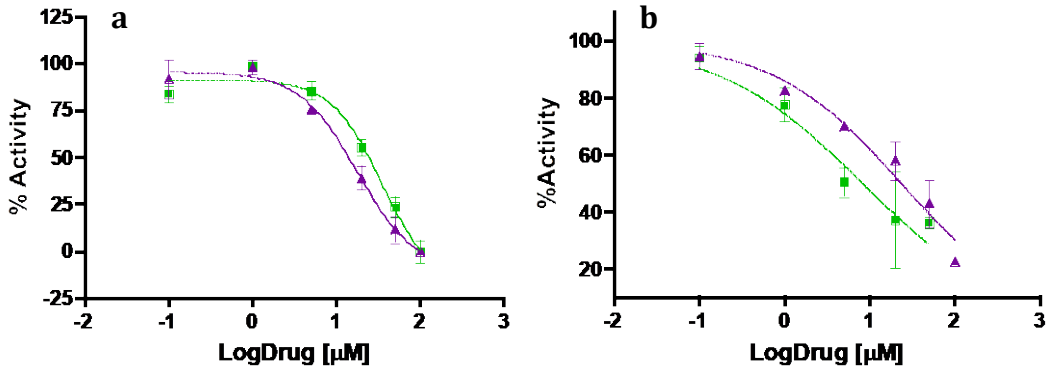

Figure 2.24 - *In vitro* assay for (a) α-glucosidase I and (b) α-glucosidase II inhibition by the DNJ-ER retaining signal constructs DNJ-KKAA (**37**, ⑤) and DNJ-KDEL(**36**, ⑩). Data is derived from from peak areas (NP-HPLC) and is reported as mean activity by comparison to a control in the absence of inhibitor. Data is reported as % ±SEM of at least triplicate measurements and fitted with a sigmodial curve (contrains: low=0, high=100).

Table 2.3 – Obtained IC_{50} values for rat α-glucosidase I and II inhibition.

Enzyme Substrate	α-Glucosidase I $Glc_3Man_7GlcNAc_1$	α-Glucosidase II $Glc_1Man_7GlcNAc_1$
DNJ-KKAA (37)	34.6 ± 1.5 μM	8.2 ± 1.4 μM
DNJ-KDEL (36)	17.5 ± 1.3 μM	23.5 ± 1.2μM
***N*B-DNJ (4)**	2.3 ± 1.1 μM	2.1 ± 1.2 μM
***N*-(5-carboxypentyl)-DNJ (8)**	23.9 ± 1.2 μM	15.6 ± 1.1 μM

While both peptide constructs (**36** and **37**) have higher IC_{50} than *N*B-DNJ (**4**), they both still possess inhibitory activity in the μM range. The inclusion of the ER peptide into the construct did not increase considerably the IC_{50} values relative to the precursor *N*-(5-carboxypentyl)-DNJ (**8**). Interestingly, the IC_{50} values for DNJ-KDEL (**36**) were comparable against both α-Glucosidase I and II, however the IC_{50} values of DNJ-KKAA (**37**) decreased 5-fold from α-Glucosidase I to α-Glucosidase II. In fact, the IC_{50} value of DNJ-KKAA (**37**) is comparable to *N*B-DNJ (**4**). Without more studies, it is impossible to define the nature of this isozyme specificity. Nevertheless, considering that both peptides are of similar length, their differences in IC_{50}s might point to the relative importance of the small hydrophobic amino acid Ala, instead of the acidic Glu in the P3 locus distal to the DNJ moiety as a possible cause for this difference. It is known that for up to 9

methylenes, the hydrocarbon chain length correlates with an increase in inhibitory activity.[60] Therefore, it is possible that the first two Ala residues in the peptide **37** are acting in the same manner as the alkyl chain by anchoring the DNJ moiety in the active site by hydrophobic interactions.

3.3.2. FOS analysis of treated cells

Prior to cell-based studies to assess cellular glucosidase inhibition, an assessment of the cytotoxicity of these constructs was completed. An MTS proliferation assay was performed in CHO-K1 cells using **36** and **37** (Figure 2.25). As desired, this study showed no cytotoxicity after 1 and 3-day incubations with either **36** or **37** for up to 500 μM concentration.

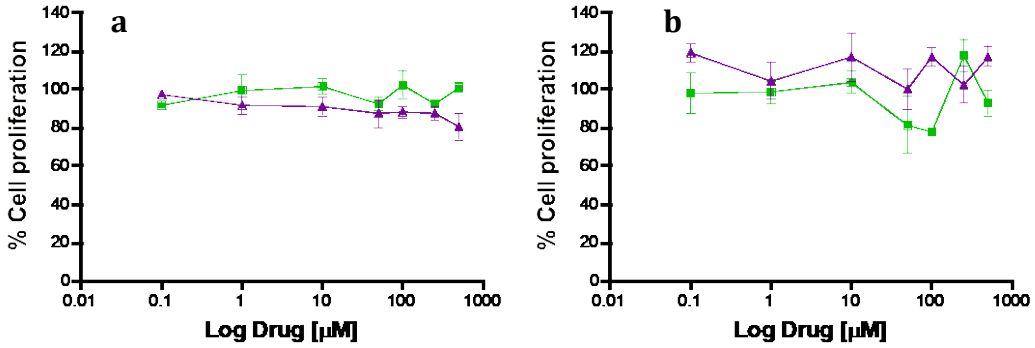

Figure 2.25 - Cell proliferation assay for DNJ-ER retaining signal constructs (⑤ DNJ-KKAA (**37**), ⑩ DNJ-KDEL (**36**)) in CHO-K1 cells, after (a) 1-day and (b) 3-day treatments. Determined by MTS proliferation assay and reported as percentage of DMSO-treated cells.

After determining that these ER-retention DNJ constructs were not cytotoxic, CHO-K1 cells were treated with them at varying concentrations over 24 h. Cell lysates were analysed for cytosolic free oligosaccharides derived from *N*-glycosylated glycoproteins following ERAD (see Figure 2.5) with the 2-AA labelling protocol developed by the Butters' group.[42] The appearance of mono and triglucosylated species followed by HPLC is correlated with the inhibition of α-glucosidases I and II in the ER lumen (Figure 2.26). Figure 2.27 tracks the appearance of $Glc_1Man_5GlcNAc_1$, $Glc_1Man_4GlcNAc_1$, $Glc_3Man_5GlcNAc_1$ and $Glc_3Man_7GlcNAc_1$, normalised to the amount of $Man_3GlcNAc_1$ in each sample. $Man_3GlcNAc_1$ is a lysosomal degradation product that remains unaffected by

treatment with α-glucosidase inhibitors, and thus is a good species to use as an internal standard to allow comparison between different assays.

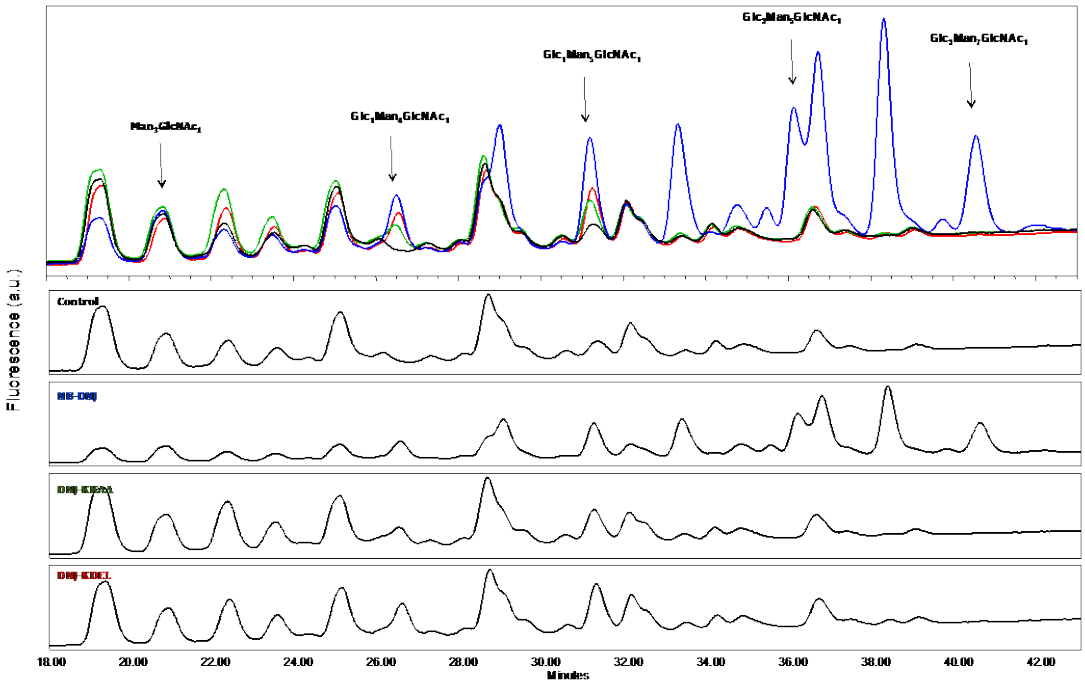

Figure 2.26 – NP-HPLC traces of FOS analysis for CHO-K1 cells in the presence or absence of 500 μM ③ *N*B-DNJ (**4**), ③ DNJ-KKAA (**37**) and ③ DNJ-KDEL (**36**) for 24 h. FOS used for analysis are indicated.

As can be observed in Figure 2.27, *N*B-DNJ (**4**) at low concentrations (100 μM) inhibits mostly α-glucosidase II, generating a majority of monoglucosylated species. As the concentration of inhibitor increases, triglucosylated species appear, indicating inhibition of α-glucosidase I. At high concentrations (500 μM) of *N*B-DNJ (**4**) it can also be observed that the amounts of monoglucosylated species slightly decrease compared to the lower concentrations of inhibitor. This counterintuitive observation can be explained by the fact that monoglucosylated species are both, products of α-glucosidase I hydrolysis and substrates for α-glucosidase II, and thus as inhibition of α-glucosidase I starts to increase, the substrate pool for α-glucosidase II decreases. For DNJ-KKAA (**37**) and DNJ-KDEL (**36**) treatments, the inhibition of α-glucosidases was lower. Except for the higher concentrations of DNJ-KDEL (**36**) where tri-glucosylated species start to appear, the inhibitory activity is mostly against α-glucosidase II, as can be observed by the dose-dependent increase of mono-glucosylated glycans.

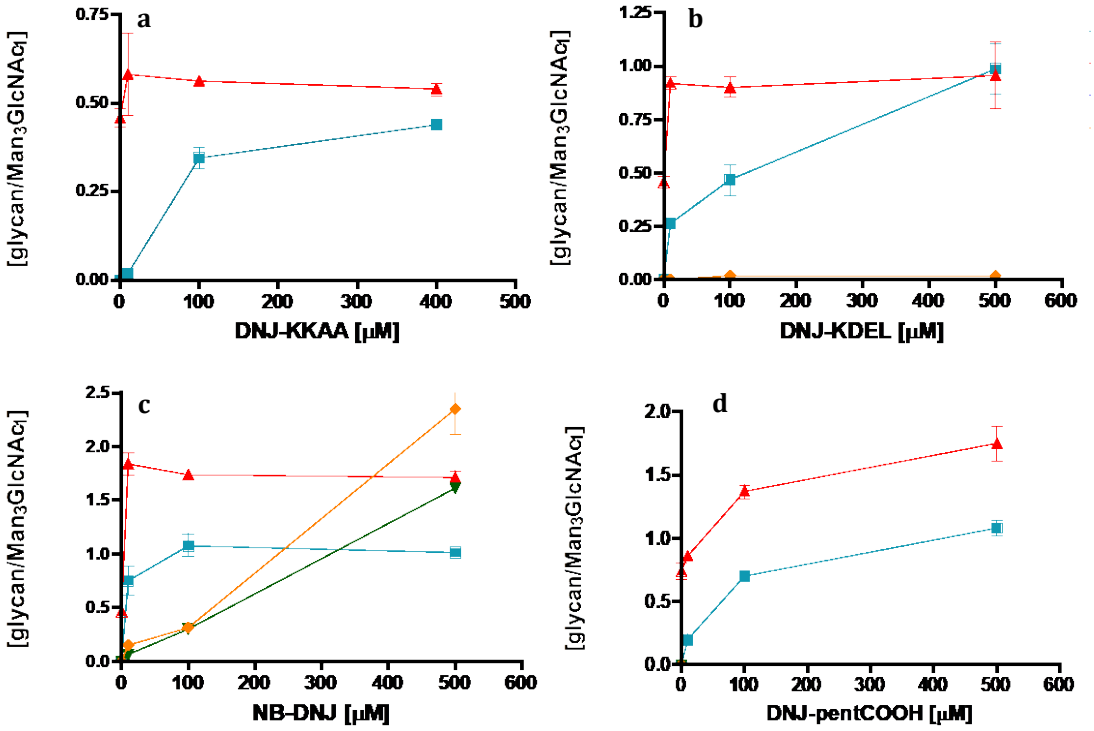

Figure 2.27 – FOS analysis after 24 h treatment of CHO-K1 cells with varying concentrations of (a) DNJ-KKAA (**37**), (b) DNJ-KDEL (**36**), (c) *N*B-DNJ (**4**), or (d) *N*-(5-carboxypentyl)-DNJ (**8**). Values normalised to concentration of $Man_3GlcNAc_1$ (⑤ $Glc_1Man_4GlcNAc_1$, ⑩ $Glc_1Man_5GlcNAc_1$, ⓿ $Glc_3Man_5GlcNAc_1$, ❶ $Glc_3Man_7GlcNAc_1$).

While the inhibition by all compounds cannot be compared directly at similar concentrations because of the different rates of inhibition of α-glucosidases I and II, a comparison can be established at lower concentrations where inhibitory activity is almost linear, and the resulting ratios can be followed throughout the concentration range. It can be observed that DNJ-KDEL (**36**) has close to 50% inhibitory activity *in cellulo* compared to *N*B-DNJ (**7**), while DNJ-KKAA (**37**) has around 25% of *N*B-DNJ's inhibition in cells. While there is no doubt that many factors can influence the results obtained, such as the different methods and ease to cross the plasma membrane of each compound, the intracellular localisation or the charge of each molecule in the different compartments of the cell, a rough comparison between compounds can be made taking into consideration the results presented so far. DNJ-KDEL (**36**) showed a 10-fold higher IC_{50} than *N*B-DNJ (**4**) for both α-glucosidases *in vitro*, however cell treatment required only a 2-fold excess of the peptide construct to obtain the same level of inhibition in cells. Assuming that the *in vitro* activity is comparable to the activity *in cellulo* for

both compounds, KDEL-DNJ (**36**) seems to be 5 times more effective at reaching α-glucosidase I in the ER. Using a parallel reasoning, DNJ-KKAA (**37**) was comparable to *N*B-DNJ (**4**) *in vitro* for α-glucosidase II, but showed only a quarter of the inhibitory activity of *N*B-DNJ (**4**) as shown by the appearance of monoglucosylated species. This indicates that DNJ-KKAA (**37**) is 4-fold less active than *N*B-DNJ (**9**) in cells.

Compared to *N*-(5-carboxypentyl)-DNJ (**8**), DNJ-KDEL (**36**) seems to be more efficient overall since the appearance of tri-glucosylated species indicates that it reaches α-glucosidase I, while *N*-(5-carboxypentyl)-DNJ (**8**) does not generate any triglucosylated glycans (Figure 2.27-d). *N*-(5-carboxypentyl)-DNJ (**8**) seems to be about 50% more efficient than DNJ-KKAA (**37**) at inhibiting α-glucosidase II even though its activity *in vitro* is three times lower.

Based on these results, DNJ-KKAA (**37**) was abandoned for subsequent studies, since its activity *in cellulo* was significantly less than its *in vitro* inhibition suggested. While DNJ-KDEL (**36**) was more efficient than *N*B-DNJ (**4**), the net effect of its inhibitory activity was still no better than had been obtained before. Nevertheless, the use of ER-retaining peptides not only intended to increase the concentration of DNJ (**1**) in the ER, but also to retain DNJ (**1**) there and allow a constant increase of its concentration during long term treatments and higher perseverance after treatment is finalised. Two experiments were designed to study the ability of DNJ-KDEL (**36**) to fulfil these expectations.

3.3.3. FOS analysis of long term treated cells

The first of these studies was simply a longer treatment of CHO-K1 cells, after which the FOS were analysed as described above. Figure 2.28 illustrates the results obtained for $Glc_1Man_4GlcNAc_1$. As can be observed, at the high concentration used (100 μM), the percentage of $Glc_1Man_4GlcNAc_1$ generated by DNJ-KDEL (**36**) inhibition compared to the amount of glycan generated during *N*B-DNJ (**4**) inhibition after 3 days of treatment is higher than after a single day of treatment. The change is very small, but nevertheless significant. The change is observable but not significant at lower concentrations. This small increase in ratio seems to point to a higher accumulation of DNJ-KDEL (**36**) in the ER over time, compared to *N*B-DNJ (**4**). If compared to the acid precursor *N*-(5-

carboxypentyl)-DNJ (**8**), the increase is quite significant with a longer treatment. In contrast to *N*B-DNJ (**4**) and DNJ-KDEL (**36**), longer treatment with *N*-(5-carboxypentyl)-DNJ (**8**) does not appear to induce higher inhibition with time, pointing to a mechanism that prevents its accumulation in the ER lumen.

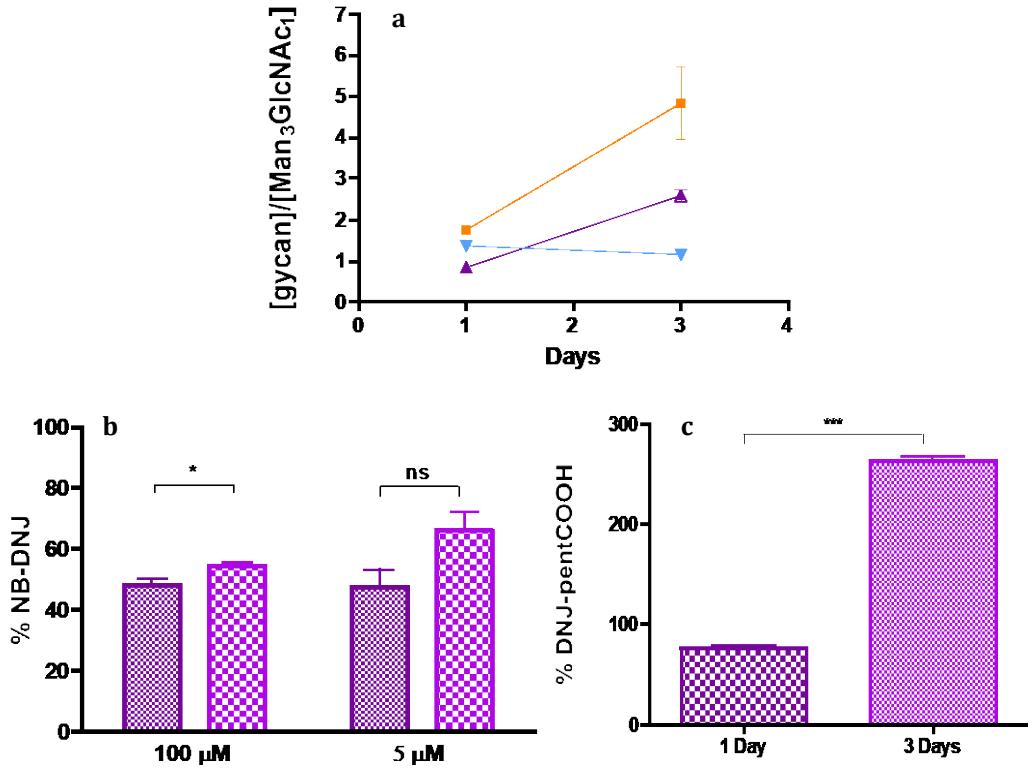

Figure 2.28 - FOS analysis for long-term treatment of CHO-K1 cells with ER-retaining peptide constructs. (a) 2-AA labelled $Glc_1Man_4GlcNAc_1$ after 1 and 3-day treatments at 100 µM ⑤ *N*B-DNJ (**4**), ⑩ DNJ-KDEL (**36**) or ⓪ *N*-(5-carboxypentyl)-DNJ (**8**). Values normalised to concentration of $Man_3GlcNAc_1$ (b) Percentage $Glc_1Man_4GlcNAc_1$ from values obtained with *N*B-DNJ at 100 µM and 5 µM after 1 and 3-day treatments. (c) Percentage $Glc_1Man_4GlcNAc_1$ from values obtained with *N*-(5-carboxypentyl)-DNJ (**8**) at 100 µM after 1 and 3-day treatments. Statistical analysis performed using Graphpad Prism 4.0 – Student's *t*-test; ns $p>0.05$; * $p<0.05$, ** $p<0.01$, *** $p<0.001$; n=3.

Figure 2.29 summarises the results obtained for long-term treatment of cells in relation to $Glc_1Man_5GlcNAc_1$. For 100 µM treatments, *N*B-DNJ (**4**) causes an increase in this glycan parallel to $Glc_1Man_4GlcNAc_1$. Treatment with DNJ-KDEL (**36**) over long time causes a much slower increase of the glycan amount at high concentrations, while *N*-(5-carboxypentyl)-DNJ (**8**) does not induce a change over long-term treatment. The difference in accumulation rates can be explained by considering that $Glc_1Man_5GlcNAc_1$ is a precursor for $Glc_1Man_4GlcNAc_1$. *N*B-DNJ (**4**) generates enough monoglucosylated glycans to allow us to see changes in both $Glc_1Man_5GlcNAc_1$ and $Glc_1Man_4GlcNAc_1$. DNJ-KDEL (**36**) on the other

hand, produces less net amount of glycans, and thus it is likely that most of the produced $Glc_1Man_5GlcNAc_1$ is transformed into $Glc_1Man_4GlcNAc_1$ making the direct comparison over longer treatments inconsistent for similar DNJ-KDEL (**36**) and *N*B-DNJ (**4**) high concentrations. At lower inhibitor concentrations, the accumulation rates over longer treatments is more dramatic, indicating higher DNJ-KDEL (**36**) accumulation compared to *N*B-DNJ (**4**). At lower inhibitor concentrations, the level of glycans produced is at a similar lower amounts for both inhibitors, thus allowing direct comparison over longer treatments for this glycan. Similarly to $Glc_1Man_5GlcNAc_1$, comparison with *N*-(5-carboxypentyl)-DNJ (**8**) at high concentrations shows an increase for DNJ-KDEL (**36**) treatments compared to *N*-(5-carboxypentyl)-DNJ (**8**).

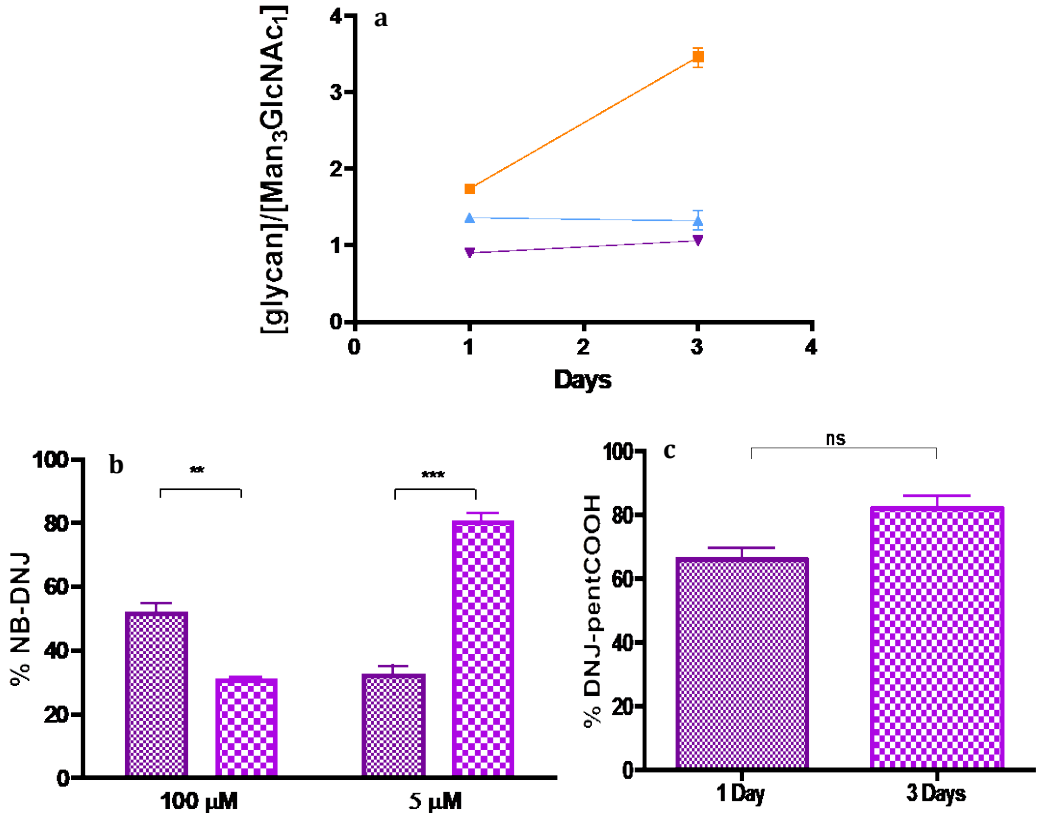

Figure 2.29 – FOS analysis for long-term treatment of CHO-K1 cells with ER-retaining peptide constructs. (a) 2-AA labelled $Glc_1Man_5GlcNAc_1$ after 1 and 3 day treatments (⑤ *N*B-DNJ (**4**), ⑩ DNJ-KDEL (**36**) and ⓪ *N*-(5-carboxypentyl)-DNJ (**8**)). Values normalised to concentration of $Man_3GlcNAc_1$ (b) Percentage $Glc_1Man_5GlcNAc_1$ from values obtained with *N*B-DNJ at 100 µM and 5 µM after 1 and 3-day treatments. (c) Percentage $Glc_1Man_5GlcNAc_1$ from values obtained with *N*-(5-carboxypentyl)-DNJ (**8**) at 100 µM after 1 and 3 day treatments. Statistical analysis performed using Graphpad Prism 4.0 – Student's *t*-test; ns $p>0.05$; * $p<0.05$, ** $p<0.01$, *** $p<0.001$; n=3.

In relation to triglucosylated glycans (Figure 2.30), while no measurable species appear after 24 h treatments with DNJ-KDEL (**36**) and *N*-(5-carboxypentyl)-DNJ (**8**), longer treatments generate some $Glc_3Man_5GlcNAc_1$. The pattern for accumulation of this glycan mimics the observations for $Glc_1Man_5GlcNAc_1$, with lower concentrations of DNJ-KDEL (**36**) generating a higher percentage of the triglucosylated species obtained with *N*B-DNJ (**4**). However, this can be simply explained again by the net amount of glycans generated. Since no measurable species were obtained after a single day of treatment, no comparison can be made regarding the accumulation rates for *N*B-DNJ (**4**) and DNJ-KDEL (**36**), however the appearance of triglucosylated species does confirm the cumulative effect of inhibition over time.

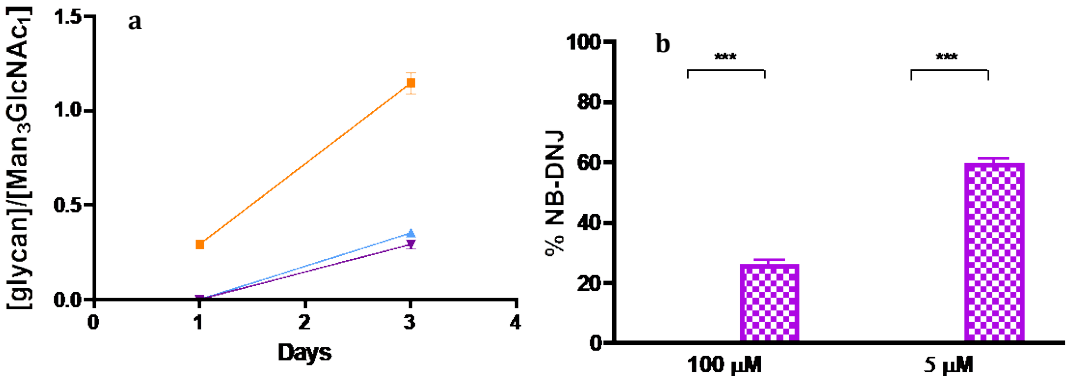

Figure 2.30 - FOS analysis for long-term treatment of CHO-K1 cells with ER-retaining peptide constructs (a) 2-AA labelled $Glc_3Man_5GlcNAc_1$ after 1 and 3 day treatments (⑤ *N*B-DNJ (**4**), ⑩ DNJ-KDEL (**36**) and ⓿ *N*-(5-carboxypentyl)-DNJ (**8**)). Values normalised to concentration of $Man_3GlcNAc_1$ (b) Percentage $Glc_3Man_5GlcNAc_1$ from values obtained with *N*B-DNJ at 100 µM and 5 µM after 1 and 3-day treatments. Statistical analysis performed using Graphpad Prism 4.0 – Student's *t*-test; ns $p>0.05$; * $p<0.05$, ** $p<0.01$, *** $p<0.001$; n=3.

3.3.4. FOS analysis for recovery of treated cells

The second study analysed the reversibility of DNJ-KDEL (**36**) treatment compared to *N*B-DNJ (**4**) and *N*-(5-carboxypentyl)-DNJ (**8**). For this purpose, CHO-K1 cells were treated for 24 h with the compounds at 100 µM, after which the media was replaced with drug-free media and the cells were incubated for another 24 h.

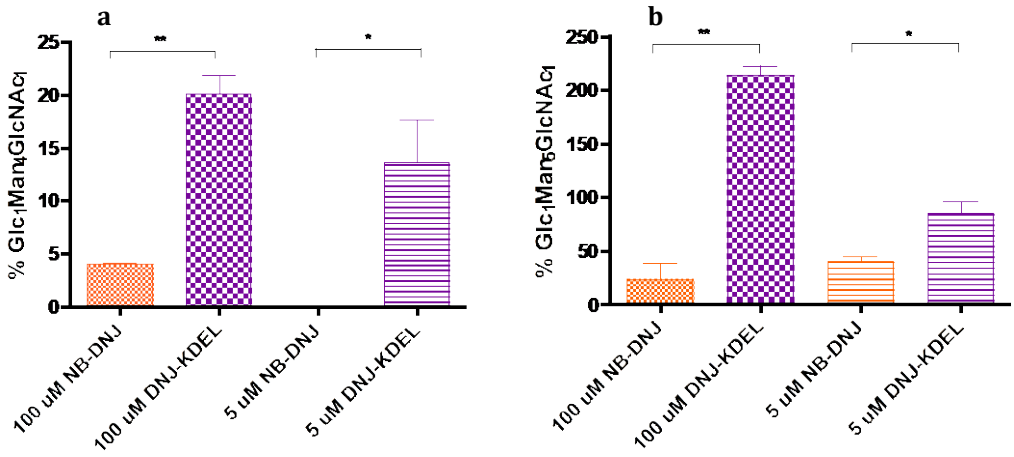

Figure 2.31 -Percentage 2-AA labelled glycans after 24 h recovery in drug-free media from values obtained after 24 h drug treatments (a) $Glc_1Man_4GlcNAc_1$ and (b) $Glc_1Man_5GlcNAc_1$. (⑤ *N*B-DNJ (**4**) and ⑤ DNJ-KDEL (**36**)). Statistical analysis performed using Graphpad Prism 4.0 – Student's *t*-test; ns p>0.05; * p<0.05, ** p<0.01, *** p<0.001; n=3.

As the results for $Glc_1Man_4GlcNAc_1$ indicate (Figure 2.31), while *N*B-DNJ (**9**) inhibition is completely reversible at low concentrations and only a 4% activity remains after 24 h for higher concentrations, DNJ-KDEL (**36**) maintains 20% activity after 24 h recovery and this effect can be observed even at low drug concentrations. In relation to $Glc_1Man_5GlcNAc_1$, treatment with DNJ-KDEL (**36**) sees levels of the glycan doubling for the recovery 24 h, while cells treated with *N*B-DNJ (**4**) recovered to have only 20% $Glc_1Man_5GlcNAc_1$ from Day-1 left. The observations for $Glc_1Man_5GlcNAc_1$ can be explained by the fact that even during normal conditions, this species is present as a FOS. It is therefore more persistent in the cytoplasm than other monoglucosylated species. The doubling of $Glc_1Man_5GlcNAc_1$ 24 h after treatment has been stopped is another indication of the persistent effect of DNJ-KDEL (**36**), while the cells treated with *N*B-DNJ (**4**) were well under way to recovery of normal levels (only 20% excess glycan after 24 h).

3.3.5. Fluorescently labelled ER-retaining peptides

In an effort to complement these results, fluorescently labelled ER retaining peptides were prepared with the objective of quantitating the uptake of labelled peptides using flow cytometry and tracking the cellular localisation of these short peptides through fluorescence microscopy. The first approach to the

synthesis was a direct on resin coupling between fluorescein isothiocyante (FITC) and the free amino group of the ER-retaining peptides previously prepared. This reaction would lead to the formation of the thiourea **40** (Figure 2.32). The acidic cleavage from the resin and purification of the residue led to the isolation of two compounds; a FITC thiohydantoin (**41**) from the last α-amino acid of the peptide sequence and the truncated peptide **42**. This reaction is known as Edman degradation,[116] and consists of an initial formation of a thiourea, followed by nucleophilic attack of the sulfur atom of the thiourea on to the carbonyl group of the α-amino acid next to it, forming a cyclic FITC-thiocabamoyl derivative, which under acidic conditions rearranges to the thiohydantoin. This problem was solved by the use of a 6-carbon linker before the addition of FITC, introduced as an extra Fmoc-protected amino acid by Fmoc-aminocaproic acid (**43**).[117]

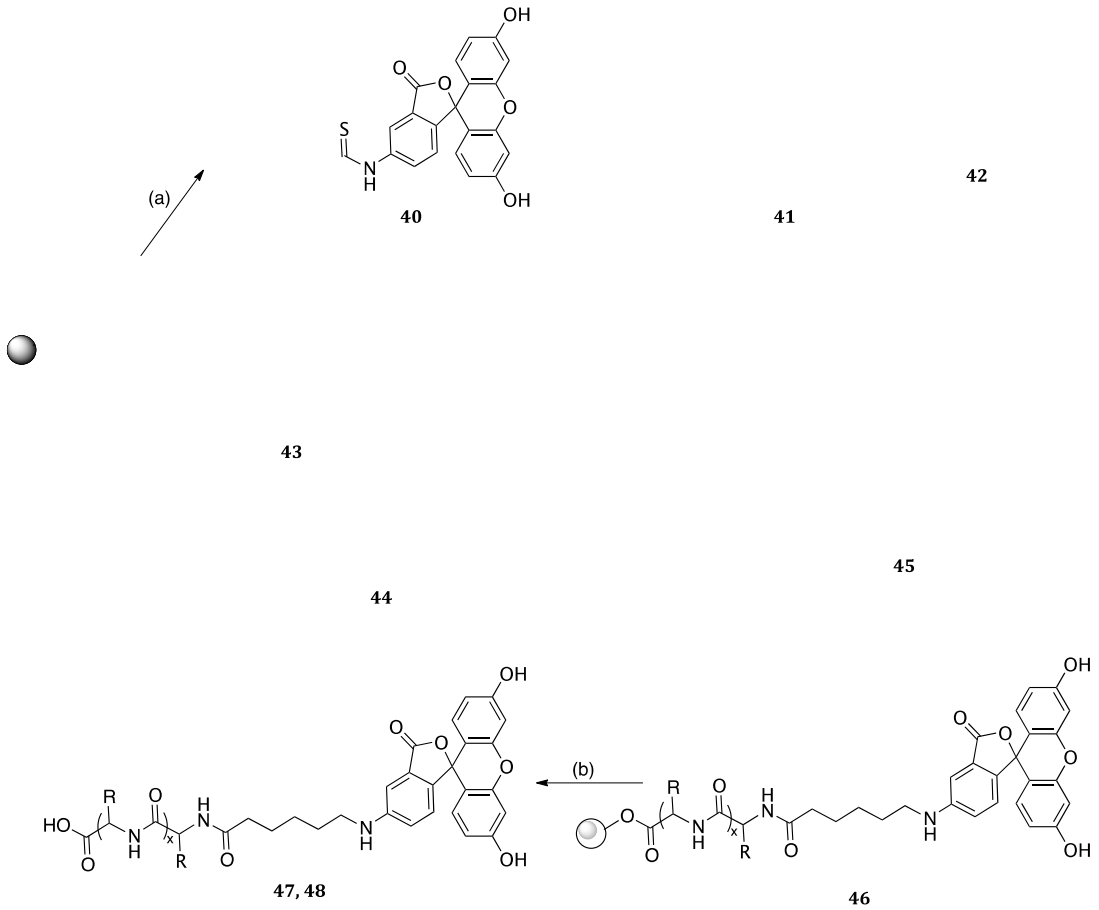

Figure 2.32 – General scheme for the formation of a fluorescein thiohydantoin and the synthesis of FITC labelled ER-retaining peptides. *Reagents and conditions*: (a) FITC, DIPEA; (b) TFA; (c) HOBt, DIC; (d) 20% piperidine in DMF.

Thus, after cleavage from the resin, the desired compounds FITC-KKAA (**47**) and FITC-KDEL (**48**) could be isolated with 18% and 5% overall yield respectively, after semi preparative scale HPLC. ^{1}H NMR analysis indicated that the purity of these compounds was higher than 98%. These fluorescently labelled peptides were used for FACS studies mimicking the assays done to measure α-glucosidase inhibition (concentration dependent treatments, long term treatment and a 24 h reversibility assay), as well as an immunofluorescence (IF) localisation study. While the difference between DNJ (**1**) and FITC is significant in both size and nature, these studies attempted to determine whether the use of ER-retaining signals could be extended to small molecules administered by supplemented media, since most of the studies so far take advantage of these signals as part of the synthetic process for new proteins. These FACS experiments (Figure 2.33) were performed after treatment with trypsin and multiple washes in order to avoid artifactual readings caused by labelled peptides associated with the cell surface instead of intracellular values.[130]

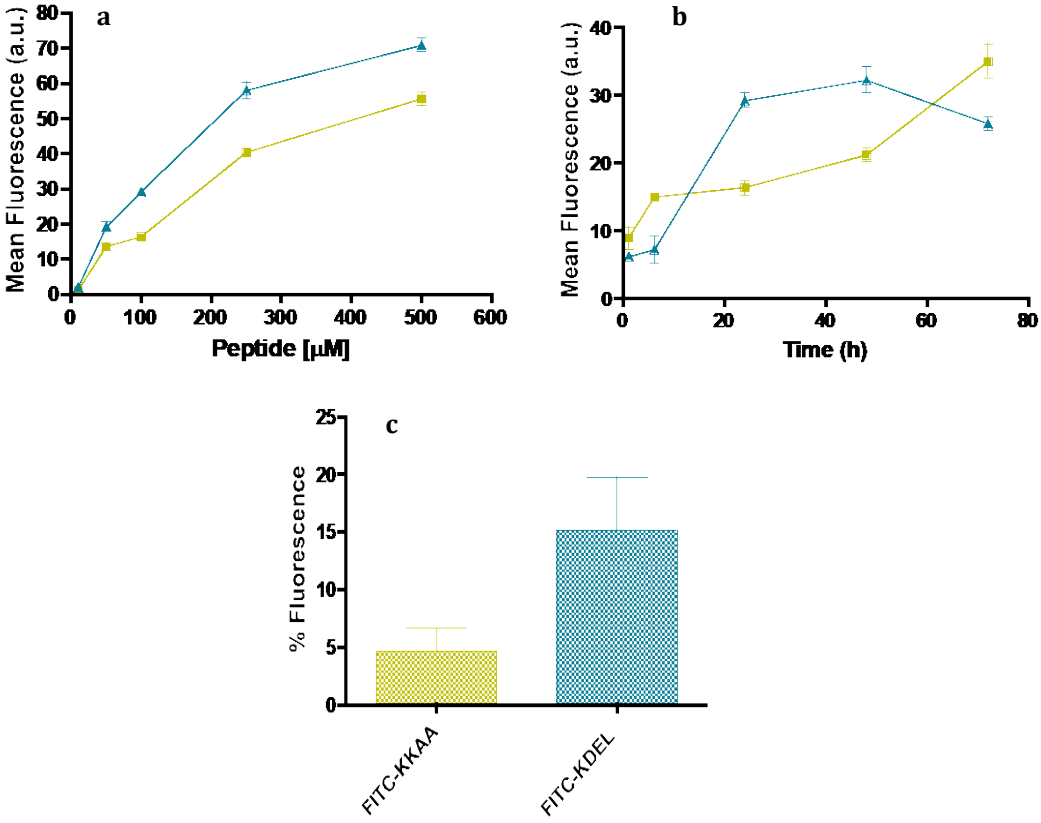

Figure 2.33– FACS results for (a) 24 h treatment with increasing compound concentration (50, 100, 250, and 500 μM), (b) Mean fluorescence after increasing duration treatments (30 min, 6, 24, 48 and 72 h) with 100 μM drug, (c) Percentage fluorescence of 24 h treatment after 24 h drug-free recovery (⑤ FITC-KKAA (**47**) and ⑤ FITC-KDEL (**48**)).

The increasing concentrations of both FITC labelled peptides (**47** and **48**) resulted in increased fluorescence. Within the range of concentrations tested, the relationship was not linear. After a fast increase, the uptake appeared to reach plateau for the higher concentrations. Nevertheless, without further studies at higher concentrations and specific assays to determine the method of internalisation, nothing more can be concluded from this assay apart from a dose-dependent increase in fluorescence for treatments with up to 250 μM labelled peptide. Regarding long-term treatment with 100 μM labelled peptides, after a period of fast uptake of FITC-KKAA (**47**), the rate decreases and it remains constant for the length of the treatment, allowing the accumulation of FITC labelled peptide through time. FITC-KDEL (**48**) initially had a slower uptake but the rate increased significantly after 6 h and seemed to have reached the maximum uptake after 24 h, maintaining an almost constant level of FITC-KDEL (**48**) for the subsequent 24 h, and then decreasing for the last 24 h of treatment. The behaviour of FITC-KKAA (**47**) matches the expectation of its accumulation over time, whereas the accumulation is due to ER retention or simply by prolonged internalisation, it cannot be determined with these data. The pattern for FITC-KDEL (**48**) is different and slightly puzzling. It cannot be reasoned that after 24 h, a saturation point is reached since treatment with higher concentrations led to higher fluorescence than the values obtained after 24 or 48 h during this assay. However, it is possible that equilibrium is reached after 24 h for FITC-KDEL (**48**) and maintained for 24 h before peptide degradation starts to decrease the intracellular concentration. Whether this equilibrium extends to localisation in the ER or not is still an unknown.

Finally, the reversibility study of the fluorescently labelled peptides gave a similar result for FITC-KDEL (**48**) as the one obtained for DNJ-KDEL (**36**) in the inhibitory assay, with close to 20% retention of the fluorescence (or inhibitory activity) of the previous day. FITC-KKAA (**47**) only showed about 5% fluorescence retention from the previous day measurements. This could be explained if the faster rate of internalisation showed in the previous experiment was caused by easier diffusion across the membrane, allowing the construct to both, enter and leave the cells faster than FITC-KDEL (**48**).

In an attempt to determine if the effects presented so far are indeed the results of ER retention, a microscopy study was undertaken with the FITC-labelled peptides. The cells were treated with 200 μM FITC-KKAA (**47**) or FITC-KDEL (**48**) for 24 h, and after fixation, an ER marker (PDI antibody) was added for IF microscopy (Figure 2.34).

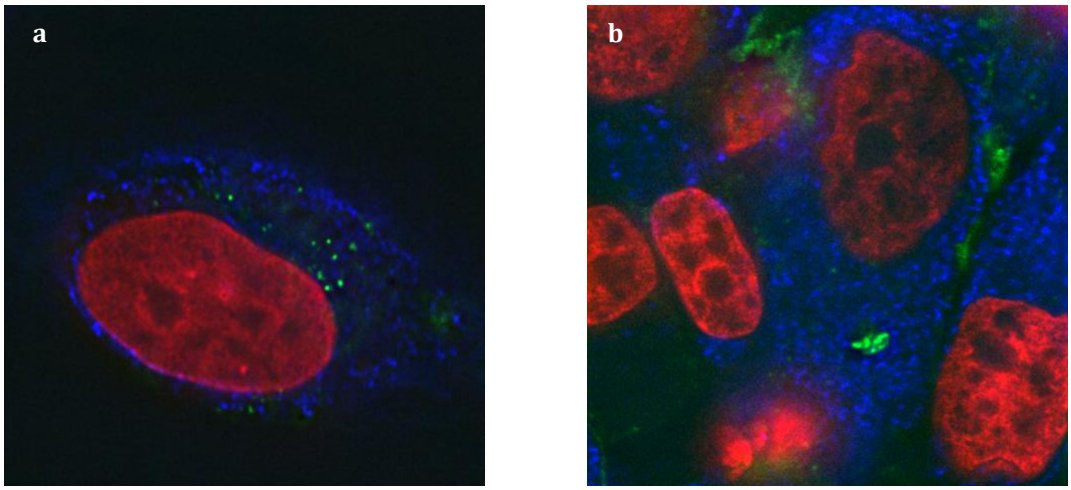

Figure 2.34– IF microscopy for 24 h treatments with (a) FITC-KDEL (**48**) or (b) FITC-KAAA (**47**) with DAPI for nucleus staining and a monoclonal mouse PDI primary antibody with an AlexaFluor 633 anti-mouse secondary antibody.

The resulting images for the IF microscopy experiment were inconclusive. There were detectable amounts of fluorescently labelled peptides within the cells, however the colocalisation with the ER marker was inconclusive. The FITC signal was spread throughout the cells, with a few small spots of high fluorescence within the area occupied by the ER. However, none of these spots seemed to overlap with the ER signal. Moreover, they seem to localise with gaps in the pattern generated by the ER antibody. It is possible that the FITC tagged peptide takes longer than 24 h to localise to the ER, and in the meantime, it is spread throughout the cell. It is also possible that since the primary antibody immunolocalises to a membrane bound protein, it would not colocalise to a small soluble peptide in the ER lumen. Yet another possibility is that the strong FITC signals observed are the result of compound precipitation or aggregation with other cell components, and the remaining cell-wide spread of the tagged peptide emits too-low fluorescence to obtain meaningful colocalisation results. Whether

the fluorescently labelled peptides colocalise with endosomes or other cell organelles (if any), cannot be concluded without further studies involving a wider range of antibodies.

3.4. Cell Penetrating Peptide-DNJ constructs

3.4.1. *In vitro* inhibition

Similarly to the experiments for ER-retaining peptides, an *in vitro* study of α-glucosidase I and II hydrolysis inhibition, with 2-AA labelled $Glc_3Man_7GlcNAc_1$ and $Glc_1Man_7GlcNAc_1$ as respective substrates, was carried out. The enzymes and substrates were incubated with 0.1, 1, 5, 20, 50 and 100 μM DNJ-CPP (**38** or **39**) to obtain the IC_{50} values summarised in Table 2.4, compared to the well studied *N*B-DNJ (**4**) and the free acid DNJ precursor *N*-(5-carboxypentyl)-DNJ (**8**).

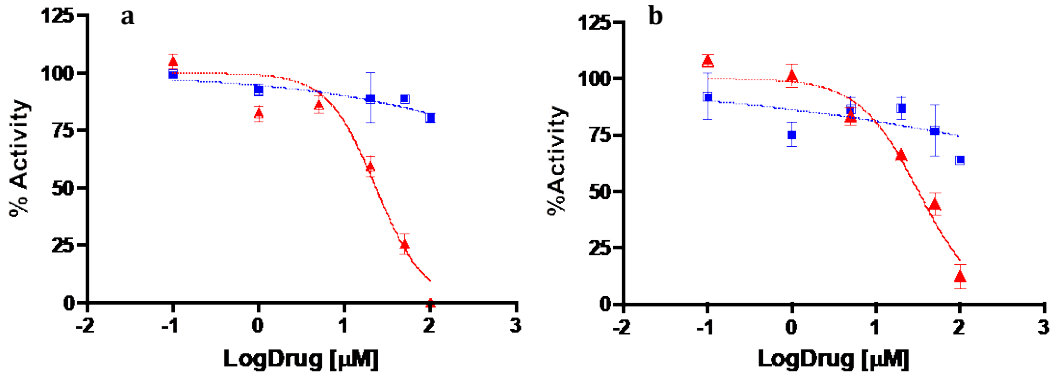

Figure 2.35- *In vitro* assay for (a) α-glucosidase I and (b) α-glucosidase II inhibition by the DNJ-CPPs constructs (⑤ DNJ-MAP (**39**), ⑩ DNJ-TAT (**38**)). Data is derived from from peak areas (NP-HPLC) and is reported as mean activity by comparison to a control in the absence of inhibitor. Data is reported as % ±SEM of at least triplicate measurements and fitted with a sigmodial curve (contrains: low=0, high=100).

Table 2.4 –Obtained IC_{50} values of rat α-Glucosidase I and II inhibition

Enzyme Substrate	α-Glucosidase I $Glc_3Man_7GlcNAc_1$	α-Glucosidase II $Glc_1Man_7GlcNAc_1$
DNJ-MAP (39)	>100 μM	>100 μM
DNJ-TAT (38)	23.3 ± 1.1 μM	42.1 ± 1.1 μM
***N*B-DNJ (4)**	2.3 ± 1.1 μM	2.1 ± 1.2 μM
***N*-(5-carboxypentyl)-DNJ (8)**	23.9 ± 1.2 μM	15.6 ± 1.1 μM

Similarly to the ER-retaining peptide constructs, DNJ-TAT's *in vitro* inhibitory activity was 10-fold higher than *N*B-DNJ (**4**) for α-glucosidases I and 20-fold higher for α-glucosidase II. DNJ-MAP (**39**) was surprisingly inefficient at inhibiting both glucosidases within the concentration range tested. As mentioned before, without structural studies, it is impossible to determine the factors that influence the activity of both constructs, however the lack of activity of DNJ-MAP (**39**) could be attributed to the nature of the peptide. The amphipathic α-helix is capable of strong interactions with both hydrophobic and hydrophilic residues, if the peptide associates with a particular part of the enzyme, it could hinder the ability of the DNJ moiety to reach the active site. In addition, amphipathic α-helices also tend to aggregate due to the nature of their constituent amino acids, which again could hinder the ability of DNJ (**1**) to inhibit its target. DNJ-TAT (**38**) is twice as efficient inhibiting α-Glucosidase I compared to α-Glucosidase II, however it is still 10-fold less active than *N*B-DNJ (**4**). Nevertheless, just like with the ER-retaining peptide constructs, DNJ-TAT (**38**) has comparable inhibitory activity to the acid precursor *N*-(5-carboxypentyl)-DNJ (**8**).

3.4.2. FOS analysis of treated cells

Cytotoxicity analysis by MTS proliferation assay showed no toxicity after 1 and 3-day treatments with up to 500 μM DNJ-TAT (**38**) as shown in Figure 2.36.

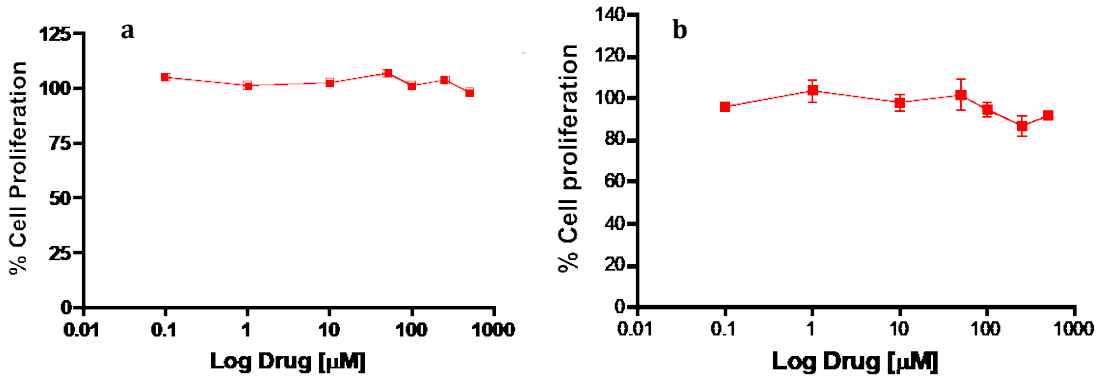

Figure 2.36- Cell proliferation assay for DNJ-TAT (**38**) in CHO-K1 cells, after (a) 1-day and (b) 3-day treatments. Determined by MTS proliferation assay and reported as percentage of a DMSO-treated control.

Satisfied that DNJ-TAT (**38**) was not cytotoxic, CHO-K1 cells were treated with it at varying concentrations over 24 h and the FOS were analysed as described

before. The results are shown in Figure 2.37. Similar tests with DNJ-MAP (**39**) showed no inhibition at all for up to 500 μM treatments.

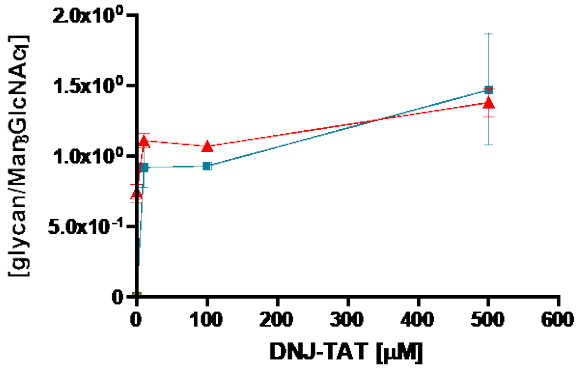

Figure 2.37 - 2-AA labelled FOS after 24 h treatments of CHO-K1 cells with varying concentrations of DNJ-TAT (**38**). Values normalised to concentration of $Man_3GlcNAc_1$ (⑤ $Glc_1Man_4GlcNAc_1$, ⑩ $Glc_1Man_5GlcNAc_1$, ⓿ $Glc_3Man_5GlcNAc_1$, ❶ $Glc_3Man_7GlcNAc_1$).

Direct comparison between $Glc_1Man_4GlcNAc_1$ obtained from DNJ-TAT (**38**) and *N*B-DNJ (**4**) treatments indicates a net 20-50% higher inhibitory activity *in cellulo*. Considering that DNJ-TAT (**38**) had a 20-fold lower *in vitro* activity, these measurements imply a 20 to 30-fold higher efficiency at reaching α-glucosidase II in the ER. Despite these promising results, it is important to point out that $Glc_1Man_5GlcNAc_1$ did not show a parallel increase to $Glc_1Man_4GlcNAc_1$, with DNJ-TAT (**38**) generating only about 60% of the $Glc_1Man_5GlcNAc_1$ produced by *N*B-DNJ (**4**). Additionally, no tri-glucosylated species were observed with DNJ-TAT (**38**) treatment. These observations could point to either an α-glucosidase II specific inhibition *in cellulo*, different kinetics than *N*B-DNJ (**4**) inhibition, or indeed a combination of both.

4. Conclusions

The *in vitro* and *in cellulo* results with the ER-retaining peptide constructs **35** and **36**, indicate that ER retaining signals could indeed be used to improve the effective concentration of drugs in the ER and prolong its effect after treatment has stopped. The main limitation at the moment is the lower inhibitory activity of DNJ-KDEL (**36**), as can be observed by its higher IC_{50} values *in vitro* (17.5 μM for α-glucosidase I and 23.5 μM for α-glucosidase II) compared to *N*B-DNJ (**4**), which currently makes the net effect on α-glucosidase inhibition lower overall than *N*B-DNJ (**4**), even if DNJ-KDEL (**36**) seemed more efficient when comparing their activities *in vitro* and *in cellulo*. While the net effect on long-term treatments is very low, this could be explained if indeed equilibrium was reached after 24 h treatment as suggested by the FACS studies. The most promising effect is the maintenance of activity after treatment has been stopped, which hints strongly to a retention mechanism that is not observed with simple alkylated DNJ. Taken together, these results seem to indicate that DNJ-KDEL (**36**) is more effective at reaching the ER, and thus inhibiting α-glucosidases, even when its *in vitro* activity is not as high as *N*B-DNJ (**4**). It appears that the main problem is that DNJ-KDEL (**36**) is less efficient at getting inside the cell, and thus its net inhibitory effect is lower than *N*B-DNJ (**4**). While the results so far are promising, these constructs still need to be optimised and more information needs to be collected about their modes of action before they can be considered for real therapeutic applications as enhanced molecules for ER localised α-glucosidase inhibition.

The CPP-DNJ constructs **38** and **39** yielded mixed results. DNJ-MAP (**39**) proved completely inefficient at inhibiting α-glucosidases *in vitro* and *in cellulo*. DNJ-TAT (**38**) on the contrary, showed close to half the activity of *N*B-DNJ (**4**) at similar concentrations for treated cells, even though its activity *in vitro* was 20-fold lower. This promising result points to the successful use of CPPs for delivery. Optimisation of the DNJ constructs via either DNJ-linker modification or the use of different CPPs with higher *in vitro* activity can lead to significant increases of intracellular α-glucosidases inhibition.

5. Future work

The use of peptides as a means to enhance DNJ's activity is a novel concept and thus requires further research before their value can be assessed. Several initial tests come to mind in relation to ER retaining peptides. The effect observed needs to be confirmed as a result of accumulation of peptide in the ER. This can be confirmed by radiolabelling of the DNJ-constructs to monitor its uptake and trafficking. The integrity of KDEL and its ability to bind KDEL receptors must also be confirmed. Immunoprecipitation of the KDEL receptor of treated cells, could lead, upon gel separation of the bound KDEL-containing components, to identification of the DNJ-KDEL constructs, thus confirming its ability to bind the receptor *in cellulo*. Improvements for the use of KDEL-DNJ (**36**) would involve primarily enhancing its ability to cross the plasma membrane to increase intracellular concentrations and thus its ability to localise to the ER. A simple method would involve using liposomes for delivery. Another possibility involves the combination of both CPPs and ER-retaining signals, in an effort to both increase efficiency while crossing the plasma membrane and localising to the ER. Regarding CPPs, two avenues are open for improvement. The first one involves systematic testing of the available CPP sequences in an effort to find the optimum combination of *in vitro* inhibition and *in vivo* activity. The second avenue focuses on the optimisation of DNJ-TAT (**38**). This construct needs to be tested in different cell lines and *in vivo*, since CPPs are renowned for their specific activity in particular environments. It must also be studied in long term experiments to determine its stability *in cellulo,* and by reversibility assays to determine its persistence profile. Regarding improvements for the actual construct, an interesting modification would involve the use of an acid-liable disulfide linker between DNJ and the TAT peptide. The cleavage of such bonds has been reported to happen spontaneously inside cells, thus releasing DNJ and allowing it to inhibit its target without hindering of the large peptide moiety. Other improvements involve the focus on making TAT more stable *in vivo*. The use of D-amino acids make peptides less liable to protease degradation and it has even been reported that the use of D-amino acids for the inverse sequence of a peptide, retains all its biological activity and provides complete degradation

protection. Modified TAT sequences and hybrid peptides would also provide sensible routes of improvement.

And of course, once these compounds cross the threshold of activity formerly set by *N*B-DNJ (**4**) and its analogues, they ought to be tested in mouse models to ascertain their activity *in vivo*. Their toxicity should be determined in comparison with available therapeutics, and their effect on α-glucosidase inhibition should be determined from FOS isolated from different tissues. Once these elements are analysed, transgenic mice with relevant diseases should be studied to ascertain the use of these compounds in the treatment and/or prevention of these diseases.

6. Experimental

6.1. Materials and general methods

All solvents used were laboratory or analytical grade and were purchased from Fisher Scientific unless otherwise stated. Anhydrous solvents were purchased from Acros. HPLC grade solvents were from AnalaR and Fisher Scientific. All commercially available reagents were purchased from Sigma or Acros unless otherwise specified, and were used as received without further purification. All amino acids, resins and reagents required for peptide synthesis were purchased from C S Bio Co (USA). Tissue culture media were from Gibco/Invitrogen (Paisley UK). Water was Milli-Q™ grade.

CHO-K1 cells were cultured in DMEM (with L-glutamate) medium containing 10% Foetal Calf Serum and 1% stock solution of penicillin-streptomycin (Invitrogen)

PDI (Protein Disulfide Isomerase) antibody, P4HB purified from mouse, was obtained from Enzo Life Sciences. Goat anti-mouse, Alexa Fluor 633 antibody, was obtained from Invitrogen.

Normal phase HPLC (Waters) analysis of FOS was carried out using a 4.6×250mm TSK gel Amide-80 column (Anachem). The chromatography system consisted of a Waters Alliance 2695 separations module and an in-line Waters 474 fluorescence detector with λ460 nm excitation and λ425 nm emission. Solvent A was CH_3CN, solvent B was water and solvent C was 100 mM ammonium hydroxide, pH 3.85 (titrated with AcOH). Program A - gradient: t=0 min, 71.6% A – 8.4 % B – 20% C, 0.8 mL/min; t=6 min, 71.6% A – 8.4 % B – 20% C, 0.8 mL/min; t=40 min, 52% A – 28 % B – 20% C, 0.8 mL/min; t=41 min, 23% A – 57 % B – 20% C, 1 mL/min; t=43 min, 23% A – 57 % B – 20% C, 1 mL/min; t=44 min, 71.6% A – 8.4 % B – 20% C, 1.2 mL/min; t=59 min, 71.6% A – 8.4 % B – 20% C, 1.2 mL/min; t=60 min, 71.6% A – 8.4 % B – 20% C, 0.8 mL/min.

Semi-preparative scale HPLC (Agilent) was performed using a protein and peptide C18 column (Vydec). The chromatography system consisted of Agilent 1100 Degasser, Quat pump and MWP modules. Spectra were collected for λ256 nm, λ214 nm, and λ495 nm absorptions with a UV/Vis detector. Solvent A was 0.1% TFA in Water and solvent B was 0.1% TFA in CH_3CN. Program B (3 mL/min flow) - gradient: t=0 min, 5% B; t=3 min, 5%; t=20 min, 40% B; t=23 min, 95% B; t=25 min, 95% B; t=28 min, 5%B; t=30 min, 5% B – 8.4 % B.

Silica gel column chromatography was carried out using Merck silica gel (60, particle size 0.040-0.063 mm (as stationary phase). Thin layer chromatography was performed using pre-coated silica gel plates (Merck 0.25mm Kieselgel 60 F_{254}) visualised by UV (254 nm) or by staining with 10% ammonium molybdate in 2 M H_2SO_4, 0.3 M dinitrophenylhydrazine (DNPH) in 20% H_2SO_4 50% aqueous EtOH or 0.1 M ninhydrin in 3% ethanolic AcOH, followed by heating.

Fluorescence spectra and UV absorbance were recorded on a Spectramax M5 microtiter plate reader (Molecular Devices).

NMR spectra were recorded on a Varian Spectrometer (500 MHz) at 30°C or a Brücker DPX (400 MHz) machine at ambient temperature. The following abbreviations are used to denote multiplicities: br-broad, s-singlet, d-doublet, t-triplet, q-quartet, dd-doublet of doublet, ddd- doublet of doublet of doublets, dt-doublet of triplets, m-multiplet. Coupling constant values (*J*) are reported to the nearest O.1 Hz. Chemical shifts are reported in parts per million (ppm) and are referenced to the residual solvent peak (^1H: $CDCl_3$ – 7.24 ppm, D_2O - 4.80 ppm, Acetone-d_6 – 2.05 ppm, MeOD-d_4 – 4.87 ppm and 3.31 ppm, or DMSO-d_6 – 2.50 ppm; ^{13}C: $CDCl_3$ – 77.23 ppm, Acetone-d_6 – 29.92 ppm and 206.68 ppm, MeOD-d_4 – 49.15 ppm, or DMSO-d_6 – 39.51 ppm).

Mass spectra were recorded on a Micromass LCT electrospray ionisation mass spectrometer with medium-high (7,000) resolution running openlynx. High-resolution mass spectra were recorded on a Brücker MicroTOF electrospray ionisation mass spectrometer with medium-high resolution (10,000).

Melting points were recorded on a Gallenkamp capillary melting point apparatus and are reported uncorrected.

Microscopy was performed using a DeltaVision wide-field deconvolution-enhanced microscope with a 100x objective and RI 1.514 immersion oil, and standard DAPI, CYAN-5, and FITC filters. Image analysis was completed using ImageJA 1.45I analysis software.

FACS analysis was performed using a BD FACScalibur Flow Cytometer (BD Science, Oxford). Acquisition was performed from 10 000 cells per sample. A blue Argon Laser (488 nm) was used to excite fluorochromes, and emission was detected with a green channel (FITC) and an orange channel (PI). Obtained data was analysed by CellQuest Pro Software.

Samples were analysed in triplicate and error is reported as standard deviation unless otherwise stated. Statistical analysis was generated using GraphPadPrism 4.0a for Macintosh using unpaired Student's *t*-test: *** $p<0.001$, ** $p<0.01$, * $p<0.05$.

All graphics were generated using GraphPrism 4.0a for Macintosh. Dose-response curves were fitted with a sigmoidal (four-parameter logistic) curve, with top constrain=100 and low constrain=0. Calibration curves were fitted with a linear regression curve.

^{1}H NMR and MS data are reported for all synthesised compounds. ^{13}C NMR data and high resolution MS are reported for novel compounds. M.p. are presented when available. Peak assignment for novel compounds was completed with COSY and HMQC data.

6.2. DNJ synthesis

2,6-Dibromo-2,6-dideoxy-L-idono-1,4-lactone[131]

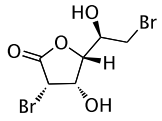

10

Commercially available D-mannono-1,4-lactone (**9**) (29 g, 162.9 mmol) was dissolved in a solution of HBr in AcOH (33% w/w, 150 mL) and stirred at RT for 2.5 h. MeOH (800 mL) was then added slowly, and the mixture was allowed to stir overnight. Solvents were then evaporated *in vacuo*. The residue was dissolved in MeOH (800 mL), followed by water (2 x 250 mL), with the solvent being evaporated each time *in vacuo*. The crude was dissolved in water (500 mL) and extracted with ether (6 x 300 mL). The combined organic fractions were dried over $MgSO_4$, the desiccant was removed by filtration and the solvent evaporated under reduced pressure. The residue was purified by silica gel chromatography (9:1 DCM:MeOH) to obtain the title compound **10** as a brown viscous oil (49% yield, 29.2 g, 79.6 mmol).

R_f 0.71 (9:1 DCM:MeOH, *p*-anisaldehyde stain).

^{1}H NMR (Acetone-d_6, 500 MHz) δ 3.67 (ddd, 2H, J=26.9 Hz, 10.4 Hz, 6.0 Hz, H1), 4.38 (td, 1H, J=5.9 Hz, 3.1 Hz, H2), 4.72 (d, 1H, J=4.9 Hz, H5), 4.82-4.86 (m, 2H, H3, H4).

LR-MS (ESI): *m/z* 304.9 $[M+H]^+$

2,6-Dibromo-D-mannitol[131]

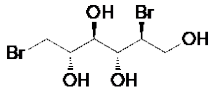

11

A solution of di-bromo lactone **10** (24 g, 79.0 mmol) in MeOH (180 mL) was cooled to 0°C in an ice bath, and $NaBH_4$ (11.1 g, 292.0 mmol) was then added slowly over a 30 min period with stirring. The reaction was stirred for further 30 min, after which HCl (32% w/w, 23.3 mL) was added slowly, and the resulting precipitate was removed by vacuum filtration. The filtrate was then stirred in the presence of Dowex 50Wx8 H^+ (5 g) for 30 min. The resin was removed by filtration, and the solvent was evaporated under reduced pressure. The residue

was dissolved in MeOH (4 x 80 mL), with the solvent being evaporated each time. The di-bromo iditol **11** was obtained by crystallisation from EtOH (30 mL) as white square planar crystals (43% yield, 10.5 g, 34.2 mmol).

R_f 0.50 (4:1 DCM:MeOH, molybdate stain)

^{1}H NMR (D_2O, 500 MHz) δ 3.42 (dd, 1H, J=10.6 Hz, 7.1 Hz, H1a), 3.51 (dd, 1H, J=10.6 Hz, J=5.0 Hz, H1b), 3.76-3.81 (m, 3H, H1, H5, H6), 3.87 (dd, 1H, J=12.4 Hz, 5.6 Hz, H4), 3.90 (t, 1H, J=6.2 Hz, H3), 4.14 (t, 1H, J=6.2 Hz, H2).

LR-MS (ESI): m/z 330.9 $[M+Na]^+$

2,6-Dibromo-3,4-*O,O*-isopropylidene-D-mannitol[121]

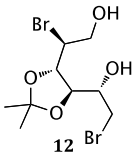

12

p-TsOH (79 mg, 0.46 mmol) was added slowly to a solution of the dibromoiditol **11** (1.42 g, 4.6 mmol) in acetone (19 mL). The reaction mixture was stirred at RT for 10 min, after which it was poured onto cold aqueous $NaHCO_3$ (saturated, 50 mL), and extracted with EtOAc (3 x 50 mL). The combined organic fractions were dried over $MgSO_4$, the desiccant was removed by filtration and the solvent evaporated under reduced pressure. The residue was purified by silica gel chromatography (9:1 DCM:MeOH) to obtain the protected di-bromo iditol **12** as a white viscous oil (64% yield, 1.01 g, 2.9 mmol).

R_f 0.52 (9:1 DCM:MeOH, molybdate stain).

^{1}H NMR ($CDCl_3$, 500 MHz) δ 1.43 (d, 6H, J=3.7 Hz, 2xMe), 2.49 (br-s, 2H, 2xOH), 3.52 (d, 1H, J=1.3 Hz, H1a), 3.53 (d, 1H, J=0.7 Hz, H1b), 3.99-4.02 (m, 3H, H5, H6), 4.20-4.24 (m, 2H, H4, H3), 4.32 (dt, 1H, J=7.3 Hz, 5.4 Hz, H2).

LR-MS (ESI): m/z 346.8 $[M+H]^+$

(*R*)-2-Amino-1-{(4*R*,5*S*)-5-[(*S*)-1-bromo-2-({*tert*-butyldimethylsilyl}oxy) ethyl]-2,2-dimethyl-1,3-dioxolan-4-yl}ethanol[121]

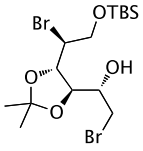

13

TBS-Cl (4.08 g, 27.2 mmol) was added with stirring to a solution of the protected di-bromo iditol **12** (8.54 g, 24.7 mmol) in pyridine (40 mL). The reaction mixture was allowed to stir overnight. MeOH (80 mL) was then added to the reaction mixture, and the organic solvents were removed under reduced pressure. The residue was dissolved in MeOH (60 mL) and aqueous NH_3 (28% v/v, 19.1 mL) was added to the solution. The reaction mixture was allowed to stir at RT for 12 h, after which the solvent was evaporated under reduced pressure. The residue was purified by silica gel chromatography (4:1 DCM:MeOH) to obtain the desired amino compound **13** as a clear viscous oil (82% yield, 7.81 g, 19.9 mmol).

R_f 0.55 (4:1 DCM:MeOH, ninhydrin stain)

^{1}H NMR ($CDCl_3$, 500 MHz) δ 0.10 (s, 6H, 2x*t*Bu Me), 0.90 (s, 9H, 3x*t*Bu Me), 1.46 (d, 6H, *J*=6.3 Hz, 2xMe), 3.96 (d, 2H, *J*=7.2 Hz, H1), 4.09-4.20 (m, 3H, H3, H4), 4.34 (dd, 1H, *J*=8.2 Hz, 1.9 Hz, H2).

LR-MS (ESI): *m/z* 399.1 $[M+H]^+$

6-*O*-[(*tert*-Butyldimethylsilyl)]oxy-3,4-*O*-isopropylidene-1-deoxynojirimycin[121]

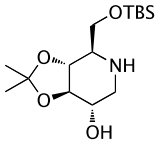

15

Sodium acetate (117 mg, 1.43 mmol) was added to a solution of the amino compound **13** (45 mg, 0.11 mmol) in nitromethane (1 mL). The reaction mixture was heated under reflux conditions overnight. The insoluble components were removed by filtration, and the filtrate was then evaporated under reduced pressure. The residue was purified by silica gel chromatography (99:1 DCM:MeOH) to obtain a compound as a white powder (81% yield, 29 mg). This

main product was shown to be an elimination by-product of the reaction. A second fraction was collected from the column (4:1 DCM:MeOH), not visible by TLC (visualisation with molybdate, ninhydrin, *p*-anisaldehyde, H_2SO_4 and DNPH stains), to obtain the title compound **15** as a white powder (10% yield, 3.5 mg, 0.01 mmol).

^{1}H NMR ($CDCl_3$, 500 MHz) δ 0.09 (s, 6H), 0.90 (s, 9H), 1.40 (d, 3H, *J*=7.7 Hz), 1.47 (d, 3H, *J*=15.0 Hz), 2.90-2.99 (m, 1H), 3.73 (dd, 1H, *J*=9.8 Hz, 2.6 Hz), 3.81 (dd, 1H, *J*=13.0 Hz, 5.2 Hz), 3.92-3.94 (m, 1H), 4.02-4.08 (m, 2H), 4.17 (dd, 1H, *J*=12.9 Hz, 4.7 Hz), 4.29-4.34 (m, 1H).

LR-MS (ESI): *m/z* 318.2 $[M+H]^+$

1-Deoxynojirimicin[121]

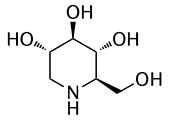

1

HCl (32% v/v, 210 µL) was added to a solution of the protected DNJ **15** (52 mg, 0.07 mmol) in MeOH (800 µL), and the reaction mixture was stirred at RT for 30 min. The organic solvent was then evaporated under reduced pressure, and the residue was washed with cold ether (2 x 1 mL) and dried under vacuum to give a white powder as a mixture of products, including DNJ (**1**) (26.8 mg).

No clean NMR spectrum obtained.

LR-MS (ESI): *m/z* 164.1$[M+H]^+$ (corresponding to DNJ (**1**))

1,2-*O,O*-isopropylidene-α-D-glucorono-3,6-lactone[119]

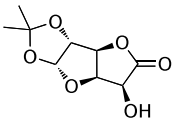

17

H_2SO_4 (32 mL) was added slowly to a solution of glucoronolactone **16** (227.0 mmol, 40 g) in acetone (960 mL). The reaction mixture was stirred at RT for 5 h, after which sodium bicarbonate was then added until the reaction mixture reached neutral pH. The insoluble material was removed by filtration, and the filtrate evaporated under reduced pressure. The crude product was dissolved in DCM (100 mL) and filtered. The filtrate was evaporated under reduced pressure

and the residue was crystallised from hot toluene to obtain glucoronoloactone acetonide **17** as white needle crystals (93% yield, 257.6 mmol, 45.6 g).

R_f 0.75 (EtOAC, molybdate stain).

^{1}H NMR ($CDCl_3$, 500 MHz) δ 1.36 (s, 3H, Me), 1.53 (s, 3H, Me), 4.52 (1H, d, *J*=4.4 Hz, H5), 4.83-4.84 (m, 2H, H2, H3), 4.95 (dd, 1H, *J*=4.2 Hz, 3.0 Hz, H4), 6.00 (d, 1H, *J*=3.6 Hz, H1).

m.p.: 124.5.-125-3°C (lit.[132] m.p. 120.5-121.5°C)

LR-MS (ESI): *m/z* 239.0 $[M+Na]^+$

1,2-*O,O*-isopropylidene-β-L-idurono-3,6-lactone[119]

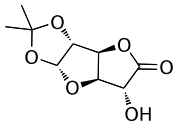

18

A solution of acetonide **17** (237.0 mmol, 51.21 g) in DCM (425 mL) and pyridine (56.3 mL) was cooled down to -30°C in an acetonitrile/dry ice bath. Triflic anhydride (260.0 mmol, 43.9 mL) was added drop wise over a 1 h period. The reaction was stirred for a further 1 h period at -30°C, after which the reaction mixture was washed with aqueous HCl (2 M, 3 x 500 mL). The organic phase was then concentrated under reduced pressure and the crude triflate was dissolved in DMF (210 mL). Sodium trifluoroacetate (474.0 mmol, 64.5 g) was added slowly and the reaction mixture was stirred at RT for 1 h. The resulting mixture was then diluted with aqueous sodium bicarbonate (saturated, 400 mL) and extracted with EtOAc (3 x 500 mL). The combined organic fractions were concentrated under reduced pressure and the residue was crystallised from hot toluene. The resulting crystals were collected by filtration to afford the iduronolactone acetonide **18** as white crystals (91% yield, 214.9 mmol, 46.4 g).

R_f 0.45 (2:1 petroleum ether/EtOAc, molybdate stain)

^{1}H NMR ($CDCl_3$, 500 MHz) δ 1.36 (s, 3H, Me), 1.52 (s, 3H, Me), 4.34 (1H, d, *J*=2.0 Hz, H5), 4.80 (d, 1H, *J*=3.2, H4), 4.84 (d, 1H, *J*=3.7 Hz, H2), 5.07 (d, 1H, *J*=3.2 Hz H3), 5.94 (d, 1H, *J*=3.7 Hz, H1).

m.p.: 133.8-135.3°C (lit.[133] m.p. 133-135°C)

LR-MS (ESI): *m/z* 239.0 $[M+Na]^+$

5-Azido-1,2,-*O,O*-isopropylideneglucoronolactone[119]

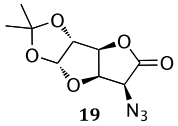

19

A solution of the lactone **18** (800 mg, 3.7 mmol) in a mixture of DCM (8 mL) and pyridine (880 µL) was cooled down to -30°C in an acetonitrile/dry ice bath. Triflic anhydride (685 µL, 4.07 mmol) was then added portion-wise over a period of 1 h while stirring, and the resulting mixture was allowed to stir for a further 1 h. The reaction mixture was then washed with aqueous HCl (2M, 3 x 10 mL) and the organic phase was concentrated under reduced pressure. The crude triflate was dissolved in DMF (9 mL) and the solution was cooled down to 20°C in an ice/NaCl bath. Sodium azide (240 mg, 3.7 mmol) was then added to the solution and the reaction was allowed to proceed for 1 h while stirring. After this time, brine (50 mL) was added and the mixture was extracted with EtOAc (3 x 50 mL). The combined organic fractions were evaporated and the residue was purified by silica gel chromatography (13:7 hexane:EtOAc) to obtain the azido glucoronolactone **19** as a clear oil that crystallised overnight to white needle crystals (66% yield, 591 mg, 2.5 mmol).

R_f 0.41 (2:1 hexane/EtOAc, molybdate stain).

^{1}H NMR ($CDCl_3$, 500 MHz) δ 1. 37 (s, 3H, Me), 1.54 (s, 3H, Me), 4.09 (d,1H, J=4.3 Hz, H5), 4.86 (d, 2H, J=2.9, H2, H3), 5.04 (dd, 1H, J=4.3 Hz, 2.6 Hz, H4), 6.04 (d, 1H, J=3.5 Hz, H1).

m.p.: 81.5-82.0°C (lit.[134] m.p. 82-84°C)

LR-MS (ESI): m/z 264.1 $[M+H]^+$

5-Azido-1,2,-*O,O*-isopropylideneglucoronolactol[119]

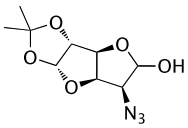

20

A solution of the azido lactone **19** (23.9 g, 99.1 mmol) in DCM (120 mL) was cooled down to -78 °C in an acetone/dry ice bath, and DIBAL-H in hexane (1M, 113 mL, 113 mmol) was added over 30 min while stirring. The reaction mixture was allowed to react for a further 30 min, and then it was diluted with DCM (500

mL) and a saturated aqueous solution of potassium sodium tartrate (600 mL) was added. The mixture was allowed to stir overnight, after which the organic phase was collected and the aqueous phase was extracted with DCM (5 x 300 mL). The collected organic fractions were dried over $MgSO_4$, the desiccant was removed by filtration and the solvent evaporated under reduced pressure. The residue was purified by silica gel chromatography (1:1 hexane:EtOAc) to obtain the desired difuranose **20** as a pale orange powder (72% yield, 17.3 g, 71.1 mmol).

R_f 0.32 (2:1 hexane/EtOAc, molybdate stain).

^{1}H NMR ($CDCl_3$, 500 MHz) δ 1.36 (s, 3H, Me), 1.51 (s, 3H, Me), 3.48 (t, 1H, *J*=4.8 Hz, H5), 4.65 (d, 1H, *J*=4.0 Hz, H3), 4.77 (d, 1H, *J*=3.6 Hz, H2), 5.01 (t, 1H, *J*=4.2 Hz, H4), 5.41 (dd, 1H, *J*=7.6 Hz, 4.4 Hz, H6), 6.11(d, 1H, *J*=3.5 Hz, H1).

m.p.: 112.8-115.4°C (lit.[119] m.p. 110-112°C)

LR-MS (ESI): *m/z* 266.1 $[M+Na]^+$

5-Azido-1,2,-*O,O*-isopropylidene-β-D-glucofuranose[119]

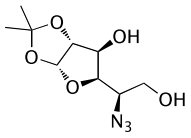

21

A solution of the difuranose **20** (4.49 g, 18.5 mmol) in MeOH (30 mL) was cooled down to -20°C in a NaCl/ice bath. $NaBH_4$ (177 mg, 4.8 mmol) was added to the solution, and the reaction mixture was stirred for 1 h. Glacial AcOH was then added until $NaBH_4$ was neutralised, and the solvent was removed under reduced pressure. The residue was purified by silica gel chromatography (1:1 hexane:EtOAc) to obtain the glucofuranose **21** as a colourless viscous oil (93% yield, 4.22 g, 17.2 mmol).

R_f 0.45 (1:1 hexane: EtOAc, molybdate stain).

^{1}H NMR ($CDCl_3$, 500 MHz) δ 1.33 (s, 3H, Me), 1.57 (s, 3H, Me), 3.85 (dd, 1H, *J*=11.1 Hz, 5.7 Hz, H6a), 3.87-3.91 (m, 1H, H5), 4.01 (dd, 1H, *J*=11.2 Hz, 3.5 Hz, H6b), 4.13-4.16 (m, 1H, H4), 4.35 (d, 1H, *J*=2.7 Hz, H3), 4.55 (d, 1H, *J*=3.6 Hz, H2), 5.96 (d, 1H, *J*=3.6 Hz, H1).

LR-MS (ESI): *m/z* 268.1 $[M+Na]^+$

1-Deoxynojirimycin[119]

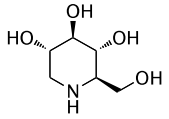

1

Dowex 50Wx8 H^+ (200 mg) was added to a solution of the glucofuranose **21** (140 mg, 0.57 mmol) in water (1 mL). The mixture was allowed to stir for 2 h at 70°C, after which the resin was removed by filtration and Pd/C (10%, 20 mg) was added to the solution. The flask was flushed with H_2 and the reaction mixture was allowed to stir for two days under a H_2 atmosphere, with continued flushing of the solution with H_2. The solids were then removed by filtration through a celite path and the filtrate was evaporated *in vacuo*. The residue was dissolved in MeOH (3 x 2 mL) with the solvent being evaporated each time *in vacuo* at a temperature under 20°C until crystals started to precipitate. The product was allowed to crystallise overnight, and the crystals were then collected by filtration and dried under vacuum to obtain DNJ **1** (99% yield, 92.3 mg, 56.7 mmol).

R_f 0.61 (14:1 MeOH:H_2O, ninhydrin stain).

^{1}H NMR ($CDCl_3$, 500 MHz) δ 2.89 (t, 1H, *J*=12.1 Hz, H1a), 3.12 (ddd, 1H, *J*=10.5 Hz, 5.1 Hz, 3.3 Hz, H5), 3.42 (dd, 1H, *J*=12.9 Hz, 5.6 Hz, H1b), 3.42 (t, 1H, *J*=9.3 Hz, H3), 3.51 (t, 1H, *J*=9.9 Hz, H4), 3.71 (ddd, 1H, *J*=10.9 Hz, 8.5 Hz, 5.2 Hz, H2), 3.78 (dd, 1H, *J*=12.8 Hz, 5.2 Hz, H6a), 3.85 (dd, 1H, *J*=12.8 Hz, 3.2 Hz, H6b).

m.p.: 215.8-218.0°C (lit.[135] m.p. 200-202°C)

LR-MS (ESI): *m/z* 164.1 $[M+H]^+$

6.3. Synthesis of DNJ constructs

Methyl 6-hydroxyhexanoate[136]

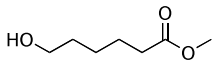

24

Methanolic sulfuric acid (90%, 15 mL) was added to a solution of ε-Caprolactone **23** (15 g, 0.13 mol) in MeOH (25 mL). The mixture was heated under conditions of reflux for 10 min and then allowed to cool to RT. An aqueous solution of sodium hydroxide (0.5 M, 60 mL) was then added to the reaction mixture before extraction with ethyl acetate (3 x 100 mL). The combined organic fractions were washed with brine (100 mL), dried over $MgSO_4$, the desiccant was removed by

filtration and the solvent evaporated under reduced pressure. The desired product **24** was isolated as a colourless oil (95% yield, 18.2 g, 0.12 mol) and used without further purification.

^{1}H NMR ($CDCl_3$, 500 MHz) δ 1.34-1.42 (m, 2H, H4), 1.53-1.67 (m, 4H, H3, H5), 2.30-2.34 (m, 2H, H2), 2.52 (s-br, 1H, OH), 2.65 (t, 1H, *J*=6.5 Hz, H6), 2.66 (s, 3H, Me).

Methyl 6-oxohexanoate

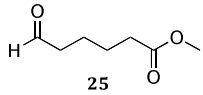

25

A solution of methyl-6-hydroxyhexanoate **24** (2.0 g, 12.7 mmol) in a mixture of DMSO and DCM (1:5, 30 mL) was cooled to 0°C in an ice bath. Sulfur trioxide pyridine adduct (4.36 g, 27.4 mmol) and triethylamine (7.6 mL, 54.8 mmol) were added and the suspension was allowed to stir for 30 min. The reaction mixture was diluted with ethyl acetate (250 mL) and washed with water (2 x 50 mL), saturated aqueous ammonium iodide (50 mL) and brine (50 mL). The organic phase was dried over $MgSO_4$, the desiccant was removed by filtration and the solvent evaporated *in vacuo*. The residue was purified by silica gel chromatography (4:1 petrol: EtOAc) to obtain the desired aldehyde **25** as a clear oil (44% yield, 0.87 g, 5.8 mmol).

^{1}H NMR ($CDCl_3$, 500 MHz) δ 1.64-1.68 (m, 4H, H3, H4), 2.30-2.36 (m, 2H, H2), 2.45-2.48 (m, 2H, H5), 3.67 (s, 3H, Me), 9.77 (s, 1H, CHO).

LR-MS (ESI): *m/z* 167.1 $[M+Na]^+$

***N-(*Methyl-5-carboxypentyl)-deoxynojirimycin**[137]

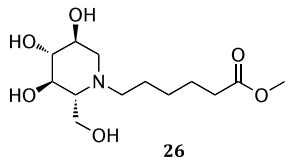

26

Pd/C (10%, 25 mg) was added to a solution of methyl-6-oxohexanoate **25** (70 µL) and DNJ (45 mg, 0.28 mmol) in a mixture of MeOH, water and acetic acid (5:4:0.3 v/v/v, 500 µL). The reaction mixture was stirred under a hydrogen atmosphere for 12 h, and then filtered through a celite path. The filtrate was evaporated under reduced pressure to give the crude product **26** as a clear oil.

The crude product was used without further purification.

LR-MS (ESI): *m/z* 292.2 $[M+H]^+$ (corresponding to *N*-(Methyl-5-carboxypentyl)-deoxynojirimycin (**26**)).

No clean NMR spectra obtained

N-(5-Carboxypentyl)deoxynojirimycin[138]

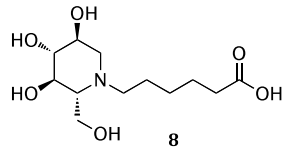

8

A solution of the protected DNJ construct **26** (40 mg, 0.14 mmol) in aqueous NaOH (0.4 M, 5 mL) was allowed to stir for 2 h. The reaction mixture was then passed over a column packed with Dowex AG50Wx12 H^+, and eluted from the column with ammonium hydroxide. The resulting solution was lyophilised to dryness to yield the crude product as a mixture of compounds that could not be purified.

LR-MS (ESI): *m/z* 300.2 $[M+Na]^+$ (corresponding to *N*-(5-carboxypentyl)-deoxynojirimycin (**8**)).

No clean NMR spectra obtained

6-Hydroxyhexanoic acid[139]

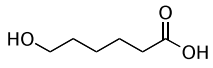

27

A solution of ε-caprolactone **23** (5 g, 43.85 mmol) in aqueous NaOH (0.5 M, 100 mL) was allowed to stir at RT for 12 h. The reaction was neutralised with Dowex 50Wx8 H^+ resin (5 g), filtered and extracted with EtOAc (5 x 75 mL). The combined organic fractions were dried over $MgSO_4$, the desiccant was removed by filtration and the solvent evaporated under reduced pressure to give the hydroxyacid **27** as a clear oil (84% yield, 4.86 g, 36.8 mmol). The product was used without further purification.

^1H NMR ($CDCl_3$, 500 MHz) δ 1.42-1.49 (m, 2H, H4), 1.59-1.65 (m, 2H, H3), 1.67-1.73 (2H, m, H5), 2.40 (t, 2H, *J*=7.4 Hz, H2), H, 3.69 (t, 2H, *J*=6.5 Hz, H6).

^{13}C {^1H} NMR ($CDCl_3$, 125 MHz) δ 24.40 (C4), 25.21(C3), 32.26 (C5), 33.52 (C2), 62.64 (C6), 177.42 (C1).

LR-MS (ESI): *m/z* 131.1 $[M+H]^+$

6-(*tert*-Butyldimethylsilyloxy)hexanoic acid[140]

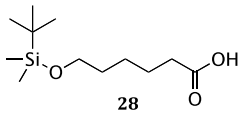

28

2.4 equivalents of imidazole (2.53 g, 36.8 mmol) were added to a solution of 6-hydroxyhexanoic acid (**27**) (2.02 g, 15.3 mmol) in dry DMF (21 mL). The reaction mixture was stirred for 10 min at RT, after which *tert*-butyldimethylsilyl chloride (3.00 g, 19.9 mmol) was added. The reaction mixture was then stirred at RT for another 30 min. The solvent was then evaporated under reduced pressure and the residue was dissolved in H_2O (50 mL). This aqueous solution was shaken with EtOAc (3 x 100 mL) and the combined organic fractions were dried over $MgSO_4$, the desiccant was removed by filtration and the solvent evaporated *in vacuo*. Product **28** was obtained in quantitative yield (3.76 g, 15.3 mmol) as a clear oil. The product was used without further purification.

Rf 0.35 (17:3 hexane:EtOAc, bromocresol green stain).

^{1}H NMR ($CDCl_3$, 500 MHz) δ 0.05 (s, 6H, 2 x Me), 0.90 (s, 9H, 3 x *t*Bu Me), 1.37-1.43 (m, 2H, H4), 1.52-1.58 (m, 2H, H3), 1.61-1.69 (m, 2H, H5), 2.38 (t, 2H, *J*=7.5 Hz, H2), 3.64 (t, 2H, *J*=6.5 Hz, H6).

^{13}C {^{1}H} NMR ($CDCl_3$, 125 MHz) δ -5.32 (Si Me), 18.31 (Si *t*Bu), 24.48 (*t*Bu Me), 25.33 (C4), 25.92 (C3), 32.38 (C5), 34.05 (C2), 62.89 (C6), 179.84 (C1).

LR-MS (ESI): *m/z* 269.1 $[M+Na]^+$

1-Benzyl-6-(*tert*-butyldimethylsilyloxy)hexanoate[140]

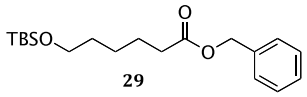

29

K_2CO_3 (16.85 g, 121.9 mmol) was added to a solution of the protected hydroxyacid **28** (6.00 g, 24.4 mmol) in dry acetone (105 mL). The resultant suspension was stirred for 10 min at RT, after which benzyl bromide (3.77 mL, 31.7 mmol) was added drop wise to the reaction mixture. The reaction was then stirred under conditions of reflux for 18 h, after which it was cooled down to RT,

the insoluble material removed by filtration and the filtrate was evaporated *in vacuo*. The residue was purified by silica gel chromatography (9:1 petroleum ether:EtOAc) to give the benzyl-protected product **29** as a clear oil (70% yield, 6.22 g, 16.99 mmol).

^{1}H NMR ($CDCl_3$, 500 MHz) δ 0.06 (s, 6H, 2 x Me), 0.91 (s, 9H, 3 x *t*Bu Me), 1.35-1.41 (m, 2H, H4), 1.51-1.57 (m, 2H, *J*=7.1 Hz, H3), 1.66-1.72 (m, 2H, *J*=7.6 Hz, H5), 2.40 (t, 2H, *J*=7.6 Hz, H2), 3.62 (t, 2H, *J*=6.5 Hz, H6), 5.13 (s, 2H, CH_2Ph), 7.31-7.42 (m, 5H, Ph).

^{13}C {^{1}H} NMR ($CDCl_3$, 125 MHz) δ -5.29 (Si Me), 18.33 (Si *t*Bu), 24.78 (*t*Bu Me), 25.43 (C4), 25.95 (C3), 32.45 (C5), 34.33 (C2), 62.94 (C6), 66.06 (*C*H_2Ph), 128.52, 128.52, 136.13 (Ph), 173.52 (C1).

LR-MS (ESI): *m/z* 365.0 $[M-H]^-$

Benzyl-6-hydroxyhexanoate[140]

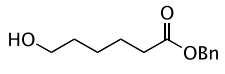

30

A solution of the fully protected hydroxyacid **29** (100 mg, 0.27 mmol) in dry THF (200 µL) was cooled down to 0°C in an ice bath. A solution of TBAF in THF (1 M, 410 µL, 0.41 mmol) was added drop wise to the reaction mixture. The reaction was stirred at RT for 3 h, after which the solvents were evaporated *in vacuo*. The residue was subjected to silica gel chromatography (9:1 hexane:EtOAc) to obtain the product **30** as a clear oil (89% yield, 54 mg, 0.24 mmol).

R_f 0.35 (9:1 hexane:EtOAc, UV).

^{1}H NMR ($CDCl_3$, 500 MHz) δ 1.38-1.44 (m, 2H, H4), 1.55-1.61 (m, 2H, H3), 1.66-1.72 (m, 2H, H5), 2.40 (t, 2H, *J*=7.6 Hz, H2), 3.65 (t, 2H, *J*=6.5 Hz, H6), 5.13 (s, 2H, CH_2Ph), 7.31-7.38 (m, 5H, Ph).

^{13}C {^{1}H} NMR ($CDCl_3$, 125 MHz) δ 24.63 (C4), 25.26 (C3), 32.27 (C5), 34.21 (C2), 62.55 (C6), 66.13 (*C*H_2Ph), 128.17, 128.53, 136.06 (Ph), 173.51 (C1).

LR-MS (ESI): *m/z* 245.1 $[M+H]^+$

Benzyl-6-oxohexanoate

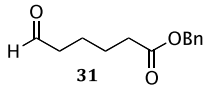

31

Dess-Martin Periodinane (229 mg, 0.54 mmol) was added to a solution of Bn-6-hydroxyhexanoate (**30**) (100 mg, 0.45 mmol) in dry DCM (1 mL). The reaction mixture was stirred for 3 h, after which the insoluble material was removed by filtration. The filtrate was evaporated *in vacuo* and the residue was immediately purified by flash chromatography (17:3 petroleum ether:EtOAc) to obtain the aldehyde **31** as a clear glass (45% yield, 44.1 mg, 0.20 mmol).

TLC analysis of **31** after 24 h showed the appearance of degradation products, indicating the need for its immediate use in subsequent reactions.

R_f 0.76 (9:1 hexane:EtOAc, DNPH stain).

^{1}H NMR ($CDCl_3$, 500 MHz) δ 1.65-1.74 (m, 4H, H3, H4), 2.42 (t, 2H, J=7.0 Hz, H2), 2.48 (dt, 2H, J=6.9 Hz, 1.3 Hz, H5), 5.14 (s, 2H, CH_2Ph), 7.32-7.40 (m, 5H, Ph), 9.76 (s, 1H, CHO).

^{13}C {^{1}H} NMR ($CDCl_3$, 125 MHz) δ 21.48 (C3), 24.35 (C4), 33.94 (C2), 43.44 (C5), 66.24 (*C*H_2Ph), 128.22, 128.56, 135.96 (Ph), 173.00 (C1), 201.92 (C6).

HPLC trace (Program B):

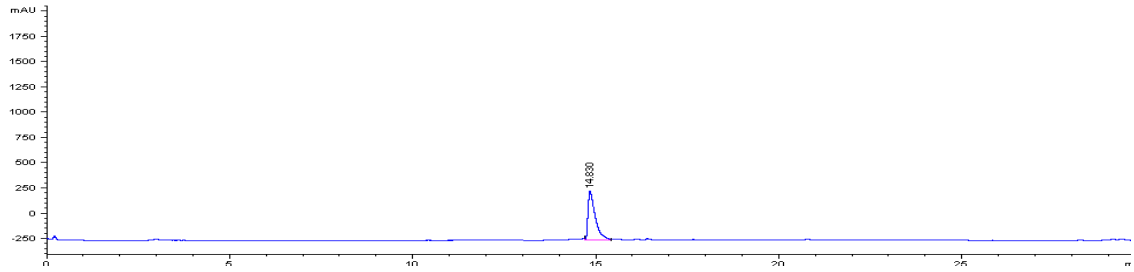

***N*-[(5-Benzyloxycarbonyl)penty]deoxynojirimycin**

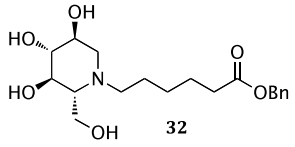

32

Activated 3Å molecular sieves, compound **31** (450 mg, 2.06 mmol) and $NaCNBH_3$ on solid support (1.13 g, 2.26 mmol) were added sequentially to a solution of DNJ (**1**) (100 mg, 0.61 mmol) in dry MeOH (30 mL). The reaction mixture was stirred for 3 h at RT and then filtered and evaporated *in vacuo*. The residue was purified by semi-preparative scale HPLC with program B (R_t = 15.37 min). The

relevant fractions were lyophilised to dryness to obtain the desired product **32** as a white powder (57% yield, 128.2 mg, 0.35 mmol).

^{1}H NMR (MeOD-d_4, 500 MHz) δ 1.39-1.46 (m, 2H, H4), 1.69-1.75 (m, 4H, H3, H5), 2.45 (t, 2H, *J*=7.3 Hz, H2), 3.00 (t, 1H, *J*=11.7 Hz, H6a), 3.04 (d, 1H, *J*=10.0 Hz, H6b), 3.18 (dt, 1H, *J*=12.0 Hz, 4.7 Hz, DNJ-H1a), 3.32-3.33 (m, 1H, DNJ-H5), 3.39 (t, 1H, *J*=9.1 Hz, DNJ-H1b), 3.46 (dd, 1H, *J*=11.9 Hz, 4.5 Hz, DNJ-H3), 3.62 (t, 1H, *J*=9.6 Hz, DNJ-H4), 3.66-3.71 (m, 1H, DNJ-H2), 3.91 (d, 1H, *J*=12.1 Hz, DNJ-H6a), 4.13 (d, 1H, *J*=12.2, DNJ-H1b), 5.14 (s, 2H, C*H*$_2$Ph), 7.31-7.37 (m, 5H, Ph).

^{13}C {^{1}H} NMR (MeOD-d_4, 125 MHz) δ 22.41 (C4), 23.96 (C3), 25.58 (C5), 33.22 (C2), 52.79 (C6), 53.53 (DNJ-C1), 65.85 (*C*H$_2$Ph), 66.09 (DNJ-C5), 67.42 (DNJ-C6), 76.72 (DNJ-C2), 115.64 (DNJ-C4), 117.97 (DNJ-C3), 127.83 (Ph C3, Ph C4), 128.15 (Ph C2), 136.26 (Ph C1), 173.46 (C1).

HR-MS: ($C_{19}H_{29}NO_6$) theoretical *m/z* 368.2068 $[M+H]^+$, found *m/z* 368.3065 $[M+H]^+$

N-(5-Carboxypentyl)deoxynojirimycin

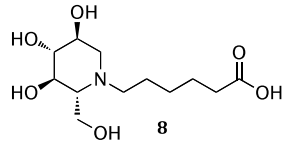

8

Pd/C (10%, 10 mg) was added to a solution of the benzyl-protected DNJ construct **32** (128.2 mg, 0.35 mmol) in MeOH (500 µL). The reaction mixture was stirred under a H_2 atmosphere for 18 h at RT, after which the suspension was filtered and evaporated under reduced pressure to obtain the deprotected DNJ acid **8** as a white powder in quantitative yield (96.8 mg, 0.35 mmol).

^{1}H NMR (D_2O, 500 MHz) δ 1.41-1.48 (m, 2H, H4), 1.66-1.72 (m, 1H, H3), 1.74-1.84 (m, 2H, H5), 2.36 (t, 2H, *J*=7.3 Hz, H2), 3.00 (t, 1H, *J*=11.7 Hz, H6a), 3.07 (d, 1H, *J*=10.3 Hz, H6b), 3.24 (dt, 1H, *J*=12.3 Hz, 5.4 Hz, DNJ-H1a), 3.28-3.36 (m, 1H, DNJ-H5), 3.42 (t, 1H, *J*=9.2 Hz, DNJ-H1b), 3.49 (dd, 1H, *J*=6.1 Hz, 4.9 Hz, DNJ-H3), 3.63 (t, 1H, *J*=7.1Hz, DNJ-H4), 3.75 (ddd, 1H, *J*=11.0 Hz, 10.2 Hz, 4.8 Hz, DNJ-H2), 3.95 (dd, 1H, *J*=12.6 Hz, 3.0 Hz, DNJ-H6a), 4.12 (dd, 1H, *J*=12.6 Hz, 1.3 Hz, DNJ-H6b).

^{13}C {^{1}H} NMR (D_2O, 125 MHz) δ 22.60 (C4), 24.03 (C3), 25.71 (C5), 33.25 (C2), 52.55 (C6), 53.44 (DNJ-C1), 56.95 (DNJ-C5), 66.13 (DNJ-C6), 66.44 (DNJ-C2), 67.54 (DNJ-C4), 76.71 (DNJ-C3), 176.06 (C1).

HR-MS: ($C_{12}H_{23}NO_6$) theoretical *m/z* 278.1598 $[M+H]^+$, found *m/z* 278.1599 $[M+H]^+$

HPLC trace (Program B):

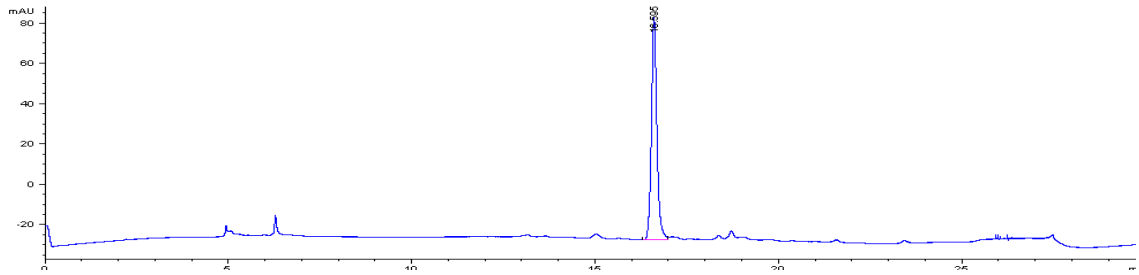

6.4. Peptide synthesis

Wang resin

AMS resin **33** (2.0 mmol, 5 g) was soaked in a 1:1 mixture of DMF and DCM (50 mL). After 3 h the solution was drained and the resin washed with DMF (3 x 10 mL). HMPA linker **34** (1.46 g, 8.0 mmol) and HOBt (1.19 g, 8.8 mmol) were then dissolved in DMF (10 mL) and added to the resin. DIC (1.24 mL, 8.0 mmol) was added to the mixture and the reaction was stirred for 1 h. The resin **35** was then drained, washed with DMF and dried *in vacuo*.

First amino acid loading

The prepared Wang resin **35** (2.0 mmol) was suspended in DMF. In a scintillation vial, DIC (2 equiv., 619 µL, 4.0 mmol) was added a solution of the desired amino acid (4 equiv., Leu for KDEL, Arg(Pbf) for polyarginine peptide, and Lys(Cbz) for the modified KKAA) in dry DMF (10 mL). The solution was stirred at RT for 5 min, after which the resulting anhydride solution was added to the resin, followed by DMAP (49 mg, 0.2 mmol). The resin was stirred at room temperature for 2 h, after which it was washed sequentially with DMF (2 x 20

mL), DCM (2 x 20 mL) and DMF (2 x 20 mL). Amino acid loading was determined by Fmoc cleavage with 20% piperidine in DMF (5 mL) of dry resin (10 mg). After 30 min, the absorbance was recorded at 290 nm and compared to a standard curve generated after treatment under the same conditions of a resin with known loading (in this case Fmoc-Ala-Wang resin with 0.74 mmol/g loading). Loading for Fmoc-Leu-Wang resin was determined to be 0.30 mmol/g. Loading for Fmoc-Arg(Pbf)-Wang resin was determined to be 0.32 mmol/g. Loading for Fmoc-Lys(Cbz)-Wang was determined to be 0.35 mmol/g.

Peptide synthesis

Peptide elongation was carried out on the required resin suspended in DMF (20 mL/g resin) by the additions of the corresponding amino acid (4 equiv., 1.5 mmol), followed by HOBt (4.4 equiv.) and DIC (4.4 equiv.). The suspension was allowed to stir for 1.5 h at RT, after which the resin was washed sequentially by DMF (2 x 20 mL), DCM (2 x 20 mL) and DMF (2 x 20 mL). Fmoc deprotection was done by treatment with piperidine in DMF (20%, 20 mL/g resin), followed by the same washing steps and the next coupling. After the sequence was completed, a final Fmoc deprotection step was performed to leave the peptide sequence with the free amino terminus.

DNJ peptide coupling

A solution of *N*-(5-carboxypentyl)-DNJ (**8**) (27.7 mg. 0.1 mmol) in DMF (1 mL) was added to a suspension of the resin with the free amino terminus (0.1 mmol) in DMF (20 mL). DIC (1.5 equiv., 23.2 μL, 0.15 mmol) and HOBt (1.5 equiv., 20.2 mg, 0.15 mmol) were added, and the reaction mixture was stirred at RT for 3 h. After this time, the resin was washed with DMF (2 x 5 mL), DCM (2 x 5 mL), MeOH (2 x 5 mL), DCM (2 x 5 mL) and DMF (2 x 5 mL).

Cleavage from resin

A solution of TFA, triisopropylsilane and water (90:7:3 v/v/v, 5 mL) was added to the prepared resin (0.1 mmol) and stirred for 3 h at RT. The resin was then removed by filtration and washed with neat TFA (2 x 500 μL). The combined filtrates were added drop wise to cold ethyl ether (100 mL). After vigorous

shaking, the resultant precipitate was centrifuged (3,000 rpm, 20 min) and the supernatant decanted. This process was repeated twice and the final pellet was dried under an argon flow, re-dissolved in a solution of *t*-BuOH/H_2O (4:1, 5 mL) and lyophilised to yield the crude DNJ-peptide construct as a white powder. The crude product was purified by semi-preparative scale HPLC – Program B. The relevant fractions were dried *in vacuo* to yield the pure DNJ-constructs **37**-**39** as white powders.

DNJ-KDEL

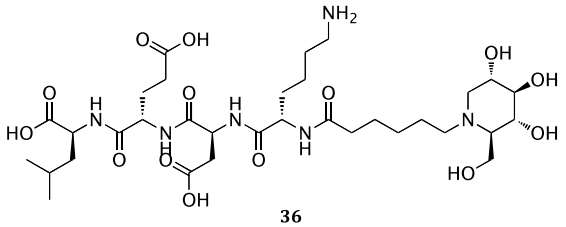

36

^{1}H NMR (MeOD-d_4, 500 MHz) δ 0.94 (d, 3H, *J*=6.4 Hz, Val Me), 0.98 (d, 3H, *J*=6.4 Hz, Val Me), 1.42-1.52 (m, 4H, Val H2, H3), 1.63-1.77 (m, 7H, H4, H2, Arg H3, Val, H3), 1.79-1.87 (m, 2H, Lys H4), 1.93-2.01 (m, 1H, Arg H2a), 2.16-2.23 (m, 1H, Lys H2b), 2.26-2.36 (m, 2H, Glu H2), 2.45 (t, 1H, *J*=7.6 Hz, H1), 2.86 (dd, 1H, *J*=17.1 Hz, 6.9 Hz, Glu H3), 2.93 (dd, 1H, *J*=17.0 Hz, 6.0 Hz, Asp H2), 2.98 (t, 2H, *J*=8.2 Hz, Lys H5), 3.05 (t, 1H, *J*=11.7 Hz, DNJ H6a), 3.07-3.09 (m, 1H, DNJ H2), 3.20-3.23 (m, 1H, H5), 3.42 (t, 1H, *J*=9.2 Hz, DNJ H4), 3.49 (dd, 1H, *J*=12.1 Hz, 4.5 Hz, DNJ H5), 3.64 (t, 1H, *J*=9.6 Hz, DNJ H3), 3.69-3.74 (m, 1H, DNJ H6b), 3.95 (d, 1H, *J*=11.0 Hz, DNJ H1a), 4.14 (d, 1H, *J*=12.2 Hz, DNJ H1b), 4.29 (t, 1H, *J*=7.1 Hz, Glu H1), 4.40-4.46 (m, 2H, Val H1, Lys H1), 4.70 (t, 1H, *J*=6.3 Hz, Asp H1), 8.04 (br-d, 1H, *J*=7.9 Hz, Val NH), 8.14 (br-d, 1H, *J*=7.9 Hz, Lys NH), 8.29 (br-d, 1H, *J*=8.3 Hz, Glu NH), 8.35 (br-d, 1H, *J*=7.4 Hz, Asp NH).

^{13}C {^{1}H} NMR (MeOD-d_4, 125 MHz) δ 21.76 (Val Me), 23.44 (Val Me), 23.74 (Val C4), 25.91 (Val C3), 25.97 (Lys C4), 27.14 (C4), 28.19 (Lys C3), 28.47 (Glu C3), 31.08 (Lys C5), 32.21 (C5), 36.04 (C3), 36.20 (C2), 40.50 (Glu C4), 41.31 (Asp C3), 51.49 (DNJ C2), 52.23 (DNJ C4), 53.95 (DNJ C6), 54.97 (DNJ C3), 67.33 (C6), 67.86 (DNJ C5), 68.83 (DNJ C1), 78.13 (Lys C6), 114.94 (Val C2), 116.38 (Lys C2), 117.20 (Glu C2), 118.69 (Asp C2), 172.77 (Glu C5), 173.45 (Asp C4), 174.14 (Val C1), 174.36 (C1), 175.71 (Lys C1), 176.18 (Glu C1), 176.72 (Asp C1).

HR-MS: ($C_{33}H_{58}N_6O_{14}$) theoretical *m/z* 763.4084 $[M+H]^+$, found *m/z* 763.4099

$[M+H]^+$

HPLC trace (Program B):

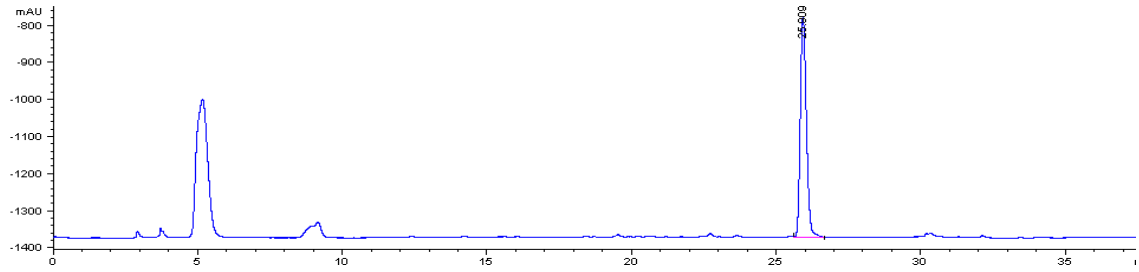

DNJ-KKAA

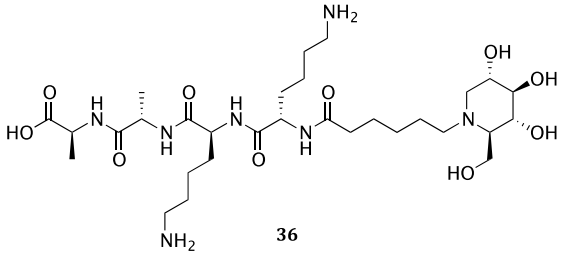

36

^{1}H NMR (MeOD-d_4, 500 MHz) δ 1.43 (dd, 6H, *J*=8.6 Hz, 7.3 Hz, Ala1 Me, Ala2 Me), 1.48-1.57 (m, 4H, Lys1 δH, Lys2 δH), 1.67-1.75 (m, 12H, H3, H5, Lys1 βH, Lys2 βH, Lys1 γH, Lys2 γH), 1.87-1.94 (m, 2H, H4), 2.32 (t, 2H, *J*=7.0 Hz, H2), 2.98 (q, 4H, *J*=7.0 Hz, Lys1 εH, Lys2 εH), 3.04 (t, 1H, *J*=11.8 Hz, DNJ H6a), 3.07-3.08 (m, 1H, DNJ H2), 3.17-3.18 (m, 1H, H6a), 3.41 (t, 1H, *J*=9.3 Hz, DNJ H4), 3.48 (d, 1H, *J*=8.8 Hz, DNJ H5), 3.64 (t, 1H, *J*=9.3 Hz, H3), 3.69-3.74 (m, 4H, DNJ H6b, H6), 3.94 (d, 1H, *J*=11.5 Hz, DNJ H1a), 4.13 (d, 1H, *J*=11.4 Hz, DNJ H1b), 4.31 (t, 1H, *J*=6.7 Hz, Ala1 αH), 4.34-4.39 (m, 3H, Lys1 αH, Lys2 αH, Ala2 αH), 8.15 (br-d, 1H, *J*=6.5 Hz, Ala2 NH), 8.21 (br-d, 1H, *J*=7.2 Hz, Ala1 NH), 8.29 (br-d, 1H, *J*=7.2 Hz, Lys2 NH), 8.35 (br-d, 1H, *J*=7.7 Hz, Lys1 NH).

^{13}C {^{1}H} NMR (MeOD-d_4, 125 MHz) δ 17.64 (Ala1 Me), 18.24 (Ala2 Me), 23.47 (C4), 23.63 (Lys1 δC), 23.83 (Lys2 δC), 23.88 (C5), 26.08 (C3), 27.23 (Lys1 γC), 28.03 (Lys2 γC), 28.06 (Lys1 βC), 28.09 (Lys2 βC), 28.22 (C2), 31.81 (Lys2 αC), 32.16 (Lys2 αC), 32.46 (Ala2 αC), 32.52 (Ala2 αC), 36.15 (DNJ C1), 40.48 (DNJ C6), 50.27 (C6), 54.31 (DNJ C4), 54.48 (DNJ C2), 54.73 (DNJ C3), 55.30 (DNJ C5), 67.38 (Lys2 εC), 68.85 (Lys1 εC), 172.91 (Ala1 CO), 174.01 (Ala2 CO), 174.33 (Lys1 CO), 174.59 (Lys2 CO), 175.98 (C1).

HR-MS: ($C_{30}H_{58}N_8O_9$) theoretical *m/z* 676.4240 $[M+H]^+$, found *m/z* 676.4213

$[M+H]^+$

HPLC trace (Program B):

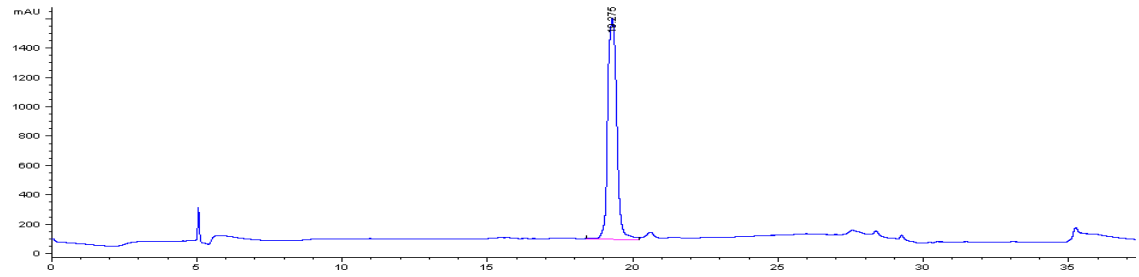

DNJ-TAT

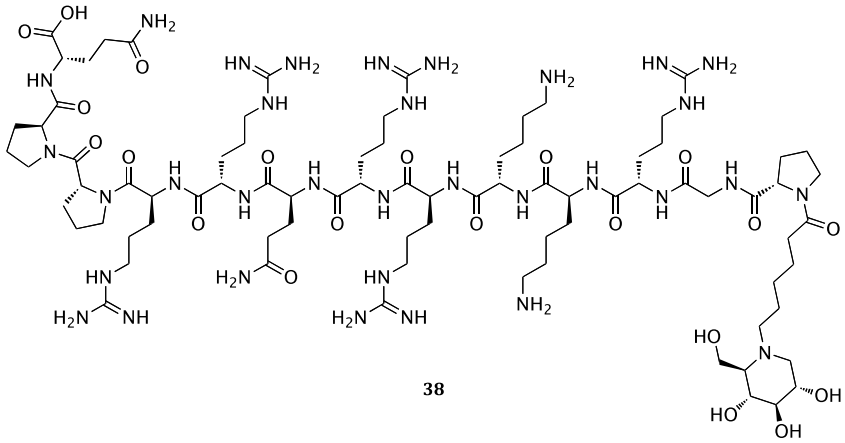

38

^{1}H NMR (D_2O, 500 MHz) δ 0.81-0.84 (m, 10H, Arg1 δH, Arg2 δH, Arg3 δH, Arg4 δH, Arg5 δH), 0.85-0.88 (m, 2H, H4), 1.20-1.22 (m, 2H, H3), 1.22-1.29 (m, 6H, Pro1 δH, Pro2 δH, Pro3 δH), 1.29-1.34 (m, 14H, Arg1 βH, Arg2 βH, Arg3 βH, Arg4 βH, Arg5 βH, Lys1 δH, Lys2 δH), 1.38-1.42 (m, 4H, Lys1 βH, Lys2 βH), 1.46-1.49 (m, 4H, Lys1 γH, Lys2 γH), 1.52-1.63 (m, 18H, Arg1 γH, Arg2 γH, Arg3 γH, Arg4 γH, Arg5 γH, Pro1 βH, Pro2 βH, Pro3 βH, H5), 1.70-1.72 (m, 2H, Lys2 εH), 1.85-1.85 (m, 2H, Lys1 εH), 2.08-2.17 (m, 2H, Gln1 βH), 2.22-2.29 (m, 2H, Gln2 βH), 2.31-2.36 (m, 2H, Gln1 δH), 2.93-2.96 (m, 8H, Pro1 γH, Pro2 γH, Pro3 γH, Gln2 δH), 3.12 (t, 2H, *J*=5.5 Hz, H6b), 3.14-3.17 (m, 1H, DNJ H2), 3.46-3.49 (m, 1H, DNJ H4), 3.52-3.54 (m, 1H, DNJ H5), 3.57-3.69 (m, 10H, Arg1 αH, Arg2 αH, Arg3 αH, Arg4 αH, Arg5 αH, DNJ H1b, DNJ H6a, DNJ H3, H6), 3.75-3.87 (m, 1H, DNJ H1a), 3.87-3.92 (m, 1H, Gln2 αH), 4.05-4.09 (m, 2H, Gly αH), 4.24-4.27 (m, 6H, Pro1 αH, Pro2 αH, Pro3 αH, Lys1 αH, Lys2 αH, Gln1 αH).

LR-MS (MALDI): *m/z* 1919.4 $[M+H]^+$

HPLC trace (Program B):

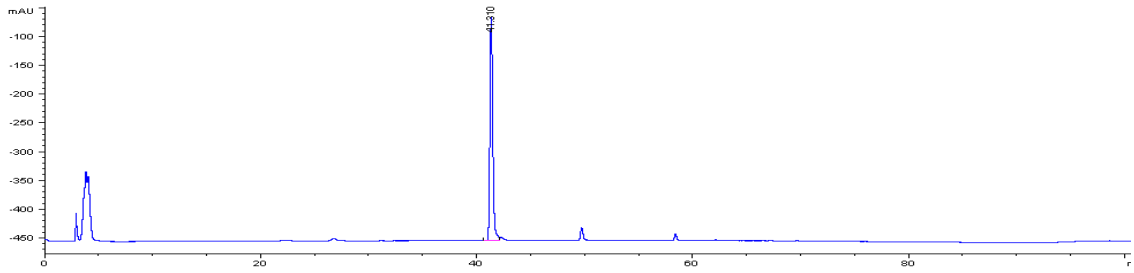

DNJ-MAP

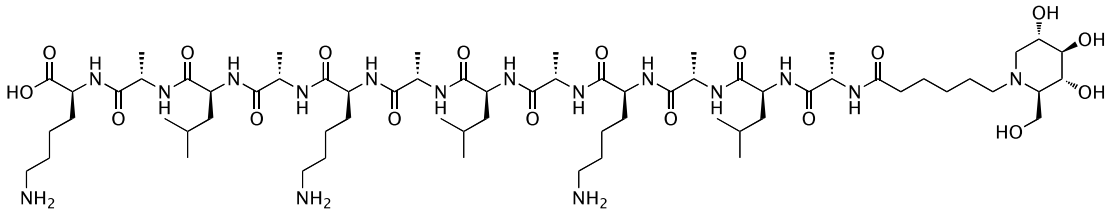

39

^{1}H NMR (D_2O, 500 MHz) δ 0.94-0.99 (m, 18H, Val1 2xMe, Val2 2xMe, Val3 2xMe), 1.30-1.48 (m, 24H, Lys1 δH, Lys2 δH, Lys3 δH, Lys1 βH, Lys2 βH, Lys3 βH, Val1 βH, Val2 βH, Val3 βH, H3, H4, H5), 1.64-1.72 (m, 12H, Lys1 εH, Lys2 εH, Lys3 εH, Lys1 γH, Lys2 γH, Lys3 γH), 1.85-1.89 (m, 3H, Val1 δH, Val2 δH, Val3 δH), 2.27-2.31 (m, 2H, H2), 2.92-2.99 (m, 6H, DNJ H3, DNJ H5, DNJ H4, DNJ H2, DNJ H6b), 3.55-3.58 (m, 2H, H6), 3.64-3.66 (m, 1H, DNJ H6a), 3.72-3.77 (m, 1H, DNJ H1b), 3.79-3.84 (m, 1H, DNJ H1a), 4.10-4.14 (m, 1H, Lys1 αH), 4.15-4.18 (m, 1H, Lys3 αH), 4.20-4.22 (m, 2H, Val2 αH, Val3 αH), 4.29-4.37 (m, 2H, Lys1 αH, Lys2 αH), 4.38-4.43 (m, 6H, Ala1 αH, Ala2 αH, Ala3 αH, Ala4 αH, Ala5 αH, Ala6 αH).

LR-MS (MALDI): *m/z* 1450.9 $[M+Na]^+$

HPLC trace (Program B):

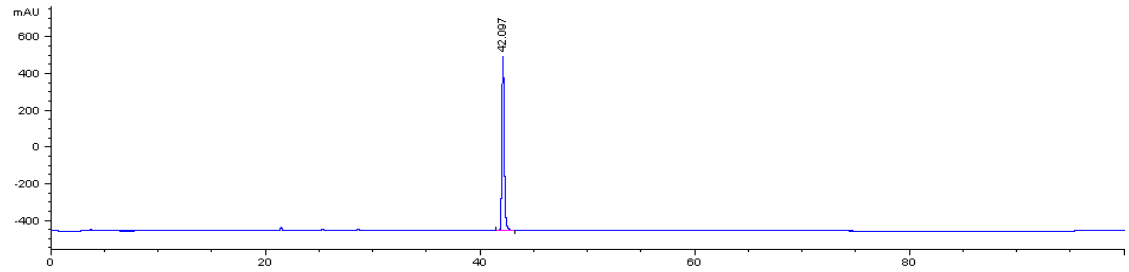

6.5. α-Glucosidase I purification

Affinity column preparation

Affi-gel 102 Gel from Bio-Rad (5 mL of packed volume) was washed with water (15 mL). *N*-(5-Carboxypentyl)-deoxynojirimycin (**8**) (27.7 mg, 0.1 mmol) was

added to water (3 mL) and the pH was adjusted with 1 M HCl to pH 5. The solution was added to the affi-gel and 1.2 M solution of EDAC (192 mg in 1 mL) was added to the mixture. The mixture was stirred at RT for 4 h and then left mixing overnight at 4°C. The gel was filtered through a scinter glass funnel and washed with 50 mM NaOAc, 0.5 M NaCl, pH 4.5 (20 mL) and 50 mM Tris/HCl, 0.5 M NaCl, pH 8 (20 mL). The functionalised affinity gel could be stored at 4°C in 0.1 M sodium phosphate, pH 7, 0.8% (w/v) Lubrol PX.

Preparation of α-glucosidase I enriched liver extract

α-Glucosidase I was purified from rat liver microsomes. 300 g of rat liver was dissected into small pieces and homogenised in 50 mM Tris/HCl buffer, pH 7.2 (1 L) using a polytron at intervals during 5-10 min, while maintaining the homogenate in an ice bath. The homogenate was then filtered through muslin and the filtrate was centrifuged at 15,000 x g for 30 min. The supernatant was recovered and centrifuged at 150,000 x g for 60 min. The pellet was then washed in the same homogenate buffer, and centrifuged at 150,000 x g for 60 min. The resulting pellet was re-suspended in 0.2 M Na Phosphate buffer, pH 6.8, 0.5% Triton X-100 (110 mL) and the suspension was stirred for 30 min 4°C. The mixture obtained was centrifuged again at 150,000 g for 30 min and the supernatant was stored to prepare α-glucosidase II extract. The pellet was re-suspended in the 0.2 M Na phosphate buffer, pH 6.8, 0.8% Lubrol PX (Buffer A), stirred for 60 min and then centrifuged at 150,000 x g for 90 min. The supernatant was finally recovered and added to *N*-(5-carboxypentyl)-deoxynojirimycin functionalised affinity gel (5 mL) and left stirring at 4°C overnight. The gel was recovered by low speed centrifugation and washed on a glass scinter funnel with buffer A (250 mL). The gel was then transferred to a 10 mL column and α-glucosidase I was eluted with 100 mM *N*B-DNJ (**4**) in Buffer A (2 x 5 mL with 15 min incubation time each). *N*B-DNJ (**4**) was then removed by dialysis (4 x 3L buffer A) with 4 h equilibration time.

The purified α-glucosidase I hydrolysed $Glc_3Man_7GlcNAc_1$ substrate (labelled with 2-Anthranilic acid [2-AA] – see section on FOS analysis) with an activity of 0.27 pmol/min/mL

6.6. α-Glucosidase II

α-Glucosidase II was prepared from rat liver by Dr. T.D. Butters, Glycobiology Institute. It was used in 80 mM Et_3N Buffer, pH 7, containing 0.5% Triton X-100, 0.1 M NaCl, 10% glycerol and 1 mg/mL BSA.

6.7. 2-AA-labelled substrates

2-AA-labelled free oligosaccharides were isolated and purified as substrates for α-glucosidases I and II from a 500 mM *N*B-DNJ (**4**) *in cellulo*, 1-day inhibition assay. The 2-AA labelled FOS were obtained as described below (see Free Oligosaccharide isolation from cells). The collected digest was passed through a 200 μL column of QEA sephardex resin Q25-200 (pre-washed with 2 x 1 mL water). The loaded resin was washed with water (2 x 1 mL) and eluted with 200 μM acetic acid (2 x 1 mL). The eluent was concentrated *in vacuo* and re-dissolved in 50% water/CH_3CN (100 μL). The resulting solution was separated by HPLC (Program A) and fluorescently labelled $Glc_3Man_7GlcNAc_1$, $Glc_3Man_7GlcNAc_1$, and $Glc_3Man_7GlcNAc_1$ were collected separately.

6.8. *In vitro* α-glucosidase I inhibition

The fluorescently labelled substrate $Glc_3Man_7GlcNAc_2$ was added to 1.5 mL Eppendorf tubes with varying concentrations of DNJ constructs and dried down under vacuum. α-Glucosidase I was added (10 μL) to obtain 25% hydrolysis in 120 min, during which linear degradation of substrate occurred. The reaction was stopped by the addition of 1 μL glacial AcOH. The samples were then dried *in vacuo* and re-suspended in 50% water/CH_3CN (60 μL) for HPLC analysis (Program A).

6.9. *In vitro* α-glucosidase II inhibition

Inhibition of α-glucosidase II was analysed in the same manner as for α-glucosidase I but using $Glc_1Man_7GlcNAc_2$ as substrate with an incubation time of 30 min to obtain 25% hydrolysis.

6.10. Free oligosaccharide isolation from cells

CHO-K1 cells were seeded in 6-well plates (2.5 x 10^5 cells/mL – 2 mL) and allowed to recover overnight. Fresh medium containing DNJ constructs (in water) or water as control was added after washing the cells with PBS (2 x 1 mL) and the cell cultures were incubated for 24 h. After this time, the medium was removed and the cells were washed with PBS (2 x 1 mL), before being scraped into PBS (2 mL). The cells were then centrifuged (2,000 rpm for 5 min), PBS was decanted and the cell pellet was re-suspended in PBS (500 μL). The cells were manually homogenised and an aliquot (30 μL) of each sample was separated for protein concentration determination. The homogenate was desalted and deproteinated by passage through a mixed-bed ion-exchange column [380 μL packed resin of AG50W-X12 (H^+ 100-200 mesh) over 500 μL packed resin of AG3-X4 (OH^-, 100-200 mesh) – 4 mL water elution] pre-equilibrated with water (4 mL). The eluent was concentrated *in vacuo* and re-suspended in water (30 μL). The FOS were labelled with 2-AA by incubating at 80°C for 1 h with labelling buffer (45 mg of anthranilic acid and 67.5 mg $NaCHBH_3$ in 1.5 mL water – 80 μL). The resulting mixture was diluted with 1 mL 97:3 CH_3CN:water, and the solution was purified by passing it through a Speed-Amide 2 column, pre-equilibrated with water and CH_3CN (1 mL each). The column was washed with CH_3CN/water (95:5, 2 mL) and eluted with water (2 x 750 μL). 0.5 M Tris/HCl buffer, pH 7.2 (175 μL) was added to each sample. The labelled FOS were finally purified by using a ConA (Concanavalin A)-Sepharose 4B column (100 μL packed resin). The column was pre-equilibrated with water (2 x 1 mL) followed by sequential washes of 1 mM $MgCl_2$, 1 mM $CaCl_2$,1 mM $MnCl_2$ (1 mL), and 50 mM Tris/HCl buffer, pH 7.2 (2 x 1 mL). The sample was added and allowed to pass through the column before washing with 50mM Tris/HCl buffer, pH 7.2 (1 mL) and water (1 mL). The ConA-bound FOS were then eluted with hot (70◦C) 0.5 M methyl α-D-mannopyranoside in 50mM Tris/HCl buffer, pH 7.2 (2 x 1 mL). Aliquots (50 μL) of each 2-AA labelled FOS sample were diluted with CH_3CN (50 μL) and analysed by HPLC (Program A). Glucose units were determined, following comparison with a 2-AA-labelled glucose oligomer ladder (derived from a partial hydrolysate of dextran) external standard using Peak Time software (developed in-house).

The peak area of each 2-AA-labelled species was measured using Waters Empower software.

6.11. Protein analysis

Protein levels were determined using a bicinchoninic acid (BCA) protein assay (Pierce Biotechnology) according to manufacturer's instructions. In summary, BCA working solution was prepared by adding $CuSO_4$ solution (200 μL of 4% $CuSO_4 \bullet H_2O$ in water) to BCA solution (10 mL) immediately before use. BSA standards (0-1,000 μg/mL) and homogenated samples (25 μL - see above) were aliquoted in a clear 96-well plated, and the BCA working solution (200 μL) was added to each well. The plate was covered and incubated at 37◦C for 30 min, after which the absorbance at 562 nm was measured. Protein concentrations were determined by comparison to a standard curve generated with known concentrations of BSA standard (200, 400, 600, 800 and 1000 μg/mL in water).

6.12. Cytotoxicity determination

Each compound's cytotoxicity was determined using the MTS Cell proliferation assay (Promega) according to manufacturer's instructions. In summary, cells were seeded at 5,000 cells/well for 1-day assays and 2,000 cells/well for 3-day assays in clear 96-well plates. The cells were allowed to settle for 4 h, and then the media was replaced with drug containing media in various concentrations. A 2% MTS solution pH 6.5 was prepared (42 mg in 21 mL of PBS) and filtered through a 0.2 μm sterile filter. The provided PMS solution (100 μL) was diluted with 2% MTS solution (2 mL) just before use. After 24 h or 72 h of incubation with the drugs, the media was supplemented with the PMS/MTS dilution (20 μL/ well). The plate was incubated for further 4 h and the absorbance was then measured at 490 nm. The percentage cytotoxicity was determined by comparison with the cell number of untreated controls.

6.13. Synthesis of Fluorescent ER-retaining peptide constructs

KDEL and KKAA peptides were synthesised as described previously. 1.2 equivalents of FITC (140 mg, 0.36 mmol) and 1.2 equivalents of DEA (50 μL, 0.36 mmol) were added to a suspension of the resins (0.3 mmol) in DMF (30 mL). The

reaction mixtures were allowed to stir at RT for 3 h, after which they were washed and cleaved with the conditions described previously.

As described in the previous section, fluorescein thiohydantoine was obtained in a 55% yield (m.p. 178.0-180.0°C).

Addition of Fmoc-aminohexanoic acid as an extra amino acid in the peptide sequence, following by the same treatment with FITC as described above generated the desired FITC labelled amino acids.

FITC- KDEL

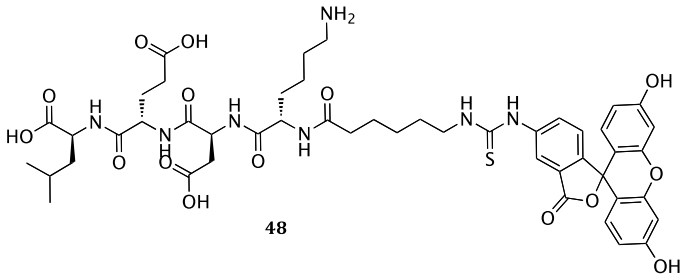

48

Compound **48** was obtained as an orange powder (5% overall yield, 15 mg, 0.015 mmol).

^{1}H NMR (MeOD-d$_4$, 500 MHz) δ 0.97 (dd, 3H, *J*=15.3 Hz, 6.3 Hz, Val Me), 1.03 (dd, 3H, *J*=7.7 Hz, 6.3 Hz, Val Me), 1.44-1.53 (m, 4H, Lys βH, H4), 1.65-1.80 (m, 12H, Glu βH, Asp βH, Val βH, Lys δH, H3, H5), 1.86-1.93 (m, 1H, Val δH), 2.84 (d, 2H, *J*=5.5 Hz, Glu δH), 2.97 (t, 4H, *J*=7.5 Hz, Lys γH, H2), 4.31-4.42 (m, 3H, Lys αH, Glu αH, Asp αH), 4.63 (t, 1H, *J*=5.6 Hz, Val αH), 4.60-4.69 (m, 4H, Lys εH, H6), 6.58 (dd, 2H, *J*=8.6 Hz, 2.5 Hz, FITC PhB H2), 6.68-6.71 (m, 4H, FITC PhB H4, FITC PhB H5), 7.15-7.19 (m, 1H, FITC PhA H6), 7.74-7.80 (m, 1H, FITC PhA H2), 8.17-8.27 (m, 1H, FITC PhA H3).

LR-MS (ESI): *m/z* 1006.5 [M+H]$^+$

HPLC trace (Program B):

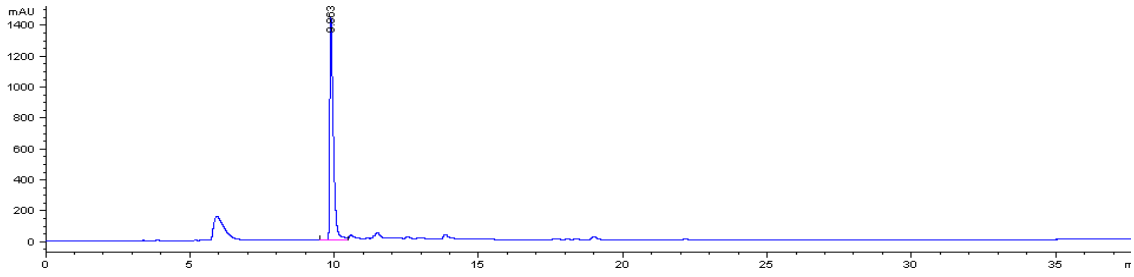

FITC-KKAA

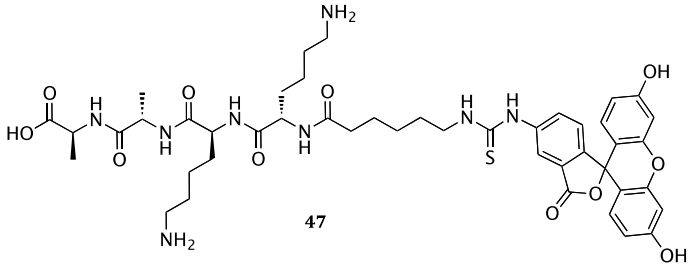

47

Compound **47** was obtained as an orange powder (18% overall yield, 48.2 mg, 0.054 mmol).

^{1}H NMR (D_2O, 500 MHz) δ 1.22-1.33 (m, 14H, H3, H4, Lys1 γH, Lys2 γH, Ala1 βH, Ala2 βH), 1.48-1.62 (m, 10H, Lys1 βH, Lys2 βH, H5, Lys1 γH, Lys2 γH), 2.15-2.24 (m, 2H, H2), 2.85-2.87 (m, 4H, Lys1 εH, Lys2 εH), 3.43-3.47 (t, 2H, *J*=7.5 Hz, H6), 4.11-4.21 (m, 4H, Ala1 αH, Ala2 αH, Lys1 αH, Lys2 αH), 6.78 (dd, 2H, *J*=9.1 Hz, 2.1 Hz, FITC PhB H2), 6.90 (d, 2H, *J*=2.3 Hz, FITC PhB H4), 7.17 (t, 3H, *J*=8.7 Hz, FITC PhA H6, FITC PhB H5), 7.56 (d, 1H, *J*=7.1 Hz, FITC PhA H2), 7.93 (s, 1H, FITC PhA H3).

^{13}C {^{1}H} NMR (MeOD-d_4, 125 MHz) δ 16.15 (Ala1 Me), 16.79 (Ala2 Me), 22.02 (Lys1 δH), 22.43 (Lys2 δH), 25.13 (Lys1 βH), 26.05 (Lys βH), 26.53 (C4), 26.74 (C3), 28.18 (C5), 30.78 (Lys1 γH), 31.13 (Lys2 γH), 35.06 (C2), 35.14 (Ala2 αC), 39.06 (Ala1 αC), 39.10 (Lys2 αC), 39.12 (Lys1 αC), 48.80 (FITC C), 48.82 (C6), 52.79 (Lys2 εC), 53.35 (Lys1 εC), 102.15 (FITC PhA C2), 104.66 (FITC PhA C3), 104.95 (FITC PhA C4), 105.32 (FITC PhA C6), 107.49 (FITC PhA C5), 110.40 (FITC PhA C1), 112.64 (FITC PhB C5), 112.66 (FITC PhB C4, FITC PhB C6), 114.24 (FITC PhB C2), 129.06 (FITC PhB C1), 129.11 (FITC PhB C3), 172.18 (FITC CO), 172.74 (C1), 172.98 (Ala2 CO), 173.17 (Ala1 CO), 174.19 (Lys2 CO), 175.00 (Lys1 CO), 188.75 (CS).

m.p.: 126.0-127.2°C

LR-MS (ESI): *m/z* 919.7 $[M+H]^+$

HPLC trace (Program B):

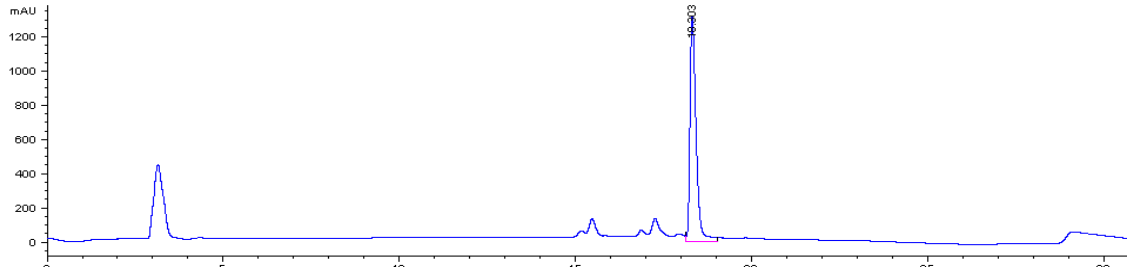

6.14. Fluorescence microscopy and immunolocalisation

12 mm coverslips were washed with EtOH and allowed to dry. The dry coverslips were set in 24-well plates and covered with a solution of poly-L-lysine bromide (120 μL of 50 μg/mL in water). The coverslips were incubated at 37°C for 1 h. The coverslips were then washed with water and allowed to dry. 20,000 cells per well were added in media (100 μL) and incubated overnight. The media was then drained and replaced by media containing the FITC labelled peptides (100 μM) and the cells were incubated for a further 24 h. After this time, the media was removed and the coverslips were washed with PBS (2 x 1 mL). The cells were then fixed with 4% paraformaldehyde in PBS (100 μL) at RT for 30 min. The coverslips were then washed with cold PBS (2 x 2 mL), and then blocked with a 5% BSA solution in PBS (1 mL) for 1 h. After removing the BSA solution from the wells, the cells were permeabilised with 1% Triton-X-100 solution in PBS (1 mL) for 20 min. The cells were then washed twice by incubation with 1% Tween-20 in PBS (1 mL) for 10 min, followed by removal of the solution. A solution of PDI antibody (1:500 dilution, 80 μL) in 5% BSA in PBS was added to each coverslip and incubated for 1 h at RT. The unbound primary antibody was washed away with 1% Tween-20 in PBS (3 x 1 mL for 15 min). The secondary antibody (Alexa Fluor 633, 1:500 dilution, 80 μL) was added to each coverslip and incubated at RT for 1 h, protected from light. The coverslips were then washed with 1% Tween-20 in PBS (3 x 1 mL for 15 min) to remove excess antibody. Finally, the coverslips were mounted on the slides by adding a drop of Vectashield mounting medium (with DAPI) to the slide and sealing the slide with nail varnish.

6.15. FACS

Cells were seeded at 2 x 10^4 cells (400 μL) per well in a 24-well plate for 3 day-long experiments and at 5 x 10^4 cells per well for 1-day experiments and allowed to recover overnight. The media was then exchanged for media containing FITC-labelled peptides and incubated for the required amount of time, after which the media was removed and the cells were washed with PBS (2 x 1 mL). The cells were detached by treatment with trypsin-containing EDTA (100 μL) for 20 min at 37°C, after which trypsin was neutralised by addition of 20% FCS in media (400 μL). The cells were centrifuged at 2000 rpm for 5 min, and the media was discarded. The pellet was re-suspended in PBS containing PI (1:500 dilution, 1 mL) and analysed directly by FACS.

7. References

1. Fischer, P.B.; Karlsson, G.B.; Butters, T.D.; Dwek, R.A. and Platt, F.M. *N*-Butyldeoxynojirimycin-mediated inhibition of human immunodeficiency virus entry correlates with changes in antibody recognition of the V1/V2 region of gp120. *Journal of Virology*. 1996;70(10):7143-52.

2. Karlsson, G.B.; Butters, T.D.; Dwek, R.A. and Platt, F.M. Effects of the imino sugar *N*-butyldeoxynojirimycin on the *N*-glycosylation of recombinant gp120. *The Journal of Biological Chemistry*. 1993;268(1):570-6.

3. Dwek, R.A.; Butters, T.D.; Platt, F.M. and Zitzmann, N. Targeting glycosylation as a therapeutic approach. *Nature Reviews. Drug Discovery*. 2002;1(1):65-75.

4. Gabius, H-J. ed. *The Sugar Code*. 1st ed. Wiley-Blackwell; 2009:569.

5. Burda, P. and Aebi, M. The dolichol pathway of *N*-linked glycosylation. *Biochimica et Biophysica Acta*. 1999;1426(2):239-57.

6. Alberts, B.; Johnson, A.; Lewis, J.; Raff, M.; Roberts, K. and Watson, J.D. eds. *Molecular Biology of the Cell*. 4th ed. London: Garland Science; 2002.

7. Yan, Q. and Lennarz, W.J. Oligosaccharyltransferase: a complex multisubunit enzyme of the endoplasmic reticulum. *Biochemical and Biophysical Research Communications*. 1999;266(3):684-9.

8. Silberstein, S. and Gilmore, R. Biochemistry, molecular biology, and genetics of the oligosaccharyltransferase. *The FASEB Journal*. 1996;10:849-58.

9. Kelleher, D.J. and Gilmore, R. An evolving view of the eukaryotic oligosaccharyltransferase. *Glycobiology*. 2006;16(4):47R-62R.

10. Helenius, A. and Aebi, M. Roles of *N*-linked glycans in the endoplasmic reticulum. *Annual Review of Biochemistry*. 2004;73:1019-49.

11. Helenius, J.; Ng, D.T.W.; Marolda, C.L.; Water, P.; Valvano, M.A. and Aebi, M. Translocation of lipid-linked oligosaccharides across the ER membrane requires Rft1 protein. *Nature*. 2002;415(6870):447-50.

12. Shailubhai, K.; Pukazhenthi, B.S.; Saxena, E.S.; Varma, G.M. and Vijay, I.K. Glucosidase I, a transmembrane endoplasmic reticular glycoprotein with a luminal catalytic domain. *The Journal of Biological Chemistry*. 1991;266(25):16587-93.

13. Grinna, L.S. and Robbins, P.W. Substrate specificities of rat liver microsomal glucosidases which process glycoproteins. *The Journal of Biological Chemistry*. 1980;255(6):2255-8.

14. Trombetta, E.S.; Simons, J.F. and Helenius, A. Endoplasmic reticulum glucosidase II is composed of a catalytic subunit, conserved from yeast to mammals, and a tightly bound noncatalytic HDEL-containing subunit. *The Journal of Biological Chemistry*. 1996;271(44):27509-16.

15. Wilson, C.M. and High, S. Ribophorin I acts as a substrate-specific facilitator of *N*-glycosylation. *Journal of Cell Science*. 2007;120(Pt 4):648-57.

16. Ware, F.E.; Vassilakos, A.; Peterson, P.A.; Jackson, M.R.; Lehrman, M.A. and Williams, D.B. The molecular chaperone Calnexin binds Glc1Man9GlcNAc2 oligosaccharide as an initial step in recognizing unfolded glycoproteins. *The Journal of Biological Chemistry*. 1995;270(9):4697-704.

17. Lindquist, J.A., Hämmerling, G.J. and Trowsdale, J. ER60/ERp57 forms disulfide-bonded intermediates with MHC class I heavy chain. *The FASEB Journal : Official publication of the Federation of American Societies for Experimental Biology*. 2001;15(8):1448-50.

18. Deprez, P.; Gautschi, M. and Helenius, A. More than one glycan is needed for ER glucosidase II to allow entry of glycoproteins into the calnexin/calreticulin cycle. *Molecular Cell*. 2005;19(2):183-95.

19. Taylor, S.C.; Ferguson, A.D.; Bergeron, J.J.M. and Thomas, D.Y. The ER protein folding sensor UDP-glucose glycoprotein-glucosyltransferase modifies substrates distant to local changes in glycoprotein conformation. *Nature Structural & Molecular Biology*. 2004;11(2):128-34.

20. Caramelo, J.J. and Parodi, A.J. How sugars convey information on protein conformation in the endoplasmic reticulum. *Seminars in Cell & Developmental Biology*. 2007;18(6):732-42.

21. Ellgaard, L. and Helenius, A. Quality control in the endoplasmic reticulum. *Nature Reviews. Molecular Cell Biology*. 2003;4(3):181-91.

22. Roth, J.; Yam, G.H-F.; Fan, J.; Hirano, K.; Gaplovska-Kysela, K.; Le Fourn, V.; Guhl, B.; Santimaria, R.; Torossi, T.; Ziak, M. and Zuber, C. Protein quality control: the who's who, the where's and therapeutic escapes. *Histochemistry and Cell Biology*. 2008;129(2):163-77.

23. Spiro, R.G. Glucose residues as key determinants in the biosynthesis and quality control of glycoproteins with *N*-linked oligosaccharides. *The Journal of Biological Chemistry*. 2000;275(46):35657-60.

24. Tang, B.L.; Wang, Y.; Ong, Y.S. and Hong, W. COPII and exit from the endoplasmic reticulum. *Biochimica et Biophysica Acta*. 2005;1744(3):293-303.

25. Tokunaga, F.; Brostrom, C.; Koide, T. and Arvan, P. Endoplasmic reticulum (ER)-associated degradation of misfolded *N*-linked glycoproteins is suppressed upon inhibition of ER mannosidase I. *The Journal of Biological Chemistry*. 2000;275(52):40757-64.

26. Weng, S. and Spiro, R.G. Demonstration that a kifunensine-resistant alpha-mannosidase with a unique processing action on *N*-linked oligosaccharides occurs in rat liver endoplasmic reticulum and various cultured cells. *The Journal of Biological Chemistry*. 1993;268(34):25656-63.

27. Vashist, S.; Kim, W.; Belden, W.J.; Spear, E.D.; Barlowe, C. and Ng, D.T. Distinct retrieval and retention mechanisms are required for the quality control of endoplasmic reticulum protein folding. *The Journal of Cell Biology*. 2001;155(3):355-68.

28. Carvalho, P.; Goder, V.; Rapoport, T.A. Distinct ubiquitin-ligase complexes define convergent pathways for the degradation of ER proteins. *Cell*. 2006;126(2):361-73.

29. Gauss, R., Jarosch, E.; Sommer, T. and Hirsch, C. A complex of Yos9p and the HRD ligase integrates endoplasmic reticulum quality control into the degradation machinery. *Nature Cell Biology*. 2006;8(8):849-54.

30. Mancini, R.; Aebi, M. and Helenius, A. Multiple endoplasmic reticulum-associated pathways degrade mutant yeast carboxypeptidase Y in mammalian cells. *The Journal of Biological Chemistry*. 2003;278(47):46895-905.

31. Weng, S. and Spiro, R.G. Demonstration of a peptide: *N*-glycosidase in the endoplasmic reticulum of rat liver. *Biochemistry Journal*. 1997;322:655-61.

32. Suzuki, T.; Park, H. and Lennarz, W.J. Cytoplasmic peptide:*N*-glycanase (PNGase) in eukaryotic cells: occurrence, primary structure, and potential functions. *The FASEB Journal : Official publication of the Federation of American Societies for Experimental Biology*. 2002;16(7):635-41.

33. Suzuki, T.; Kitajima, K.; Emori, Y.; Inoue, Y. and Inoue, S. Site-specific de-*N*-glycosylation of diglycosylated ovalbumin in hen oviduct by endogenous peptide:

N-glycanase as a quality control system for newly synthesized proteins. *Proceedings of the National Academy of Sciences of the United States of America*. 1997;94(12):6244-9.

34. Katiyar, S.; Li, G. and Lennarz, W.J. A complex between peptide:*N*-glycanase and two proteasome-linked proteins suggests a mechanism for the degradation of misfolded glycoproteins. *Proceedings of the National Academy of Sciences of the United States of America*. 2004;101(38):13774-9.

35. Lee, J-H.; Choi, J.M.; Lee, C.; Yi, K.J. and Cho, Y. Structure of a peptide:*N*-glycanase-Rad23 complex: insight into the deglycosylation for denatured glycoproteins. *Proceedings of the National Academy of Sciences of the United States of America*. 2005;102(26):9144-9.

36. Wiertz, E.J.H.J.; Tortorella, D.; Bogyo, M.; Yu, J.; Mothes, W.; Jones, T.; Rapoport, R.A. and Ploegh, H.L. Sec61-mediated transfer of a membrane protein from the endoplasmic reticulum to the proteasome for destruction. *Nature*. 1996:432-8.

37. Misaghi, S.; Pacold, M.E.; Blom, D.; Ploegh, H.L. and Korbel, G.A. Using a small molecule inhibitor of peptide: *N*-glycanase to probe its role in glycoprotein turnover. *Chemistry & Biology*. 2004;11(12):1677-87.

38. Cacan, R.; Mir, A-M.; Verbert, A.; Verbert, A. an Krag, S.S. Occurrence of a cytosolic neutral chitobiase activity involved in oligomannoside degradation: a study with Madin-Darby bovine kidney (MDBK) cells. *Biochemistry Journal*. 1996;313:597-602.

39. Tulsiani, D.R. and Touster, O. Substrate specificities of rat kidney lysosomal and cytosolic alpha-D-mannosidases and effects of swainsonine suggest a role of the cytosolic enzyme in glycoprotein catabolism. *The Journal of Biological Chemistry*. 1987;262(14):6506-14.

40. Durrant, C. and Moore, S.E.H. Perturbation of free oligosaccharide trafficking in endoplasmic reticulum glucosidase I-deficient and castanospermine-treated cells 1. *Biochemistry Journal*. 2002;247(May 2001):239-47.

41. Cacan, R.; Duvet, S.; Labiau, O.; Verbert, A.; and Krag, S.S. Monoglucosylated oligomannosides are released during the degradation process of newly synthesized glycoproteins. *The Journal of Biological Chemistry*. 2001;276(25):22307-12.

42. Yanagida, K.; Natsuka, S. and Hase, S. Structural diversity of cytosolic free oligosaccharides in the human hepatoma cell line, HepG2. *Glycobiology*. 2006;16(4):294-304.

43. Mellor, H.R.; Neville, D.C.A.; Harvey, D.J.; Platt, F.M.; Dwek, R.A. and Butters, T.D. Cellular effects of deoxynojirimycin analogues: uptake, retention and inhibition of glycosphingolipid biosynthesis. *The Biochemical Journal*. 2004;381(Pt 3):861-6.

44. Alonzi, D.S.; Neville, D.C.A.; Lachmann, R.H.; Dwek, R.A. and Butters, T.D. Glucosylated free oligosaccharides are biomarkers of endoplasmic-reticulum alpha-glucosidase inhibition. *The Biochemical Journal*. 2008;409(2):571-80.

45. Saint-Pol, A.; Codogno, P. and Moore, S.E. Cytosol-to-lysosome transport of free polymannose-type oligosaccharides. Kinetic and specificity studies using rat liver lysosomes. *The Journal of Biological Chemistry*. 1999;274(19):13547-55.

46. Moore, S.E.; Bauvy, C. and Codogno, P. Endoplasmic reticulum-to-cytosol transport of free polymannose oligosaccharides in permeabilized HepG2 cells. *The EMBO Journal*. 1995;14(23):6034-42.

47. Moore, E.H. and Spiro, G. Demonstration that golgi endo-cu-D-mannosidase provides a pathway for the formation of complex oligosaccharides of glycoproteins. *Biological Chemistry*. 1990;265(22):13104-12.

48. Moore, S.E. and Spiro, R.G. Characterization of the endomannosidase pathway for the processing of *N*-linked oligosaccharides in glucosidase II-deficient and parent mouse lymphoma cells. *The Journal of Biological Chemistry*. 1992;267(12):8443-51.

49. Zuber, C.; Spiro, M.J.; Guhl, B.; Spiro, R.G. and Roth, J. Golgi apparatus immunolocalization of endomannosidase suggests post-endoplasmic reticulum glucose trimming: implications for quality control. *Molecular Biology of the Cell*. 2000;11(12):4227-40.

50. Kamiya, Y.; Yamaguchi, Y.; Takahashi, N.; Arata, Y.; Kasai, K-I.; Ihara, Y.; Matsuo, I.; Ito, Y.; Yamamoto, K. and Kato, K. Sugar-binding properties of VIP36, an intracellular animal lectin operating as a cargo receptor. *The Journal of Biological Chemistry*. 2005;280(44):37178-82.

51. Ahner, A. and Brodsky, J. Checkpoints in ER-associated degradation: excuse me, which way to the proteasome? *Trends in Cell Biology*. 2004;14(9):474-8.

52. Nishikawa, S.I.; Fewell, S.W.; Kato, Y. and Brodsky, J.L. Endo T. Molecular chaperones in the yeast endoplasmic reticulum maintain the solubility of proteins for retrotranslocation and degradation. *The Journal of Cell Biology*. 2001;153(5):1061-70.

53. Kukushkin, N.V.; Alonzi, D.S.; Dwek, R.A. and Butters, T.D. Demonstration that endoplasmic reticulum-associated degradation of glycoproteins can occur downstream of processing by endomannosidase. *The Biochemical Journal*. 2011;438(1):133-42.

54. Winchester, B. and Fleet, G.W. Amino-sugar glycosidase inhibitors: versatile tools for glycobiologists. *Glycobiology*. 1992;2(3):199-210.

55. Brumshtein, B.; Aguilar-Moncayo, M.; García-Moreno, M.I.; Ortiz Mellet, C.; Garcia Fernandez, J.M.; Silman, I.; Shaaltiel, Y.; Aviezer, D.; Sussman, J.L. and Futerman, A.H. 6-Amino-6-deoxy-5,6-di-*N*-(*N*'-octyliminomethylidene)nojirimycin: synthesis, biological evaluation, and crystal structure in complex with acid beta-glucosidase. *ChemBioChem : a European Journal of Chemical Biology*. 2009;10(9):1480-5.

56. Asano, N.; Nash, R.J.; Molyneux, R.J. and Fleet, G.W.J. Sugar-mimic glycosidase inhibitors: natural occurrence, biological activity and prospects for therapeutic application. *Tetrahedron: Asymmetry*. 2000;11(8):1645-80.

57. Saunier, B.; Kilker, R.D.; Tkacz, J.S.; Quaroni, A. and Herscovics, A. Inhibition of *N*-linked complex oligosaccharide formation by 1-deoxynojirimycin, an inhibitor of processing glucosidases. *The Journal of Biological Chemistry*. 1982;257(23):14155-61.

58. Butters, T. Molecular requirements of imino sugars for the selective control of *N*-linked glycosylation and glycosphingolipid biosynthesis. *Tetrahedron: Asymmetry*. 2000;11(1):113-24.

59. Borges de Melo, E.; Silveira Gomes, A. and Carvalho, I. α- and β-Glucosidase inhibitors: chemical structure and biological activity. *Tetrahedron*. 2006;62(44):10277-302.

60. Mellor, H.R.; Nolan, J.; Pickering, L.; Wormald, M.R.; Platt, F.M.; Dwek, R.A.; Fleet, G.W.J. and Butters, T.D. Preparation, biochemical characterization and biological properties of radiolabelled *N*-alkylated deoxynojirimycins. *Biochemistry Journal*. 2002;233:225-33.

61. Platt, F.M.; Neises, G.R.; Dwek, R.A. and Butters, T.D. *N*-butyldeoxynojirimycin is a novel inhibitor of glycolipid biosynthesis. *The Journal of Biological Chemistry*. 1994;269(11):8362-5.

62. Tan, A., Broek, L. van den; Boeckel, S. van; Ploegh, H. and Bolscher, J. Chemical modification of the glucosidase inhibitor 1-deoxynojirimycin. Structure-activity relationships. *The Journal of Biological Chemistry*. 1991;266(22):14504-10.

63. Platt, F. and Cox, T. Substrate reduction therapy. In: *Gaucher Disease*. CRC Press; 2006:355-76.

64. Cox, T.; Lachmann, R.; Hollak, C.; Aerts, J.; van Weely, S.; Hrebicek, M.; Platt, F.; Butters, T.; Dwek, R.; Moyses, C.; Gow, I.; Elstein, D.; and Zimran, A. Novel oral treatment of Gaucher's disease with *N*-butyldeoxynojirimycin (OGT 918) to decrease substrate biosynthesis. *The Lancet*. 2000;355:1481-5.

65. Zedek, S. Sustained therapeutic effects of oral miglustat 918 in type I Gaucher disease. *Glycobiology*. 2004;27:757-66.

66. Platt, F.M.; Neises, G.R.; Karlsson, G.B.; Dwek, R.A. and Butters, T.D. *N*-butyldeoxygalactonojirimycin inhibits glycolipid biosynthesis but does not affect *N*-linked oligosaccharide processing. *The Journal of Biological Chemistry*. 1994;269(43):27108-14.

67. Durantel, D.; Branza-nichita, N.; Carroue, S.; Butters, T.D.; Dwek R.A. and Zitzmann, N. Study of the mechanism of antiviral action of iminosugar derivatives against bovine viral diarrhea virus. *Journal of Virology*. 2001;75(19):8987-98.

68. Zitzmann, N.; Mehta, A.S.; Carrouée, S.; Butters, T.D.; Platt, F.M.; McCauley, J.; Blumberg, B.S.; Dwek, R.A. and Block, T.M. Imino sugars inhibit the formation and secretion of bovine viral diarrhea virus, a pestivirus model of hepatitis C virus: implications for the development of broad spectrum anti-hepatitis virus agents. *Proceedings of the National Academy of Sciences of the United States of America*. 1999;96(21):11878-82.

69. Gruters, R.A.; Neefjes, J.; Tersmette, M.; Goede, R.E.Y.; Tulp, A.; Huisman, H.G.; Miedema, F. and Ploegh, H.L. Interference with HIV-induced syncytium formation and viral infectivity by inhibitors of trimming glucosidase. *Letters to Nature*. 1987;330(5):74-7.

70. Walker, B.D.; Kowalski, M.; Goh, W.C.; Kozarsky, K.; Krieger, M.; Rosen, C.; Rohrschneider, L.; Haseltine, W.A. and Sodroski, J. Inhibition of human immunodeficiency virus syncytium formation and virus replication by

castanospermine. *Proceedings of the National Academy of Sciences of the United States of America*. 1987;84(22):8120-4.

71. Fischer, P.B.; Karlsson, G.B.; Dwek, R.A. and Platt, F.M. *N*-butyldeoxynojirimycin-mediated inhibition of human immunodeficiency virus entry correlates with impaired gp120 shedding and gp41 exposure. *Journal of Virology*. 1996;70(10):7153-60.

72. Tierney, M.; Pottage, J.; Kessler, H.; Fischl, M.; Richman, D.; Merigan, T.; Powderly, W.; Smith, S.; Karim, A. and Sherman, J. The tolerability and pharmacokinetics of N-butyl-deoxynojirimycin in patients with advanced HIV disease (ACTG 100). *The AIDS Clinical Trials Group (ACTG) of the National Institute of Allergy and Infectious Diseases.* 1995:549-53.

73. Block, T.M.; Lu, X.; Mehta, A.S.; Blumberg, B.; Tennant, B.; Ebling, M.; Korba, B.; Lansky, D.M.; Jacob, G.S. and Dwek, R. Treatment of chronic hepadnavirus infection in a woodchuck animal model with an inhibitor of protein folding and trafficking. *Nature Medicine*. 1998;4(5):610-4.

74. Pavlović, D.; Neville, D.C.A.; Argaud, O.; Blumberg, B.; Dwek, R.A.; Discher, W.B. and Zitzmann, N. The hepatitis C virus p7 protein forms an ion channel that is inhibited by long-alkyl-chain iminosugar derivatives. *Proceedings of the National Academy of Sciences of the United States of America*. 2003;100(10):6104-8.

75. Branza-Nichita, N.; Durantel, D.; Carroue, S.; Dwek, R.A. and Zitzmann, N. Antiviral effect of *N*-butyldeoxynojirimycin against bovine viral diarrhea virus correlates with misfolding of E2 envelope proteins and impairment of their association into E1-E2 heterodimers. *Journal of Virology*. 2001;75(8):3527-36.

76. Butters, T.D.; Dwek, R.A. and Platt, F.M. Imino sugar inhibitors for treating the lysosomal glycosphingolipidoses. *Glycobiology*. 2005;15(10):43R-52R.

77. Kolter, T. and Sandhoff, K. Recent advances in the biochemistry of sphingolipidoses. *Brain Pathology (Zurich, Switzerland)*. 1998;8(1):79-100.

78. Sawkar, A.R.; Cheng, W-C.; Beutler, E.; Wong, C.; Balch, W.E. and Kelly, J.W. Chemical chaperones increase the cellular activity of N370S beta-glucosidase: a therapeutic strategy for Gaucher disease. *Proceedings of the National Academy of Sciences of the United States of America*. 2002;99(24):15428-33.

79. Yam, G.H-F.; Zuber, C. and Roth, J. A synthetic chaperone corrects the trafficking defect and disease phenotype in a protein misfolding disorder. *The*

FASEB Journal : Official publication of the Federation of American Societies for Experimental Biology. 2005;19(1):12-8.

80. Fan, J.Q.; Ishii, S.; Asano, N. and Suzuki, Y. Accelerated transport and maturation of lysosomal alpha-galactosidase A in Fabry lymphoblasts by an enzyme inhibitor. *Nature Medicine*. 1999;5(1):112-5.

81. Asano, N.; Ishii, S.; Kizu, H.; Ikeda, K.; Yasuda, K.; Kato, A.; martin, O.R. and Fan, J.Q. *In vitro* inhibition and intracellular enhancement of lysosomal alpha-galactosidase A activity in Fabry lymphoblasts by 1-deoxygalactonojirimycin and its derivatives. *European Journal of Biochemistry / FEBS*. 2000;267(13):4179-86.

82. Tropak, M.B.; Reid, S.P.; Guiral, M.; Withers, S.G. and Mahuran, D. Pharmacological enhancement of beta-hexosaminidase activity in fibroblasts from adult Tay-Sachs and Sandhoff patients. *The Journal of Biological Chemistry*. 2004;279(14):13478-87.

83. Tominaga, L.; Ogawa, Y.; Taniguchi, M.; Ohno, K.; Matsuda, J.; Oshima, A.; Suzuki, Y. and Nanba, E. Galactonojirimycin derivatives restore mutant human beta-galactosidase activities expressed in fibroblasts from enzyme-deficient knockout mouse. *Brain & Development*. 2001;23(5):284-7.

84. Norez, C.; Noel, S.; Wilke, M.; Bijvelds, M.; Jorna, H.; Melin, P.; DeJonge, H. and Becq, F. Rescue of functional delF508-CFTR channels in cystic fibrosis epithelial cells by the alpha-glucosidase inhibitor miglustat. *FEBS Letters*. 2006;580(8):2081-6.

85. Orive, G.; Hernández, R.M.; Gascón, A.R.; Domínguez-Gil, A. and Pedraz, J.L. Drug delivery in biotechnology: present and future. *Current Opinion in Biotechnology*. 2003;14(6):659-64.

86. Allen, T.M. and Cullis, P.R. Drug delivery systems: entering the mainstream. *Science (New York, N.Y.)*. 2004;303(5665):1818-22.

87. Snyder, E.L. and Dowdy, S.F. Cell penetrating peptides in drug delivery. *Pharmaceutical Research*. 2004;21(3):389-93.

88. Emr, S.D. A mechanism of protein localization: the signal hypothesis and bacteria. *The Journal of Cell Biology*. 1980;86(3):701-11.

89. Frankel, A.D. and Pabo, C.O. Cellular uptake of the tat protein from human immunodeficiency virus. *Cell*. 1988;55:1189-93.

90. Green, M. and Loewenstein, P.M. Autonomous functional domains of chemically synthesized human immunodeficiency virus tat trans-activator protein. *Cell*. 1988;55(6):1179-88.

91. Derossi, D.; Joliot, A.H.; Chassaing, G. and Prochiantz, A. The third helix of the *Antennapedia* homeodomain translocates through biological membranes. *The Journal of Biological Chemistry*. 1994;269(14):10444-50.

92. Patel, L.N.; Zaro, J.L. and Shen, W-C. Cell penetrating peptides: intracellular pathways and pharmaceutical perspectives. *Pharmaceutical Research*. 2007;24(11):1977-92.

93. Sebbage, V. Cell-penetrating peptides and their therapeutic applications. *Bioscience Horizons*. 2009;2(1):64-72.

94. Tréhin, R. and Merkle, H.P. Chances and pitfalls of cell penetrating peptides for cellular drug delivery. *European Journal of Pharmaceutics and Biopharmaceutics : Official journal of Arbeitsgemeinschaft für Pharmazeutische Verfahrenstechnik e.V*. 2004;58(2):209-23.

95. Pham, W.; Kircher, M.F.; Weissleder, R. and Tung, C-H. Enhancing membrane permeability by fatty acylation of oligoarginine peptides. *ChemBioChem : A European Journal of Chemical Biology*. 2004;5(8):1148-51.

96. Wender, P.A.; Mitchell, D.J.; Pattabiraman, K.; Pelkey, E.T.; Steinman, L. and Rothbard, J.B. The design, synthesis, and evaluation of molecules that enable or enhance cellular uptake: peptoid molecular transporters. *Proceedings of the National Academy of Sciences of the United States of America*. 2000;97(24):13003-8.

97. Scheller, A.; Oehlke, J.; Wiesner, B.; Dathe, M.; Krause, E.; Beyermann, M.; Melzing, M. and Bienert, M. Structural requirements for cellular uptake of alpha-helical amphipathic peptides. *Journal of Peptide Science : An official publication of the European Peptide Society*. 1999;5(4):185-94.

98. Järver, P. and Langel, U. Cell-penetrating peptides- a brief introduction. *Biochimica et Biophysica Acta*. 2006;1758(3):260-3.

99. Richard, J.P.; Melikov, K.; Vives, E.; Ramos, C.; Verbeure, B.; Gait, M.J.; Chernomordik, L.V. and Lebleu B. Cell-penetrating peptides. A reevaluation of the mechanism of cellular uptake. *The Journal of Biological Chemistry*. 2003;278(1):585-90.

100. Green, I.; Christison, R.; Voyce, C.J.; Bundell, K.R. and Lindsay, M.A. Protein transduction domains: are they delivering? *Trends in Pharmacological Sciences*. 2003;24(5):213-5.

101. Kerkis, A.; Hayashi, M.A.F.; Yamane, T. and Kerkis, I. Properties of cell penetrating peptides (CPPs). *IUBMB Life*. 2006;58(1):7-13.

102. Foerg, C. and Merkle, H.P. On the biomedical promise of cell penetrating peptides : limits versus prospects. *Journal of Pharmaceutical Sciences*. 2008;97(1):144-62.

103. Elliott, G. and O'Hare, P. Intercellular trafficking of VP22-GFP fusion proteins. *Gene Therapy*. 1999;6(1):149-51.

104. Thorén, P.E.; Persson, D.; Karlsson, M. and Nordén, B. The *Antennapedia* peptide penetratin translocates across lipid bilayers - the first direct observation. *FEBS Letters*. 2000;482(3):265-8.

105. Bian, J.; Popovic, Z.B.; Benejam, C.; Kiedrowski, M.; Rodriguez, L.L. and Penn, M.S. Effect of cell-based intercellular delivery of transcription factor GATA4 on ischemic cardiomyopathy. *Circulation Research*. 2007;100(11):1626-33.

106. Brigidou, J.; Legrand, C.; Meryl, J. and Rabie, A. The retro-inverso form of a homeobox-derived short peptide is rapidly internalised by cultured neurones: a new basis for an efficient intracellular delivery system. *Biochemical and Biophysical Research Communications*. 1995;214(2):685-93.

107. Schwarze, S.R. *In Vivo* protein transduction: delivery of a biologically active protein into the mouse. *Science*. 1999;285(5433):1569-72.

108. Muratovska, A. and Eccles, M.R. Conjugate for efficient delivery of short interfering RNA (siRNA) into mammalian cells. *FEBS Letters*. 2004;558(1-3):63-8.

109. Rothbard, J.B.; Garlington, S.; Lin, Q.; Kirschberg, T.; Kreider, E.; McGrane, P.L.; Wender, P.A.; Khavari, P.A. Conjugation of arginine oligomers to cyclosporin A facilitates topical delivery and inhibition of inflammation. *Nature Medicine*. 2000;6(11):1253-7.

110. Delcroix, M. and Riley, L.W. Cell-penetrating peptides for antiviral drug development. *Pharmaceuticals*. 2010;3(3):448-70.

111. Munro, S. and Pelham, H.R. A C-terminal signal prevents secretion of luminal ER proteins. *Cell*. 1987;48(5):899-907.

112. Jackson, M.R.; Nilsson, T. and Peterson, P.A. Identification of a consensus motif for retention of transmembrane proteins in the endoplasmic reticulum. *The EMBO Journal*. 1990;9(10):3153-62.

113. Alberts, B.; Bray, D.; Lewis, J.; Raff, M.; Roberts, K. and Watson, J.D. *Molecular Biology of the Cell*. 3rd ed. New York: Garland Science; 1994.

114. Semenza, J.C.; Hardwick, K.G.; Dean, N. and Pelham, H.R. ERD2, a yeast gene required for the receptor-mediated retrieval of luminal ER proteins from the secretory pathway. *Cell*. 1990;61(7):1349-57.

115. Lewis, M.J. and Pelham, H.R. Sequence of a second human KDEL receptor. *Journal of Molecular Biology*. 1992;226(4):913-6.

116. Pelham, H.R.; Hardwick, K.G. and Lewis, M.J. Sorting of soluble ER proteins in yeast. *The EMBO Journal*. 1988;7(6):1757-62.

117. Jackson, M.R.; Nilsson, T. and Peterson, P.A. Retrieval of transmembrane proteins to the endoplasmic reticulum. *The Journal of Cell Biology*. 1993;121(2):317-33.

118. Cosson, P. and Letourneur, F. Coatomer interaction with di-lysine endoplasmic reticulum retention motifs. *Science*. 1994;263 (5153):1629-31.

119. Best, D.; Wang, C.; Weymouth-Wilson, A.C.; Clarkson, R.A.; Wilson, F.X.; Nash, R.J.; Miyauchi, S.; Kato, A. and Fleet, G.W.J. Looking glass inhibitors: scalable syntheses of DNJ, DMDP, and (3*R*)-3-hydroxy-l-bulgecinine from D-glucuronolactone and of L-DNJ, L-DMDP, and (3*S*)-3-hydroxy-D-bulgecinine from L-glucuronolactone. *Tetrahedron: Asymmetry*. 2010;21(3):311-9.

120. Hughes, A.B. and Rudge, A.J. Deoxynojirimycin: synthesis and biological activity. *Natural Product Reports*. 1994;11(December):135.

121. Song, X. and Hollingsworth, R.I. Facile syntheses of 1-deoxynojirimycin (DNJ) and 1-deoxymannojirimycin (DMJ). *Tetrahedron Letters*. 2007;48(17):3115-8.

122. State, N.Y. and Yamazaki, N. Total dynthesis of nojirimycin and 1-deoxynojirimycin. *Synthesis*. 1987;3337(3):3337-42.

123. Zhang, G-L.; Chen, C.; Xiong, Y.; Zhang, L-H.; Ye, J.; Ye, X-S. Synthesis of *N*-substituted iminosugar derivatives and their immunosuppressive activities. *Carbohydrate Research*. 2010;345(6):780-6.

124. Gilbert, E.E. The reactions of sulfur trioxide, and of its adducts, with organic compounds. *Chemical Reviews*. 1962;62(6):549-89.

125. Corey, E.J. and Venkatswarlu, A. Protection of hydroxyl groups as *tert*-butyldimethylsilyl derivatives. *Journal of the American Chemical Society*. 1972;94(17):6190-1.

126. Dess, D.B. and Martin, J.C. A useful 12-I-5 triacetoxyperiodinane (the Dess-Martin periodinane) for the selective oxidation of primary or secondary alcohols and a variety of related 12-I-5 species. *Journal of the American Chemical Society*. 1991;113(19):7277-87.

127. Abdel-Magid, A.F.; Carson, K.G.; Harris, B.D.; Maryanoff, C.A. and Shah, R.D. Reductive amination of aldehydes and ketones with sodium triacetoxyborohydride. Studies on direct and indirect reductive amination procedures. *The Journal of Organic Chemistry*. 1996;61(11):3849-62.

128. Lloyd-Williams, P.; Albericio, F. and Giralt, E. *Chemical approaches to the synthesis of Peptides and Proteins*. Barcelona: CRC Press; 1997:278.

129. Gross, E. and Meienhofer, J. eds. *The Peptides: Analysis, Synthesis, Biology*. London: Academic Press; 1979:435.

130. Jullian, M.; Hernandez, A.; Maurras, A.; Puget, K.; Amblard, M.; Martinez, J. an Subra, G. *N*-terminus FITC labeling of peptides on solid support: the truth behind the spacer. *Tetrahedron Letters*. 2009;50(3):260-3.

131. Pedersen, C.; Bock, K. and Lundt, I. Synthesis of bromodeoxy sugars from hexoses, alditols and aldonic acids. *Synthesis*. 1978;50(1):1385-400.

132. Bashayal, B.P.; Chow, H-F.; Fellows, L.E. and Fleet, G.W.J. The synthesis of polyhydroxylated amino acids from glucoronolactone: enantiospecific synthesis of 2*S*, 3*R*, 4*R*, 5*S*-trihydroxypipecolic acid, 2*R*, 3*R*, 4*R*, 5*S*-trihydroxypipecolic acid and 2*R*, 3*R*, 4*R*-dihydroxyproline. *Synthesis*. 1987;43(2):415-22.

133. Horton, D. and Tsai, J-H. Preparation of derivatives of L-Idose and L-iduronic acid from 1,2-*O*-Usopropylidene-α-D-glucofuranose by way of acetylenic intermediates. *Carbohydrate Research*. 1977;58:89-103.

134. Krulle, T.M.; Davis, B.; Ardron, H.; Long, D.D.; Hindle, N.A.; smith, C.; Brown, D.; Lane, A.L.; Watkin, D.J.; Marquessb, D.G. and Fleet, G.W.J. Kinetic and thermodynamic azides from α-triflates and γ-lactones: intermediates for the incorporation of polyhydroxylated D- and L-α-amino acids into combinatorial libraries. *Tetrahedron*. 1996:1271-2.

135. Murao, S. and Miyata, S. Isolation and characterization of a new trehalase inhibitor, S-GI. *Agricultural and Biological Chemistry*. 1980;44(1):219-21.

136. Bosone, E.; Farina, P.; Guazzi, G.; Innocenti, S.; Marotta, V. and Valcavi, U. New synthesis of methyl 7-oxoheptanoate: an useful intermediate for the preparation of 2-(6-methoxycarbonylhexyl)-cyclopent-2-en-1-one. *Synthesis*. 1983;1983(11):942-4.

137. Steiner, A.J.; Stütz, A.E.; Tarling, C.A.; Withers, S.G. and Wrodnigg, T.M. Iminoalditol-amino acid hybrids: synthesis and evaluation as glycosidase inhibitors. *Carbohydrate Research*. 2007;342(12-13):1850-8.

138. Hettkamp, H.; Legler, G.; and Bause, E. Purification by affinity chromatography of glucosidase I, an endoplasmic reticulum hydrolase involved in the processing of asparagine-linked oligosaccharides. *European Journal of Biochemistry / FEBS*. 1984;142(1):85-90.

139. Bookser, B.C.; Kasibhatla, S.R.; Appleman, J.R. and Erion, M.D. AMP deaminase inhibitors. 2. Initial discovery of a non-nucleotide transition-state inhibitor series. *Journal of Medicinal Chemistry*. 2000;43(8):1495-507.

140. Nicolaou, K.C.; Hwang, C.K.; Marron, B.E.; DeFrees, S.A.; Couladouros, E.A.; Abe, Y.; Carroll, P.J. and Snyder, J.P. Bridging of macrodithionolactones to bicyclic systems. Synthesis and modeling of oxapolycyclic frameworks. *Journal of the American Chemical Society*. 1990;112(8):3040-54.

CHAPTER 3

Beauveriolides and their reduction of Amyloid-β by ACAT inhibition

1. Project objectives

The aims of this project are two-fold:

I) To improve the synthetic route which gives access to the beauveriolide cyclodepsipeptide family aiming to increase the overall yield, decrease the number of steps and allow more flexibility than the current synthetic methods.

II) To develop an IF-FACS-based method for rapid monitoring of Amyloid β (Aβ) reduction as a consequence of Acyl CoA: cholesterol acyl transferase (ACAT) inhibition by beauveriolides.

2. Introduction

Alzheimer's disease (AD) is the most common form of dementia, with 35.6 million people living with it in 2010, and the numbers predicted to rise rapidly in the next few years.[1] The Wentworth group is interested in several aspects of chemical biology, amongst them, the possible therapeutic application of the naturally occurring cyclodepsipeptides beuveriolides in the treatment of AD.[2]

The present introduction provides a general background on the topic and highlights key relevant information. The first section contains a brief history of the development of beauveriolides, an introduction to ACAT inhibition, and its links to atherosclerosis and AD. The second section provides a description of Alzheimer's disease and Aβ metabolism, as well as available treatments. The third section describes the link between Aβ metabolism and cholesterol, and the role of beauveriolides as ACAT inhibitors. Finally, a brief review is provided on available synthetic routes for the beauveriolide family.

The results and discussion section is divided into two subsections. The first one is focused on the synthesis of beauveriolide III and method improvements. The second one focuses on the development of a FACS-based method for monitoring

Aβ reduction as an effect of ACAT inhibition by beauveriolide III. The conclusions section provides a summary of the results obtained as well as the key conclusions that could be drawn from the results obtained. The future work section highlights the next experiments that need to be done to complete the results obtained and explore the avenues of research opened by the current work. Finally, the experimental section provides detailed procedures for the synthesis and assays completed, as well as characterisation of the synthetic products generated. References for this project are provided at the end of the chapter.

2.1. Beauveriolides

Beauveriolides are a family of fungal metabolites that have shown promising biological applications as ACAT inhibitors.[3] The first compound related to this family, beauvericin, was initially isolated from *Beauveria bassiana* for its insecticide properties.[4] Further isolations from various fungal strains yielded several structurally related compounds that were collectively termed beauveriolides.[5,6,7,8] Beauveriolides I (**49**) and III (**50**) (Figure 3.1) were first isolated from *Beauveria* sp. FO-6979 during a screening of microbial metabolites for inhibitors of lipid droplet accumulation.[9]

The core structure of the beauveriolides consists of a 13-membered depsipeptide ring formed by a β-hydroxyacid and three variable amino acids. Beauveriolides I (**49**) and III (**50**) are the most studied compounds of the family in the context of ACAT inhibition; their structure comprises (3*S*,4*S*)-3-hydroxy-4-methyloctanoic acid, L-Phe, L-Ala, and D-Leu or a D-*allo*-Ile respectively.

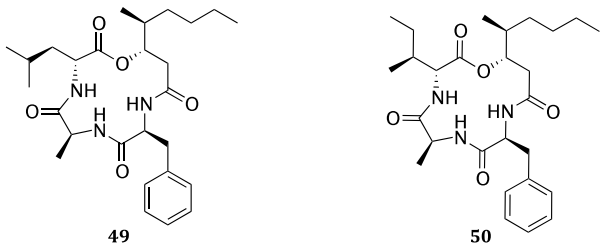

49 **50**

Figure 3.1 - Structures of beauveriolide I (**49**) and beauveriolide III (**50**).

New derivatives are starting to emerge in the hope of improving activity, stability and ACAT isoform specificity. A study in 2008 tested 105 beauveriolide derivatives and concluded that the 3*S*-configuration of the hydroxyacid (Figure

3.2-part 1) was necessary for inhibition, a smaller residue in the Ala position (Figure 3.2-part 2) lead to higher inhibitory activity, and larger residues such as a bisphenyl moiety in place of the Phe amino acid (Figure 3.2-part 3) increased the activity 10-fold, but resulted in loss of selectivity between ACAT-1 and ACAT-2.[10]

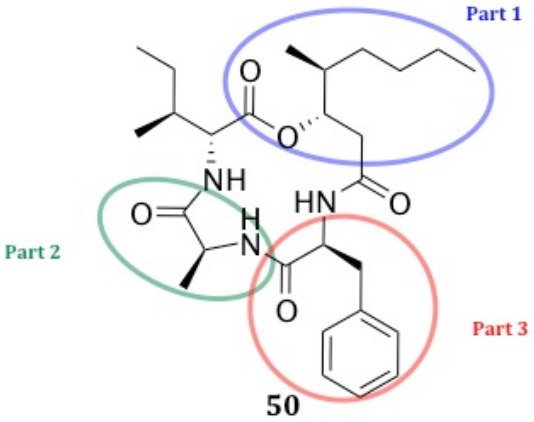

Figure 3.2 - Key parts for analogue development of beauveriolides.

2.2. ACAT inhibition

The beauveriolide's target, ACAT, is an enzyme which catalyses the transfer of fatty acid acyl groups from one molecule to another. There are two isozymes of ACAT in mammals, ACAT-1 and ACAT-2. ACAT-1 is present in most cells, while ACAT-2 is predominantly expressed in liver and intestines. Inhibition studies with beauveriolides I (**49**) and III (**50**), show that they inhibit both isozymes in enzyme micelles, with selectivity towards ACAT-1 in cell-based studies.[11,12]

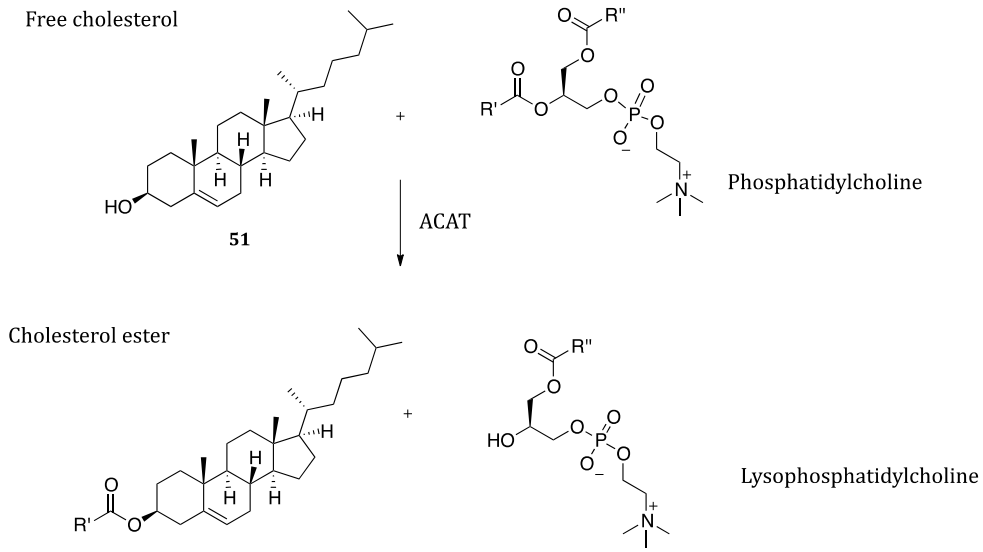

Figure 3.3 - General process of cholesterol esterification catalysed by ACAT.

In nearly all mammalian cells, ACAT catalyses the intracellular esterification of cholesterol (**51**) (Figure 3.3). This transformation has several significant biological effects, but probably the main one is further limiting cholesterol's poor aqueous solubility.[13] This change in solubility increases the intracellular accumulation of cholesteryl esters (CE) as lipid droplets within the cytoplasm and reduces the toxic accumulation of free cholesterol. Whilst all cells need cholesterol, not all are capable of degrading it. When a cell contains excess cholesterol, its only possibility is to esterify it to send it back to the liver, which has the ability to catabolise it into bile acids for disposal.[14] ACAT mediates this esterification reaction, thus enabling the cells to get rid of excess cholesterol. ACAT is also involved in the production and release of apoB-containing lipoproteins.[15]

2.2.1. Atherosclerosis

ACAT first drew attention as a potential target for the treatment of atherosclerosis.[16,17] This disease is characterized by dyslipidemia and hypercholesterolemia. In addition, macrophages accumulate in the arterial walls scavenging oxidized-low density lipoproteins (LDL) and liberating free cholesterol (FC) which is stored as CEs in lipid droplets in the cytoplasm. This process eventually transforms the macrophages into the so-call foam cells which are one of the first observations in atherosclerosis.[18] Inhibition of ACAT reduces the intracelluar accumulation of cholesterol as lipid droplets, thereby making ACAT inhibitors potential drugs for the treatment of atherosclerosis.

Among the eight beauveriolides that have been isolated, beauveriolides I (**49**) and III (**50**) are the two most active inhibitors of CE synthesis in macrophages with IC_{50} values of 0.78 and 0.41 μM respectively.[19] They significantly reduce the amount of lipid droplets in the cytoplasm.[19] Beauveriolide III (**50**) has also been tested *in vivo* using LDL-receptor knockout mice. When these mice are fed a high cholesterol diet, they develop atherosclerosis in the aorta and heart. Treatment with beauveriolide III (25 mg/kg·day) over 2 months reduced the atherosclerotic lesions by 50% without any toxicity.[19]

2.2.2. Alzheimer's disease

A more recent connection links ACAT and Alzheimer's Disease (AD).[20] The progressive degeneration of several cognitive and memory functions is characteristic of AD, but no common cause has yet been identified. Several factors, including old age, genetic and environmental elements, contribute to the development of AD. Nevertheless, one characteristic pathological feature is present in all types of AD, the accumulation of Aβ in the brain.[21,22]

2.2.3. Amyloid-β

Aβ is a 38-43 amino acid-long peptide product of the degradation of Amyloid Precursor Protein (APP). The normal function of APP is still unknown, although studies suggest it can have a role in metal-binding,[23] protease inhibition,[24] and synaptic plasticity.[25] Nevertheless, it is known that APP is a type I transmembrane protein with a large extracellular domain and a short cytoplasmic region. APP can be secreted or processed in the endosomal/lysosomal pathway without secretion and it can be cleaved by α, β or/and γ- secretases. Production of Aβ is a normal physiological function, but its accumulation in the brain is linked to AD pathogenesis. Aβ is unfolded in its native state, but it has a propensity to fold and polymerise forming soluble oligomers and insoluble fibrils. These fibrils tend to accumulate in the normal amyloidogenic β-sheet conformation.[21] Located in the plasma membrane, α-secretase can cleave APP within the Aβ domain, thus preventing the formation of Aβ. However, when APP is cleaved suquentially by β-secretase and γ-secretase, Aβ is generated.[26] β-Secretase cleavage generates a C-terminal fragment (C99), which is then cleaved by γ-secretase to generate Aβ (Figure 3.4).

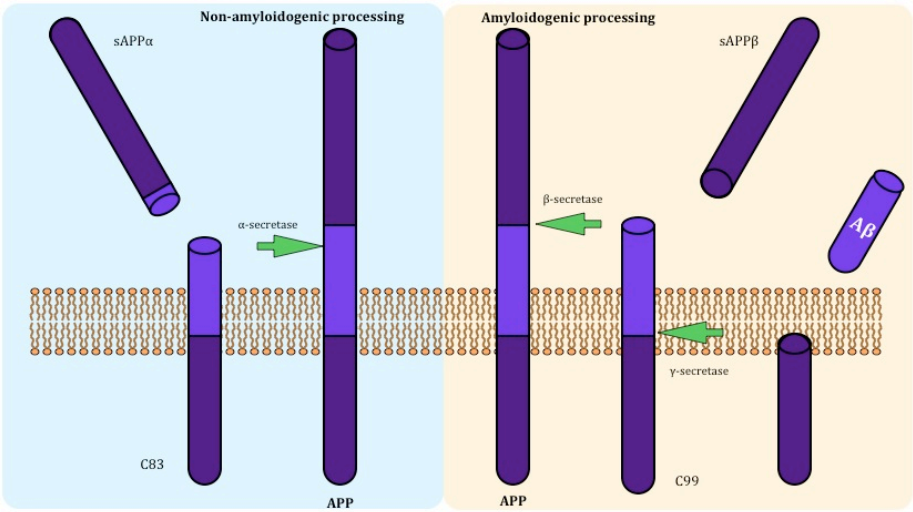

Figure 3.4 - APP processing and formation of Amyloid-β

γ-Secretase can cleave the C99 fragment at different sites within the transmembrane domain of APP, generating several isoforms of Aβ. The most common isoforms are $Aβ_{38}$, $Aβ_{40}$, and $Aβ_{42}$; with the numbers referring to the number of amino acids in the Aβ sequence. It appears that the shorter isoforms ($Aβ_{38}$ and $Aβ_{40}$) are less cytotoxic than $Aβ_{42}$.[27] The smaller isoform, $Aβ_{40}$, is the most frequent form of Aβ (~90% of the total Aβ), however $Aβ_{42}$ is the most amyloidogenic isoform, and while not the principal isoform (only ~10% of the total), it is the predominant species found in senile plaques.[28-30] Mutations in APP have also been associated with early-onset AD and increased production of $Aβ_{42}$. The ratio between $Aβ_{40}/Aβ_{42}$ seems to accelerate the aggregation of Aβ into fibrils.[30] Whether the fibrils, the protofibrils, the oligomers, or the monomers are the most pathogenic form of Aβ is yet to be determined.

2.2.3.1. Amyloid Cascade Hypothesis

The 'Amyloid cascade hypothesis' has been widely accepted as a description of the role of Aβ in AD. This theory suggests that the characteristic pathological effects of AD (neurofibrillary tangle formation, inflammation, neuronal loss and synaptic disruptions) can be traced to the misprocessing, misfolding and aggregation of Aβ.[21,22,31] Although Aβ plaques were initially considered to be the primary cause for the amyloid cascade, recent evidence suggests that Aβ oligomers might be the actual neurotoxic element.[21,32] The origin of Aβ oligomers

is still under debate. One explanation places the oligomers as an intermediate step in the formation of plaques, starting from the monomeric Aβ (monomer => oligomer => protofibril => fibril => plaque [Figure 3.5]).[33,34,35]

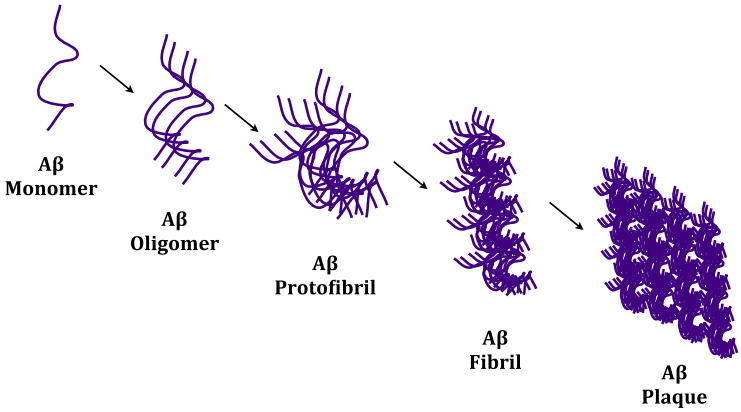

Figure 3.5 - Amyloid plaque formation.

An alternative hypothesis proposes the formation of the Aβ oligomers as an independent process from plaque formation, giving rise to stable oligomers that prevent further aggregation.[36] In either case, it is unknown whether Aβ is secreted as a monomer[37] or if it aggregates intracellularly and then is released as an oligomer.[38]

2.2.3.2. Cellular localisation of Aβ

Another aspect of Aβ metabolism that has yet to be fully characterised is the intracellular localisation of APP and its processing intermediates (Figure 3.6). It is known that after synthesis in the ER, APP moves to the trans-Golgi for post-translational modifications.[30] It is then transported through secretory vesicles to the plasma membrane. Some APP is cleaved at this point by α-secretase, while some is recycled through endosomes back to the Trans-Golgi network (TGN), whilst a portion of the material is subjected to the lysosomal degradation pathway.[39,30]

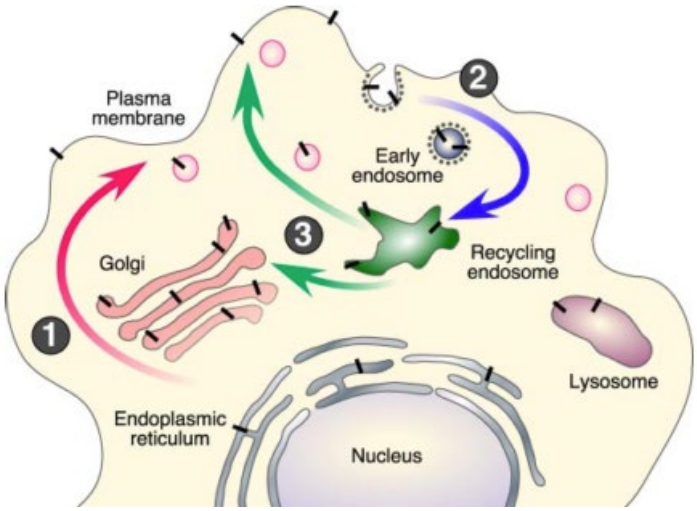

Figure 3.6 - Intracellular trafficking of APP. (Step 1) APP travels to the plasma membrane where it is secreted; (Step 2) Secreted APP is rapidly internalised into endosomes; (Step 3) APP is recycled to the plasma membrane or degraded in the lysosome.
Taken from Thinakaran, G. and Koo, E. *The Journal of Biological Chemistry*, 2008. Vol. 283 (44), pp. 29,615-9.

The location of Aβ production is still under debate. β-Secretase has been found mainly in the later Golgi, TGN and endosomes, thus indicating that Aβ production occurs mainly during the endocytic recycling steps of APP. Several studies have also found γ-secretases in different cell compartments including the ER, ER-Golgi Intermediate Complex (ERGIC), Golgi, TGN, endosomes and the plasma membrane.[26] The location of γ-secretase seems to be cell dependent. IF microscopy studies have found indications that neuronal cells have intracellular concentrations of Aβ whereas non-neuronal cell lines have γ-secretase associated with the plasma membrane, thus secreting Aβ as soon as it is produced.[28]

2.2.4. Current treatments for Alzheimer's Disease

Regarding current treatments for AD, at present, there are no drugs on the market that can provide a cure for AD. Current treatments focus on relieving symptoms and slowing the progression of the disease.[40] The therapeutics may be broadly assigned to one of two classes, acetylcholinesterase (AChE) inhibitors and *N*-methyl-D-aspartate (NMDA) receptor antagonists.[1] AChE inhibitors target the enzyme responsible for breaking down acetylcholine, a neurotransmitter

that is significantly reduced during AD.[41] NMDA receptor antagonists compete with glutamate for its binding site on the NMDA receptor. Once bound, glutamate maintains the receptor in an activated state, allowing electrical signals to be transmitted in the central nervous system (CNS).[42] NMDA receptors are very harmful factors in excitotoxicity. Glutamate is released in excess during AD, thus NMDA receptor antagonists attempt to reduce the damage generated by excessive stimulation.[42]

Regarding Aβ processing, there are a number of therapeutic strategies under study and they predominantly fall into one of three categories: inhibitors of Aβ aggregation, inhibitors of secretase activity or antibodies against Aβ oligomers.[40] Inhibitors of Aβ aggregation tend to be small molecules that prevent aggregation or chelate metals that trigger misfolding.[43] Inhibitors of secretase activity target either β- or γ- secretases, thus preventing the formation of Aβ.[44,45] The antibodies against Aβ oligomers have been shown to negate the toxic effect of the oligomers *in vivo*.[46]

2.3. Alzheimer's disease and cholesterol

Another therapeutic approach to AD relies on regulating the lipid environment and cholesterol homeostasis. Recently, a connection between intracellular cholesterol levels and accumulation of Aβ has been documented.[20] The initial evidence of this link came from genetic studies that highlighted four genes related to AD by point mutations. The first three genes are related to Aβ metabolism (APP, presenilin-1, and presenilin-2). While APP is the precursor protein of Aβ, the presenilins are subcomponents of the γ-secretase complex.[47] All three mutations cause either an increased level of Aβ or higher propensity to aggregate. The fourth gene codes for apolipoprotein E – type 4 (ApoE-ε4) a lipid-binding protein, which among other functions, shuttles lipids between cells. Mutations in ApoE-ε4 remain the single most important factor in determining the risk of developing AD.[48]

In addition to the genetic markers, studies have shown that AD patients have increased levels of total systemic cholesterol and LDL cholesterol compared to age-matched controls.[49] Further observations showed that treatment with

statins not only reduced cholesterol levels, but also reduced levels of Aβ.[50] There has even been some speculation about the role of Aβ being involved in cholesterol homeostasis.[51]

Cholesterol-related treatments of AD involve affecting cholesterol biosynthesis, cholesterol esterification and targeting ApoE-ε4. Regarding cholesterol biosynthesis, the most studied method is the use of statins as inhibitors of HMG-CoA. This enzyme catalyses the rate-limiting step in the synthesis of cholesterol. Statins have shown significant success in the treatment of hypercholesterolemia and cardiovascular disease.[52,53] However, despite the great promise shown in AD transgenic cells and mouse model studies,[40,54] human trials have been inconclusive.[40] Therapies involving ApoE-ε4 focus on using ApoE mimetics to stabilise its function as well as trying to change the pathogenic E4 form to E3 by either pharmacokinetics or genetic manipulation.[55,56]

The final strategy to treat AD involving cholesterol revolves around the inhibition of ACAT, since studies have shown that intracellular CE levels correlate to levels of Aβ secretion and production. It has also been shown that ACAT modulates the generation of Aβ by regulating the equilibrium between FC and CE.[57,58,59] One theory suggests that the levels of CEs direct APP into an *N*-terminal processing pathway that leads to proteosomal degradation and thus reduction of the APP pool. This pathway would bypass the traditional amyloidogenic and non-amyloidogenic processing pathways.[20]

ACAT inhibition by CP-113,818 (Fisher, **52** – Figure 3.7) has been shown to reduce production of Aβ by 50% in cell models,[57] while a mouse-model study of this ACAT inhibitor showed very promising results reducing plaque formation by up to 99% in APP-producing transgenic mice.[58] This study used amyloid staining, thioflavin and Aβ staining, as well as sandwich ELISA for detecting changes in the cortex and hippocampus of treated mice. It also showed that treated mice showed a significant improvement on cognitive functions, achieving levels comparable to non-transgenic mice.[58-60] Unfortunately, ACAT inhibition studies have encountered problems with bioavailability[60] and toxicity to the adrenal gland.[61,62] In addition, human trials have thus far been unsuccessful in affecting cholesterol levels and Aβ production.[13,14]

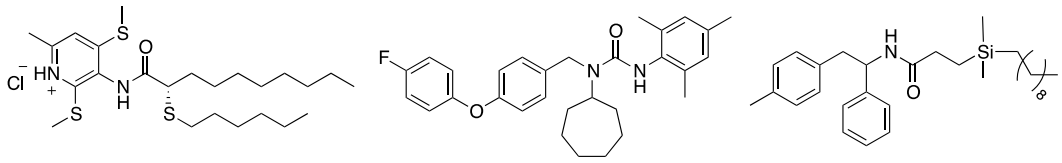

52 **53** **54**

Figure 3.7 - Examples of ACAT inhibitors. CP-113,818 (**52**),[63] FR179254 (**53**) and Sandoz 58-035 (**54**).[57]

2.3.1. Aβ reduction by beauveriolides

Beauveriolides have been found to be highly effective at reducing atherosclerotic plaques in mouse models without inducing any adrenal toxicity.[2] The exact mechanism of ACAT inhibition by beauveriolides is unknown, however their structure is significantly different from traditional ACAT inhibitors (Figures 3.1 and 3.7).

The initial tests of beauveriolides in the context of Aβ reduction have recently been completed.[2] The study was carried out in transgenic APP-expressing CHO cells (7WD10 cell line) treated with beauveriolides I (**49**) and III (**50**). CE levels were measured using the Amplex Red cholesterol assay and shown to decrease by up to 95% after 48 h of treatment with beauveriolide III (**50**, 5 μM). Secreted Aβ levels measured by sandwich ELISA were also shown to decrease by up to 65% after 4 days of treatment with beauveriolide III (**50**, 5 μM).[64]

2.4. Beauveriolide chemical synthesis

As these natural products showed promising biological applications, the need for an effective synthesis became apparent. The first total synthesis of a beauveriolide (beauveriolide I, **49**) was published in 2005 by the Liang group. (Figure 3.8).[64]

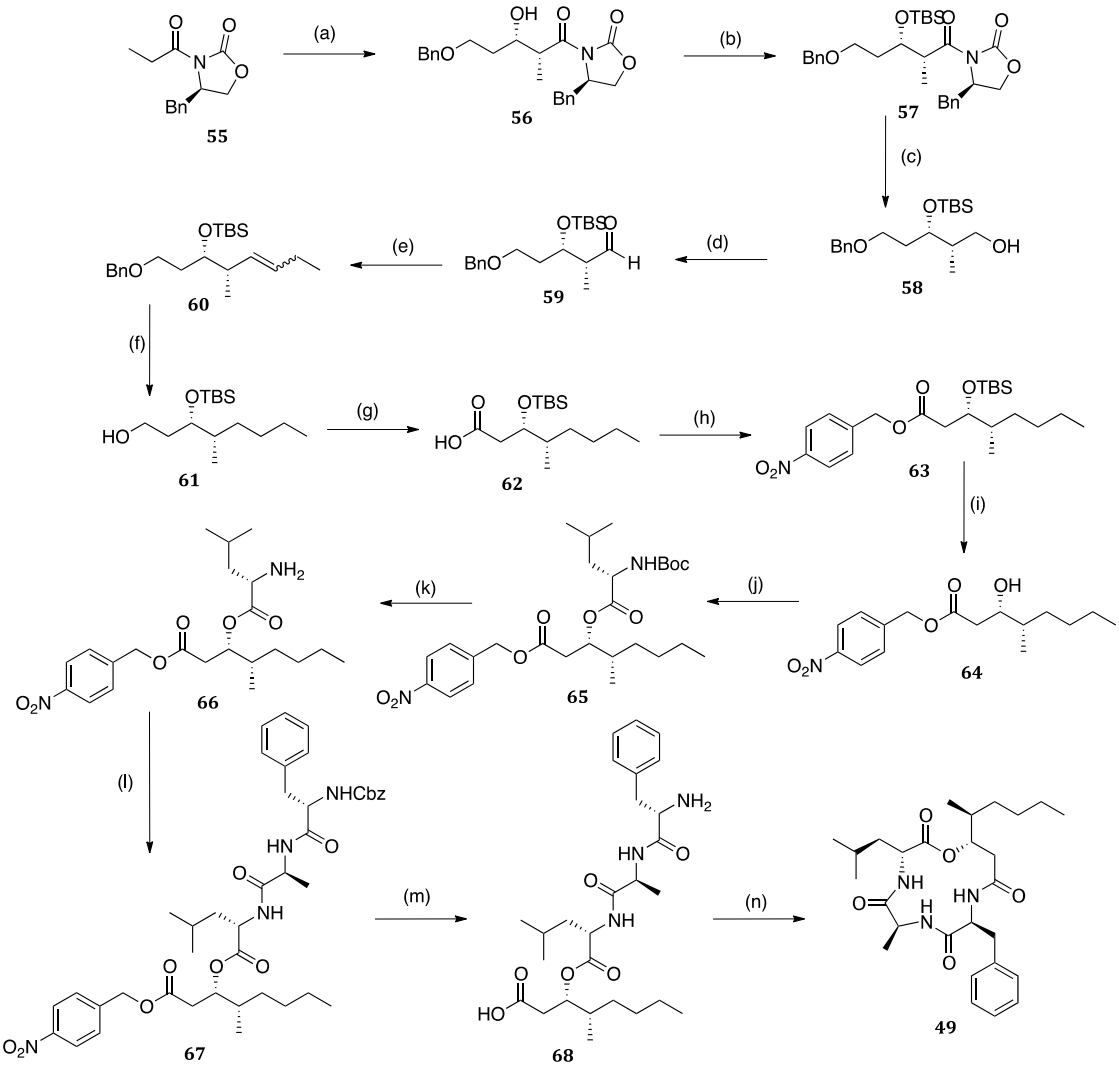

Figure 3.8 – Total synthesis of beauveriolide I by Tian, *et.al.*[64] *Reagents and conditions*: (a) 3-benzyloxypropionaldehyde, $TiCl_4$, DIPEA, NMP (97%); (b) TBS-Cl, imidazole (79%); (c) $LiBH_4$ (73%); (d) $(COCl)_2$, NEt_3 (90%); (e) $[Ph_3PCH_2CH_2CH_3]\cdot Br$, *n*-BuLi (91%); (f) H_2, 10% Pd/C (82%); (g) $NaIO_4$, $RuCl_3$ (cat.) (78%); (h) 4-nitro-benzyl bromide, DIPEA (66%); (i) HF·Py (70%); (j) DCC, DMAP, *N*-Boc-D-Leu; (k) HCl/EtOAc; (l) *N*-Cbz-L-Phe-L-Ala, EDCI, DIPEA, HOSu; (m) H_2, 10% Pd/C; (n) BOP, DMAP (68%).

As the authors describe, the two challenges of the synthesis are the macrocyclisation of the depsipeptide and the homochiral assembly of the β-hydroxyacid part of the molecule. The cyclisation can take place by either macrolactonisation or macrolactamisation. Their research demonstrated that cyclisation by ester formation was not viable under the conditions tested and settled on a ring closure by amide formation. The formation of the β-hydoxyacid component was achieved by a diastereoselective aldol condensation using Evans' auxiliary **55** under Crimmin's conditions with 3-benxyloxypropionaldehyde. TBS

protection of the resultant β-hydroxyacid gave silylether **56**, from which the auxiliary was removed under reducing condition using $LiBH_4$ to give the primary alcohol **58**. The alcohol **58** was then oxidised under Swern conditions to give aldehyde **59**, which was then subjected to a Wittig olefination reaction to give alkene **60** as a mixture of geometric isomers. A simultaneous debenzylation and alkene reduction by catalytic hydrogenation lead to primary alcohol **61**, which was then oxidised with $NaIO_4$ and $RuCl_3$ to yield acid **62**. This product was then esterified with 4-nitrobenzyl bromide to give ester **63**. Desilylation with HF·pyr complex gave alcohol **64**, which was then esterified with Boc-*N* protectected D-Leu to give ester **65**. Boc removal using TFA gave the secondary amine **66**, which was then coupled to Cbz-*N*-Phe-Ala for the installment of the remaining two amino acids to five CBz-tripeptide **67**. Simultaneous removal of the 4-nitrobenzyl ester and Cbz groups using catalytic hydrogenation generated amino acid **68**, which underwent macrolactamisation to yield beauveriolide I (**49**). The full synthesis consisted of ten core steps, with six extra reactions for protecting group manipulation, with an overall yield of less than 9% (although it is important to mention that the reaction yields are not explicitly reported for 4 steps of the synthesis).

Another synthesis developed in the Takahashi lab (Figure. 3.9) was published in 2006.[10,65] In this work, the assembly of the linear depsipeptide **80** was achieved on-resin using a tritryl-linker. The β-hydroxy acid **77** was synthesised by the condensation of (*S*)-oxazolidinone (**69**) and hexanoyl chloride, followed by introduction of the desired 3*S,4S* stereochemistry in two steps. The first step involved an Evans' asymmetric alkylation of the intermediary amide using NaHMDS and MeI. For the second step the chiral auxiliary was removed from product **70** under basic conditions (aq. LiOH). Activation of the resultant carboxylate **71** with carbonyl diimidazole (CDI) was followed by nucleophilic addition with ethylmagnesium malonate, which after decarboxylation yielded β-keto ester **72**. Asymmetric hydrogenation of ketone **72** under high pressure (90 atm) installed the desired *3S*-stereochemistry of the secondary alcohol in ester **73**. The establishment of the desired stereochemistry was followed by a transesterification from ethyl **73** to benzyl ester **75**, which was then esterified with Boc-D-*allo*-Ileu (**76**). After benzyl ester deprotection under reductive

conditions, the resultant acid **77** provided the β-hydroxyacid building block that could be added onto an Ala-Phe dipeptide pre-synthesised on resin (**78**) to complete the linear assembly of all the components of the depsipeptide **79**. Once the assembly was complete, the depsipeptide was cleaved from the resin and beauveriolide III (**50**) was obtained after solution-phase macrolactamisation using EDAC in 51% yield. The total synthesis consisted of nine core steps, with two extra reactions for protecting group manipulation. The overall yield for the total synthesis was 20%.

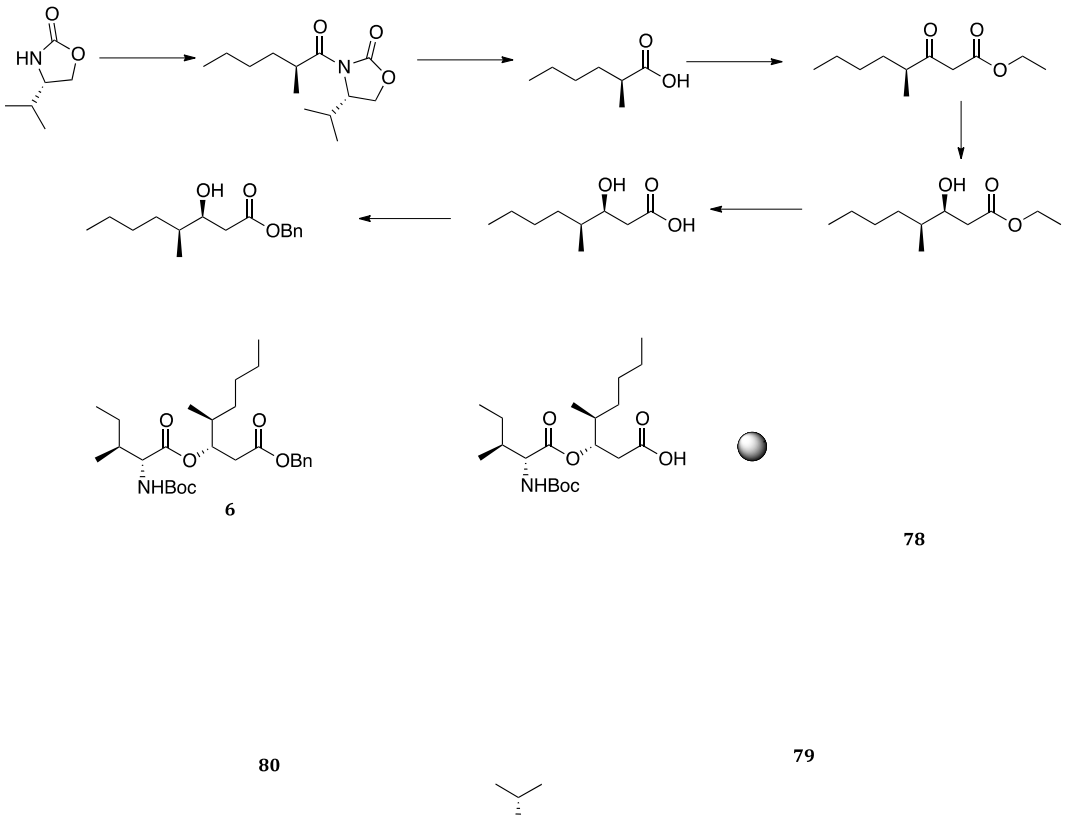

Figure 3.9 – Total synthesis of beauveriolide III by Nagai, T.; et.al.[63] *Reagents and conditions*: (a) i. *n*-BuLi; ii. NaHMDS, IMe (97%); (b)LiOH; (c)CDI, $(EtO_2CCH_2CO_2)_2Mg$ (63%); (d) $RuCl_2[(R)$-binap], H_2, 90 atm; (e)LiOH; (f) Cs_2CO_3, BnBr (85%); (g) Boc-D-*allo*-Ileu, DCC, DMAP; (h) H_2, 10% Pd/C (84%); (i) PyBrop, *i*-Pr_2NEt; (j) HCl (91%); (k) EDAC·HCl, *i*-Pr_2NEt (51%).

A different total synthesis for beauveriolides I (**49**) and III (**50**) was developed in 2009 in the Wentworth laboratory.[2] This synthesis (Figure 3.10) suffered the same problems in attempting macrolactonisation for ring closure as reported in

Liang's synthesis,[64] and therefore employed a HATU/HOAt activation for macrolacamisation. The synthesis starts with the PMB protection of 1,3-propanediol (**81**), the resulting alcohol **82** is then subjected to a Swern oxidation to form the PMB-protected aldehyde **83**. The aldehyde **83** is then used in a *cis*-crotylation with *cis*-2-butene and (+)-*B*-methoxydiisopinocampheylboron (+MDPCB) to introduce the desired 3*S*,4*S* stereochemistry.

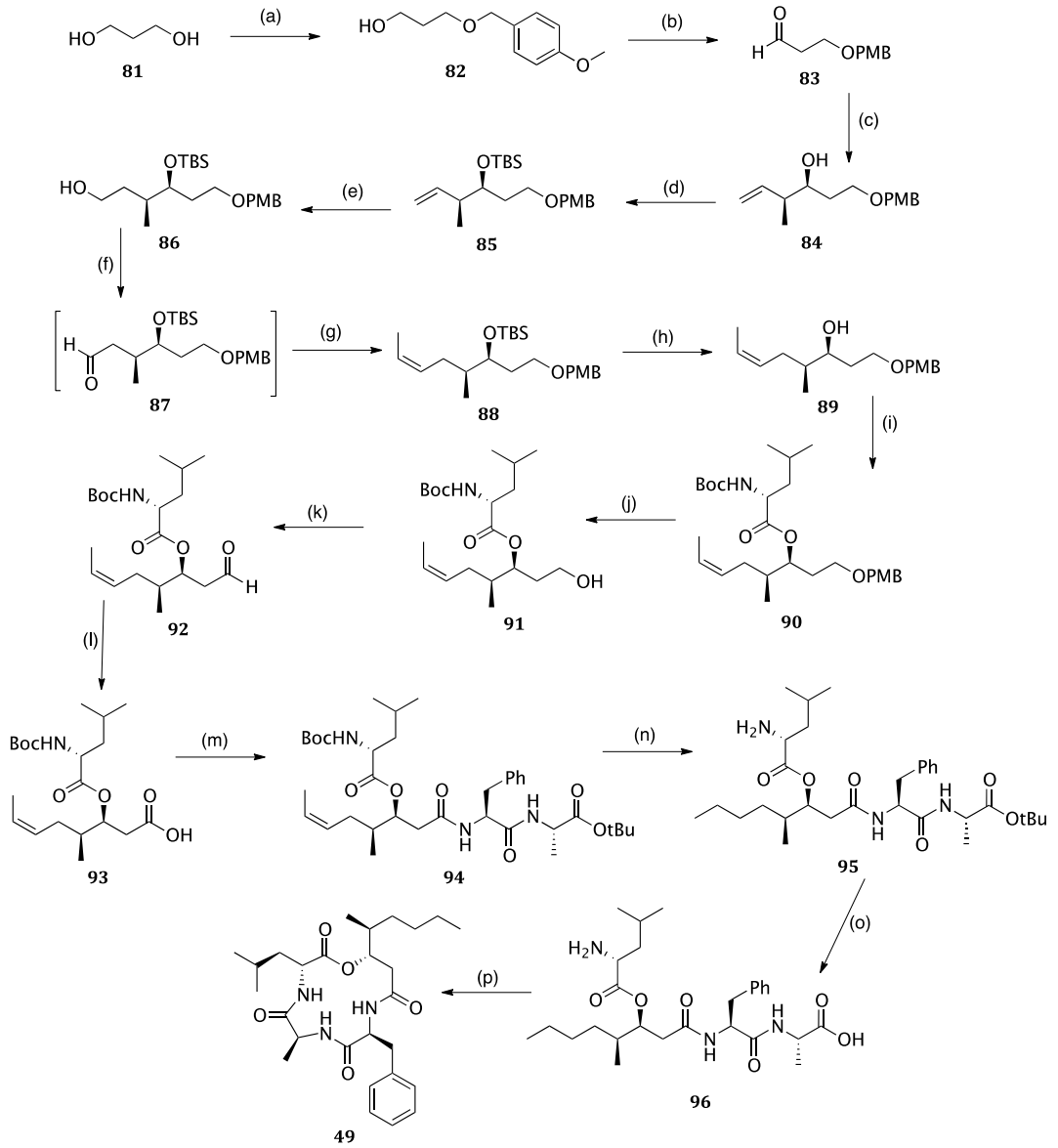

Figure 3.10 – Total synthesis of beauveriolide I by Witter, et.al.[2] *Reagents and conditions*: (a) 1. *p*-anisaldehyde, *p*-TsOH. 2. DIBAL-H; (b) Oxalyl chloride, DMSO, NEt_3; (c) *cis*-2-butene, KO*t*Bu, +MDPCB, $BF_3{\cdot}OEt_2$ (78%); (d) TBS-triflate, 2,6-lutidine (95%); (e) 9-BBn, H_2O_2, NaOH (82%); (f) TPAP, NMO (96%); (g) $EtPPh_3$, NaHMDS (83%); (h) TBAF (97%); (i) DIC, DMAP, *N*-Boc-D-Leu, $Sc(OTf)_3$ (87%); (j) DDQ; (k) Dess-Martin periodinane; (l) $NaClO_2$, NaH_2PO_4, 2-methyl-2-butene; (m) EDC, HOBt, Phe-Ala-O*t*Bu: (55% over four steps); (n) H_2, Pd/C; (o) TFA (quant.); (p) HATU, HOAt, collidine (74%).

TBS protection of the homoallylic alcohol **84** is followed by a hydroboration of the terminal double bond to introduce a primary alcohol and form compound **86**, which is then oxidised by TPAP. The resulting aldehyde **87** is immediately used in a Wittig olefination to yield the *cis*-alkene **88**, which upon deprotection, can be coupled to Boc-D-Leu. The PMB-protected hydroxy group in compound **90** is deprotected, and sequentially oxidised to the aldehyde **92** by Dess-Martin periodinane and then to the acid **93** by treatment with $NaClO_2$, NaH_2PO_4 and 2-methyl-2-butene. The acid can then be coupled to a Phe-Ala-O*t*Bu dipeptide (**117**), which upon deprotection yields the depsipeptide **96**. As mentioned before, the cyclisation is achieved by a HATU/HOAt macrolactamisation. The synthesis consists of ten core reactions, and six additional protecting group manipulation steps. The overall yield for the synthesis is 16% with the PMB-protected aldehyde **84** as starting point.

3. Results and Discussion

Despite the fact that there exists more than one synthetic route for beauveriolides, these compounds are still rare commodities because their syntheses are labour intensive and require expensive reagents. Since the objective of this project was to develop a method to monitor Aβ changes as a result of ACAT inhibition by beauveriolide III, a significant amount of compound was needed.

3.1. Beauveriolide synthesis

It was decided to use the synthesis by Witter, *et.al.*[2] as a starting point, mainly because the synthetic methodology to prepare stereoselectively the β-hydroxyacid moiety was the most efficient and cost-effective of the three published synthesis (Figure 3.11). Both Liang's[64] and Takahashi's[63] syntheses utilise a chiral auxiliary (**55** in Figure 3.8 and **69** in Figure 3.9) which, although commercially available, is not commercially viable on a large scale. Moreover, Takahashi's synthesis employs an asymmetric catalytic hydrogenation step which requires high pressure equipment (90 atm).

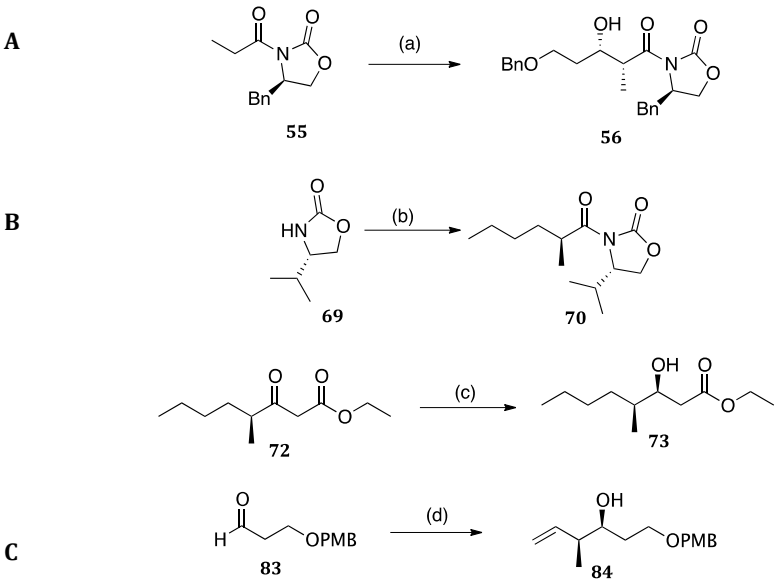

Figure 3.11 – Introduction of *S,S*-stereochemistry in β-hydroxyacid by (A) Liang's synthesis,[64] (B) Takahashi's synthesis, [63] and (C) Wentworth's synthesis.[2] *Reagents and conditions*: (a) 3-Benzyloxypropionaldehyde, $TiCl_4$, DIPEA, NMP (97%); (b) i. *n*-BuLi; ii. NaHMDS, IMe (97%); (c) $RuCl_2$[(*R*)-BINAP], H_2, 90 atm; (d) +MDPCB, $BF_3{\cdot}OEt_2$ (78%).

A major point of improvement in Wentworth's synthesis was detected in the synthetic sequence to transform compound **84** into alkene **89** (Figure 3.12). After establishing the desired stereochemistry with the enantio and diastereoselective *cis*-crotylation, the next five reactions were involved in elongating the hydrocarbon chain of the β-hydroxy ether **84**. Although the yield of this sequence is good (60% over 5 steps), the atom efficiency is very low and some protocols are tedious (such as the purification from the mixture after the Wittig reaction).

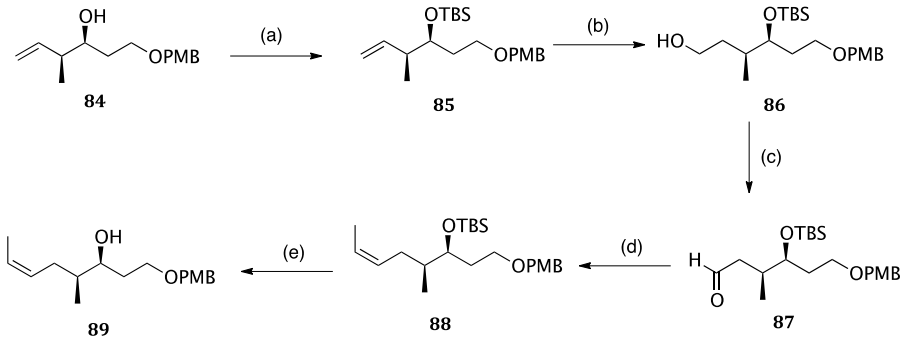

Figure 3.12 – Reactions for the elongation of the hydrocarbon chain of the β-amino acid in the synthesis by Witter, et.al.[2] *Reagents and conditions*: (a) TBS-triflate, 2,6-lutidine (95%); (b) 9-BBn, H_2O_2, NaOH (82%) (c) TPAP, NMO (96%); (d) $EtPPh_3$, NaHMDS (83%); (f) TBAF (97%).

Cross-metathesis represents a more efficient way to achieve the same purpose. This reaction allows the functionalisation of simple alkenes, or in this context, the extension of a hydrocarbon chain across a double bond (Figure 3.13-a). Although Grubbs' 1st generation catalyst (Figure 3.13-b, **97**) has been shown to display a wide tolerance of functional groups, it reacts poorly in cross-metathesis reactions involving homoallylic alcohols.[66] Hoveyda-Grubbs' 2nd generation catalyst (**98**) overcomes this lack of activity.[67] The only difference introduced by the use of a cross-metathesis reaction is the position of the alkene as shown in Figure 3.13-c and d. However, as the alkene is reduced during the final steps of the synthesis, its position has no bearing to the rest of the synthesis

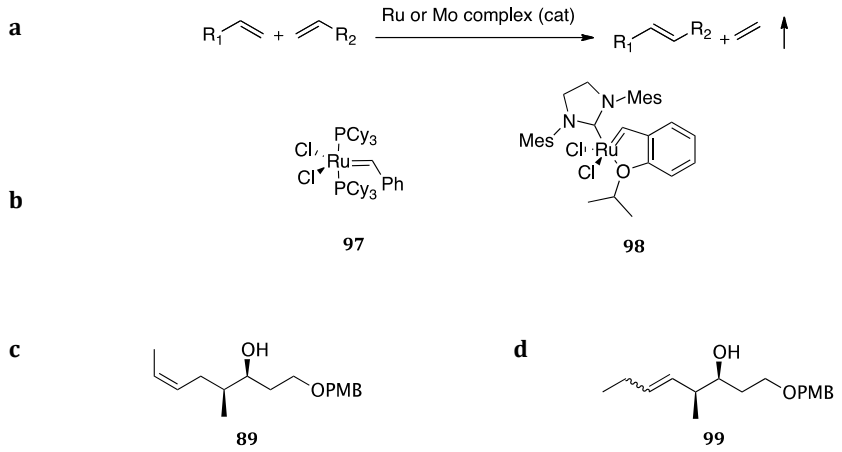

Figure 3.13 – (a) General cross-metathesis scheme[68]; (b)Grubbs' 1st generation catalyst (**97**) and Hoveyda-Grubbs' 2nd generation catalyst (**98**); (c) Position of alkene bond in product generated by the established synthesis; (d) Position of alkene bond in product generated by cross-metathesis.

Having made these observations, the synthesis of beauveriolide III was initiated using the published protocol described in Figure 3.10. 1,3-propanediol (**81**) was protected with PMB by a two-step protocol. Reaction with one equivalent of *p*-anisaldehyde in the presence of a catalytic amount of *p*-TsOH led to the formation of 1,3-dioxolane, which was reduced in the presence of DIBAL-H to yield compound **82** in 61% yield. The alcohol was then transformed to aldehyde **83** by a Swern oxidation with a 68% yield. While the reported yields for these reactions are almost quantitative, the results obtained show lower yields because the work was done on a large scale (>100 g) and thus priority was given to collect completely pure fractions as opposed to maximising yields.

The next step in the synthesis was Brown's crotylation of compound **83** to generate the desired stereochemistry in the homoallylic alcohol **84**.[68] The reaction consists on the addition of a previously formed homochiral borane to aldehyde **83** as shown in Figure 3.14. Metalation of *cis*-butene by *n*-BuLi/KO*t*Bu was followed by treatment with +MDPCB and $BF_3{\cdot}OEt_2$. It is accepted that the addition of borane to the carbonyl carbon of an aldehyde such as **83** occurs preferentially on one face of a putative six-membered transition state (**100**).[69] *Z*-alkenes generate selectively *erythro*-isomers, while *E*-alkenes form *threo*-isomers selectively.

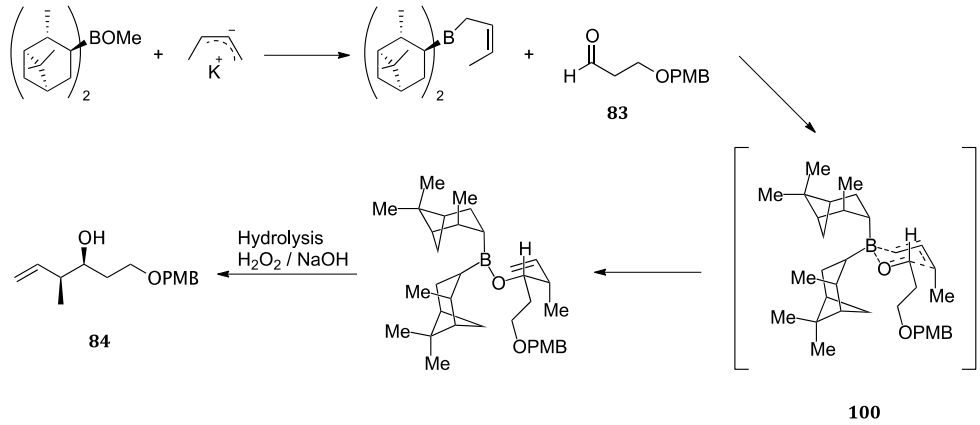

Figure 3.14 – Reaction mechanism for Brown's *cis*-crotylation.

The resulting alcohol **84** was TBS protected (**85**) to allow a hydroboration-oxidation reaction by treatment with 9-BBN. The primary alcohol **86** was obtained in 79% yield, and was then oxidised to the aldehyde **87** using TPAP and NMO. The aldehyde **87** was used directly in a Wittig reaction to obtain alkene **88** with a yield of 50% over two reactions. This compound was finally deprotected to obtain the free alcohol **89**. Alcohol **89** was used to test the proposed cross-metathesis reaction in order to compare the two methods.

Initially, a readily available racemic homoallylic alcohol **101** was used in a 100 mg scale for the reaction shown in Figure 3.15 to determine if the cross-metathesis would tolerate the substrate. Both 1-butene and *trans*-3-hexene would lead to the same product because they can form the same propylidene complex upon reaction with the catalyst **98**. *Trans*-3-hexene was chosen because it is easier to handle as a liquid instead of using 1-butene as a gas. 5% of the ruthenium complex was used as a catalyst and dichloromethane (DCM) as solvent since they are the most common conditions used for this type of reaction.

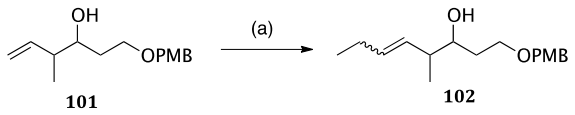

101 **102**

Figure 3.15 – Cross-metathesis test reaction. *Reagents and conditions*: (a) 20 equiv. *trans*-3-hexene, 0.05 equiv. Hoveyda-Grubbs 2nd generation cat., DCM, heated under reflux, 12 h (71%).

The reaction proceeded as desired with a 71% yield. The next step involved the use of the desired (*S*,*S*)-alcohol **84** as the starting material (Figure 3.16). The reaction proceeded successfully, with no racemisation and with quantitative

conversion as determined by NMR. The reaction produced a 10:1 mixture of *trans* to *cis* isomers as seen by NMR (*J*=15.3 Hz for *trans* and *J*=10.7 Hz for *cis* isomers).

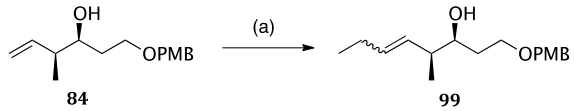

Figure 3.16 – Cross-metathesis test reaction II. *Reagents and conditions*: (a) 20 equiv. *trans*-3-hexene, 0.05 equiv. Hoveyda-Grubbs 2nd generation cat., DCM, heated under reflux, 12 h.

At this stage Grubbs' 1st generation catalyst (**97**) was also tested in the reaction, mainly because it was available in the lab. Interestingly, no conversion was observed after several hours of heating under reflux conditions. This result is in accordance with the generally accepted inactivity of complex **97** with homoallylic substrates.[67] A study of the reaction conditions was completed next, with the objective of using the lowest amount of catalyst to obtain full conversion of the substrate. Table 3.1 shows the conditions tested with the obtained conversion percentage from starting material to product as determined by NMR.

First, different solvents were chosen to study the effects of solvent polarity and coordination strength on reaction conversion. The rest of the reaction conditions were fixed: 2% of catalyst **98**, 5 equivalents of alkene, the same amount of dry solvent, RT and reaction performed under an inert atmosphere. Conversion was measured after 6 h of reaction by direct ^{1}H NMR from reaction mixtures.

Hexane showed poor conversion, most likely because the ruthenium complex **98** was very insoluble in this apolar solvent. Diethyl ether, tetrahydrofurane (THF) and acetonitrile are more polar solvents and the catalyst could dissolve well in them, but still these reactions only proceeded with low conversions. This may be explained by the fact that they are coordinating solvents and, as such, they can compete with substrates to complex the metal centre and form stable adducts. This effect is pronounced because alkenes themselves are weak coordinators and the solvent is present in vast excess to the alkene.[70]

Table 3.1 – Optimisation of the cross-metathesis reaction between compound **84** and *trans*-3-hexene.

Optimisation condition	Solvent	*trans*-3-hexene equivalents	Conc. (M)	Cat. (%)	Time (h)	Temperature (°C)	Conversion (%)
Solvent	Hexane	5	0.2	2	6	RT	11.5
	$(Et)_2O$	5	0.2	2	6	RT	6.1
	THF	5	0.2	2	6	RT	2.0
	CH_3CN	5	0.2	2	6	RT	0.0
	Acetone	5	0.2	2	6	RT	21.3
	DMF	5	0.2	2	6	RT	18.0
	EtOAc	5	0.2	2	6	RT	35.5
	DCM	5	0.2	2	6	RT	43.5
Concentration	DCM	5	1	2	6	RT	41.5
	DCM	5	0.04	2	6	RT	2.9
Reagent equiv.	DCM	10	0.2	2	6	RT	38.7
	DCM	2	0.2	2	6	RT	6.5
Time/Cat./	DCM	5	0.2	2	15	Reflux	100
Temperature	DCM	5	0.2	1	3	Reflux	100
	DCM	5	0.2	0.5	12	Reflux	86.0

Acetone, dimethylformamide (DMF) and ethyl acetate are also polar solvents, but form adducts with the Ru complex to a lower extent than the solvents above, thus conversion is higher in these solvents. Ultimately, DCM is the solvent that gives the highest conversion, probably because of its high polarity coupled with a low coordination propensity.

Based on these observations, DCM was used to test the remaining conditions: alkene equivalents, temperature and concentration. As can be seen in Table 3.1, high dilution (0.04 M) of substrates and catalyst led to a low conversion, while no differences where observed between 1M and 0.2M. Regarding the equivalents of *trans*-3-hexene used, lower equivalents led to low conversion, however there was no significant difference between the use of 5 and 10 equivalents of *trans*-3-hexene on product conversion. The next test analysed the effect of concentration on the reaction. Further tests indicated that an increase in the reaction temperature to reflux conditions in DCM led to full conversion in 1.5 h. Employing 1% of catalyst increased reaction time to 3 h to achieve full conversion, while the use of 0.5% catalyst did not show full conversion after 12

h, perhaps because of catalyst decomposition during the prolonged reaction time.

These optimisation studies determined the use of 5 equivalents of *trans*-3-hexene and 1% catalyst **98**, heating under reflux conditions for 3 h of a 0.2 M solution of the allylic alcohol **84** in dry DCM under an inert atmosphere to obtain complete conversion to the desired product **99**, which was isolated and characterised after chromatography purification of the reaction mixture with an 89% yield in a scale to 50 mg of starting material **84**. The ^{1}H NMR spectrum of the product **99** can be observed in Figure 3.17.

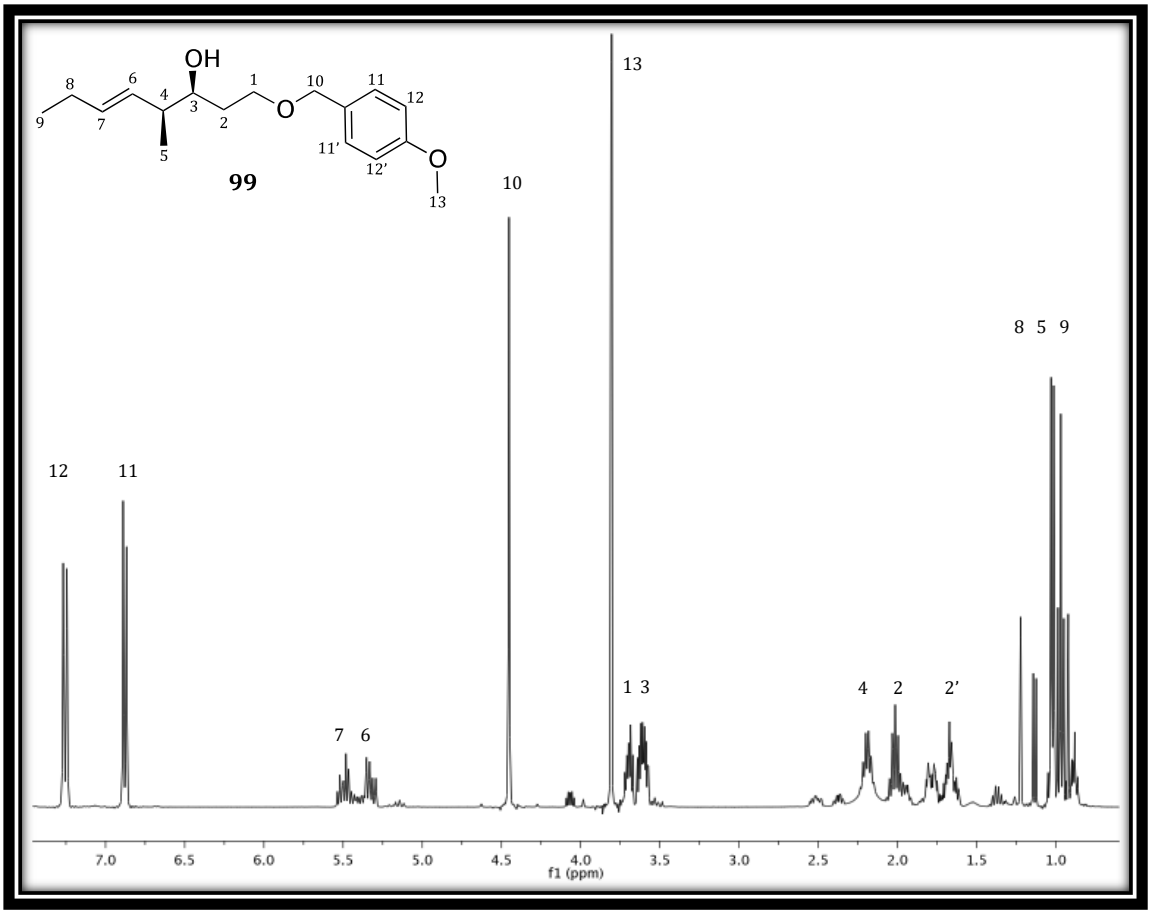

Figure 3.17 - Spectroscopic characterisation by ^{1}H NMR of cross-metathesis product **99.**

Table 3.2 provides a comparison between the synthesis of the isomers **89** and **99** with the published protocol and the cross-metathesis approach. Comparing both methods to elongate the hydrocarbon chain in β-hydroxyester **84**, the developed metathesis reaction is better in yield (89% compared to 60%), cost, atom efficiency and simplicity.

Table 3.2. Summary of products and yields for the synthesis of beauveriolide III (**50**)

Published Method					New method	
Compound	Reaction yield (%)	Overall yield (%)	Reported yield (%)	Reported overall yield (%)	Compound	Reaction Yield (%)
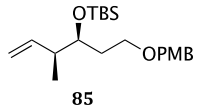 **85**	69	69	95	95	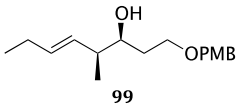 **99**	89
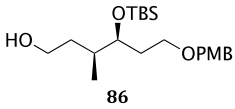 **86**	71	49	82	78		
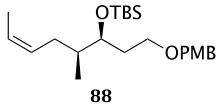 **88**	50	24.5	79	62		
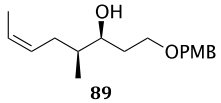 **89**	90	22.5	97	60		

Milligrams quantities of beauveriolide III (**50**) were required to develop a FACS based method of Aβ reduction by ACAT inhibition. For this reason, large quantities of alkene **84** were prepared. However, only a test-scale synthesis of **50** was conducted following the published synthesis. The introduced cross-metathesis was used by Dr. Jaime Escribano Cabeza, post-doctoral fellow in the Wentworth lab, to complete, scale up and further modify the remaining steps in the synthesis of beauveriolide III (**50**).

Figure 3.18 shows the remaining tested steps for the published synthesis of **50**. The synthesis is continued when alcohol **89** is esterified with the Boc-protected D-amino acid, *n*-Boc-D-*allo*-Ileu by the action of DIC and DMAP in 54% yield. The PMB protection is then removed by DDQ, and subsequent oxidations of the alcohol **104** to the aldehyde **105** by Dess-Martin periodinane (57% yield), and then to the acid **106** by $NaClO_2$, $NaHPO_4$ and 2-methyl-2-butene (76% yield) are conducted. The resulting acid **106** is then coupled to the free amine of a previously prepared Phe-Ala-O*t*Bu (**117**) dipeptide. Deprotection of the depsipeptide **107** and alkene reduction by treatment with H_2 and Pd/C yields

compound **109**, which allows a final macrolactonisation to the desired beauveriolide III (**50**) by HATU and HOAt in a 76% yield.

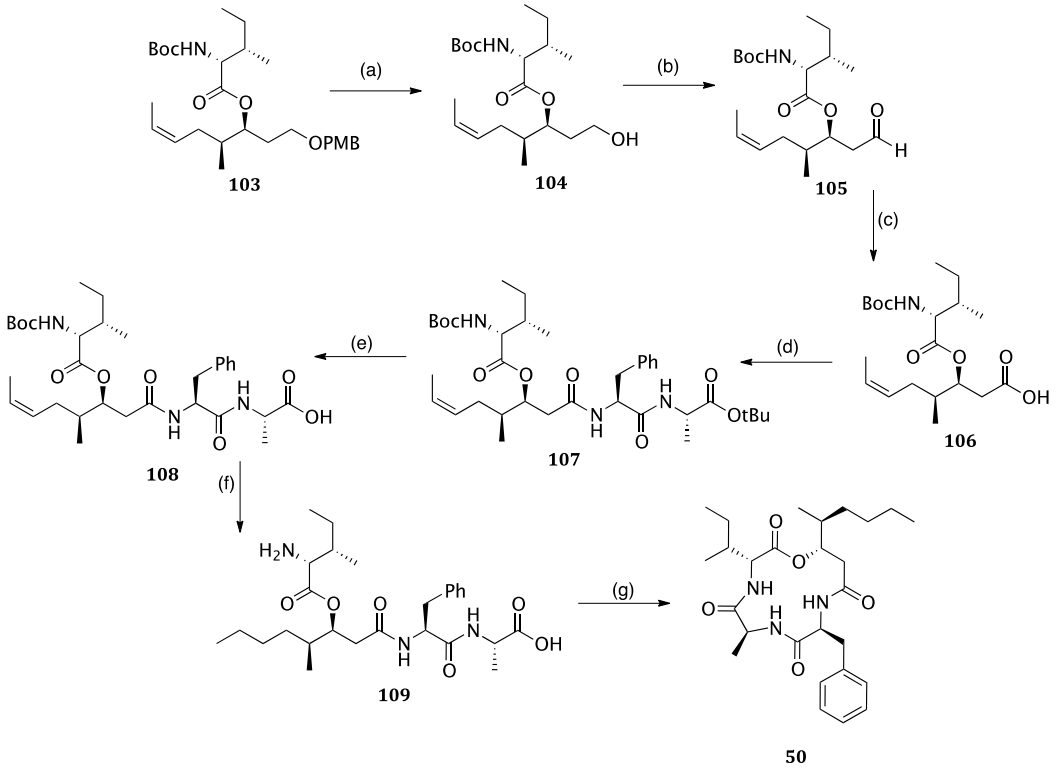

Figure 3.18 – Synthesis of beauveriolide III from **89** with method by Witter, et.al.[2] *Reagents and conditions*: (a) DDQ; (b) Dess-Martin Periodinane; (c) $NaClO_2$, NaH_2PO_4, 2-methyl-2-butene; (d) EDC, HOBt, Phe-Ala-OtBu; (e) TFA; (f) H_2, Pd/C; (g) HATU, HOAt, Collidine.

Further optimisation of the reactions after cross-metathesis by Dr. Jaime Escribano Cabeza have reduced the number of reaction steps to five. The improved synthesis, with the cross-metathesis product **99** is presented in Figure 3.19. The cross-metathesis reaction was scaled-up to yield more than 1 g of compound **99** in a 93% yield of isolated product. The alcohol **99** was then reacted with *n*-Boc-D-*allo*-Ileu in the presence of DMAP, DIC an $Sc(OTf)_3$ to yield ester **110** in a 76% yield. Hydrogenation of the double bond and deprotection of the PMB ether was achieved quantitatively in the presence of H_2 and catalytic amounts of Pd/C for prolonged reaction times (48 h). Oxidation of hydroxyl group in **111** was in this case completed with $KMnO_4$ (excess) in a biphasic reaction mixture using Bu_4NBr as phase transfer agent.[30] Acid **112** was obtained in quantitative yield after an aqueous extraction. Coupling of the carboxylic acid **112** with Phe-Ala-O*t*Bu (**117**), deprotection and macrolactamisation were done

employing the same reaction conditions as the published synthesis to give beauveriolide III (**50**) with a 71% yield after 5 steps.

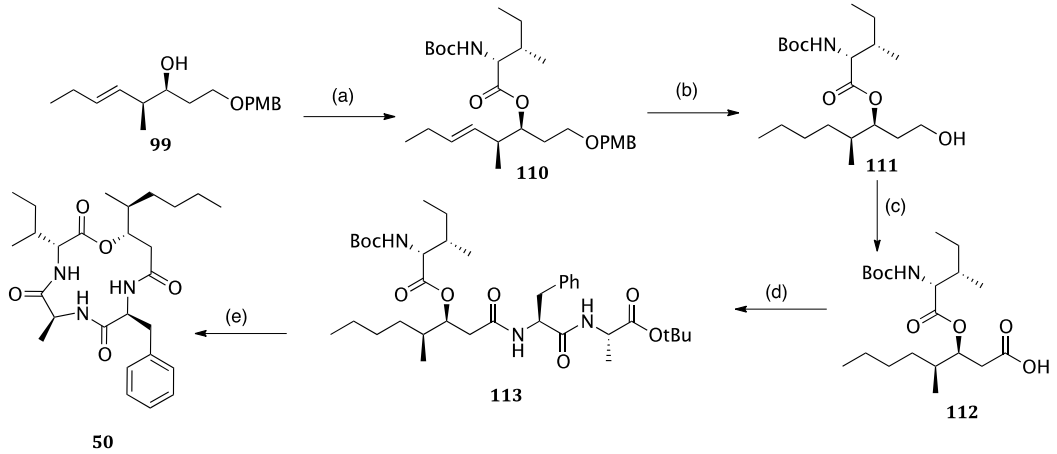

Figure 3.19 – Synthesis of beauveriolide III from **50**. *Reagents and conditions*: (a) DIC (2.4 equiv.), DMAP (2 equiv.), *N*-Boc-D-*allo*-Ile (2 equiv.), $Sc(OTf)_3$ (0.4 equiv.), –10°C→10°C, 3h, (75%, 97% brsm); (b) H_2, Pd/C (5%), EtOAc, RT, 48 h, (quant.); (c) $KMnO_4$ (3 equiv.), Bu_4NBr (0.5 equiv.), DCM/H_2O/AcOH (5:3:0.2), 40°C, 5 h (quant.); (d) EDC (1.05 equiv.), HOBt (1.05 equiv,), Phe- Ala-CO_2*t*Bu (**116**), DCM, 0°C→RT, 20h (quant.); (e) i. DCM/TFA (1:1), RT, 7h; ii. HOAt (5 equiv.), 2,4,6-collidine (10 equiv.), HATU (2.5 equiv.), 0°C→RT, DMF, 22 h (71%).

With these further improvements, the overall % yield for the synthesis of beauveriolide III (**50**) was increased to 45% from the 16% published yield. The significant increased yield is complemented by the reduction of the number of reactions required (Table 3.3), cutting down the reagents, materials and time required for the total synthesis. A ^1H NMR spectrum of the obtained beauveriolide III (**50**) is shown in Figure 3.20.

Table 3.3. Summary of products and yields for the synthesis of beauveriolide III (**50**).

	Published Synthesis[2]	Tested published synthesis[2]	Modified Synthesis
Overall yield	16%	3%	45%
Synthetic steps	16	16	10
PG manipulation steps	6	6	3

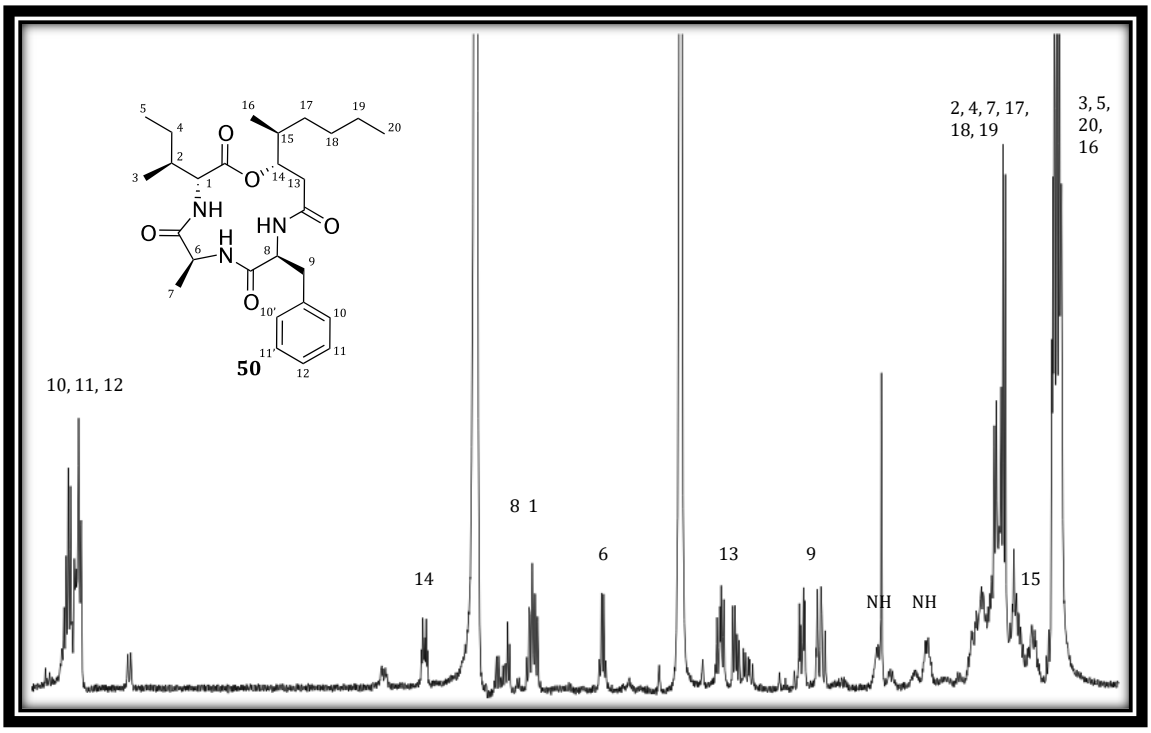

Figure 3.20 - Spectroscopic characterisation by ^{1}H NMR of beauveriolide III (**50**).

3.2. Reduction in Aβ by beauveriolide III

Once enough beauveriolide III (**50**) was available (~50 mg), a study for the development of a method for detection of Aβ changes as a result of ACAT inhibition was undertaken. One of the most common methods to monitor changes in cellular Aβ secretion is a sandwich ELISA-based analysis of the secreted Aβ in the culture media. While this method yields meaningful results, it is expensive, time consuming, and requires large amounts of compound to treat large numbers of cells to get measurable results, as well as multiple sample manipulations before screening. For these reasons, it was decided to explore IF-based flow cytometry (IF-FACS) as an alternative to monitor Aβ changes. This technique requires significantly lower cell numbers, and consequently lower amounts of compound to treat them. It also yields fast results and requires just a pair of antibodies for detection. Furthermore, it is a robust quantitative technique and can be coupled to measure other factors by IF with different excitation wavelengths.

3.2.1. Intracellular Aβ measurements

Ideally, any analysis would be able to detect intracellular changes of Aβ. For this purpose, 7WD10 (transgenic CHO cells expresing human APP) cells were treated for 1, 2, and 3 days with either beauveriolide III (**50**, 10 μM) or a reference ACAT inhibitor (FR179254, **53**, 10 μM). After removing the treated media, the washed cells were detached by incubation with trypsin to remove any surface-bound Aβ. The cells were then analysed by IF with the Aβ-binding primary antibody (4G8) and a 488 Alexa Fluor secondary antibody. The same experiment was repeated but instead of using trypsin as a method for detachment, the cells were scraped from the surface of the culture plates. The different detachment methods were intended to determine whether membrane bound Aβ affected the results obtained.

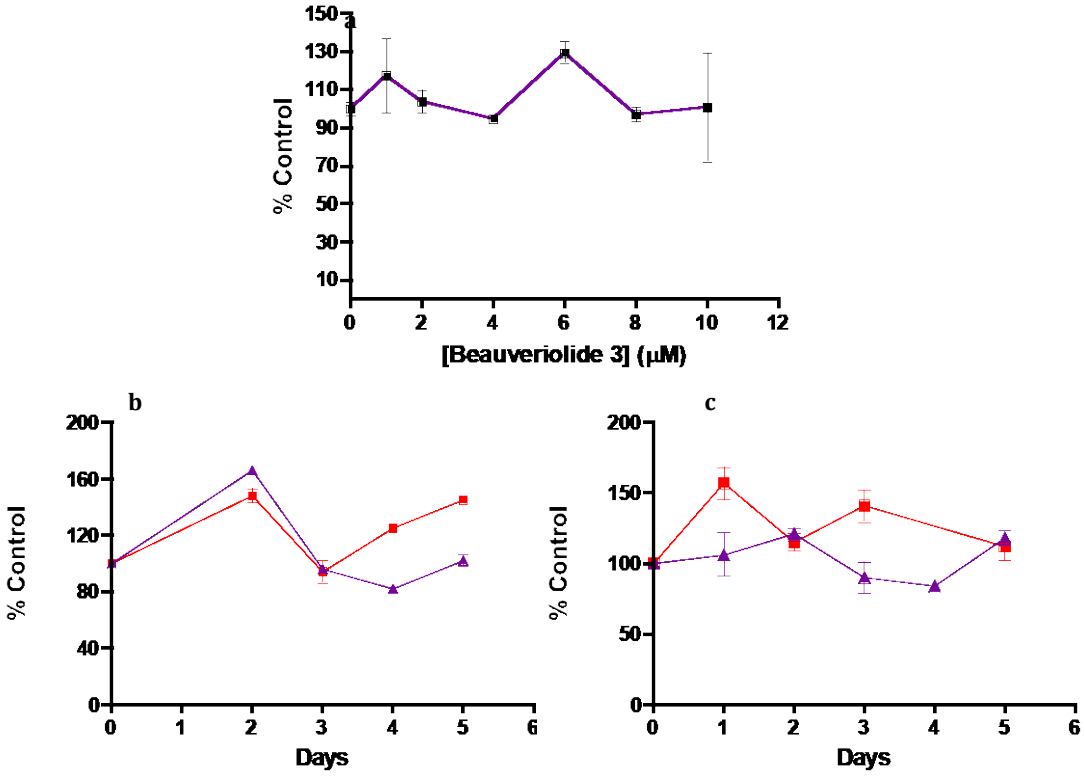

Figure 3.21 – FACS measurements of intracellular Aβ following treatment with ACAT inhibitors. (a) FACS measurements for 7WD10 cells after 24 h treatment with varying concentrations of beauveriolide III (**50**), reported as percent from DMSO treated control cells. (b) FACS measurements for 7WD10 cells treated with 10 μM ■ FR179254 (**53**) or ▲ beauveriolide III (**50**) for varying lengths of time and detached by scraping, reported as percent from DMSO treated control cells. (c) FACS measurements for 7WD10 cells treated with 10 μM ■ FR179254 (**53**) or ▲ beauveriolide III (**50**) for varying lengths of time and detached by trypsin treatment for 15 min at 27°C, reported as percent from DMSO treated control cells, all results normalised to protein content. Data reported as means of three separate samples, and error as std. dev.

As can be observed in Figure 3.21, no change in Aβ concentration could be detected by increasing concentrations of ACAT inhibitor after 24 h, even though 1 μM treatment with beauveriolide III (**50**) has previously been reported to elicit a 10% reduction in secreted Aβ after 24 h treatment measurable by ELISA. Moreover, in the same study, treatments with 1 μM beauveriolide III (**50**) generated up to 60% reduction of secreted Aβ over 3-day treatments.[39] IF-FACS analysis showed no change in Aβ concentration inside the cells over time, for cells treated for up to 5 days with either beauveriolide III (**50**) or FR179254 (**53**).

No difference was observed when different detachment methods were used, however variability from day to day seemed to be slightly smaller with trypsin treatment. While the exact mechanics for Aβ surface association are unknown, the peptide is loosely associated with the membrane and thus any manipulations have the potential to disrupt surface bound Aβ and introduce an element of variability.

It has been reported that different cell-lines have different locations for γ-secretase.[71] The general model for Aβ processing states that APP travels to the plasma membrane where it is secreted. Non-amyloidogenic processing occurs in the plasma membrane where α-secretase cleaves in the middle of the Aβ domain.[2] Some of the secreted APP is rapidly internalised and trapped into endosomes, which either recycle APP to the plasma membrane or target it for lysosomal degradation.[71] Amyloidogenic processing by β and γ-secretases seems to occur in these endosomes. Nevertheless, some studies indicate that non-neuronal cells localise γ-secretase to the plasma membrane, and thus Aβ is secreted as it is produced.[72] No localisation studies have been found for γ-secretase in 7WD10 cells, and thus only speculations can be done on the Aβ processing in the cell model used.

Since 7WD10 cells are transgenic CHO cells, and thus non-neuronal, it is possible that γ-secretase is located primarily in the plasma membrane and therefore most Aβ produced is likely to be secreted immediately. This would explain why the developed assay fails to detect any changes in intracellular Aβ concentration. A

previous IF-microscopy study with 7DW10 cells shows that Aβ distribution is not changed following addition of an ACAT inhibitor (as shown in Figure 3.22).[72] Another study separated the different organelles of treated cells and found that while concentrations of $A\beta_{40}$ did no vary, $A\beta_{42}$ was increased in late endosomes of treated cells.[67] Both studies are not necessary contradictory since the antibody used for IF-microscopy in the first study recognises both $A\beta_{40}$ and $A\beta_{42}$, and since $A\beta_{40}$ is much more abundant than $A\beta_{42}$, the signal might have simply overwhelmed $A\beta_{42}$ changes. Similarly, the antibody used in this case for the FACS assay recognised both $A\beta_{40}$ and $A\beta_{42}$. The fact that no change was observed with either increasing inhibitor concentration and over time can therefore be attributed to the fact that intracellular levels of $A\beta_{40}$ remain constant in 7WD10 cells, and that any changes for $A\beta_{42}$ were overwhelmed by the population of $A\beta_{40}$.

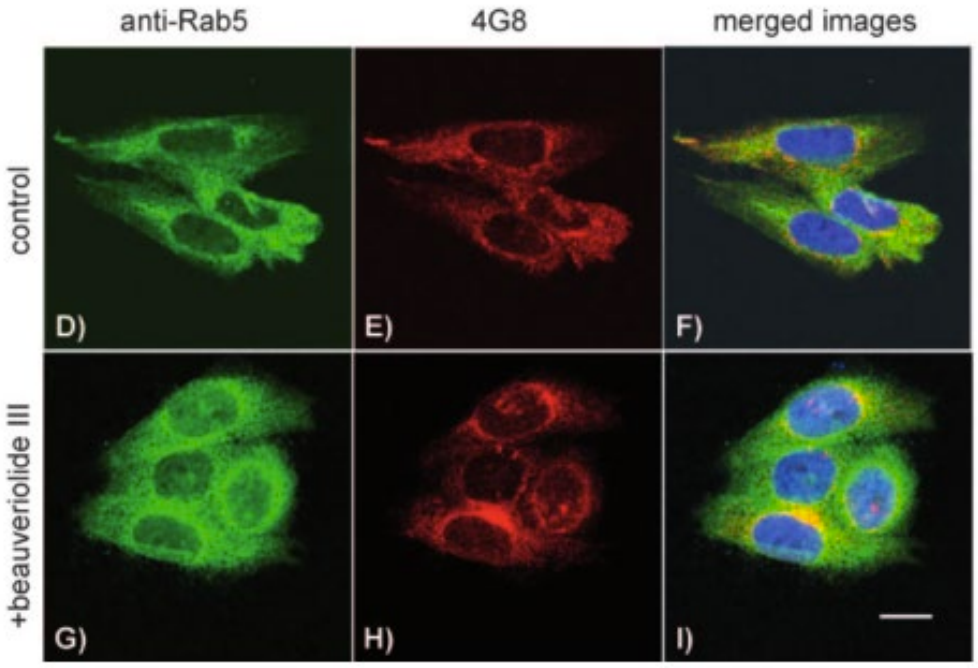

Figure 3.22 – Confocal microscopy images of 7WD10 cells incubated with D)-F) 0.1%DMSO or G)-I) beauveriolide III (1 μM) for 48 h. Cells were fixed with paraformaldehyde and immunolabelled with either rabbit anti-Rab5 antibody with an Alexa-488-labelled (green) secondary antibody (D,G), or the murine anti-Aβ antibody 4G8, with an Alexa-543-labelled (red) secondary antibody (E,H). Nuclei were stained with DAPI. Yellow color in merged image (F,I) corresponds to colocalised Rab5 and Aβ.
Taken from Witter, D., et.al. *ChemBioChem*. 2009, Vol. 10 (8), pp. 1344-1347.

3.2.2. Membrane-bound Aβ detection

Since it did not prove possible to detect intracellular changes in Aβ production, it was decided to attempt detecting changes in secreted media by analysing membrane-bound Aβ. Previous IF-microscopy studies have been able to detect surface-bound Aβ by limiting the number of washing steps and fixing the cells with paraformaldehyde.[28] It only remained to be seen if the membrane-bound Aβ correlated to the secreted amounts of Aβ and whether the developed IF-FACS protocol would be sensitive enough to detect any changes.

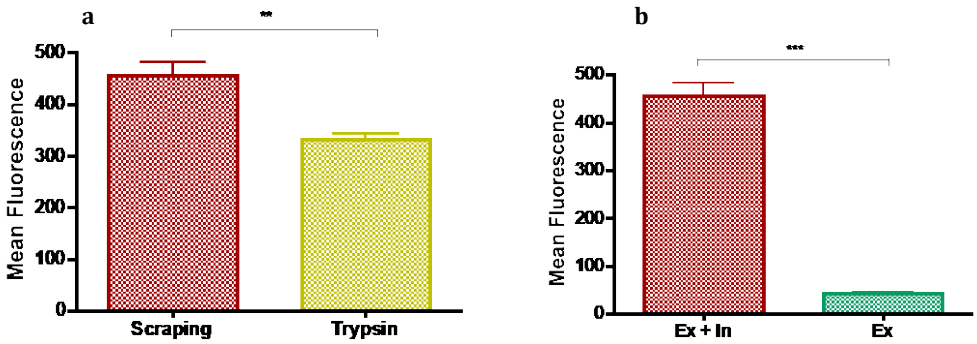

Figure 3.23 – IF-FACS measurements for Aβ with different detachment methods and treatments for 7WD10. (a) Mean fluorescence for cells detached by scraping or trypsin treatment (15 min at 37°C); (b) Mean fluorescence for cell treated with (Extracellular and intracellular Aβ) and without (Extracellular Aβ) 0.1% Triton X-100 in PBS (30 min) for permeabilisation after fixation with paraformaldehyde. Statistical analysis performed using Graphpad Prism 4.0 – Student's *t*-test; ns $p>0.05$; * $p<0.05$, ** $p<0.01$, *** $p<0.001$; n=3.

The method for detachment and treatment of the Aβ expressing cells generated important differences when applied to this assay (Figure 3.23). There was a difference of 100 fluorescence units for trypsin treated cells versus scraped cells (both permeabilised for the same period of time), presumably attributed to the membrane bound Aβ removed with trypsin treatment. However, there were only about 50 fluorescence units observed when scraped cells were analysed without permeabilisation, to detect only membrane bound Aβ. The difference in fluorescence intensity may be explained by the fact that cell permeabilisation tends to split clumps of scraped cells and thus non-permeabilised cells tend to remain in clumps, limiting access to antibodies. Nevertheless, some fluorescence was detected for membrane-bound Aβ, permitting measurements related to ACAT inhibition.

Following the same conditions as the previous experiment (albeit for the permeabilisation step), the results for IF-FACS showed a heterogeneous population (Figure 3.24). After analysis, it was shown that the larger population (FSC>240, R2 in Figure 3.24-b) was most likely formed by clumps with non-specific immunoreactivity since the DMSO-treated control average measurements were equal to the negative control measurements provided by non-APP expressing CHO cells as shown in Figure 3.25-b.

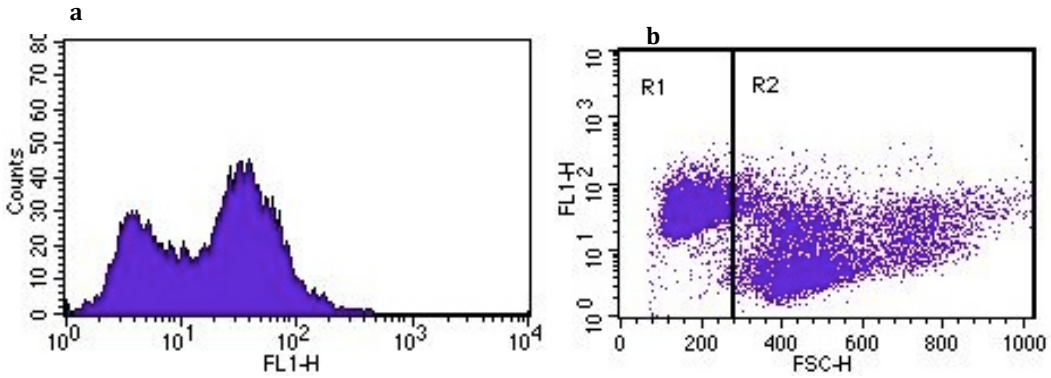

Figure 3.24 – Sample of FACS data collected after Aβ immunolabelling of 7WD10 cells. (a) Histogram of collected data points reported as fluorescence (FL1-H) vs. number of cells (Counts); (b) Dot plot of collected data sorted as forward scatter (FSC-H) vs. fluorescence (FL1-H), with defined regions for small counts (R1, <240 FSC) and large counts (R2, >240 FSC).

The small population (FSC<240, R1 in Figure 3.24-b) showed a distinct difference between positive and negative controls and the population had overall larger fluorescence. In fact, the gated high-fluorescence population (>10^1 FL1-H, Figure 3.24-a) fluorescence mean correlated with the gated small population (FSC<240, R1 in Figure 3.24-a) fluorescence mean. These observations support the hypothesis of the identity of the larger population, since clumped cells restrict the binding of the antibody.

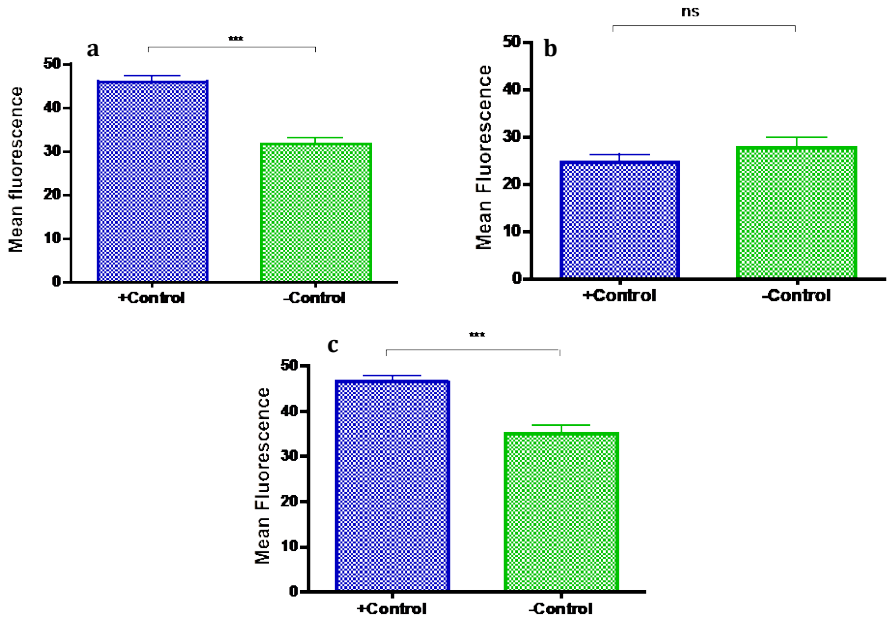

Figure 3.25 – Comparison of populations obtained by IF-FACS for CHO-K1 (-Control) and 7WD10 (+Control) cells, when no permeabilisation is conducted after fixation for labelling of extracellular Aβ only. (a) Small population (R1, <240 FSC) from dot plot; (b) Big population (R2, >240 FSC) from dot plat; c) High fluorescence population (>10^1 FL1-H) from histogram. Statistical analysis performed using Graphpad Prism 4.0 – Student's *t*-test; ns $p>0.05$; * $p<0.05$, ** $p<0.01$, *** $p<0.001$; n=3.

Unfortunately, the analysis of changes in the small population yielded no better results than the ones obtained for the intracellular measurements. As shown in Figure 3.26, no significant difference could be observed for cells treated with ACAT inhibitor over time. The effect was the same for the synthesised beauveriolide III (**50**) and the commercially available ACAT inhibitor Sandoz 58-035 (**54**).

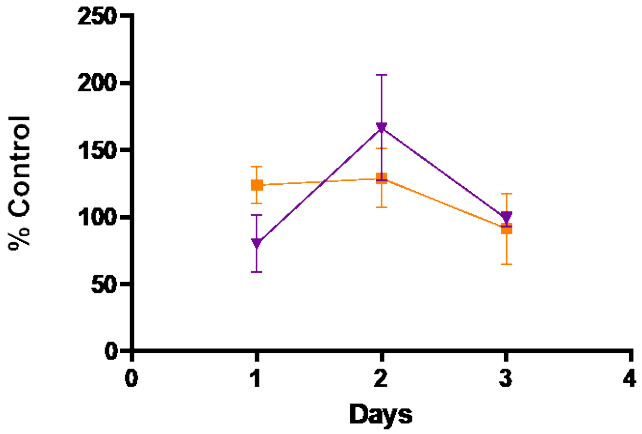

Figure 3.26 – IF-FACS results for extracellular Aβ concentration of 7WD10 cells treated with 10 μM ▼ beauveriolide III (**50**) or ■ Sandoz 58-035(**54**), after 1,2 and 3-day treatments. Results

reported as percentage from 0.1% DMSO-treated control cells after normalisation to protein levels.

3.2.3. Cholesterol esters measurement

In order to determine whether the effects observed were due to the inability of the assay to detect changes in Aβ instead of unexpected metabolic effects in the cells, the assay was complemented with cholesterol (**51**) measurements to confirm ACAT inhibition. Total cholesterol and FC (**51**) measurements were made with Amplex Red Cholesterol Assay from small samples of the treated cell cultures used to determine extracellular Aβ levels. Both measurements were used to determine the changes in CE levels that would indicate ACAT inhibition.

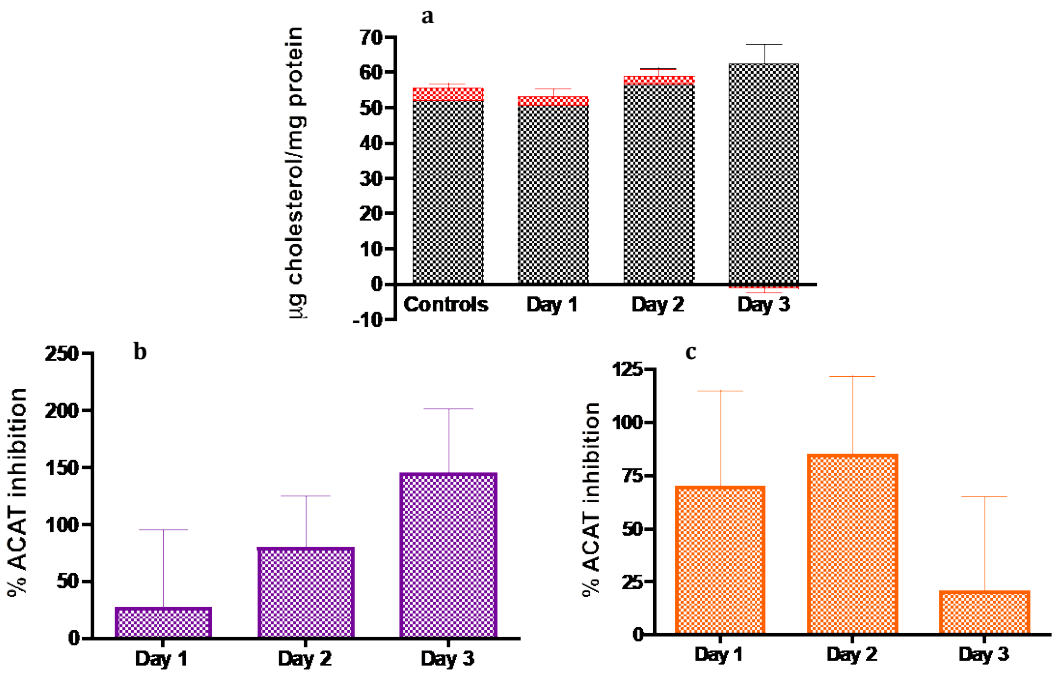

Figure 3.27 – Cholesterol measurements for 7WD10 cells treated with ACAT inhibitors for 1,2 and 3 days. (a) Total cholesterol for cells treated with 10 µM beauveriolide III reported as the combination of ■ free cholesterol and ■ cholesterol esters. Controls are average means for 0.1% DMSO-treated controls for 1,2 and 3-day treatments; (b) ACAT inhibition after 1,2 and 3-day treatments with 10 µM beauveriolide III, reported as percentage of cholesterol esters compared to 0.1 DMSO-treated control cells; (c) ACAT inhibition after 1,2 and 3-day treatments with 10 µM Sandoz 58-035, reported as percentage of cholesterol esters compared to 0.1 DMSO-treated control cells.

As expected, both beauveriolide III (**50**) and Sandoz 58-035 (**54**) showed a decrease in the percentage of CE levels in cells over time without significant

changes in total cholesterol (Figure 3.27- a). Presented as %ACAT inhibition as determined by amount of CE relative to untreated cells, beauveriolide III (**50**) achieved almost complete inhibition by the second day. At similar concentrations, ACAT inhibitor Sandoz 58-035 (**54**) achieved almost complete inhibition after 24 h as reported previously.[63] Treatment for 3 days with Sandoz 58-035 (**54**) showed a decrease in ACAT inhibition as seen by the re-appearance of CE. This fact could be caused by decomposition of the inhibitor in media at the 37°C incubation temperature or other unknown mechanisms, however further investigation on this observation was beyond the scope of this project.

4. Conclusions

In the synthesis of beauveriolide III (**50**), the adoption of a cross-metathesis reaction in place of the published five reactions required for elongation of the β-amino acid in Witter's, *et.al*.[2] synthesis has been fully established. The method has been used to generate beauveriolide III (**50**) in milligram quantities, as well as other beauveriolide analogues. Further optimisations in the reactions following cross-metathesis have led an improvement of the overall yield for the total synthesis of beauveriolide III (**50**) from the reported 16% to 45%.

The development of a FACS method for Aβ detection in treatments for ACAT inhibition requires further optimisation. While Aβ was detected during both intracellular and membrane-bound Aβ measurements, no changes were observed in its concentration following treatment with ACAT inhibitors. No changes were detected with either increasing amounts of inhibitor or long term treatments. Total cholesterol and cholesterol ester measurements indicated successful ACAT inhibition, and thus the lack of confirmation of the Aβ level reduction was more likely a problem of the assay design as opposed to a true metabolic observation. It is probable that the lack of detectable changes is a result of the location of γ-secretase in the plasma membrane on the cell model used, causing most Aβ to be secreted immediately upon production. Nevertheless, it is encouraging to note that IF-FACS can be used to detect Aβ in cell models even when its intracellular amount is likely to be very low. Perhaps further research would lead to a successful combination of antibodies and cell treatment that would allow IF-FACS to be adopted as a method of fast screening for Aβ reduction.

5. Future work

The natural continuation for the first part of this project is the continuous improvement of the available synthetic methods for beauveriolides. Part of this work has already been completed by Dr. Jaime Escribano Cabeza's work on the oxidation steps following cross-metathesis. In addition, the fast pace of research in asymmetric catalysis is likely to provide in the near future a way of improving or replacing the *cis*-crotylation that introduces the desired stereochemistry in the available protocol. Equally, the cyclisation by macrolactonisation is still open to improvement by treatment with different coupling and activating reagents. A systematic study of the optimal reaction conditions has previously been prohibitive due to the cost involved in producing the starting material for the reaction. However, this project's contribution to the improvement of the synthesis might allow this reaction to be further optimised. Testing of carbodiimide activation and different triazoles such as PyBOP are logical starting points for this optimisation.

The use of IF-FACS as a mean to monitor Aβ changes is a novel concept and thus requires extensive optimisation before its use as an analytical tool can be validated. While the studies performed did not provide any positive results, they did open several possibilities for exploration. The two main elements that might provide the key to unlock this methodology are the cell-line and the primary antibody used. A neuronal APP-expressing cell line is more likely to mimic the normal metabolic pathways of Aβ and have γ-secretase as part of the endosomal pathway. This differential localisation of γ-secretase might be enough to allow tracking of Aβ changes by intracellular measurements. Another avenue worthy of study is the use of an anti-$A\beta_{42}$ antibody with minimal cross-reactivity to $A\beta_{40}$ or APP. While the normal amounts of $A\beta_{42}$ are often low and might not be enough to detect any trends by IF-FACS, $A\beta_{42}$ changes have been detected in 7WD10 cells by other methods and thus provide a hopeful avenue for research. The use of an $A\beta_{42}$ provides the additional advantage that this isoform is the most cytotoxic form of Aβ, and thus if readings can be made for $A\beta_{42}$, the results obtained will be directly relevant to effects on AD.

6. Experimental

6.1. Materials and general methods

All solvents used were laboratory or analytical grade and were purchased from Fisher Scientific unless otherwise stated. Anhydrous solvents were purchased from Acros. HPLC grade solvents were from either AnalaR and or Fisher Scientific. All commercially available reagents were purchased from Sigma or Acros unless otherwise specified, and were used as received without further purification. All amino acids, resins and reagents required for peptide synthesis were purchased from C S Bio Co (USA). Tissue culture media were from Gibco/Invitrogen (Paisley UK). Water was Milli-Q™ grade.

CHO-K1 cells were cultured in DMEM medium (with L-glutamate) containing 10% foetal calf serum and 1% stock solution of penicillin-streptomycin (Invitrogen). 7WD10 cells are a stably transfected CHO cell-line expressing human APP751 gene and were donated by Prof. T. Y. Change (Darmouth Medical School, Hannover, NH). 7WD10 cells were cultured in DMEM medium (with L-glutamate) containing 10% foetal calf serum, 0.5% 4G8 antibiotic and 1% stock solution of penicillin-streptomycin (Invitrogen).

Amyloid-β 17-24 monoclonal antibody, 4G8 purified from mouse, was obtained from Covance. Goat anti-mouse, Alexa Fluor 488 antibody, was obtained from Invitrogen.

Semi-preparative scale HPLC (Agilent) was performed using a protein and peptide C18 column (Vydec). The chromatography system consisted of Agilent 1100 Degasser, Quat pump and MWP modules. Spectra were collected for λ256 nm, λ214 nm, and λ495 nm absorptions with a UV/Vis detector. Solvent A was 0.1% TFA in Water and solvent B was 0.1% TFA in CH_3CN. Program A (3 mL/min flow) - gradient: t=0 min, 5% B; t=3 min, 5%; t=20 min, 40% B; t=23 min, 95% B; t=25 min, 95% B; t=28 min, 5%B; t=30 min, 5% B – 8.4 % B.

Silica gel column chromatography was carried out using Merck silica gel (60,

particle size 0.040-0.063 mm (as stationary phase). Thin layer chromatography was performed using pre-coated silica gel plates (Merck 0.25mm Kieselgel 60 F_{254}) visualised by UV (254 nm) or by staining with 10% ammonium molybdate in 2 M H_2SO_4, 0.3 M dinitrophenylhydrazine (DNPH) in 20% H_2SO_4 50% aqueous EtOH or 0.1 M ninhydrin in 3% ethanolic AcOH, followed by heating.

Fluorescence spectra and UV absorbance were recorded on a Spectramax M5 microtiter plate reader (Molecular Devices).

NMR spectra were recorded on a Varian Spectrometer (500 MHz) at 30°C or a Brücker DPX (400 MHz) machine at ambient temperature. The following abbreviations are used to denote multiplicities: br-broad, s-singlet, d-doublet, t-triplet, q-quartet, dd-doublet of doublet, ddd- doublet of doublet of doublets, dt-doublet of triplets, m-multiplet. Coupling constant values (*J*) are reported to the nearest 0.1 Hz. Chemical shifts are reported in parts per million (ppm) and are referenced to the residual solvent peak (^{1}H: $CDCl_3$ – 7.24 ppm, D_2O - 4.80 ppm, Acetone-d_6 – 2.05 ppm, MeOD-d_4 – 4.87 ppm and 3.31 ppm, or DMSO-d_6 – 2.50 ppm; ^{13}C: $CDCl_3$ – 77.23 ppm, Acetone-d_6 – 29.92 ppm and 206.68 ppm, MeOD-d_4 – 49.15 ppm, or DMSO-d_6 – 39.51 ppm).

Mass spectra were recorded on a Micromass LCT electrospray ionisation mass spectrometer with medium-high (7,000) resolution running openlynx. High-resolution mass spectra were recorded on a Brücker MicroTOF electrospray ionisation mass spectrometer with medium-high resolution (10,000).

Melting points were recorded on a Gallenkamp capillary melting point apparatus and are reported uncorrected.

FACS analysis was performed using a BD FACScalibur Flow Cytometer (BD Science, Oxford). Acquisition was performed from 10 000 cells per sample. A blue Argon Laser (488 nm) was used to excite fluorochromes, and emission was detected with a green channel (FITC) and an orange channel (PI). Obtained data was analysed by CellQuest Pro Software.

Samples were analysed in triplicate and error is reported as standard deviation unless otherwise stated. Statistical analysis was generated using GraphPrism 4.0a for Macintosh using unpaired Student's *t*-test: *** $p<0.001$, ** $p<0.01$, * $p<0.05$.

All graphics were generated using GraphPrism 4.0a for Macintosh. Calibration curves were fitted with a linear regression curve.

^{1}H NMR and MS data are reported for all synthesised compounds. ^{13}C NMR data and high resolution MS are reported when available.

6.2. Beauveriolide III synthesis

3-[(4-Methoxybenzyl)oxy]propanol[2]

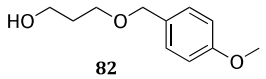

82

p-Anisaldehyde (109.5 mL, 0.9 mol) and a catalytic amount of *p*-toluenesulfonic acid (270 mg, 1.57 mmol) were added to a solution of 1,3-propanediol (**81**) (64.6 mL, 0.9 mol) in toluene (120 mL). The reaction mixture was then heated under reflux conditions on a Dean-Stark apparatus overnight, after which the reaction mixture was allowed to cool down to RT. The solvent was then evaporated under reduced pressure and the residue was dissolved in toluene (3 x 20 mL) with the solvent being evaporated *in vacuo* each time to remove any remaining water. The resulting yellow oil was dissolved in toluene (150 mL) and cooled in an ice bath to 0°C. An ice cooled solution of DIBAL-H (1.5 M, 200 mL, 1.13 mol) in toluene (553 mL) was prepared and added drop wise while stirring. The reaction was allowed to stir overnight at RT and then cooled down to 0°C in an ice bath. Methanol (90 mL) and water (80 mL) were added slowly and the reaction was stirred for 1 h, After which the insoluble material was removed by filtration through a celite path. The filtrate was then washed with toluene (200 mL) and the solvents evaporated *in vacuo*. The brown oil residue was purified by silica gel

chromatography (17:3 DCM:EtOAc) to generate the PMB-protected alcohol **82** as a clear oil (61% yield, 107.6 g. 0.55 mol).

^{1}H NMR ($CDCl_3$, 500 MHz) δ 1.81-1.89 (m, 2H, H2), 3.65 (t, 2H, *J*=5.7 Hz, H3), 3.78 (t, 2H, *J*=5.7 Hz, H1), 3.82 (s, 3H, OMe), 4.47 (s, 2H, CH_2Ph), 6.89 (d, 2H, *J*=9 Hz, Ph H2), 7.26 (d, 2H, *J*=9 Hz, Ph H3).

^{13}C {^{1}H} NMR ($CDCl_3$, 125 MHz) δ 32.34 (C2), 55.50 (C3), 62.61 (C1), 69.36 (*C*H_2Ph), 73.17 (OMe), 114.09 (Ph C3), 129.50 (Ph C2) , 130.44 (Ph C4), 159.51 (Ph C1).

LR-MS (ESI): *m/z* 219.4 $[M+Na]^+$

3-[(4-Methoxybenzyl)oxy]propanal[2]

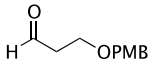

83

A dilution of DMSO (79.5 mL) in DCM (168 mL) was added slowly to a solution of oxalyl chloride (41.2 mL, 0.48 mol) in DCM (479 mL) previously cooled down to -78°C in an acetone/dry ice bath. A solution of PMB-propanol (**82**) (78.83 g, 0.40 mol) in DCM (325 mL) was then added drop wise to the cooled mixture and the reaction was allowed to stir for 20 min. Triethylamine (278.5 mL) was then added and the reaction mixture was allowed to warm up to RT over 45 min while stirring. The reaction was then diluted with water (500 mL) and extracted with DCM (2 x 500 mL). The organic fraction was further washed with brine (2 x 500 mL) and dried over $MgSO_4$, the desiccant was removed by filtration and the solvent evaporated *in vacuo*. The crude orange oil was then purified by silica gel chromatography (4:1 DCM:EtOAc). Aldehyde **83** was isolated as a yellow oil (68% yield, 52.53 g, 0.27 mol).

R_f 0.73 (9:1 DCM:EtOAC, DNPH stain)

^{1}H NMR ($CDCl_3$, 500 MHz) δ 2.68 (td, 2H, *J*=6 Hz, 1.5 Hz, H2), 3.79 (t, 2H, *J*=6 Hz, H3), 3.81 (s, 3H, OMe), 4.47 (s, 3H, CH_2Ph), 6.88 (d, 2H, *J*=8.5 Hz, Ph H2), 7.25 (d, 2H, *J*=9 Hz, Ph H3), 9.79 (t, 1H, *J*=1.7 Hz, CHO).

^{13}C {^{1}H} NMR ($CDCl_3$, 125 MHz) δ 44.12 (C2), 55.14 (C3), 63.77 (*C*H_2Ph), 73.15 (OMe), 114.09 (Ph C3), 129.57 (Ph C2), 130.18 (Ph C4), 159.56 (Ph C1), 201.39 (C1).

LR-MS (ESI): *m/z* 217.1 $[M+H]^+$

(3*S*,4*S*)-1-[(4-Methoxybenzyl)oxy]-4-methyl-5-hexen-3-ol[2]

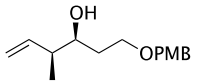

84

Cis-2-butene was bubbled into THF (24 mL) for 15 min to give a saturated solution, which was added to a solution of sodium *tert*-butoxide (6.49 g, 57.9 mmol) in anhydrous THF (58 mL) at -78°C in an acetone/dry ice bath. *n*-Butyllithium (23.2 mL, 57.9 mmol) was added drop wise to the cooled reaction mixture and the bright yellow resulting mixture was allowed to stir at -40°C in an acetonitrile/dry ice bath for 20 min. The reaction solution was then cooled down again to -78°C and a solution (+)-*B*-methoxydiisopinocampheylboron (22.3 g, 70.5 mmol) in THF (12 mL) was then added to the reaction. The resulting clear solution was allowed to stir for 35 min at -78°C. $BF_3{\cdot}Et_2O$ (8.92 mL, 70.5 mmol) was then quickly added to the reaction, followed immediately by a solution of the PMB protected aldehyde **83** (4.88 g, 25.17 mmol) in THF (30 mL). The reaction was allowed to stir at -78°C for 4 hours after which an aqueous solution of NaOH (3 M, 60 mL) was added to the reaction followed by H_2O_2 (30% v/v, 60 mL). The resulting mix was allowed to warm up to RT while stirring overnight, after which it was diluted with water (400 mL) and extracted with EtOAc (3 x 200 mL). The combined organic fractions were dried over $MgSO_4$, the desiccant was removed by filtration and the solvent evaporated under reduced pressure. The crude yellow oil was purified by silica gel chromatography (17:3 hexane:EtOAc) to give the homoallylic alcohol **35** as a yellow viscous oil (49% yield, 3.07 g, 12.3 mmol).

R_f 0.61 (9:1 DCM:EtOAc, DNPH stain)

^{1}H NMR ($CDCl_3$, 500 MHz) δ 1.06 (d, 3H, *J*=6.8 Hz, C4 Me), 1.65-1.81 (m, 2H, H2), 2.2 (q, 1H, *J*=6.8 Hz, H4), 3.59-3.73 (m, 3H, H1, H3), 3.81 (s, 3H, OMe), 4.41 (s, 2H, CH_2Ph), 5.03-5.08 (m, 2H, H6), 5.83 (ddd, 1H, *J*=17.6 Hz, 10.3 Hz, 7.7 Hz, H5), 6.89 (d, 2H, *J*=8.6 Hz, Ph H3), 7.29 (d, 2H, *J*=9.9 Hz, Ph H2).

^{13}C {^{1}H} NMR ($CDCl_3$, 125 MHz) δ 15.26 (C4 Me), 33.75 (C2), 44.09 (C4), 55.51 (C1), 69.39 (*C*H_2Ph), 73.33 (OMe), 74.80 (C3), 114.09 (Ph C3), 115.12 (Ph C4), 129.53 (Ph C2), 130.30 (Ph C1), 141.26 (C6), 159.52 (C5).

LR-MS (ESI): *m/z* 285.0 $[M+Cl]^-$

(3*S*,4*S*)-3-[(*tert*-Butyldimethylsilyl)oxy]-1-[(4-methoxybenzyl)oxy]-4-methyl-5-hexene[2]

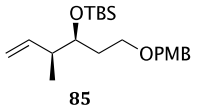

85

2,6-Lutidine (7.58 mL, 65.3 mmol) was added to a solution of the alcohol **84** (8.15 g, 32.6 mmol) in DCM (200 mL) cooled down to 0°C in an ice bath. TBS triflate (9 mL, 39.2 mmol) was then added and the reaction mixture was allowed to stir for 2 h at RT. The reaction mixture was then further diluted with DCM (200 mL) and extracted with aqueous sodium bicarbonate (sat., 2 x 200 mL). The combined aqueous fractions were back-extracted with DCM (2x100 mL) and the combined organic fractions were then dried over $MgSO_4$, the desiccant was removed by filtration and the solvent evaporated under reduced pressure. The residue was purified by silica gel chromatography (DCM) to obtain the TBS protected alkene **85** as a pale yellow oil (69% yield, 8.19 g, 22.5 mmol).

R_f 0.92 (9:1 DCM:EtOAc, DNPH stain).

^{1}H NMR ($CDCl_3$, 500 MHz) δ 0.01 (s, 3H, Si Me), 0.02 (s, 3H, Si Me), 0.86 (s, 9H, *t*Bu 3xMe), 0.95 (d, 3H, *J*=6.9 Hz, H4 Me), 1.62-1.76 (m, 2H, H2), 2.26-2.30 (m, 1H, H4), 3.46-3.49 (m, 2H, H1), 3.68-3.70 (m, 1H, H3), 3.78 (s, 3H, OMe), 4.42 (q, 2H, *J*=11.1 Hz, CH_2Ph), 4.95-5.01 (m, 2H, H6), 5.89 (ddd, 1H, *J*=17.4 Hz, 10.6 Hz, 6.8 Hz, H5), 6.86 (d, 2H, *J*=8.6 Hz, Ph H3), 7.24 (d, 2H, *J*=8.6 Hz, Ph H2).

^{13}C {^{1}H} NMR ($CDCl_3$, 125 MHz) δ 14.42 (Si Me), 15.26 (Si *t*Bu), 21.24 (*t*Bu Me), 33.76 (C4 Me), 48.11 (C2), 60.59 (C4), 69.37 (C1), 73.22 (*C*H_2Ph), 74.77 (OMe), 114.08 (C3), 115.10 (Ph C3), 120.37 (Ph C4), 129.52 (Ph C2), 130.30 (Ph C1), 159.51 (C4), 171.31 (C5).

LR-MS (ESI): *m/z* 365.4 $[M+H]^+$

(3*S*,4*S*)-4-[(*tert*-Butyldimethylsilyl)oxy]-6-[(4-methoxybenzyl)oxy]-3-methylhexanol[2]

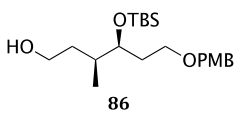

86

9-BBN (57.86 mL, 28.9 mmol) was added to a solution of protected alkene **85** (3.51 g, 9.6 mmol) in THF (200 mL). The reaction mixture was heated under reflux conditions for 3 h and then cooled down to 0°C in an ice bath. Water (5 mL) was added slowly, followed by (30% H_2O_2 v/v, 20 mL) and aqueous NaOH (3 M, 39 mL). The reaction mixture was allowed to stir at 0°C for 30 min and then a further 3 h at RT. The mixture was then diluted with an aqueous solution of Na_2SO_3 (sat., 30 mL) and extracted with EtOAc (2 x 50 mL). The combined organic fractions were washed with brine (1 x 50 mL), dried over $MgSO_4$, the desiccant was removed by filtration and the solvent evaporated *in vacuo*. The residue was purified by silica gel chromatography (6:1 hexane:EtOAc) to obtain TBS protected alcohol **86** as a clear oil (71% yield, 2.6 g, 6.8 mmol).

R_f 0.52 (9:1 DCM: EtOAc, molybdate stain).

^{1}H NMR ($CDCl_3$, 500 MHz) δ 0.03 (s, 3H, Si Me), 0.05 (s, 3H, Si Me), 0.85-0.87 (m, 12H, *t*Bu 3xMe), 1.33-1.37 (m, 1H, H4), 1.70-1.76 (m, 4H, H2, H5), 3.45-3.50 (m, 2H, H1), 3.56-3.61 (m, 1H, H6'), 3.64-3.69 (m, 1H, H3), 3.73-3.76 (m, 1H, H6"), 3.78 (s, 3H, OMe), 4.43 (q, 2H, *J*=11.7 Hz, CH_2Ph), 6.86 (d, 2H, *J*=8.6 Hz, Ph H3), 7.24 (d, 2H, *J*=8.3 Hz, Ph H2).

^{13}C {^{1}H} NMR ($CDCl_3$, 125 MHz) δ -4.80 (Si Me), -4.33 (Si Me), 17.12 (C4 Me), 18.02 (Si *t*Bu), 25.82 (*t*Bu Me), 31.97 (C2), 35.20 (C5), 37.34 (C4), 55.23 (C6), 61.97 (OMe), 66.94 (C3), 72.53 (C1), 73.28 (*C*H_2Ph), 113.70 (Ph C3), 129.26 (Ph C2), 130.53 (Ph C4), 159.08 (Ph C1).

LR-MS (ESI): *m/z* 383.4 $[M+H]^+$

tert-Butyl[(3*S*,4*S*,*Z*)-1-(4-methoxybenzyloxy)-4-methyl-6-oct-en-3-yloxy]dimethylsilane[2]

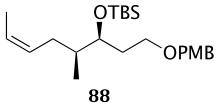

88

NMO (1.05 g, 8.9 mmol) was added to a solution of TBS-protected alcohol **86** (2.63g, 6.9 mmol) in DCM (58 mL). The reaction mixture was cooled to 0°C in an ice bath and TPAP (193.5 mg, 0.55 mmol) was added, followed by 5Å activated molecular sieves. The reaction mixture was then stirred for 3 h, after which the reaction mixture was passed through a flash silica gel column (5:1 DCM:EtOAc).

The solvent was evaporated and the crude aldehyde **87** was dissolved in dry THF (17 mL). A solution of NaHMDS (0.5 M, 42 mL) in THF (20.6 mmol) was added slowly to a solution of $EtPPh_3$ (8.64 g, 20.6 mmol) in dry THF (106 mL) under Argon. The resulting solution was stirred at 0°C for 15 min after which the aldehyde **87** solution was added drop wise with stirring. The reaction was allowed to warm up to RT while stirring over 3 h, and was then cooled to 0°C and cold water (206 mL) was added slowly. The mixture was then extracted with hexane (3 x 200 mL) and the combined organic fractions were washed with brine (1 x 200 mL) and dried over $MgSO_4$, the desiccant was removed by filtration and the solvent evaporated under reduced pressure. The residue was purified by silica gel chromatography (9:1 hexane:EtOAc) to give the final TBS-protected alkene **88** as a clear oil (50% yield, 1.35 g, 3.45 mmol).

R_f 0.90 (DCM, molybdate stain)

^{1}H NMR ($CDCl_3$, 500 MHz) δ 0.01 (s, 3H, Si Me), 0.05 (s, 3H, Si Me), 0.80 (d, 3H, *J*=6.9 Hz, C4 Me), 0.86 (s, 9H, *t*Bu 3xMe), 1.62-1.77 (m, 6H, H8, H4, H2), 1.81-1.88 (m, 1H, H5'), 2.13-.217 (m, 1H, H5"), 3.44-3.48 (m, 2H, H1), 3.70-3.73 (m, 1H, H3), 3.78 (s, 3H, OMe), 4.43 (q, 2H, *J*=11.4 Hz, CH_2Ph), 5.31-5.38 (m, 1H, H6), 5.42-5.49 (m, 1H, H7), 6.86 (d, 2H, *J*=8.5 Hz, Ph H3), 7.23 (d, 2H, *J*=5.2 Hz, Ph H2).

^{13}C {^{1}H} NMR ($CDCl_3$, 125 MHz) δ -4.23 (Si Me), -4.14 (Si Me), 13.15 (C8), 14.63 (Si *t*Bu), 18.36 (C4 Me), 26.16 (*t*Bu Me), 29.43 (C4), 29.92 (C5), 33.44 (C2), 39.38 (C3), 67.58 (OMe), 72.58 (C1), 72.84 (*C*H_2Ph), 114.00 (Ph C3), 124.65 (C7), 129.46 (Ph C2), 130.04 (C6), 130.97 (Ph C4), 159.27 (Ph C1).

LR-MS (ESI): *m/z* 393.5 $[M+H]^+$

(3*S*,4*S*,*Z*)-1-[(4-Methoxybenzyl)oxy]-4-methyl-6-octen-3-ol[2]

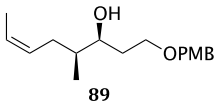

89

A solution of TBAF in THF (1M, 3.81 mL, 3.81 mmol) was added under inert atmosphere to a solution of the protected alkene **88** (1.35 g, 3.46 mmol) in dry THF (28 mL) previously cooled to 0°C in an ice bath. The reaction mixture was allowed to stir overnight, after which it was extracted with DCM (2 x 100 mL). The combined organic fractions were further washed with brine (2 x 100 mL),

dried over $MgSO_4$, the desiccant was removed by filtration and the solvent evaporated under reduced pressure. The residue was purified by silica gel chromatography (9:1 DCM:EtOAC) to obtain the deprotected alcohol **89** as a clear oil (90% yield, 0.86 g, 3.11 mmol).

R_f 0.85 (9:1 DCM: EtOAc, molybdate stain)

^{1}H NMR ($CDCl_3$, 500 MHz) δ 0.92 (d, 3H, *J*=6.8 Hz, H8), 1.54-1.59 (m, 1H, H5'), 1.64 (dd, 3H, *J*=6.7 Hz, 0.6 Hz, C4 Me), 1.67-1.71 (m, 1H, H5"), 1.77-1.87 (m, 1H, H2'), 1.94-2.01 (m, 1H, H2"), 2.16-2.23 (m, 1H, H4), 2.73 (br-s, 1H, OH), 3.66 (dt, 2H, *J*=8.9 Hz, 4.3 Hz, H1), 3.70-3.76 (m, 1H, H3), 3.82 (s, 3H, OMe), 4.47 (s, 2H, CH_2Ph), 5.40-5.46 (m, 1H, H7), 5.50-5.56 (m, 1H, H6), 6.90 (d, 2H, *J*=8.5 Hz, Ph H3), 6.72 (d, 2H, *J*=9.3 Hz, Ph H2).

^{13}C {^{1}H} NMR ($CDCl_3$, 125 MHz) δ 13.10 (C4 Me), 14.17 (C8), 30.65 (C4), 34.01 (C5), 39.41 (C2), 55.50 (C3), 69.66 (OMe), 73.22 (C1), 74.71 (*C*H_2Ph), 114.08 (Ph C3), 125.08 (C7), 126.48 (Ph C4), 129.48 (Ph C2), 130.33 (C6), 159.52 (Ph C1).

LR-MS (ESI): *m/z* 279.4 $[M+H]^+$

(2*R*,3*S*)-[(3*S*,4*S*,*Z*)-1-[(4-Methoxybenzyl)oxy]-4-methyl-6-octen-3-yl] 2-(*tert*-butoxycarbonylamino)-3-methylpentanoate[2]

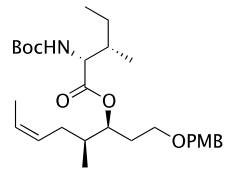

103

DIC (143 µL, 0.91 eq) was added to a solution of *N*-Boc-D-*allo*-isoleucine (175.9 mg, 0.76 mmol) in dry DCM (5 mL) previously cooled down to -10°C. The reaction mixture was allowed to stir 5 min, after which DMAP (92.9 mg, 0.76 mmol), $Sc(OTf)_3$ (74.8 mg, 0.15 mmol) and a solution of the deprotected alcohol **89** (105.7 mg, 0.38 mmol) in DCM (1 mL) were added sequentially. The reaction mixture was allowed to react for 5 h at RT with stirring. After this time, the mixture was washed with aqueous $NaHCO_3$ (sat., 2 x 10 mL), and water (1 x 20 mL). The organic fraction was then dried over $MgSO_4$, the desiccant was removed by filtration and the solvent evaporated *in vacuo*. The residue was purified by silica gel chromatography (DCM) to obtain the title compound **103** as a clear oil (54% yield, 100 mg, 0.2 mmol).

R_f 0.85 (DCM, molybdate stain).

^{1}H NMR ($CDCl_3$, 500 MHz) δ 0.87 (dd, 3H, *J*=13.5 Hz, 6.9 Hz, C4 Me), 0.91-0.99 (m, 6H, Ileu 2xMe), 1.19-1.29 (m, 2H, H4), 1.46 (s, 9H, Boc 3xMe), 1.57-1.60 (m, 2H, Ileu βH), 1.67 (d, 1H, *J*=5.9 Hz, Ileu γH), 1.74-1.77 (m, 1H, H2'), 1.88-1.97 (m, 3H, H8), 2.06-2.15 (m, 1H, H2"), 3.39-3.37 (m, 4H, H5, H3, Ileu αH), 3.82 (s, 3H, OMe), 4.17 (q, 2H, *J*=7.1 Hz, CH_2Ph), 5.06-5.14 (m, 2H, H1), 5.33-5.56 (m, 1H, H7), 5.41-5.56 (m, 1H, H6), 6.90 (d, 2H, *J*=8.6 Hz, Ph H3), 7.27 (d, 2H, *J*=8.5 Hz, Ph H2).

^{13}C {^{1}H} NMR ($CDCl_3$, 125 MHz) δ 11.77 (Ileu Me), 12.94 (Ileu Me), 13.56 (C5), 14.53 (C4 Me), 26.25 (Ileu γC), 28.34 (Boc Me), 30.63 (C8), 33.60 (C2), 37.33 (Ileu βC), 38.96 (C4), 56.95 (C3), 58.69 (C1), 62.92 (Ileu αC), 71.19 (OMe), 75.03 (*C*H_2Ph), 79.83 (Boc *t*Bu), 125.37 (Ph C3), 125.65 (Ph C4), 126.79 (C6), 128.08 (C7), 128.71 (Ph C2), 155.82 (Ph C1), 173.15 (Ileu CO), 173.71 (Boc CO).

LR-MS (ESI): *m/z* 492.4 $[M+H]^+$

(3*S*,4*S*,*Z*)-1-Hydroxy-4-methyl-6-octen-3-yl-(2*R*,3*S*)-[(*tert*-butoxycarbonyl)amino]-3-methylpentanoate[2]

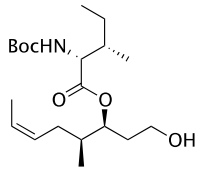

104

A solution of DDQ (19.4 mg, 0.086 mmol) in water (30 µL) was added to a solution of the compound **103** (42 mg, 0.086 mmol) in DCM (500 µL). The reaction was allowed to stir at RT for 1.5 h and then it was diluted with DCM (4 mL) and washed with aqueous sodium bicarbonate (sat., 2 x 2 mL) and brine (2 x 2 mL). The organic fractions were combined, dried over $MgSO_4$, the desiccant was removed by filtration and the solvent evaporated under reduced pressure. The residue was then purified by preparative scale TLC (9:1 DCM:EtOAC) to obtain alcohol **104** as a clear oil (82% yield, 25.9 mg, 0.07 mmol).

R_f 0.34 (9:1 DCM:EtOAc, molybdate stain).

^{1}H NMR ($CDCl_3$, 500 MHz) δ 0.90 (dd, 3H, *J*=15.8 Hz, 6.9 Hz, C4 Me), 0.92-0.99 (m, 6H, Ileu 2xMe), 1.46 (s, 9H, Boc Me), 1.58-1.61 (m, 4H, H8, H4), 1.64 (d, 1H, *J*=6.7 Hz, Ileu γH), 1.73-1.84 (m, 4H, Ileu βH, H5), 1.94-2.03 (m, 1H, H2'), 2.08-2.21 (m, 1H, H2"), 3.52-3.60 (m, 1H, H3), 3.60-3.69 (m, 1H), 4.34-4.40 (m, 1H, Ileu αH),

4.95 (d, 1H, *J*=8.2 Hz, H1'), 5.06-5.12 (m, 1H, H1"), 5.35-5.43 (m, 1H, H7), 5.53-5.56 (m, 1H, H6).

^{13}C {^{1}H} NMR ($CDCl_3$, 125 MHz) δ 11.71 (Ileu Me), 12.86 (Ileu Me), 14.42 (C5), 26.32 (C4 Me), 28.03 (Ileu γC), 30.35 (Boc Me), 34.67 (C8), 37.44 (C2), 38.94 (Ileu βC), 57.11 (C4), 58.62 (C3), 62.86 (C1), 71.24 (Boc *t*Bu), 79.67 (Ileu αC), 125.55 (C6), 128.14 (C7), 155.92 (Ileu CO), 173.63 (Boc CO).

LR-MS (ESI): *m/z* 372.4 $[M+H]^+$

(3*S*,4*S*,*Z*)-4-Methyl-1-oxo-6-octen-3-yl-(2*R*,3*S*)-[(*tert*-butoxycarbonyl)amino]-3-methylpentanoate[2]

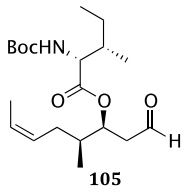

105

Dess-Martin periodinane (148 mg, 0.35 mmol) was added slowly to a solution of alcohol **104** (25.9 mg, 0.07 mmol) in DCM (2 mL). The reaction mixture was allowed to stir at RT for 30 min, after which aqueous $NaHCO_3$ (sat., 2 mL) and aqueous $Na_2S_2O_3$ (sat., 2 mL) were added and the mixture was stirred for further 30 min. The reaction mixture was then extracted with EtOAc (3 x 10 mL) and the combined organic fractions were dried over $MgSO_4$, the desiccant was removed by filtration and the solvent evaporated under reduced pressure. The residue was purified by preparative scale TLC (9:1 DCM:EtOAc) to obtain the aldehyde **105** as a clear oil (57% yield, 14.6 mg, 0.04 mmol).

R_f 0.77 (9:1 DCM: EtOAc, molybdate stain).

^{1}H NMR ($CDCl_3$, 500 MHz) δ 0.89 (d, 3H, *J*=6.8 Hz, C4 Me), 0.92-0.99 (m, 6H, Ileu 2xMe), 1.38 (s, 9H, Boc 3xMe), 1.40-1.43 (m, 1H, Ileu γH), 1.51 (d, 3H, *J*=6.0 Hz, H8), 1.58 (d, 1H, *J*=5.3 Hz, H4), 1.63-1.71 (m, 2H, Ileu βH), 1.73-1.78 (m, 1H, H5'), 1.78-1.82 (m, 1H, H5"), 3.56-3.59 (m, 1H, H3), 4.22-4.33 (m, 1H, Ileu αH), 4.83-3.86 (m, 1H, H2"), 4.98-5.04 (m, 1H, H2'), 5.26-5.31 (m, 1H, H6), 5.43-5.47 (m, 1H, H7), 9.68 (s, 1H, COH).

LR-MS (ESI): *m/z* 370.5 $[M+H]^+$

(3*S*,4*S*,*Z*)-3-{[(2*R*,3*S*)-2-[(*tert*-Butoxycarbonyl)amino]-3-methylpentanoyloxy}-4-methyl-6-octenoic acid[2]

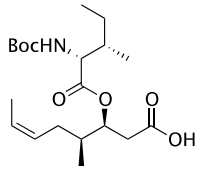

106

2-Methyl-2-butene was bubbled through water (35 µL) for 15 min to create a saturated solution, which was added drop wise to a solution of the aldehyde **105** (14.6 mg, 39.6 µmol) in butanol (162 µL). After stirring for 15 min at RT, a solution of $NaClO_2$ (48.9 mg, 0.41 µmol) and NaH_2PO_4 (35.6 mg, 0.39 µmol) in water (163 µL) was added slowly. The reaction mixture was allowed to stir overnight and then was diluted with water (1 mL) and extracted with DCM (3 x 1 mL). The combined organic fractions were dried over $MgSO_4$ the desiccant was removed by filtration and the solvent evaporated *in vacuo*. The residue was purified by preparative scale TLC to give the title compound **106** as a clear oil (76% yield, 11.5 mg, 29.9 µmol).

^{1}H NMR ($CDCl_3$, 500 MHz) δ 0.84-0.95 (m, 9H, Ileu 2xMe, C4 Me), 1.44 (s, 9H, Boc Me), 1.55-1.66 (m, 5H, Ileu γH, H4, H8), 1.79-1.98 (m, 2H, Ileu βH), 2.10-2.18 (m, 1H, H5'), 2.58-2.74 (m, 1H, H5"), 3.56-3.74 (m, 2H, H3), 4.24-4.38 (m, 1H, Ileu αH), 4.89-5.00 (m, 2H, H2), 5.26-5.39 (m, 1H, H6), 5.49-5.61 (m, 1H, H7).

LR-MS (ESI): *m/z* 408.4 $[M+Na]^+$

Fmoc-Ala-O*t*Bu

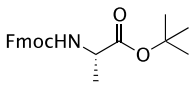

114

H_2SO_4 (16 µL) was added to a solution of Fmoc-Ala (0.5 g, 1.6 mmol) in DCM (5 mL) with stirring. Isobutylene was bubbled through the solution for 1 h, after which the solution was washed with aqueous $NaCO_3$ (sat., 2 x 5 mL) and water (2 x 5 mL). The aqueous fractions were back-extracted with DCM (3 x 10 mL) and

the combined organic phases were dried over $MgSO_4$, the desiccant was removed by filtration and the solvent evaporated *in vacuo*. The residue was purified with silica gel chromatography to obtain the protected amino acid **114** as a clear viscous oil (81% yield, 0.47 g, 1.3 mmol).

R_f 0.85 (9:1 DCM:EtOAc, molybdate stain).

^{1}H NMR ($CDCl_3$, 500 MHz) δ 1.42 (d, 3H, *J*=7.1 Hz, Ala Me), 1.49 (s, 9H, *t*Bu 3xMe), 4.30 (dt, 2H, *J*=19.3 Hz, 7.2 Hz, Ala αH, Fmoc C*H*), 4.35-4.42 (m, 2H, Fmoc CH_2), 5.39 (br-d, 1H, *J*=7.3 Hz, Ala NH), 7.34 (td, 2H, *J*=7.4 Hz, 1.0 Hz, Fmoc Ph H2), 7.43 (t, 2H, *J*=7.4 Hz, Fmoc Ph H3), 7.62 (d, 2H, *J*=3.7 Hz, Fmoc Ph H4), 7.78 (d, 2H, *J*=12.8 Hz, Fmoc Ph H1).

LR-MS (ESI): *m/z* 390.4 $[M+Na]^+$

Ala-O*t*Bu

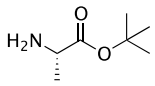

115

A solution of the protected alanine **114** (379 mg, 1.0 mmol) in a mixture of piperidine and DMF (20% v/v, 30 mL) was stirred for 30 min at RT. After this time the solvent was removed under reduced pressure and the residue was triturated with cold ether (50 mL). The insoluble material was removed by filtration and the solid residue was dried *in vacuo* to obtain the title compound **115** as a white powder (24% yield, 36 mg, 0.24 mmol).

^{1}H NMR (D_2O, 500 MHz) δ 1.35 (d, 3H, *J*=7.2 Hz, Ala Me), 1.70 (s, 9H, *t*Bu 3xMe), 3.67-3.71 (m, 1H, Ala αH).

m.p.: 177.7-178.4°C (lit. m.p.[73] 162-163°C)

LR-MS (ESI): *m/z* 146.1 $[M+H]^+$

Cbz-Phe-Ala-O*t*Bu

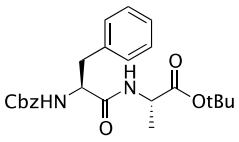

116

DIPEA (260 µL, 1.5 mmol) was added to a solution of Cbz-protected phenylalanine (445 mg, 1.5 mmol) in THF (5 mL) at 0°C. The solution was stirred

for 5 min, after which the deprotected alanine **115** (170 mg, 1.5 mmol) was added, followed by HOBt (202 mg, 1.5 mmol) and DCC (339 mg, 1.6 mmol). The reaction was stirred for 1 h at 0°C, then for a further 1 h at RT. The insoluble material was then removed by filtration, and the filtrate was diluted with EtOAc (20 mL) and extracted with aqueous $NaHCO_3$ (sat., 3 x 10 mL). The organic phase was dried over $MgSO_4$, the desiccant was removed by filtration and the solvent removed under reduced pressure. The residue was purified by silica gel chromatography (9:1 hexane:EtOAc) to obtained the fully protected dipeptide **116** as a white powder (66% yield, 420 mg, 0.99 mmol).

R_f 0.78 (9:1 DCM:EtOAc, molybdate stain).

^{1}H NMR ($CDCl_3$, 500 MHz) δ 1.34 (d, 3H, J=7.1 Hz, Ala Me), 1.47 (s, 9H, *t*Bu 3xMe), 3.07 (dd, 2H, J=13.7 Hz, 6.8 Hz, Phe βH), 3.13-3.16 (m, 1H), 4.35-4.40 (m, 1H, Ala αH), 4.44-4.45 (m, 1H, Phe αH), 5.11 (s, 2H, Cbz CH_2Ph), 5.29 (br-s, 1H, Ala NH), 6.34 (br-d, 1H, J=6.2 Hz, Phe NH), 7.19-7.39 (m, 10H, Cbz Ph, Phe Ph).

^{13}C {^{1}H} NMR ($CDCl_3$, 125 MHz) δ 18.38 (*t*Bu Me), 27.85 (Ala Me), 38.54 (Phe βC), 48.67 (*t*Bu), 66.87 (Ala αC), 81.91 (Phe αC), 92.20 (Cbz *C*H_2Ph), 126.89 (Phe Ph C3) 127.88 (Cbz Ph C3), 128.01 (Phe Ph C2), 128.10 (Cbz Ph C2), 128.50 (Phe Ph C1), 129.26 Cbz Ph C1), 136.18 (Phe Ph C4), 136.25 Cbz Ph C4), 155.82 (Cbz CO), 170.21 (Ala CO), 171.15 (Phe CO).

Phe-Ala-O*t*Bu

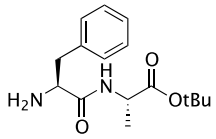

117

Pd/C (10%, 42 mg) was added to a solution of the dipeptide **116** (42 mg, 0.99 mmol) in a mixture of methanol and *tert*-butanol (1:1, 5 mL). The reaction mixture was flushed with H_2 and allowed to stir for 1 h under a H_2 atmosphere. The insoluble material was then removed by filtration through a celite pad and the solvent was evaporated under reduced pressure to obtain the deprotected dipeptide **117** as a white power (53% yield, 152 mg, 0.52 mmol). The crude product was used without further purification.

R_f 0.63 (9:1 DCM:EtOAc, ninhydrin stain).

^{1}H NMR ($CDCl_3$, 500 MHz) δ 1.38 (d, 3H, *J*=7.1 Hz, Ala Me), 1.48 (s, 9H, *t*Bu 3xMe), 2.80 (dd, 1H, *J*=13.7 Hz, 9.2 Hz, Phe βH'), 3.29 (dd, 1H, *J*=13.7 Hz, 4.0 Hz, Phe βH"), 3.68-3.69 (m, 1H, Phe αH), 4.44-4.50 (m, 1H, Ala αH), 7.24-7.34 (m, 5H, Phe Ph).

^{13}C {^{1}H} NMR ($CDCl_3$, 125 MHz) δ 18.59 (*t*Bu Me), 27.97 (Ala Me), 40.89 (Phe βC), 48.26 (*t*Bu), 56.30 (Phe αC), 81.80 (Ala αC), 126.28 (Phe Ph C3), 128.64 (Phe Ph C2), 129.35 (Phe Ph C1), 137.71 (Phe Ph C4), 172.21 (Phe CO), 173.60 (Ala CO).

m.p.: 53.4-54.7°C

LR-MS (ESI): *m/z* 293.2[M+H]$^+$

(3*S*,4*S*,*Z*)-1-[((*S*)-1-{[(*S*)-1-(*tert*-Butoxy)-1-oxopropan-2-yl]amino}-1-oxo-3-phenylpropan-2-yl)amino]-4-methyl-1-oxo-6-octen-3-yl-(2*R*,3*S*)-[(*tert*-butoxycarbonyl)amino]-3-methylpentanoate[2]

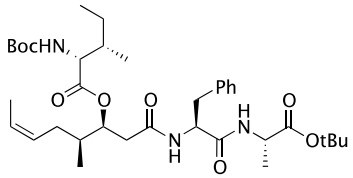

107

HOBt (34 mg, 0.25 mmol), DCC (57.2 mg, 0.28 mmol) and dipeptide **117** (73.6 mg, 0.25 mmol) were added to a solution of the acid **89** (97 mg, 0.25 mmol) in THF (5 mL) previously cooled down to 0°C in an ice bath. The reaction mixture was allowed to stir for 1 h at 0°C, and a further 1 h at RT. The solid residue was removed by filtration, and the solvents were removed under reduced pressure. The residue was purified by preparative scale TLC (9:1 DCM:EtOAc) to obtain compound **107** as a coulourless oil (80% yield, 134.1 mg, 0.2 mmol).

^{1}H NMR ($CDCl_3$, 500 MHz) δ 0.83-0.95 (m, 15H, H8, C4 Me, Ileu 2xMe, Ala Me), 1.12-1.20 (m, 1H, H4), 1.21-1.40 (m, 25H, *t*Bu 3xMe, Ileu βH, Ileu γH), 1.43 (s, 9H, Boc *t*Bu 3xMe), 1.68-1.74 (m, 1H, H5'), 1.87-1.95 (m, 1H, H5"), 2.41-2.48 (m, 2H, Phe βH), 3.01-3.12 (m, 2H, H2), 4.28-4.35 (m, 2H, Ala αH, Phe αH), 4.62 (q, 1H, *J*=7.1 Hz, Ileu αH), 5.04-5.13 (m, 2H, Ala NH, Phe NH), 5.27-5.34 (m, 1H, H3), 5.47-5.53 (m, 1H, Ileu NH), 6.35 (d, 1H, *J*=6.9 Hz, H6), 6.53-6.59 (m, 1H, H7), 7.21-7.30 (m, 5H, Phe Ph).

^{13}C {^{1}H} NMR ($CDCl_3$, 125 MHz) δ 11.71 (Ileu Me), 12.87 (Ileu Me), 13.70 (C4 Me), 14.09 (C8), 14.45 (Ala Me), 29.33, (Ileu γC), 33.68 (C5), 35.99 (C4), 37.29 (Ileu βC), 39.07 (C2), 49.44 (Phe βC), 54.65 (Ala αC), 57.05 (Phe αC), 60.38 (Ileu αC), 74.99 (*t*Bu), 79.77 (Boc *t*Bu), 81.94 (C3), 125.66 (Phe Ph C3'), 126.97 (Phe Ph C3''), 127.82 (Phe Ph C2'), 128.48 (Phe Ph C2''), 128.60 (C6), 129.25 (Phe Ph C4), 136.61 (C7), 155.88 (Phe Ph C1), 169.48 (Ala CO), 170.01 (Phe CO), 171.46 (C1), 172.29 (Boc CO).

LR-MS (ESI): *m/z* 670.1 $[M+H]^+$

(*S*)-2-[(*S*)-2-({(3*S*,4*S*)-3-[(2*R*,3*S*)-2-Amino-3-methylpentanoyl]oxy}-4-methyloctanamido)-3-phenylpropanamido]propanoic acid

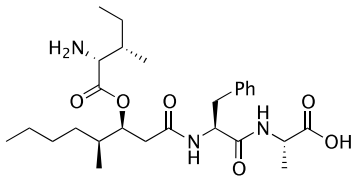

109

Pd/C (10%, 0.2 mg) was added to a solution of the fully protected alkene **107** (12 mg, 0.02 mmol) in MeOH (2 mL). The suspension was flushed with H_2 for 5 min, after which it was allowed to stir overnight under a H_2 atmosphere. The catalyst was removed by filtration through a celite path, after which the solvent was evaporated under reduced pressure. The residue was dissolved in MeOH (0.5 mL) and TFA (40 µL) was added slowly. The reaction mixture was allowed to stir for 30 min at RT, after which the solvents were evaporated under reduced pressure. Cold ether (1 mL) was added slowly, and the resulting suspension was centrifuged. The solvent was decanted and the residue was dissolved in *t*-BuOH (100 µL) and subjected to semi-preparative scale HPLC (Program A) to isolate the desired product **109** as a white powder (11% yield, 1.1 mg, 2.2 µmol) .

LR-MS (ESI): *m/z* 506.1 $[M+H]^+$

Beauveriolide III[2]

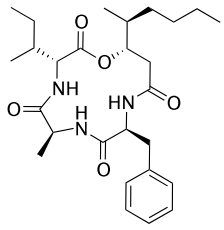

50

HATU (1.1 mg, 2.85 μmol), HOAt (0.6 mg, 4.8 μmol) and collidine (0.8 mg, 6.6 μmol) were added with stirring to a solution of the acid **109** (1.1 mg 2.2 μmol) in DMF (20 μL), previously cooled down to -10°C in a salt/ice bath. The reaction mixture was allowed to warm up overnight while stirring, after which it was diluted with EtOAc (1 mL) and washed with aqueous $NaHCO_3$ (sat., 2 x 1 mL) and brine (2 x 1 mL). The organic fraction was dried over $MgSO_4$, the desiccant was removed by filtration and the solvent removed under reduced pressure. The residue was then purified by semi-preparative scale HPLC, to obtain beauveriolide III (**50**) as a white powder (76% yield, 0.8 mg, 1.6 μmol).

^{1}H NMR ($CDCl_3$/MeOD-$_{d4}$, 500 MHz) δ 0.89-0.96 (m, 14H, Ileu 2xMe, H8, H4 Me, H7), 1.08-1.14 (m, 1H, H4), 1.15-1.50 (m, 15H, Ala Me, Ileu βH, Ileu γH, H6, H5), 1.74-1.81 (m, 1H, Ala NH), 2.02-2.06 (m, 1H, Phe NH), 2.45 (dd, 1H, *J*=13.1, 11.6 Hz, Phe βH'), 2.62 (dd, 1H, *J*=12.8 Hz, 3.7 Hz, βH"), 2.91-2.99 (m, 1H, H2), 3.05-3.09 (m, 1H, Ileu NH), 3.78-3.81 (m, 1H, Ala αH), 4.30 (t, 1H, *J*=10.1 Hz, Ileu αH), 4.34 (d, 1H, *J*=9.1 Hz), 4.44 (dd, 1H, *J*=6.9 Hz, 5.2 Hz, Phe αH), 4.98-5.02 (m, 1H, H3), 6.99 (d, 1H, *J*=8.7 Hz, Phe Ph H4), 7.22-7.33 (m, 3H, Phe Ph H3, Phe Ph H2'), 8.65 (dd, 1H, *J*=19.7 Hz, 8.7 Hz, Phe Ph H2").

^{13}C {^{1}H} NMR ($CDCl_3$+MeOD-$_{d4}$, 125 MHz) δ 11.19 (C8), 14.24 (Ile Me), 14.90 (Ileu Me), 15.15 (C4 Me), 15.81 (C7), 23.31 (C6), 26.18 (Ala Me), 29.67 (C5), 30.00 (Ileu γC), 35.91 (C4), 35.93 (Ileu βC), 36.11 (Phe βC), 37.47 (C2), 49.82 (Ileu αC), 57.23 (Ala αC), 59.65 (Phe αC), 76.91 (C3), 127.30 (Phe Ph C4), 128.88 (Phe Ph C3), 129.40 (Phe Ph C2), 136.75 (Phe Ph C1), 169.83 (Ileu CO), 171.86 (C1), 171.93 (Phe CO), 172.60 (Ala CO).

LR-MS (ESI): *m/z* 488.5 $[M+H]^+$

(3*S*,4*S*,*E*)-1-[(4-Methoxybenzyl)oxy]-4-methyl-5-octen-3-ol[66]

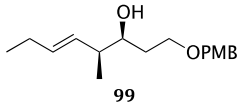

99

Trans-3-hexene (124 μL, 1 mmol) and 2nd generation Hoveyda-Grubbs catalyst (**98**, 1.2 mg, 2 μmol) were added to a solution of the homoallylic alcohol **35** (50 mg, 0.2 mmol) in DCM (1 mL). The reaction mixture was heated under reflux conditions for 3 h with stirring, after which it was cooled down to RT and the solvent was evaporated under reduced pressure. The residue was immediately purified by flash chromatography (7:3 hexane:EtOAc) to obtain the product **99** as a clear oil (89% yield, 49 mg, 0.18 mmol).

R_f 0.51 (4:1 hexane:EtOAc, molybdate stain).

^{1}H NMR ($CDCl_3$, 500 MHz) δ 0.99 (t, 3H, J=7.5 Hz, C4 Me), 1.03 (d, 3H, J=2.7 Hz, H8), 1.63-1.71 (m, 1H, H4), 1.75-1.82 (m, 1H, H2'), 1.98-2.06 (m, 1H, H2"), 2.17-2.22 (m, 2H, H7), 3.57-3.64 (m, 2H, H1), 3.67-3.72 (m, 1H, H3), 3.80 (s, 3H, OMe), 4.45 (s, 2H, CH_2Ph), 5.33 (dd, 1H, J=15.3 Hz, 7.8 Hz, H5), 5.33 (dt, 1H, J=15.3 Hz, 6.3 Hz, H6), 6.89 (d, 2H, J=8.3 Hz, Ph H2), 7.27 (d, 2H, J=9.4 Hz, Ph H3).

^{13}C {^{1}H} NMR ($CDCl_3$, 125 MHz) δ 13.9 (C4 Me), 15.8 (C8), 25.6 (C4), 33.6 (C2), 33.9 (C7), 42.9 (C1), 55.2 (C3), 69.1 (OMe), 73.0 (CH$_2$Ph), 113.8 (Ph C1), 129.3 (C5), 130.1 (C6), 131.3 (Ph C2), 132.8 (Ph C3), 159.3 (Ph C4).

LR-MS (ESI): *m/z* 279.1 $[M+H]^+$

6.3. Immunofluorescence and FACS

Standard Protocol

CHO and 7WD10 cells were seeded at a density of 5 x 10^5 cells per well in a 6-well plate and allowed to adhere overnight. The media was then aspirated and replaced with compound treated-media (or 0.1% DMSO in the case of control wells) and incubated for the required time. The media was then removed and the cells were washed with PBS (2 x 1 mL). The cells were scraped into PBS (2 mL), centrifuged at 2,000 rpm for 5 min and the pellet was suspended in PBS to give a final density of 1 x 10^6 cells per 100 μL. The cells were then transferred to a V-shape 96-well plate and spun at 1,500 rpm for 5 min. The buffer was discarded by careful pipetting and 2% paraformaldehyde (100 μL in PBS) was added to each well and allowed to mix for 20 min. The plate was then centrifuged under

the same conditions and the paraformaldehyde solution was removed. The cell pellet was washed with FACS buffer (0.02 M NaN_3, 0.1% BSA in PBS, 100 μL) and then centrifuged under the same conditions. After repeating the washing step, the cell pellet was suspended in permeabilisation buffer (0.1% saponin, 1% BSA in PBS, 100 μL) and allowed to mix for 30 min at RT. The permeabilisation buffer was then discarded and the pellet was suspended in a solution of anti-Aβ antibody (1:800 dilution in permeabilisation buffer, 50 μL) and allowed to mix for 1 h at RT. After this time, the cells were washed twice with permeabilisation buffer (100 μL) and then suspended in a solution of Alexa Fluor 488 secondary antibody (1:1,000 dilution in permeabilisation buffer, 50 μL) and allowed to stand for 1 h at RT. Following incubation with the 2° antibody, the cells were washed twice with permeabilisation buffer (100 μL) and once with FACS buffer (100 μL). The cell pellet was then resuspended in PBS (600 μL) and transferred to FACS tubes for analysis.

Membrane-bound Aβ only

The protocol was the same as the standard method but eliminating the permeabilisation step and replacing the permeabilisation buffer in the washes with FACS buffer.

Detachment method analysis

The protocol was the same as the standard method except for the detachment of cells, which instead of scraping used trypsin-EDTA (300 μL per well), followed by incubation at 37°C for 20 min, after which the cells were suspended in FCS-PBS (20%, 2 mL).

6.4. Protein content determination

Protein levels were determined using a bicinchonininc acid (BCA) protein assay (Pierce Biotechnology) as described in Chapter 2.

6.5. Amplex Red cholesterol assay

Total cholesterol and free cholesterol were determined using an Amplex Red

Cholesterol Assay Kit (Invitrogen) as per manufacturer's instructions. In summary, for total cholesterol measurements, cell samples were diluted with Triton X-100 buffer (1:1, 1% in PBS) and sonicated for 20 min at RT. Samples were then diluted with the provided reaction buffer (1:10, 0.1 M potassium phosphate, pH 7.4, 0.05 M NaCl, 5 mM cholic acid, 0.1% Triton X-100). Samples and cholesterol controls (50 μL) were added to a black-bottom 96-well plate. Working solution of Amplex Red (50 μL) containing 2 U/mL HRP, 2 U/mL cholesterol oxidase, 0.2 U/mL cholesterol esterase and 300 μM Amplex Red in DMSO was added to each well. The plate was incubated at 37°C for 30 min protected from light, after which fluorescence was measured using a 540 nm excitation and 590 nm emission detection. The assay for free cholesterol was identical to total cholesterol measurements, except in the fact that the working solution did not contain any cholesterol esterase.

7. References

1. Wimo, A. and Prince, M. *World Alzheimer Report 2010 The Global Economic Impact of Dementia*. 2010.

2. Witter, D.P.; Chen, Y.; Rogel, J.K.; Boldt, G.E. and Wentworth, P. The natural products beauveriolide I and III: a new class of beta-amyloid-lowering compounds. *ChemBioChem : A European Journal of Chemical Biology*. 2009;10(8):1344-7.

3. Tomoda, H. and Omura, S. Potential therapeutics for obesity and atherosclerosis: inhibitors of neutral lipid metabolism from microorganisms. *Pharmacology & Therapeutics*. 2007;115(3):375-89.

4. Hamill, R.L.; Higgens, C.E.; Boaz, M.E. and Gorman, M. Knockdown of ACAT-1 reduces amyloidogenic processing of APP. *Tetrahedron Letters*. 1969;(45):4255-8.

5. Isogai, A. and Kanaoka, M. Structure of a new beauveriliode beauveria A from *Bassiana*. *Structure*. 1978;42(9):1797-8.

6. Elsworth, J.F. and TownGrove, J.F. Cyclodepsipeptides from *Beauverios bassiana*. Part 2. Beauveriolides A to F and their relationship to isarolide. *Journal of the Chemical Society, Perkin Transactions 1*. 1980:1795-9.

7. Grove, J.F. Cyclodepsipeptides from *Beauverioa bassiana*. Part 3. The Isolation of beauveriolides Ba, Ca, Ja, and Ka. *Journal of the Chemical Society, Perkin Transactions 1*. 1980:2878-80.

8. Jegorov, A.; Sedmera, P.; Matha, V.; Simk, P.; Landau, Z.; Eyal, J. and Z, H. Beauveriolides L and La from *Beauveria Tenella* and *Paecilomyces Fumosoroseus*. *Phytochemistry*. 1994;37(94):1301-3.

9. Tomoda, H.; Si, S.; Yamaguchi, Y.; MAsuma, R. and Omura, S. Specific inhibitors of lipid droplet formation in mouse macrophages, produced by *Beauveria* sp. FO-6979. *Scanning*. 1999;52(1):1-6.

10. Nagai, K.; Doi, T.; Ohshiro, T.; Sunazuka, T.; Tomoda, H.; Takahashi, T. and Omura, S. Synthesis and biological evaluation of a focused library of beauveriolides. *Bioorganic & Medicinal Chemistry Letters*. 2008;18(15):4397-400.

11. Tomoda, H. and Doi, T. Discovery and combinatorial synthesis of fungal metabolites beauveriolides, novel antiatherosclerotic agents. *Accounts of Chemical Research*. 2008;41(1):32-9.

12. Ohshiro, T.; Matsuda, D.; Nagai, K.; Doi, T.; Sunazuka, T.; Takahashi, T.; Rudel, L.L.; Omura, S. and Tomoda, H. The selectivity of beauveriolide derivatives in inhibition toward the two isozymes of acyl-CoA: cholesterol acyltransferase. *Chemical & Pharmaceutical Bulletin*. 2009;57(4):377-81.

13. Harris, W.S.; Dujovne, C.A.; Bergmann, K.von; Akester, J.; Windsor, S.L.; Greene, D. and Look, Z. Effects of the ACAT inhibitor CL 277,082 on cholesterol metabolism in humans. *Clinical Pharmacology and Therapeutics*. 1990;48(2):189-94.

14. Hainer, J.W.; Terry, J.G.; Connell, J.M.; Zyruk, H.; Jenkins, R.M.; Shand D.L.; Gillies, P.J.; Livak, K.J.; Hunt, T.L. and Crouse, J.R. Effect of the acyl-CoA:cholesterol acyltransferase inhibitor DuP 128 on cholesterol absorption and serum cholesterol in humans. *Clinical Pharmacology and Therapeutics*. 1994;56(1):65-74.

15. Kusunoki, J.; Hansoty, D.K.; Aragane, K.; Fallon, J.T.; Badimon, J.J. and Fisher, E.A. Acyl-CoA : cholesterol acyltransferase inhibition reduces atherosclerosis in apoliprotein E-deficient mice. *Journal of the American Heart Association*. 2001.

16. Glass, C.K. and Witztum, J.L. Atherosclerosis: the road ahead review. *Cell*. 2001;104:503-16.

17. Nissen, S.E.; Tuzcu, E.M.; Brewer, H.B.; Sipahi, I.; Nicholls, S.J.; Ganz, P.; Schoenhagen, P.; Waters, D.D.; Pepine, C.J.; Crowe, T.D.; Davidson, M.H.; Deanfield, J.E.; Wisniewski, L.M.; Hanyok, J.J. and Kassalow, L.M. Effect of ACAT inhibition on the progression of coronary atherosclerosis. *The New England Journal of Medicine*. 2006;354(12):1253-63.

18. Ross, R. The pathogenesis of atherosclerosis: perspective for the 1990s. *Nature*. 1993;362:801-9.

19. Namatame, I.; Tomoda, H.; Ishibashi, S. and Omura, S. Antiatherogenic activity of fungal beauveriolides, inhibitors of lipid droplet accumulation in macrophages. *Proceedings of the National Academy of Sciences of the United States of America*. 2004;101(3):737-42.

20. Huttunen, H.J. and Kovacs, D.M. ACAT as a drug target for Alzheimer's disease. *Neurodegenerative Diseases*. 2008;5(3-4):212-4.

21. Haass, C. and Selkoe, D.J. Soluble protein oligomers in neurodegeneration: lessons from the Alzheimer's amyloid beta-peptide. *Nature Reviews. Molecular Cell Biology*. 2007;8(2):101-12.

22. Tanzi, R.E. and Bertram, L. Twenty years of the Alzheimer's disease amyloid hypothesis: a genetic perspective. *Cell*. 2005;120(4):545-55.

23. Ciuculescu, E-D.; Mekmouche, Y. and Faller, P. Metal-binding properties of the peptide APP170-188: a model of the ZnII-binding site of amyloid precursor protein (APP). *Chemistry (Weinheim an der Bergstrasse, Germany)*. 2005;11(3):903-9.

24. Hook, V.Y.; Sei, C.; Yasothornsrikul, S.; Toneff, T.; Kang, Y.H.; Efthimiopoulos, S.; Robakis, N.K. and van Nostrand, W. The kunitz protease inhibitor form of the amyloid precursor protein (KPI/APP) inhibits the proneuropeptide processing enzyme prohormone thiol protease (PTP). Colocalization of KPI/APP and PTP in secretory vesicles. *The Journal of Biological Chemistry*. 1999;274(5):3165-72.

25. Schmidt, C.; Lepsverdize, E.; Chi, S.L.; Das, A.M.; Pizzo, S.V.; Dityatev, A. and Schachner, M. Amyloid precursor protein and amyloid beta-peptide bind to ATP synthase and regulate its activity at the surface of neural cells. *Molecular Psychiatry*. 2008;13(10):953-69.

26. Thinakaran, G. and Koo, E.H. Amyloid precursor protein trafficking, processing, and function. *The Journal of Biological Chemistry*. 2008;283(44):29615-9.

27. Walsh, D.M. and Selkoe, D.J. A beta oligomers - a decade of discovery. *Journal of Neurochemistry*. 2007;101(5):1172-84.

28. Hartmann, T.; Bieger, S.C.; Bruhl, B.; Tienari, P.J.; Ida, N.; Allsop, D.; Roberts, G.W.; Masters, C.L.; Dotti, C.G.; Unsicker, K. and Beyreuther, K. Distinct sites of intracellular production for Alzheimer's disease A42/42 amyloid peptides. *Nature Medicine*. 1997;3(9):1016-20.

29. Selkoe, D.J. Translating cell biology into therapeutic advances in Alzheimer's disease. *Nature*. 2000;399:23-31.

30. Yin, Y.I.; Bassit, B.; Zhu, L.; Yang, X.; Wang, C.; Li, Y-M. γ-Secretase substrate concentration modulates the Abeta42/Abeta40 ratio: implications for Alzheimer Disease. *The Journal of Biological Chemistry*. 2007;282(32):23639-44.

31. Hardy, J. and Allsop, D. Amyloid deposition as the central event in the aetiology of Alzheimer's disease. *Trends in Pharmacological Sciences*. 1991;12(1986):383-8.

32. Cleary, J.P.; Walsh, D.M.; Hofmeister, J.J.; Shankar, G.M.; Kuskowski, M.A.; Selkoe, D.J. and Ashe, K.H. Natural oligomers of the amyloid-beta protein specifically disrupt cognitive function. *Nature Neuroscience*. 2005;8(1):79-84.

33. Fung, J.; Frost, D.; Chakrabartty, A. and McLaurin, J. Interaction of human and mouse Abeta peptides. *Journal of Neurochemistry*. 2004;91(6):1398-403.

34. Bitan, G.; Lomakin, A. and Teplow, D.B. Amyloid beta-protein oligomerization: prenucleation interactions revealed by photo-induced cross-linking of unmodified proteins. *The Journal of Biological Chemistry*. 2001;276(37):35176-84.

35. Khurana, R.; Ionescu-Zanetti, C.; Pope, M.; Li, J.; Nielson, L.; Ramirez-Alvarado, M.; Regan, L.; Fink, A.L. and Carter, S.A. A general model for amyloid fibril assembly based on morphological studies using atomic force microscopy. *Biophysical Journal*. 2003;85(2):1135-44.

36. Necula, M.; Kayed, R.; Milton, S. and Glabe, C.G. Small molecule inhibitors of aggregation indicate that amyloid beta oligomerization and fibrillization pathways are independent and distinct. *The Journal of Biological Chemistry*. 2007;282(14):10311-24.

37. Head, E.; Garzon-Rodriguez, W.; Johnson, J.K.; Lott, I.T.; Cotman, C.W. and Glabe, C. Oxidation of Abeta and plaque biogenesis in Alzheimer's disease and Down syndrome. *Neurobiology of Disease*. 2001;8(5):792-806.

38. Yang, A.J. Intracellular accumulation of insoluble, newly synthesized Abeta n-42 in amyloid precursor protein-transfected cells that have been treated with Abeta 1-42. *Journal of Biological Chemistry*. 1999;274(29):20650-6.

39. Kins, S.; Lauther, N.; Szodorai, A. and Beyreuther, K. Subcellular trafficking of the amyloid precursor protein gene family and its pathogenic role in Alzheimer's disease. *Neurodegenerative Diseases*. 2006;3(4-5):218-26.

40. Klafki, H-W.; Staufenbiel, M.; Kornhuber, J. and Wiltfang, J. Therapeutic approaches to Alzheimer's disease. *Brain : A Journal of Neurology*. 2006;129(Pt 11):2840-55.

41. Kaduszkiewicz, H.; Zimmermann, T.; Beck-Bornholdt, H-P and Bussche, H.van den. Cholinesterase inhibitors for patients with Alzheimer's disease: systematic

review of randomised clinical trials. *BMJ (Clinical Research ed.)*. 2005;331(7512):321-7.

42. Olney, J.W.; Labruyere, J.; Wang, G.; Wozniak, D.F.; Price, M.T. and Sesma, M.A. NMDA antagonist neurotoxicity: mechanism and prevention. *Science*. 1991; 254 (5037):1515-8.

43. Gestwicki, J.E.; Crabtree, G.R. and Graef, I.A. Harnessing chaperones to generate small-molecule inhibitors of Amyloid β aggregation. *Science*. 2011;306(5697):865-9.

44. Micchelli, C.A.; Esler, W.P.; Kimberly, W.T.; Jack, C.; Berezovska, O.; Kornilova, A. and Hyman, B.T. β-Secretase/presenilin inhibitors for Alzheimer ' s disease phenocopy Notch mutations in Drosophila 1. *The FASEB Journal*.79-81.

45. Siemers, E.R.; Quinn, J.F.; Kaye, J.; et al. Effects of a γ-secretase inhibitor in a randomized study of patients with Alzheimer disease. *Neurology*. 2006;66 (4):602-4.

46. Ma, Q-lan.; Lim, G.P.; Harris-white, M.E.; Yang, F.; Ambegaokar, S.S.; Ubeda, O.J.; Glabe, C.G.; Teter, B.; Frautschy, S.A. and Cole, G.M. Antibodies against β-amyloid reduce Aβ oligomers, glycogen synthase kinase-3β activation and S phosphorylation *in vivo* and *in vitro*. *Journal of Neuroscience Research*. 2006;384:374-84.

47. Burns, M.; Gaynor, K.; Olm, V.; Mercken, M.; LaFrancois, J.; Wang, L.; Mathews, P.M.; Noble, W.; Matsuoka, Y. and Duff, K. Presenilin redistribution associated with aberrant cholesterol transport enhances beta-amyloid production *in vivo*. *The Journal of Neuroscience : The official journal of the Society for Neuroscience*. 2003;23(13):5645-9.

48. Mahley, R.W. and Rall, S.C. Apolipoprotein E: far more than a lipid transport protein. *Annual Review of Genomics and Human Genetics*. 2000;1(59):507-37.

49. Kivipelto, M.; Helkala, E-L.; Hänninen, T.; Laakso, M.P.; Hallikainen, M.; Alhainen, K.; Soininen, H.; Tuomilehto, J. and Nissinen, A. Midlife vascular risk factors and late-life mild cognitive impairment. *Neurology*. 2001;56 (12):1683-9.

50. Hartmann, T. β and Alzheimer's cholesterol, Aβ disease molecular link I. *Review Literature And Arts Of The Americas*. 2001;24(11):45-8.

51. Grimm, M.O.W.; Grimm, H.S.; Pätzold, A.J.; Zinser, E.G.; Halonen, R.; Duering, M.; Tschlape, J.A.; de Strooper, B.; Muller, U.; Shen, J. and Hartmann, T. Regulation

of cholesterol and sphingomyelin metabolism by amyloid-beta and presenilin. *Nature Cell Biology*. 2005;7(11):1118-23.

52. Hartmann, T. Role of amyloid precursor protein, amyloid-beta and gamma-secretase in cholesterol maintenance. *Neurodegenerative Diseases*. 2006;3(4-5):305-11.

53. Istvan, E.S. and Deisenhofer, J. Structural mechanism for statin inhibition of HMG-CoA reductase. *Science*. 2001;292(5519):1160-4.

54. Jick, H.; Drachman, D.; Practice, G.; et al. Bad for the Heart, Bad For the Mind? *Science*. 2001;294(October):508-9.

55. Cedazo-Mínguez, A. Apolipoprotein E and Alzheimer's disease: molecular mechanisms and therapeutic opportunities. *Journal of Cellular and MolecularMedicine*. 2007;11(6):1227-38.

56. Wang, H.; Durham, L.; Dawson, H.; Song, P.; Warner, D.S.; Sullivan, P.M.; Vitek, M.P. and Laskowitz, D.T. An apolipoprotein E-based therapeutic improves outcome and reduces Alzheimer's disease pathology following closed head injury: evidence of pharmacogenomic interaction. *Neuroscience*. 2007;144(4):1324-33.

57. Puglielli, L.; Konopka, G.; Pack-Chung, E.; Ingano, L.A.; Berezovska, O.; Hyman, b.T.; Change, T.Y.; Tanzi, R.E. and Kovacs, D.M. Acyl-coenzyme A: cholesterol acyltransferase modulates the generation of the amyloid beta-peptide. *Nature Cell Biology*. 2001;3(10):905-12.

58. Hutter-Paier, B.; Huttunen, H.J.; Puglielli, L.; Eckman, C.B.; Kim, D.Y.; Hofmeister, A.; Moir, R.D.; Domnitz, S.B.; Frosch, M.P.; Windisch, M. and Kovacs, D.M. The ACAT inhibitor CP-113,818 markedly reduces amyloid pathology in a mouse model of Alzheimer's disease. *Neuron*. 2004;44(2):227-38.

59. Huttunen, H.J.; Greco, C. and Kovacs, D.M. Knockdown of ACAT-1 reduces amyloidogenic processing of APP. *FEBS letters*. 2007;581(8):1688-92.

60. Marzetta, C.; Savoy, Y.; Freeman, A.; Long, C.; Pettini, J.; Hagar, R.; Inskeep, P.; Davis, K.; Stucchi, A. and Nicolosi, R. Pharmacological properties of a novel ACAT inhibitor (CP-113,818) in cholesterol-fed rats, hamsters, rabbits, and monkeys. *Journal of Lipid Research.* 1994;35:1829-38.

61. Dominick, M.A.; Bobrowski, W.A.; Macdonald, J.R. and Gough, A.W. Morphogenesis of a zone-specific adrenocortical cytotoxicity in guinea pigs

administered PD 132301-2, an inhibitor of Acyl-CoA: cholesterol acyltransferase. *Toxicologic Pathology*. 1993;21(1):54-62.

62. Reindel, J.F.; Dominick, M.A.; Bocan, T.M.A.; Gough, A.W. and McGuire, E.J. Toxicologic Effects of a novel Acyl-CoA: cholesterol acyltransferase inhibitor in cynomolgus monkeys. *Toxicologic Pathology*. 1994;22(5):510-8.

63. Ross, A.C.; Go, K.J.; Heider, J.G. and Rothblat, G.H. Selective inhibition of acyl coenzyme A:cholesterol acyltransferase by compound 58-035. *The Journal of Biological Chemistry*. 1984;259(2):815-9.

64. Tian, H.; Jiao, X.; Xie, P. and Liang, X. Total synthesis of beauveriolide I. *Tetrahedron Letters*. 2005;46(49):8579-81.

65. Nagai, K.; Doi, T.; Sekiguchi, T.; Sunazuka, T.; Tomoda, H.; Takahashi, T. and Omura, S. Synthesis and biological evaluation of a beauveriolide analogue library. *Journal of Combinatorial Chemistry*. 2006;8(1):103-9.

66. Chatterjee, A.K.; Choi, T-L.; Sanders, D.P. and Grubbs, R.H. A general model for selectivity in olefin cross metathesis. *Journal of the American Chemical Society*. 2003;125(37):11360-70.

67. Brown, H.C.; Bhat, K.S. and Randad, R.S. Chiral synthesis via organoboranes. 21. Allyl- and crotylboration of α-chiral aldehydes with diisopinocampheylboron as the chiral auxiliary. *The Journal of Organic Chemistry*. 1989;54(7):1570-6.

68. Luca, L.de; Giacomelli, G. and Porcheddu, A. A very mild and chemoselective oxidation of alcohols to carbonyl compounds. *Organic Letters*. 2001;3(19):3041-3.

69. Dyer, B.S.; Jones, J.D.; Ainge, G.D.; Denis, M.; Larsen, D.S. and Painter, G.F. Synthesis and structure of phosphatidylinositol dimannoside. *The Journal of Organic Chemistry*. 2007;72(9):3282-8.

70. Slone, C.S.; Weinberger, D.A. and Mirkin, C.A. The transition metal coordination chemistry of hemilabile ligands. In: *Progress in Inorganic Chemistry*. John Wiley & Sons, Inc. 1999:233-350.

71. Yamazaki, T.; Chang, T.Y.; Haass, C. and Ihara, Y. Accumulation and aggregation of amyloid beta-protein in late endosomes of Niemann-pick type C cells. *The Journal of Biological Chemistry*. 2001;276(6):4454-60.

72. Cordero, F.M.; Gensini, M.; Goti, A. and Brandi, A. Stereoselective approach to hydroxyindolizidines: protection/deprotection of the nitrone functionality via cycloaddition/retrocycloaddition. *Organic Letters*. 2000;2(16):2475-7.

73. Michinori, W. and Meienhofer, J. Peptide synthesis using the four component condensarion (Ugi reaction). *Journal of the American Chemical Society*. 1967, 6076-82.

CHAPTER 4

Design, synthesis and evaluation of a cyclic peptide targeting influenza virus host entry

1. Project objective

The aim of this project is to explore the possibility of using a rationally designed molecule to prevent entry of the influenza virus to its host by targeting the viral host receptor.

2. Introduction

This chapter focuses on the initial stages of the development of a new prophylactic against the influenza virus. This introduction is divided in two sections. The first section provides a brief description of the influenza virus, highlighting key information on the virus properties, its host specificity and life cycle, as well as existing therapeutics. The second section focuses on cyclic peptides, their characteristics and uses as therapeutics, as well as strategies for their synthesis.

The results and discussion section is subdivided into four subsections. The first one describes the rational design of the cyclic peptide, as well as its *in silico* model and docking. The second subsection focuses on the synthesis of the cyclic peptide. The third subsection briefly describes the attempted synthesis of a fluorescent sialic acid (SA). The last subsection presents the results of the binding affinity NMR study of the cyclic peptide with sialic acid.

The conclusions section provides a summary of the results obtained as well as the key conclusions that could be drawn from them. The future work section highlights the next experiments that need to be done to complete the results obtained and explore the avenues of research opened by the current work. Finally, the experimental section provides procedures for the synthesis and assays completed, as well as characterisation of the synthetic products generated. References for this project are provided at the end of the chapter.

2.1. Influenza A virus

Influenza is a common disease caused by Influenza A, B or C viruses. These viruses belong to the *Orthomyxoviridae* family.[1] Influenza can easily spread from person to person, and its worldwide circulation in annual waves makes it a serious public health problem.[2] While most people recover within one week of infection without needing medical attention, a few cases present complications that can lead to severe illness or death.[3] Despite the fact that yearly influenza epidemics affect all age groups, young children (less than 2 years old) and adults above 65 years of age are at higher risk of presenting complications. Worldwide, annual epidemics of influenza result in about 3-5 million cases of severe illness, and about 2.5-5 million deaths.[4] Among influenza viruses, type A is the most common and the latest pandemic was caused by the H1N1 influenza A virus (Swine flu in 2009).[5]

Influenza A viruses (Figure 4.1) are RNA viruses, with a negative-sense, segmented genome.[6] Their genome is split into 8 segments coding for 11 proteins. The viral particle consists of 3 mayor components: the viral envelope, the matrix protein M1, and the core. The viral envelope is formed by a lipid bilayer and transmembrane proteins. The lipids are derived form the host plasma membrane and have been selectively enriched with cholesterol and glycosphingolipids.[7] The transmembrane proteins include Hemagglutinin (HA), Neuraminidase (NA) and the M2 ion channel. The M1 matrix protein is the link between the viral envelope and the core. The core consist of a viral nucleocapsid containing RNA, NP, nuclear export protein (NEP or NS2), and NS1, as well as the polymerase complex formed by PA, PB1 and PB2.[8]

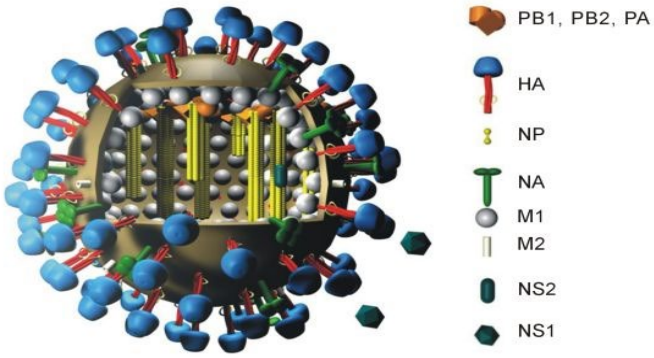

Figure 4.1 - Influenza virus and constitutive proteins.
Eickmann, M. (2005) Public domain image.

2.1.1. Host specificity

Although all components of the virus are necessary for its optimal functioning, the transmembrane proteins HA and NA are the most relevant to this project. Both proteins are immunogenic, and with M2, are exposed on the viral surface, which makes them the main targets for drug development. NA is a sialidase responsible for cleaving SA from the host to release budding virions.[8] M2 is an ion channel that has two main functions. Firstly, during endocytosis, it transfers protons from the endosome into the virus, the low pH causes HA to rearrange to expose a fusion domain that merges the viral envelope with the endosomal membrane, releasing the viral core into the cell for replication. Secondly, during assembly of the new virions in the Golgi, M2 also regulates the pH to prevent premature rearrangement of HA.[9-11]

HA is a lectin present as a homotrimer and is the major component of the protein envelope. HA's function is to recognise and bind to terminal sialic acids on glycoproteins and glycolipids located on the surface of epithelial cells in the respiratory tract and intestines.[12,13] After receptor-mediated endocytosis, the low pH generated by M2 causes HA to refold, exposing a fusion domain that translocates to the endosomal membrane effectively merging the viral envelope with the endosomal membrane and releasing the viral core into the cytosol.[10,14] Interestingly, in different influenza strains, HA also differentiates between linkages to SA, thus providing the base for viral species specificity. For example, HA from human influenza viruses bind preferentially to SA-α-2,6-Gal, while avian influenza viruses bind preferentially to SA-α-2,3-Gal (Figure 4.2).[13]

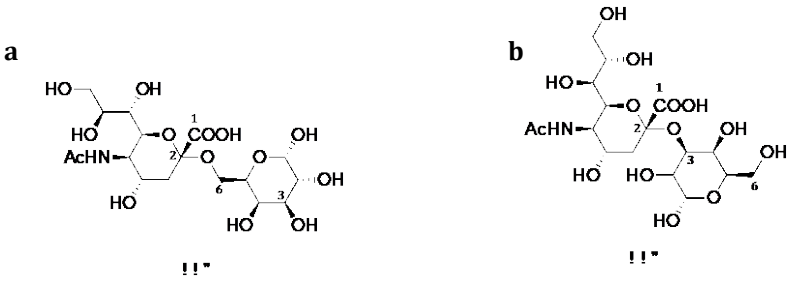

Figure 4.2 - Sialic acid-Galactose linkages recognised by human and avian influenza viruses. (a)α-2,6-sialic acid-galactose (**118**); (b) α-2,3-sialic acid-galactose (**119**).

The influenza A virus can be subdivided into different serotypes according to the antibody response to HA and NA. Mutations of these two proteins have given rise to new serotypes, some of which can and have caused pandemic outbreaks of influenza, often by jumping to a different host species.[15] Up to 2009, the research focus centred on avian flu, caused by the H5N1 serotype which is a bird-adapted highly pathogenic H5N1 strain.[16] Avian influenza viruses are not easily transmitted to humans, and human-to-human transmission is inefficient because of the highly selective nature of the HA-SA interaction. The SA-α-2,3-Gal receptors that are prevalent in birds are only present in human alveoli, and thus only prolonged contact with infected birds can lead to infection.[16-18] The same rationale explains why human–to-human transmission is also ineffective. uring infection, virus is located deep within the lungs, thus preventing the virus from being easily expelled by coughing and sneezing, the usual routes of transmission. Nevertheless, the mortality rate is very high, even if the absolute mortality rate is unknown as a consequence of moderate and asymptomatic infections going undetected.[4]

It is worth mentioning that swine possess both α-2,3 and α-2,6 SA-Galreceptors in their respiratory system, and are thus considered a potential mixing vessel for human and avian viruses. The simultaneous infection of a host with avian and human influenza A viruses can lead to the appearance of a virus with the high pathogenicity of the avian virus but with humans as its host, thereby creating the potential for a devastating pandemic such as the H2N2 and H3N2 pandemic strains.[17,19] In 2009, a close scenario became a reality with the rise of the pandemic strain H1N1 (Swine Flu). Fortunately, while the virus spread was fast and worldwide, its mortality rate was in fact lower than normal seasonal strains.[5]

2.1.2. Viral life cycle

A brief description of the viral life cycle for influenza A is shown in Figure 4.3. The cycle can be divided into five main stages: entry into the host cell, entry of the viral ribonucleoproteins (vRNPs: NP, PA, PB1 and PB2) into the nucleus, transcription and replication of the viral genome, export of vRNPs from the nucleus, and assembly and budding of the virions.[20] As mentioned before, once

HA binds a sialic acid receptor in the host cell, the virus enters the cell by endocytosis. The endosome's low pH causes the exposure of a fusion domain in HA, which fuses the endosome membrane to the viral membrane causing the release of the vRNPs into the host's cytoplasm.[21,14] All vRNPs have nuclear localisation signals, which allow their entry into the nucleus to access the host's transcription and replication machinery. vRNPs are then transported out of the nucleus by CRM1 through nuclear pores. Since the influenza virus is an enveloped virus, it uses the host's plasma membrane to bud new virions form the apical side of polarised cells. Whether the packing of new virons is through random or specific genome packing is still under study. The final release of the viron is achieved by the cleavage of sialic acid residues from plasma membrane glycoproteins by NA.[20]

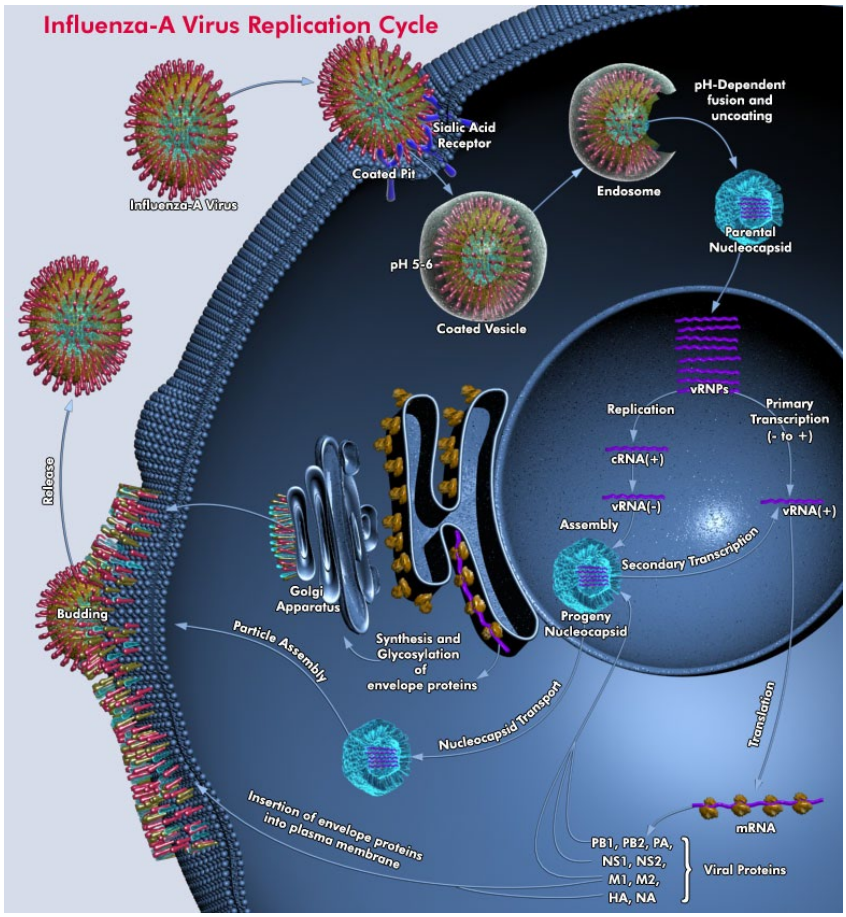

Figure 4.3 - Influenza virus life cycle
Taken from *Qiagen* (2001) GeneGlobe Pathways; Sample and Assay Technologies.

2.2. Existing therapeutics

Intensive research has been carried out in an effort to prevent and treat influenza. Among the common therapeutic approaches to treating or preventing influenza are vaccines, M2 and neuraminidase inhibitors, and other approaches like Integral Membrane Protein (IMP) inhibitors, siRNA, recombinant enzymes or entry-blocking peptides. Unfortunately, until now, all these advances still have severe limitations or could only provide an insufficient response in case of an influenza pandemic.[22]

2.2.1. Vaccines

Among healthy adults, the influenza vaccine can prevent up to 90% of influenza-specific illness, and among the elderly, it can reduce up to 80% of deaths.[4] Flu vaccines are usually developed against viral HA and NA. Unfortunately, these proteins mutate very fast and the constant change renders specific vaccines ineffective against new viruses. The WHO Global Influenza Surveillance Network, together with the National Influenza Centres, monitors the influenza viruses circulating every year. They make an annual recommendation for the type of virus that should be targeted by each year´s vaccine. The vaccine recommended usually targets the three most representative strains in circulation.[4] Although traditionally vaccines match well the epidemic viruses (16 out of 20 in the last 20 years), there is always the risk of an erroneous prediction or an unexpected strains.[23,24]

Research is also being done towards the development of a broad-spectrum vaccine. In particular, the vaccine developed by Prof. Sarah Gilbert (Oxford) targets the NP and M1 internal proteins. These proteins vary little between strains, and are also highly conserved between influenza A, B and C. This vaccine has successfully completed human clinical trials and is now undergoing further tests before it is made available to the public.[25]

2.2.2. Antivirals

Currently there are two major classes of antiviralsto treat influenza: M2 and A inhibitors.[26] Amantadine (Symmetrel, **120**) and rimantadine (Flumadine, **121**), shown in Figure 4.3, are M2 ion channe blockers. At the moment, there is a

debate on the molecular basis of this inhibition. Prof. DeGrado (U.Penn.) determined a crystal structure where rimantadine was bound to the M2 channel on the outside of the pore opening.[27] At the same time, Dr. Schnell (Oxford) determined a ^{1}H NMR structure where four rimantadine molecules were localized on the outside of the helices forming the channel.[26,28,9] Some functional studies have been done to determine which is the correct inhibition mechanism,[29] but thedefinite mode of inhibition remains an open debate. Nevertheless, single point mutations in the M2 channel (like S31N) have caused a dramatic increase in viral resistance against adamantanes.[28]

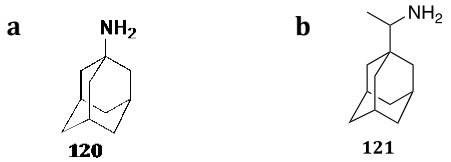

Figure 4.4 - M2 inhibitors. (a) Amantadine (**120**); (b) Rimantadine (**121**).

The current FDA approved NA inhibitors for the treatment of influenza are zanamivir (Relenza, **122**) and oseltamivir (Tamiflu, **123**) shown in Figure 4.5. Relenza was first identified using computational methods to optimise DANA,[30] a SA transition state mimic, for NA inhibition.[31] Oseltamivir is also a transition state analogue, but unlike Relenza, it is administered orally as a prodrug that is hydrolysed in the liver to the free carboxylate.[32] Both antivirals are successful when administered in the initial stages of infection, and although showing different efficiency against influenza A and B viruses, their average effect is comparable.[34] In addition to these drugs, studies are on-going for peramivir, another transition state analogue. Peramivir was developed before 2000 and has been temporarily abandoned twice because of poor bioavailability when administered orally and intramuscularly. At the moment, an intravenous version is being developed by BioCryst Pharmaceuticals.[35]

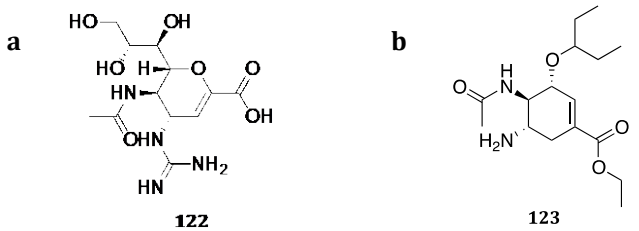

Figure 4.5 - Neuraminidase inhibitors. (a) Zanamivir (**122**); (b) Oseltamivir (**123**).

A major drawback of these antivirals is that viruses have already started developing resistance to them. Single point mutations have been shown to confer resistance to these antivirals.[36] Virus isolates from the 2007-2008 seasonal epidemic showed resistance to oseltamivir[37] and avian flu viruses have also been found to have developed resistance to NA inhibitors.[15] Apart from resistance, industrial production of these antivirals is costly and the production capacity might not be sufficient to fulfil the requirements in the case of a severe pandemic.[38]

2.2.3. Other therapeutic approaches

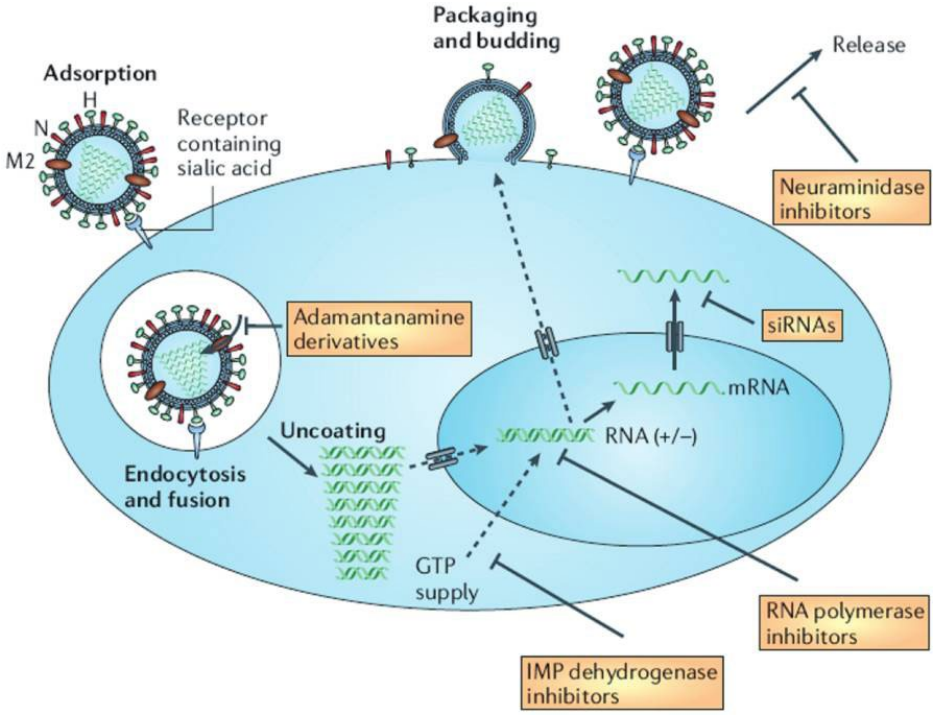

Figure 4.6 - Drug targets in the influenza virus lifecycle.
Taken from Lagoja, I.M. and Clercq, E.D. *Medicinal Research Reviews*, 2008. 28(1): p. 1-38.[39]

Given the problems associated with current influenza treatments, several academic groups and companies are currently exploring alternative therapeutics based on the viral lifecycle (Figure 4.6). IMP dehydrogenase inhibitors, such as ribavirin have been studied for potential treatment against influenza. Ribavirin is a RNA nucleotide analogue that gets incorporated into viral RNA causing fatal mutations and sometimes it can also act as an RNA polymerase inhibitor.[5] Ribavirin is available in many countries as a treatment for influenza, however there are several side-effects and its efficiency in treatment of viral infections is

still under debate. Nevertheless, its use in combination therapy is still being assessed among the pandemic preparation efforts.[40-42] Another RNA polymerase inhibitor that has been studied is T-705, a substituted pyrazine compound now in Phase I clinical trials.[22] Studies are still on-going since concerns have been raised against toxic effects and non-specificity of this class of compounds.[43] There have also been efforts to develop siRNA against influenza. For example, recently siRNA was developed against M2 and NA, reducing significantly virus titers in infected mice.[22] However there have also been concerns regarding unwanted interferon responses and toxic side effects.[44]

Sialylmimetic compounds have already proved to be effective, as demonstrated with zanamivir and oseltamivir. Further developments to this approach have generated a group of molecules collectively known as multimeric zanamivir, which show more anti-viral activity and longer stability than zanamivir. They consist of a core molecule (with either 3 or 4 free carboxylates) bound to 3 or 4 zanamivir moieties and its method of action is the same as the original drug by inhibiting viral HA.[45] Two other methods that block the initial attachment of the virus to the host are recombinant enzymes and peptides. DAS181 or Fludase (NexBio) is a recombinant sialidase with a human epithelium-anchoring domain. Its mode of action is to cleave the terminal sialic acid on epithelial cells thus eliminating the entry point for the virus.[46] Although this drug is still in clinical trials, there are already concerns on its use. Cleavage of sialic acids seems to expose cryptic receptors for *S. pneumoniae*, thus increasing cell susceptibility to another severe disease.[47] The other method under development is a 20-amino acid peptide derived from fibroblast growth factor 4 that seems to bind to HA and has shown effective activity as a broad-spectrum antiviral.[48]

2.3. Cyclic peptides

Cyclic peptides have been studied in different biological situations as therapeutic agents. They are thought to have great therapeutic potential because their reduced conformational freedom correlates to high affinity and specificity for their receptors.[49] They are also often more stable *in vivo* than their linear counterparts.[49] The concept and use of cyclic peptides has changed over time. Initially synthetic peptides were merely studied as derivatives of complex linear

molecules to facilitate their stereochemical characterisation.[48] Cyclic peptides were then considered convenient intermediates for the synthesis of biologically active peptides, and were used as peptidomimetics to mimic critical parts of larger proteins. Currently they are being designed as activetherapeutic drugs in their own right.[49] The discovery of many natural cyclic peptides has also fuelled research into cyclic peptide synthesis and methods to tailor or optimise natural products.[48]

2.3.1. Cyclic peptides used as therapeutics

The development of cyclic peptides as therapeutic drugs has been slower than the development of standard small molecule drugs mainly because their synthesis is more expensive and complex than standard small molecule drugs. Nevertheless, optimisation of cyclisation yields, the use of cheaper reagents and improved chromatographic purification methods are making the synthesis of these compounds less prohibitive.

The study of cyclic peptides can probably be divided into two fields: natural cyclic peptides and peptidomimetics.[48] A large number of natural cyclic peptides have been discovered, most of which were initially found in fungi with antibacterial properties. These peptides were relatively small, with an average of seven amino acids.[50] In recent years, the scientific community has become aware of larger cyclic peptides in nature. Circular proteins up to 78 amino acids have been found in bacteria, plants and animals.[11] A few examples of natural cyclic peptides are conotoxins, neurotoxic peptides made by marine cone snails that mostly inhibit ion channels;[51] somatostatin, a growth hormone that regulates the endocrine system by their interaction with G-coupled protein somatostatin receptors;[52] and cyclosporin A (**124**), initially studied as an anti-fungal compound but now marketed as an immunosuppressant drug that binds to cyclophillin in T-lymphocytes, which in turn inhibits calcineurin, thus preventing the activation of interleukin 2 (Figure 4.7).[53,54]

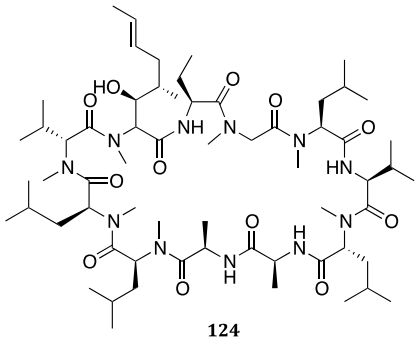

124

Figure 4.7 - Cyclosporin A.

In addition to natural products, cyclic peptides have also been studied as means to reproduce small sections of proteins. Initially, only as tools to study conformations of particular sequences,[50] but more recently also as means to reproduce antigenic epitopes or mimicking binding sites.[55] There have been several attempts to use peptides as vaccines, but these tests have had mixed results with low immune responses and insufficient cross-protection.[56] A growing application of cyclic peptides is the generation of libraries (often using phage display)[57] to find cyclic peptides that bind to a particular protein either to neutralise their activity or as recognition molecules that can be later tagged for detection.[58]

2.3.2. Cyclic peptide synthesis

Although most cyclic peptides in nature cyclise *via* disulfide bridge formation, several cyclisation techniques have been studied and optimised for synthetic peptides. The method of choice depends largely on the number and nature of the amino acids present, as well as the scale of the synthesis. Among the most important methods for cyclisation are on-resin cyclisations (Figure 4.8). Partial on-resin cyclisation involves the cleavage from the resin during the cyclising step often using peptides attached to the resin through the terminal acid.[59] Total on-resin cyclisation involves the attachment to the resin through the side-chain of an amino acid, allowing cyclisation before the final cleavage and deprotection.[60] Other methods for the synthesis of cyclic peptides involve the amide bond formation via side-chain cyclisation,[61] cyclisation via transthioesterification in cysteine rich peptides,[62] enzyme catalysed cyclisation,[63] as well as solution cyclisation.

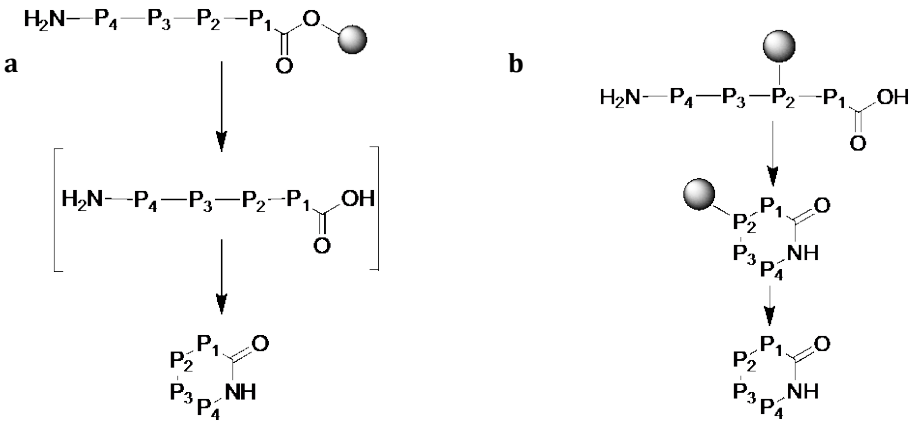

Figure 4.8 - Cyclic peptide synthetic routes. (a) Partial on-resin cyclisation and solution cyclisation; (b) Total on-resin cyclisation, amino acid side-chain attachment.

Heterodetic cyclic peptides are also common. The isopeptide bond can either be incorporated in the backbone during peptide synthesis or contribute to the final cyclisation process.[55] Thioethers, esters (depsipeptides) and disulfide bridges are isopeptides that can be accessed by synthetic methods. Thioethers are often constructed by thioalkylations, esters via a variety of macrolactonisation techniques and disulfide bridges can be obtained from simple oxidations.[59]

3. Results and Discussion

As mentioned before, the project aim was to develop a molecule that could bind to the host receptor for influenza to prevent viral entry.[64] Proteins are known for the specificity and affinity with which they bind to their targets. It is possible that if a molecule could replicate the functional groups of the protein that interact with its target, this molecule could retain enough specificity and affinity to bind to it. If a molecule could provide a competitive interaction for the viral receptor in the host cells during an infection, the decrease of infectivity might be enough to maintain the viral population below the critical threshold for a widespread infection.

3.1. Cyclic peptide design

The initial step in this project was the determination of the relevant amino acids in proteins binding sialic acid (**125**), which is the host cell receptor for the influenza virus. To this purpose, four proteins that bind SA (**125**) were explored: Sialoadhesin (Siglec-1/1QFP),[65] Hemagglutinin from an influenza A virus (1HGJ),[66] Human Siglec-7 (1O7V),[65] and Hemagglutinin-Neuraminidase (1USX) from Newcastle disease virus.[67] These proteins were selected because they have been extensively studied and the molecular basis of their interactions with SA (**125**) is well known. Figure 4.9 shows the original published results of the molecular interaction studies for these four proteins.

Siglecs are sialic acid (**125**) binding immunoglobulin-like lectins.[68] They are transmembrane proteins that modulate cellular interactions and signalling in the haematopoietic, immune and nervous system. Sialoadhesin is an adhesion molecule found in macrophages and it was the first siglec found. It binds preferentially to α(2,3)-sialic acids. Siglec-7 is part of a family of immune inhibitory CD33-related siglecs mostly found in monocytes. It shows binding preference to α(2,6)-linked SA and α(2,8)-disialic acids.[69] As mentioned before, Hemagglutinin is the influenza virus entry lectin, similar to Hemagglutinin-Neuraminidase, which has an extra domain that hydrolyses SA (**125**) once the virus is internalised. Both HA and HA-NA prefer binding α(2,6)-linked sialic acid since they belong to human-targeting viral strains.

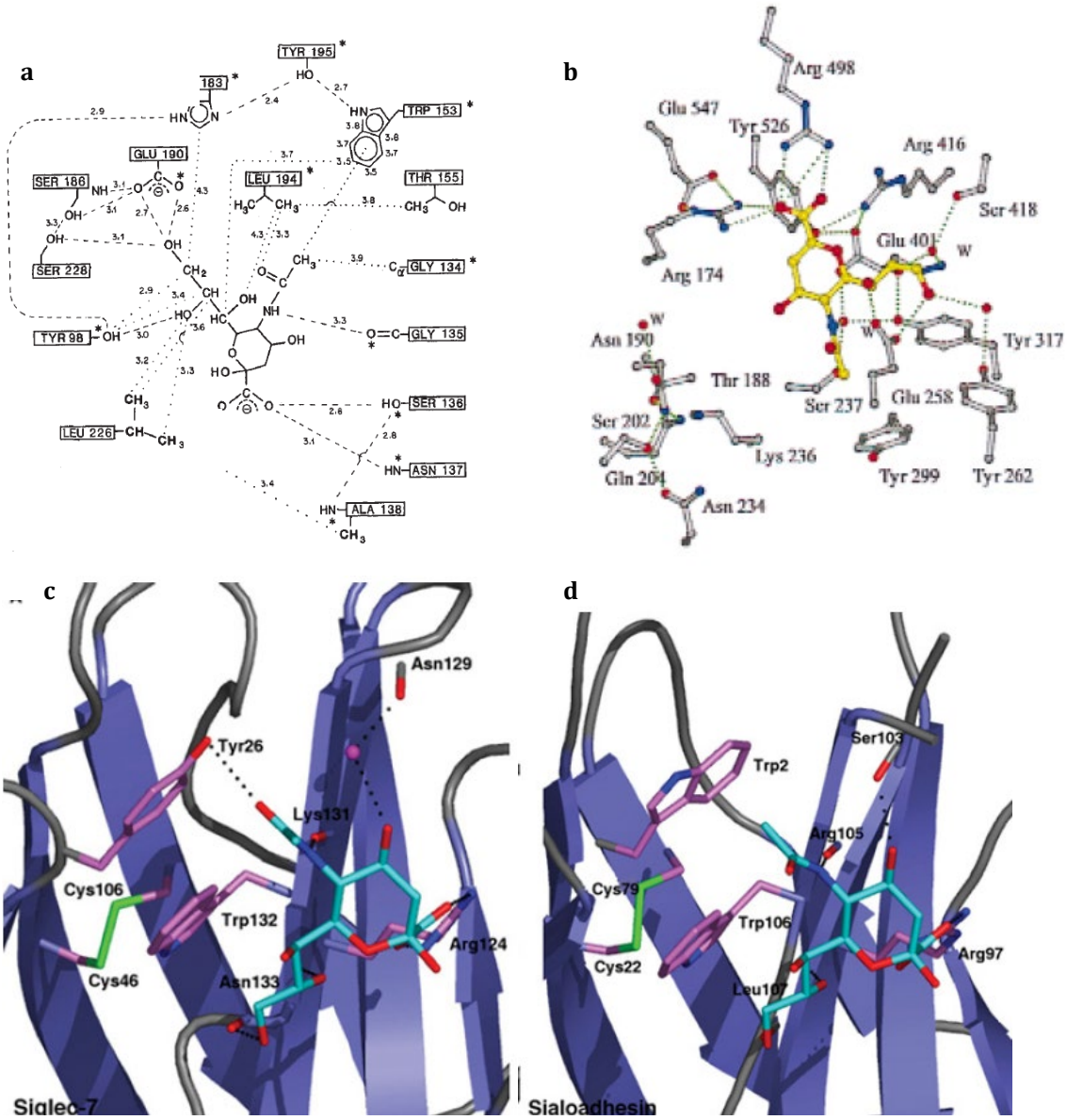

Figure 4.9 - Binding sites for sialic acid (**125**) in selected enzymes with key amino acid interactions. (a) Hemagglutinin form Influenza A virus; (b) Hemagglutinin-Neuraminidase from Newcastle disease virus; (c) Siglec-7; (d) Sialoadhesin.

Taken from (a) Weis, W.; Brown, J.H.; Cusack, S.; *et.al. Nature.* 1988; 333(2):426-31.[66]; (b) Zaitsev, V.; Itzstein, M.; Groves, D.; *et.al. Journal of Virology.* 2003; 78(7): 3733-41.[67]; (c) and (d) Attrill, H.; Takazawa, H.; Witt, S.; *et.al. Biochemistry Journal.* 2006; 397:271-8.[65]

In these proteins, the structural conformation and orientation of SA (**125**) are essentially the same. One side of the pyranose ring faces the base of the binding site, and the carboxylate, the acetamido nitrogen, and the two end hydroxyl groups (C8 and C9 – Figure 4.10) from the glycerol moiety face into the binding pocket forming hydrogen bonds with side chains of amino acids and polar atoms

in the backbone. The remaining four hydroxyl groups face out of the binding site and have no apparent interactions with the protein.

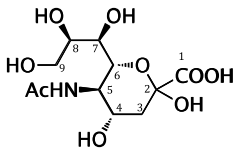

125

Figure 4.10 - Sialic acid (*N*-acetylneruaminic acid, **125**) and carbon numbering used in this chapter.

Figure 4.11 summarises the information presented in Figure 4.9, highlighting critical residues involved in binding sialic acid (**125**) within the different proteins.[69-71] As can be seen, the methyl group of the *N*-acetyl component of SA (**125**) establishes hydrophobic interactions with aromatic residues, generally Trp. The acetyl oxygen and the second hydroxyl group of the glycerol component of SA (**125**) forms hydrogen bonds with the hydroxyl groups of mostly Ser or Tyr. The remaining hydroxyl groups of the glycerol component of SA (**125**) form hydrogen bonds with Ser, Arg, Asn, Tyr and Glu; while the aliphatic backbone of the glycerol moiety establishes hydrophobic interactions with Leu or Val residues. Finally, the carboxylate of SA (**125**) is involved in the formation of two salt bridges with Arg. Based on these observations, six critical residues were chosen to form the core scaffold of the designed molecule: two Arg, Ser, Leu, Tyr and Trp.

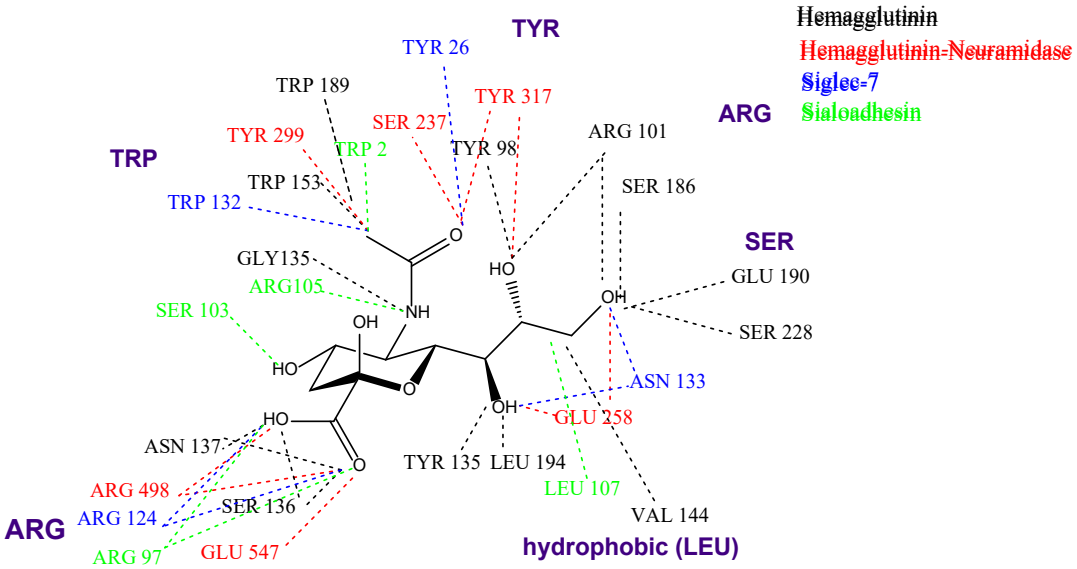

Figure 4.11 - Comparison of key amino acids interacting with sialic acid (**125**) in the binding sites of different enzymes and the six critical residueres chosen to form the molecule.

It was decided that a cyclic peptide could provide the necessary rigidity to the molecule to maintain the amino acids in roughly the same position as they are presented in a protein. Having identified the six conserved residues, the binding site of HA was used as a template for the cyclic peptide design since this protein alone contained all six conserved residues/functionalities. Leu194 matches the selected Leu, Ser186 is in place of the selected Ser, Ser 228 is used in place of Arg101 for the selected Arg, Tyr98 matches the selected Tyr, Ser136 matches the second Arg, and finally Trp153 is located in place of the selected Trp. While in Figure 4.11 it appears that the selected Trp is located between the selected Tyr and Arg residues, spatially the arrangement of the residues places Arg between the Trp and the Tyr when all critical residues are connected in a circular arrangement, as can be seen in Figure 4.12-c.

The binding site of HA was identified using ViewerLite from a published crystal structure (1HGJ) and all the residues not involved in binding of SA (**125**) were eliminated. Distances between the critical residues were obtained (measuring from the N of one residue to the carbonyl C of the next amino acid) and the resulting image can be seen in Figure 4.12-c. In general, the orientation of the amino acids in the active site of HA is ideal to the construction of the cyclic peptide, except for the Trp residue. However, since the aromatic moiety is the part forming the interactions with SA (**125**), and it is planar, Trp should be able to be presented in the same orientation as the other amino acids without affecting its ability to interact with its target in the same manner.

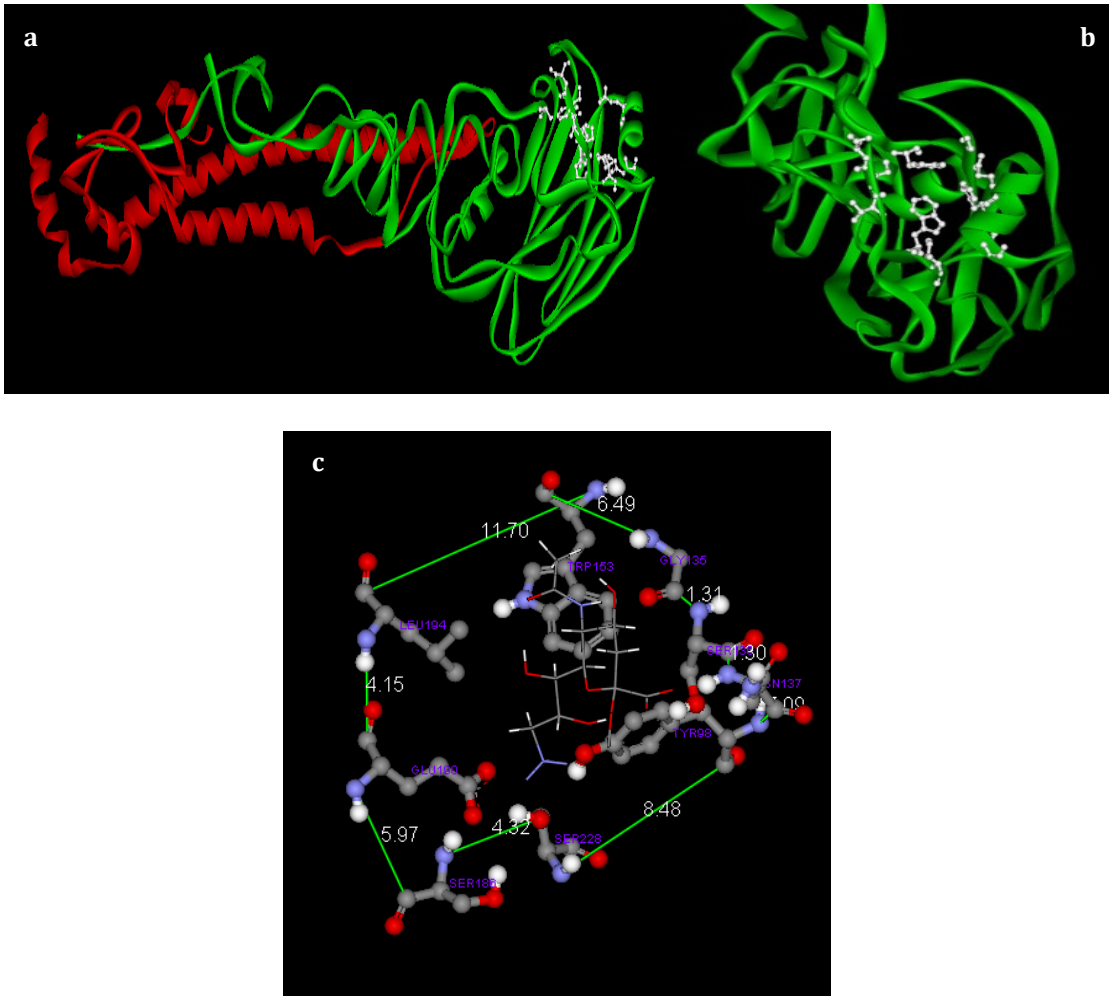

Figure 4.12 - 3D analysis of the binding site of HA with identification of important residues interacting with sialic acid (**125**). (a) Location of binding site in Hemagglutinin; (b) Key residues (in white) highlighted in HA binding site; (c) Distances (green lines and white numbers) between key residues of HA. Image rendered using ViewerLite and 2008 Schrodinger Suite, Prime module using1HGJ crystal structure from RCSB PDB.

In order to determine how many residues needed to be introduced to link the identified critical residues, the distances between the selected aminoacids in HA were analysed (Figure 4.12-c). It is known that on average, the bond distance between the α-carbon and the carbonyl carbon is 1.53 Å, 1.33 Å for the peptide bond, and 1.46 Å for the distance between the nitrogen and α-carbon (Figure 4.13).[72] Therefore, the backbone of each amino acid is roughly 4.32Å in length. However, considering that the bonds are presented at an angle, the overall linear distance from N to N in a peptide bond is roughly 3.7Å. On average the distance between amino acid and amino acid, as measured in Figure 4.12-c from N to the neighbouring carbonyl, was considered as 5Å. Table 4.1 shows the summary of

distances obtained for the critical residues in HA, and the number of amino acids, which would correspond to those distances to link the identified conserved residues.

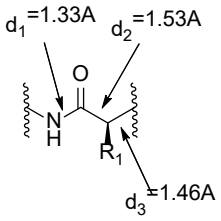

Figure 4.13 - Average distances in a peptide bond.

Table 4.1 - Summary of distances between key residues in HA and number of amino acids in target cyclic peptide.

Amino acid pair	Distance in HA (Å)	No. of amino acids	Critical amino acids
Leu194-Glu190	4.15	1	Leu/Ala
Glu190-Ser186	5.97	1	Ala/Ser
Ser 186-Ser228	4.32	1	Ser/Arg
Ser 228-Tyr98	8.48	1	Arg/Tyr
Tyr98-Asn137	1.09	0	-
Asn137-Ser136	1.30	0	Tyr/Arg
Ser136-Gly135	1.31	0	Arg/Trp
Gly135-Trp153	6.49	1	-
Trp153-Leu194	11.70	2/1	Trp/Leu

As shown in Figure 4.14 and Table 4.1, an extra Ala was added between Leu and Ser to facilitate the synthesis by using a pre-loaded resin. Considering that there was space for roughly 3 amino acids between those critical residues, a single amino acid was introduced between Leu-Ala and Ala-Ser. The distance between Ser-Arg and Arg-Tyr allowed introduction of a single amino acid between them as well. For the distance between Tyr and the subsequent Arg, Figure 4.12-c shows the distance measured including Asn 137, which was excluded from the selected residues due to lack of homology with the other enzymes. Thus, since the distances between Tyr-Asn and Asn-Arg are negligible, a single amino acid was introduced to replace Asn. Similarly, between Arg and Trp, a measurement

for Gly135 was included even though Gly was not considered for the final scaffold. The distance between Arg-Gly is negligible, and a single amino acid was introduced between Arg-Trp reflecting the distance between Gly-Trp. Finally, as mentioned before, Trp is presented in a different orientation to the rest of the amino acids, such that when measuring distances between this pair of amino acids, the resulting number included the full length of Trp. Considering the inversion of Trp, and substraction of the length of this amino acid from the reported distance, a single amino acid was introduced between Trp-Leu. In summary, a single amino acid was included between each of the critical residues (including the added Ala in this category).

For the initial peptide, alanine residues were chosen to link the conserved amino acids since it is the residue of choice when doing mutagenesis studies. However, later on it was decided to switch to glycine, not only because it provides maximum flexibility in the molecule, but also because it does not introduce any extra functionality or side chains that might interfere with the binding of the critical residues. The initial peptide including Ala residues was used for all the *in silico* studies, while the glycine-containing peptide was used for the remaining of this chapter. The cyclic peptide (**126**) resulting from the previous design is shown in Figure 4.14, and consists of 14 amino acids.

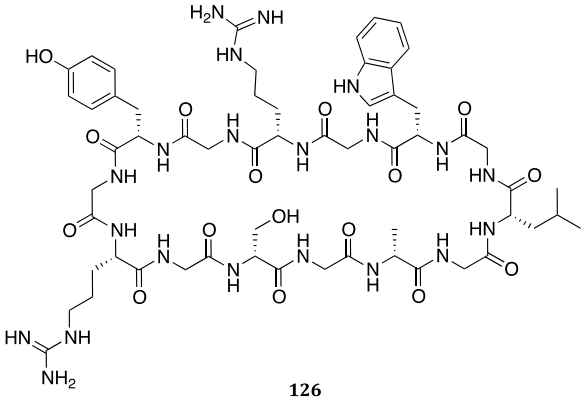

126

Figure 4.14 - Designed cyclic peptide.

3.2. *In silico* model

Having designed the target molecule, it was decided to compare its conformation to the binding site of HA *in silico*, to determine whether it could fit and overlap with the critical residues as positioned in the crystal structure. To this end a

simple 3D structure was prepared using Schrödinger Suite 2008, through the LigPrep module in Maestro. After this transformation, the structure was subjected to a model refinement in the Protein Preparation Wizard module and a minimisation process using the Prime module to predict the lowest energy conformation of the cyclic peptide. The resulting model is shown in Figure 4.15.

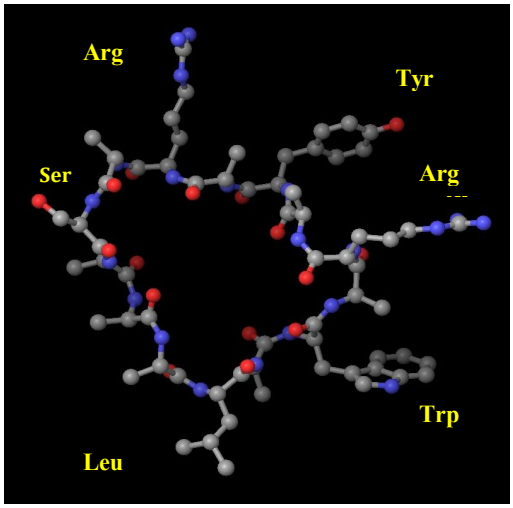

Figure 4.15 - Minimum energy 3D model of designed cyclic peptide. Image rendered using 2008 Schrodinger Suite, Prime module.

The minimum energy model was used by Dr. Kia Balali-Mood (Prof. Sansom's group, Oxford), and it allowed him to fit the peptide to the binding pocket of the crystal structure of HA (1USX). Using Gold software, he succeeded in fitting the peptide model to the binding pocket of HA with the relevant amino acids close to their original positioning (Figure 4.16). However, further studies with molecular dynamics were beyond the scope of this project since they would require a more in-depth study of the constraints required for the experiments.

The computational analysis confirmed that the designed 14-mer was the appropriate size to fit all the critical amino acids in the binding pocket and thus had the potential to form the interactions required to bind the target SA (**125**). Based on this encouraging result, the next step was the chemical synthesis of the cyclic peptide (**126**) to test its affinity to SA (**125**) *in vitro*.

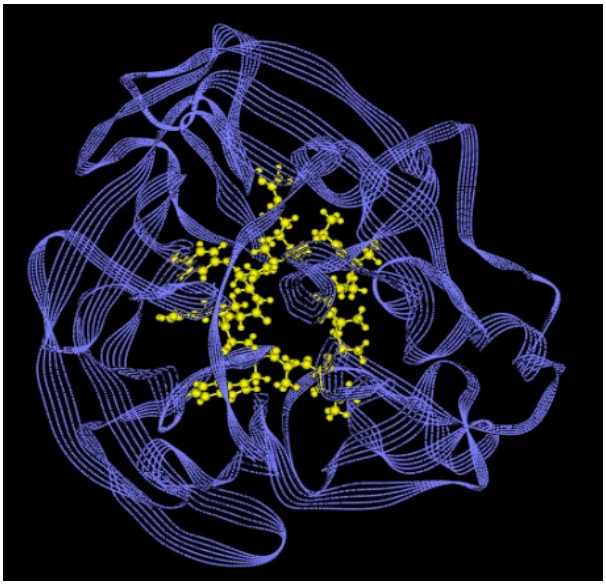

Figure 4.16 - Minimised cyclic peptide model (yellow) fitted into the binding pocket of HA-NA. Image rendered using Gold software from 1USX crystal structure in RCSB PDB.

3.3. Synthesis

The initial route tested for the synthesis of the cyclic peptide **126** was an on-resin cyclisation carried out on a peptide elongated from a Tyr loaded onto the resin through its side-chain (Figure 4.17). This synthesis was initiated with the functionalisation of an amine resin (**33**) with an HMPA linker (**34**) to form a Wang-like resin as described previously, followed by the loading of an Fmoc-Tyr-OMe (**127**) through its side chain by a Mitsunobu reaction. The full peptide was then synthesised by normal SSPS using piperidine Fmoc deprotection and DIC/HOBt as coupling reagents as described previously. The final acid deprotection was attempted by base treatment of the resin for 3 days, followed by on-resin cyclisation using TBTU (8 equiv.) and HOBt (8 equiv.) as coupling reagents, DIPEA as base, and DMF as solvent. Unfortunately, after acid treatment, MS analysis did not give proof of the desired cyclic peptide **126**, and only peptide fragments were isolated. A test cleavage from a resin sample before deprotection of the acid showed that the full peptide had been synthesised successfully, however, discolouration of the resin was observed during base treatment and the Keiser test (ninhydrin, phenol and KCN in pyridine) used to follow peptide coupling was inconclusive during cyclisation. Whether the failure was due to side

reactions during ester hydrolysis or inefficient cyclisation was not explored further.

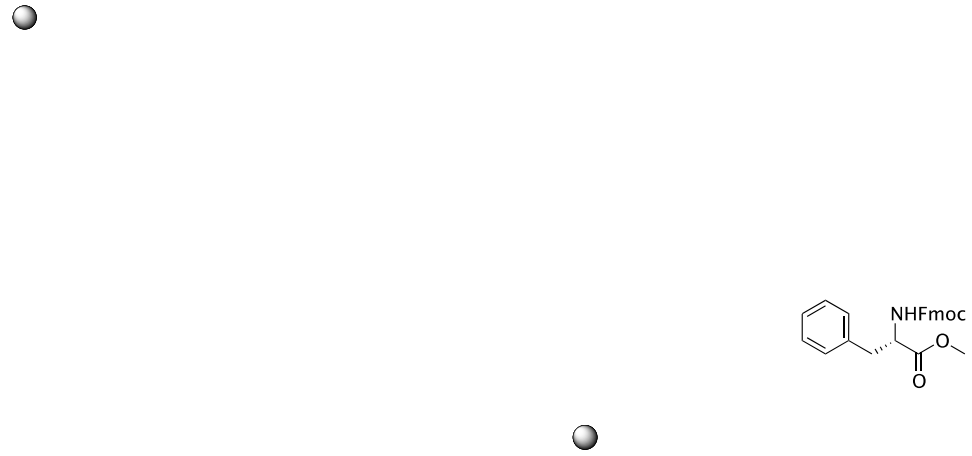

Figure 4.17 - Synthetic scheme for the cyclic peptide **126** synthesis through resin loading by a tyrosine side-chain. *Reagents and conditions*: (a)DIC, HOBt; (b) i. PPh_3, Fmoc-Tyr-OMe, DIAD; ii. Ac_2O, DIPEA (c) SPPS, i. 20% piperidine in DMF; ii. DIC, HOBt, Fmoc-aa-OH; (d) NaOH; (e) HOBt, TBTU, DIPEA.

While the normal approach for cyclic peptides involves attempting cyclisation on-resin with all residues fully protected, there have been reports of successful cyclisations performed in solution from fully deprotected linear peptides. Since the target molecule **126** is a relatively simple sequence with half the residues being glycines and no free acids or primary amines present, it was possible that a solution cyclisation would be successful in this case. For this purpose, the linear peptide **132** (Figure 4.18) was synthesised on a Fmoc-Ala-Wang resin by traditional Fmoc SPPS. Cleavage from the resin generated the desired 14-mer **132** with the two smallest neighbouring residues (Ala and Gly) as terminal amino acids, this positioning was chosen in order to maximise the chances of success during cyclisation since bulkier residues tend to have lower reaction kinetics.

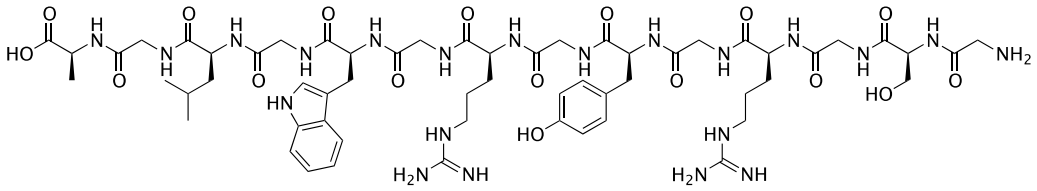

132

Figure 4.18 - Linear peptide **132**

Cyclisation was then successfully completed via a HATU/HOAt coupling (4 equiv. each) in DMF (13 mM), with a 41% yield. Figure 4.19 shows the obtained ^{1}H NMR spectrum for the linear peptide **132** and Figure 4.20 shows the MS spectrum found for the cyclic peptide **126**. It is worth noting that the splitting pattern in the ^{1}H spectra is virtually identical for both linear and cyclic peptides, however peaks are more defined for the linear peptide and chemical shifts show slight variations. For these reasons the ^{1}H spectrum of the linear peptide is shown here with the assignment of peaks as determined by COSY and ROESY experiments.

Figure 4.20 shows a LR-MS (ESI^{+}) spectrum obtained with a partially deuterated sample of the cyclic peptide **126**, and the identified peaks are indicated. The peak at 666.87 corresponds to $½[M+2H]^{2+}$ (theoretical *m/z* 666.82). The major peak at *m/z* at 667.37 correlates to the $½[M+2H]^{2+}$ where one ^{1}H has exchanged with a deuterium ^{2}H. The peak at 1446.77 is likely to be $[M+TFA+H]^{+}$ formed by residual TFA in the solvent used for HPLC purification (theoretical *m/z* 1446.65). The *m/z* equally corresponds to $[M+TFA+H]^{+}$ of the monodeuterated cyclic peptide. The peak at 1582.69 might correspond to $[M+2TFA+Na]^{+}$ (theoretical *m/z* 1582.62). Other possible identified ions are the peak at 773.44 ($½[M+4MeOH+CH_3CN+2Na]^{2+}$, theoretical *m/z* 773.38), with the same monodeuterated species at 773.95, and the peak at 789.39 ($½[M+5MeOH+CH_3CN+2Na]^{2+}$, theoretical *m/z* 789.39). High resolution MS found a *m/z* 1332.6569 $[M+H]^{+}$ corresponding to the theoretical *m/z* 1332.6556 $[M+H]^{+}$.

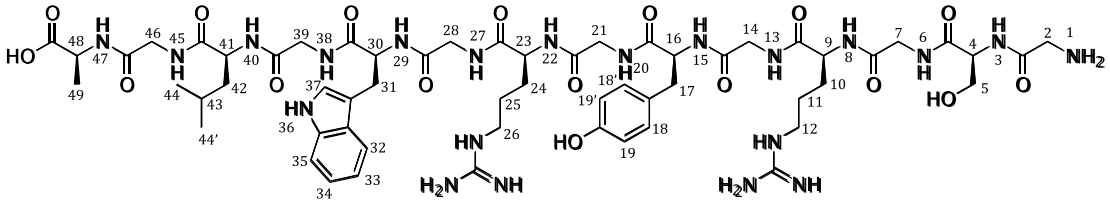

132

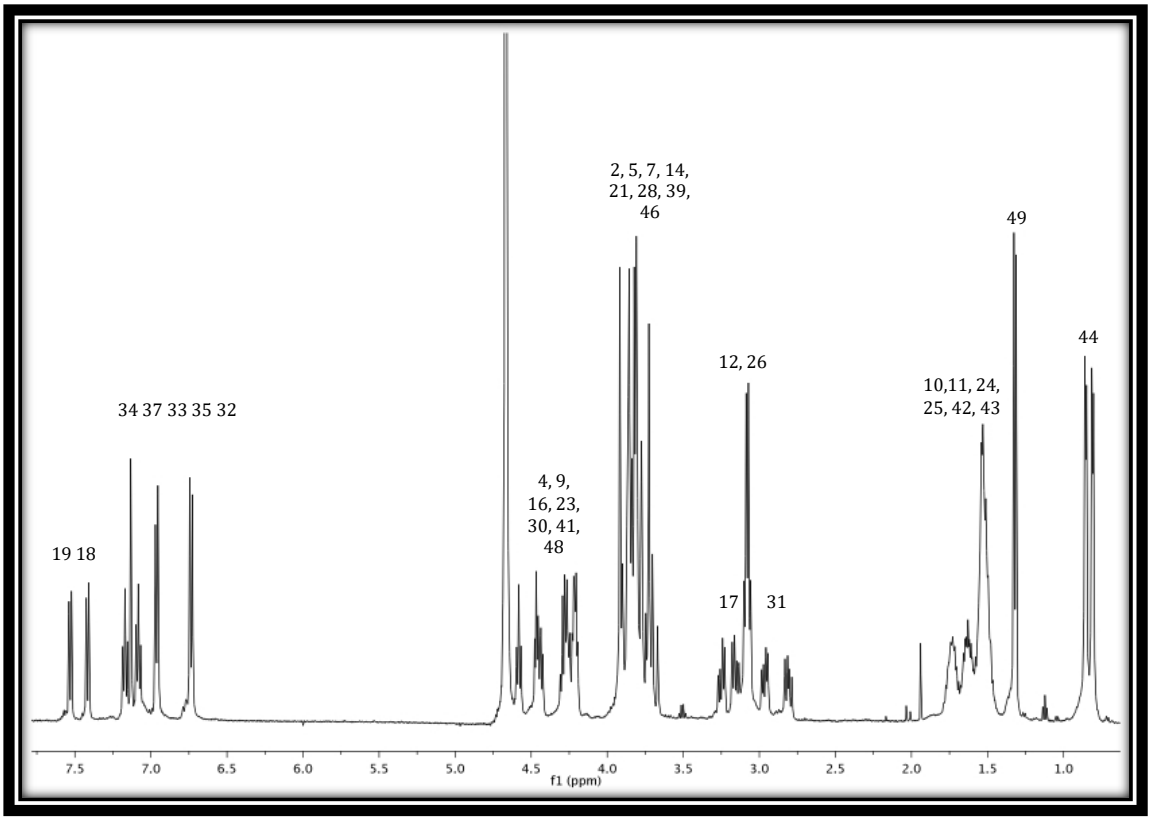

Figure 4.19 - Spectroscopic characterisation by ^{1}H NMR of linear peptide **132.**

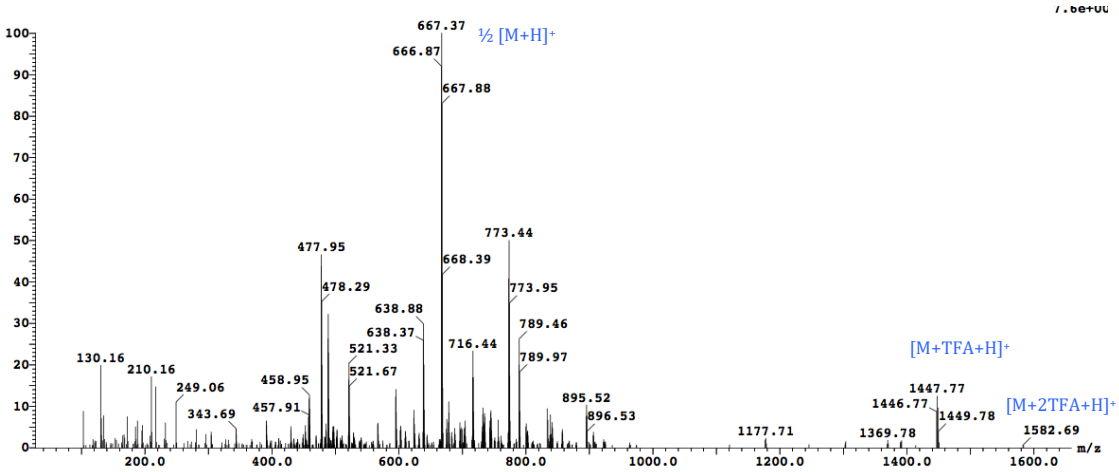

Figure 4.20 - Spectroscopic characterisation by LR-MS (ESI^{+}) of cyclic peptide **126**.

The correct peptide bond formation was confirmed by ROESY and COSY experiments in samples with 80% water (20% D_2O), to be able to observe the amide protons (Figure 4.21). The COSY spectrum allows the correlation between amide protons and α-carbon protons in the same amino acid, while the ROESY experiment allows the correlation between the amide proton and the neighbouring amino acid α-carbon. Thus for the linear peptide, the COSY spectrum shows no correlation for the *N*-terminal glycine and in the ROESY spectrum no correlation can be found for the C-terminal alanine, since it does not bear a neighbouring amide proton. However, these interactions can be found in the cyclic peptide thus confirming that cyclisation occurred at the desired location.

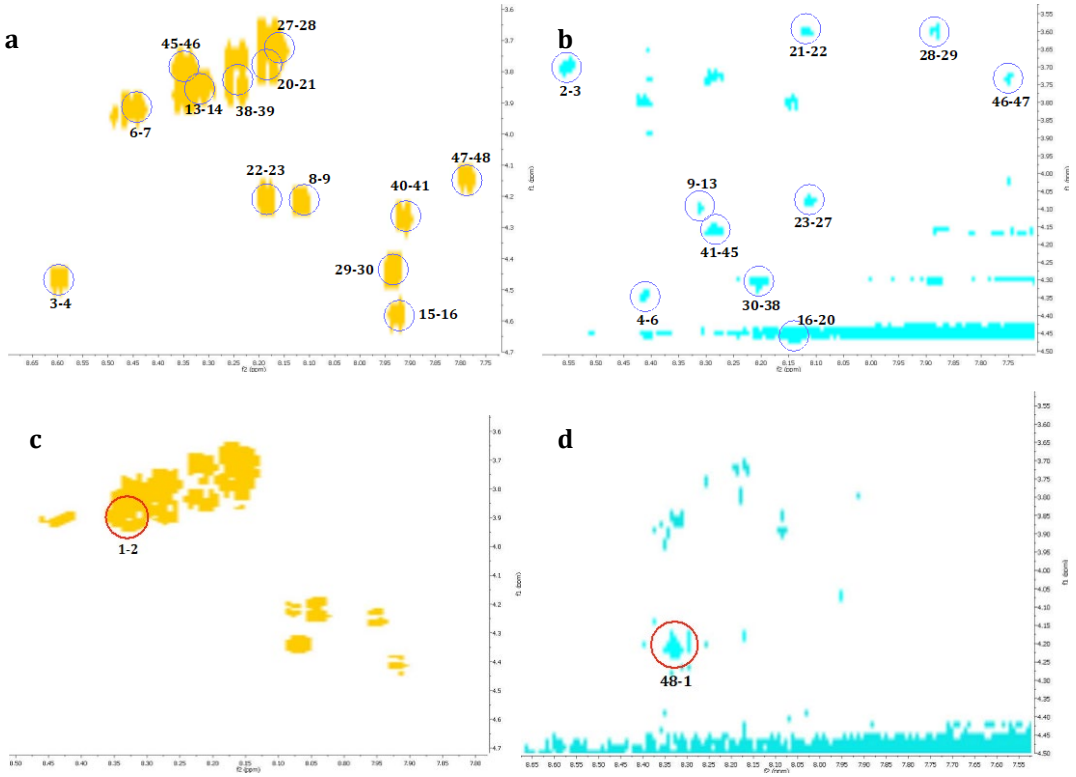

Figure 4.21 – 2D homonuclear ^1H NMR spectroscopic characterisation for linear and cyclic peptides with assignment of neighboring atoms. (a) COSY spectrum showing correlations between NH and αC ^1H in linear peptide **132**; (b) ROESY spectrum showing correlations between NH and αC+1 ^1H in linear peptide **132**; (c) COSY spectrum showing new correlation at cyclisation point between Gly αC and NH ^1H in cyclic peptide **126**; (b) ROESY spectrum showing new correlation at cyclisation point between Gly NH and Ala αC ^1H in cyclic peptide **126**.

3.4. Attempted synthesis of fluorescent sialic acid

Initially, the cyclic peptide **126** was intended to be used to determine binding affinity through fluorescence polarisation using a fluorescently tagged sialic acid. However, the synthesis of such a fluorescent probe proved to be very challenging. The synthetic strategies envisaged to prepare FITC labelled sialic acids **133** and **141** are shown in Figure 4.22 and Figure 4.24 respectively.

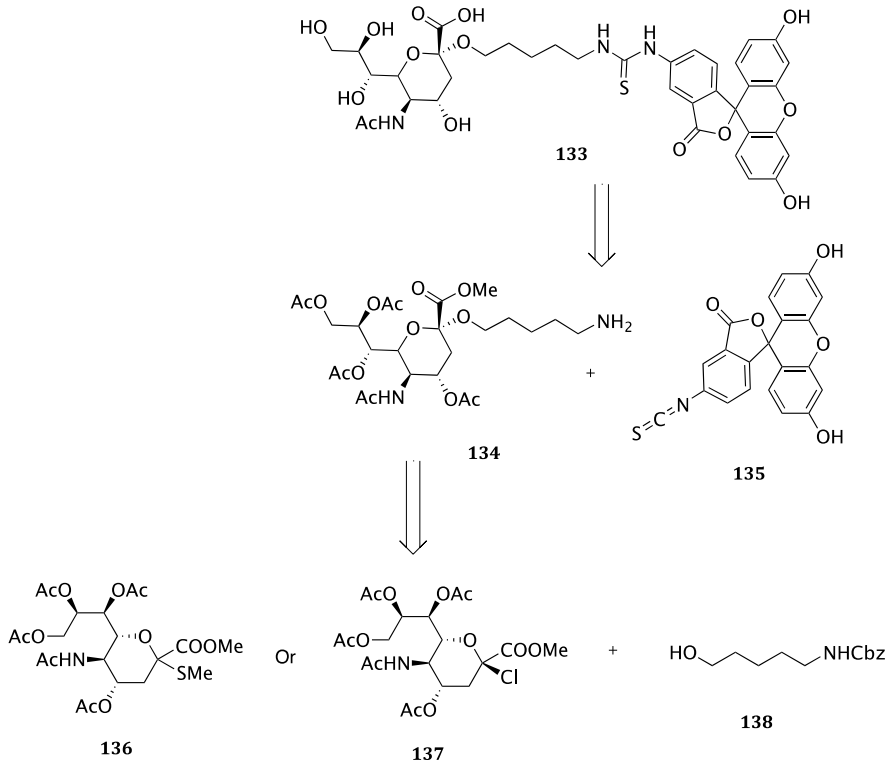

Figure 4.22 – Retrosynthetic analysis of fluorescent sialic acid **133** from glycosylation of chloride (**137**) or thioether (**136**) sialic acid donors.

The first strategy (Figure 4.22) involved the glycosylation of a sialic acid donor with a chloride (**137**) or a thioether (**136**) as leaving groups, with a Cbz protected hydroxylamine (**138**) as acceptor, which could be later deprotected to introduce the FITC moiety (**135**) by reaction with the free amino moiety.

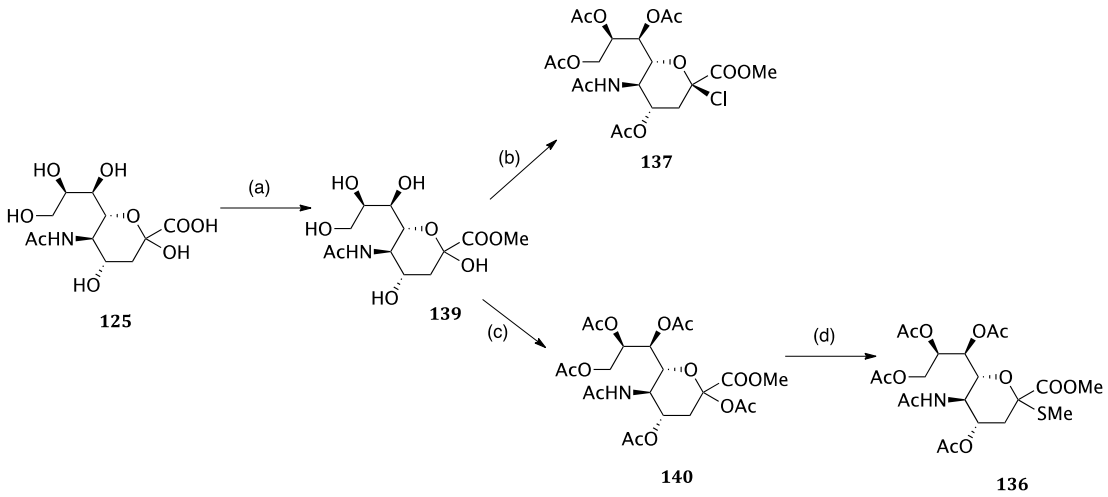

Figure 4.23 - Synthesis of sialic acid donors **136** and **137**. *Reagents and conditions*: a)Dowex 50 H^+, MeOH (quant.); (b) HCl (g), AcOH/AcCl (88%); (c) AcO_2 (79%); (d) TMS-SMe (5 equiv.), TMS-Tf (1.4 equiv.) (65%).

Both sialic acid donors (**136** and **137**) were synthesised from sialic acid (**125**) as shown in Figure 4.23. An initial esterification of the carboxylic group with MeOH in the presence Dowex 50X8 H^+ generated product **139** in quantitative yield. The methyl ester was then transformed into the chloride donor **137** by simultaneous acetylation of the hydroxyl groups and chloride introduction by HCl gas in an AcOH/AcCl mixture with an isolated yield of 88%. The thioether donor **136** was synthesised after complete acetylation of the methyl protected sialic acid **139** with acetic anhydride (72% yield), by reaction with TMS-SMe (5 equiv.) and TMS-triflate (1.4 equiv.) in a 65% yield. The Cbz protected hydroxylamine (**138**) acceptor was prepared quantitatively by a simple treatment of 5-aminopentanol with Cbz-Cl (1.4 equiv.) in THF.

The second strategy (Figure 4.24) used the same thioether donor (**136**) with a galactosyl acceptor (**143**) functionalised with Cbz-protected hydroxylamine (**138**) to provide the link to FITC (**135**) upon deprotection.

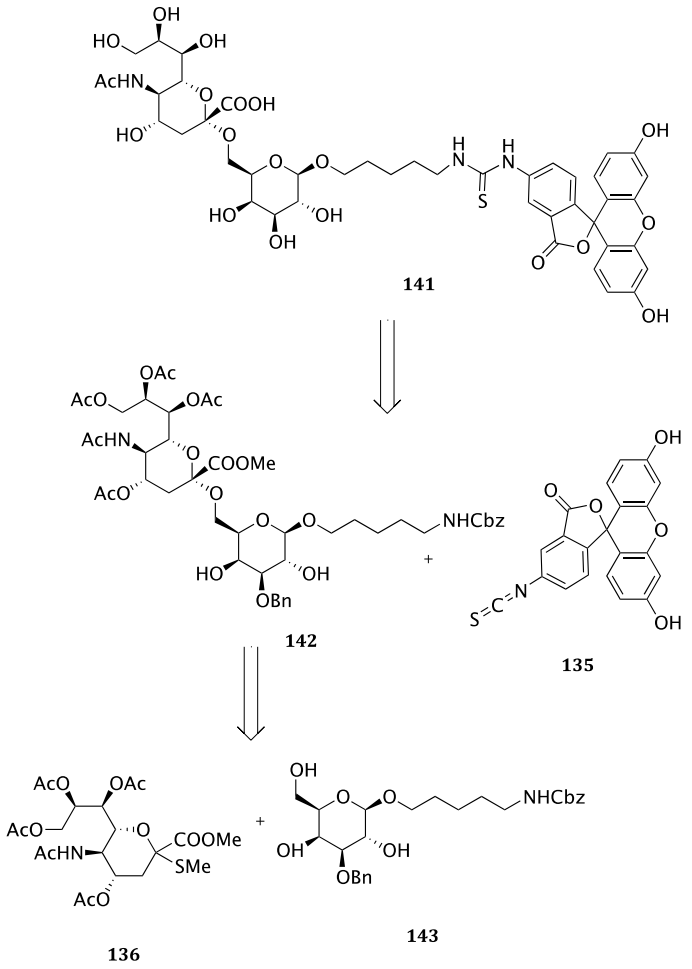

Figure 4.24 – Retrosynthetic analysis of fluorescent sialic acid **141** from glycosylation with a 3Bn-Gal acceptor and a thioether sialic acid donor (**136**).

The galactosyl acceptor (**143**) was synthesised as shown in Figure 4.25 from galactose (**144**), which was fully acetylated to **145** by treatment with Ac_2O and isolated in a 78% yield. Selective deprotection of the anomeric hydroxyl group by treatment with a 1:1 mixture of acetic acid and ethylenediamine in THF produced compound **146** in 71% yield, which was in turn transformed into a trichloroacetimidate leaving group (**147**) by treatment with CCl_3CN in dry DCM. It is worth mentioning that the reaction with CCl_3CN can lead to the formation of both α and β anomers, however addition of NaH after 2 h can drive the reaction towards the thermodynamic product, the α-anomer, which was isolated in a 75% yield.[73] The prepared galactose derivative **147** was then glycosylated by nucleophilic attack of the previously prepared Cbz-protected hydroxylamine (**138**) in the presence of $BF_3{\cdot}OEt_2$[74,75] to obtain the α-Gal compound **148** (30% yield). Finally, the galactose derivative **148** was fully deacetylated by base

treatment to **149** (90% yield), and the alcohol at C3 was selectively protected by a benzyl group to isolate **143** in a 73% yield. This selectivity was achieved by the use of dibutyltinoxide, which forms a cyclic intermediate involving the *cis*-vicinal hydroxyl at C2 which enhances the reactivity of the equatorial hydroxyl group.[76] This protection was done to avoid the formation of SA-α-2,3-Gal linkages, thus promoting the formation of SA-α-2,6-Gal linkages.

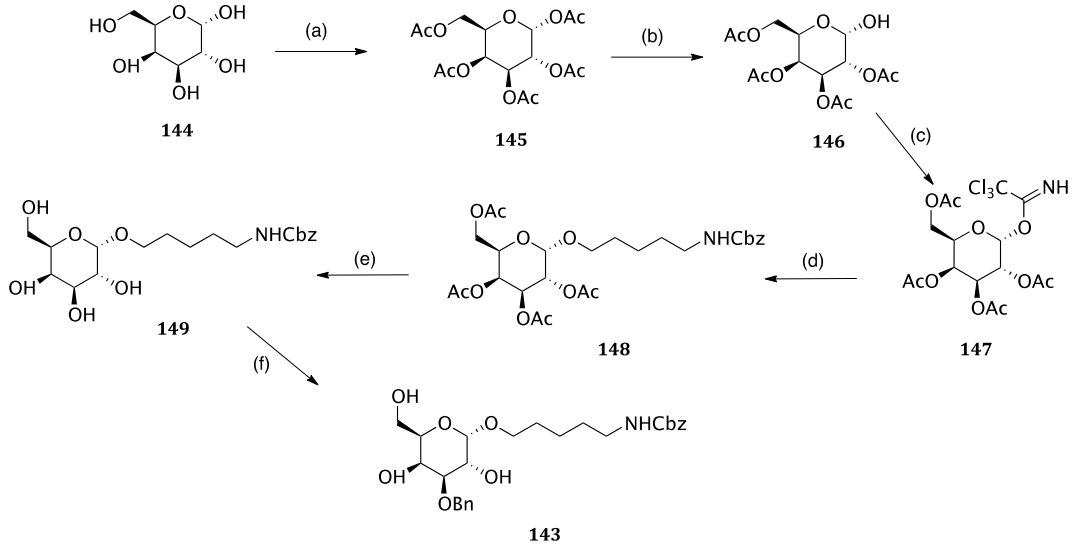

Figure 4.25 – Synthetic scheme for 3-Bn-Gal-*O*-(Cbz-aminopentanoate) (**143**). *Reagents and conditions*: (a) Ac_2O (78%); (b) H_2SO_4, ethylenediamine (71%); (c) K_2CO_3, Cl_3CCN (3 equiv.) (75%); (d) Cbz-amino-1-pentanol (**138**, 2 equiv.), $BF_3{\cdot}OEt_2$ (2 equiv.) (30%); (e) NaOAc (0.1 equiv./Ac) (90%); (f) Dibutyltin oxide (1.4 equiv.), tetrabutylammonium bromide (0.5 equiv.), benzyl bromide (12 equiv.) (73%).

Unfortunately the alcohol at C2 in SA (**125**) is very liable to dehydration due to the presence of an acid which destabilises the oxocarbenium ion intermediate formed during glycosylations and creates a tertiary anomeric centre, as well as the absence of a substituent at C3 that often assists glycosylation.[77] The product of this dehydration reaction is the alkene **150** shown in Figure 4.26, which was invariably the product obtained during the attempted reactions. Several solvent, catalyst and temperature variations were tested,[77] summarized in Table 4.2, however alkene **150** was consistently the product obtained.

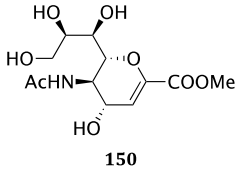

Figure 4.26 – Dehydration product from *O*-glycosylation of sialic acid.

Table 4.2 - Conditions tested for the synthesis of SA derivatives[a].

Test	Donor	Acceptor	Catalyst	Solvent	Temp.
1	137 – 1.5 equiv.	138 – 0.1 M	$Hg(CN)_2$ – 0.1 equiv.	Neat	RT
2	137 – 1.5 equiv.	138 – 0.1 M	$Hg(CN)_2$ – 0.1 equiv.	DCM	RT
3	137 – 1.5 equiv.	138 – 0.1 M	$Hg(CN)_2$ – 0.1 equiv.	CH_3NO_2	RT
4	137 – 1.5 equiv.	138 – 0.1 M	$Hg(CN)_2$ – 0.1 equiv.	DMF	RT
5	137 – 1.5 equiv.	138 – 0.1 M	$Hg(CN)_2$ – 0.1 equiv.	Benzene	RT
6	137 – 0.2 equiv.	138 - 0.1 M	Ag_2CO_3 – 0.2 equiv.	DMF	RT
7	137 – 1.5 equiv.	138 - 0.1 M	NaH – 1 equiv.	DMF	RT
8	137 – 0.2 equiv.	138 - 0.1 M	Ag_2CO_3 – 0.2 equiv.	CH_3CN	RT
9	137 – 1.5 equiv.	138 – 0.1 M	$Hg(CN)_2$ – 0.1 equiv.	CH_3NO_2	40°C
10	137 – 1.5 equiv.	138 – 0.1 M	$Hg(CN)_2$ – 0.1 equiv.	DCM	40°C
11	136 – 2 equiv.	138 - 0.1 M	DMTST - 6 equiv.	DCM	RT
12	136 – 2 equiv.	138 - 0.1 M	DMTST - 6 equiv.	CH_3CN	-40°C
13	136 – 2 equiv.	143 - 0.1 M	DMTST - 6 equiv.	CH_3CN	-40°C

[a]Standard experimental conditions used for this comparison were a total reaction volume of 1 mL, with the acceptor dissolved in the selected solvent and the donor added after the catalyst. The reaction mixture was shaken in a sealed glass vial for up to 5 days. TLC analysis was used to determine the progression of the reaction.

3.5. Dissociation constant determination by ^{1}H NMR spectroscopic analysis

Nevertheless, having successfully synthesised the cyclic peptide in sufficient quantities to obtain useful NMR data, it was decided to determine the binding affinity of the peptide to the free sialic acid through an NMR titration study. Small aliquots of a solution of SA (**125**) in D_2O were added to a 10.6 mM starting solution of the cyclic peptide **126** in D_2O. The pH was adjusted to 7.0 ± 0.1 after each SA (**125**) addition with 1M solutions of DCl and NaOD in D_2O. ^{1}H NMR spectra were recorded after each addition, and changes in chemical shifts were analysed to determine the dissociation constant (Figure 4.27).

The peaks selected for this analysis were the doublet at 7.6 ppm corresponding to Tyr H29 and the doublet at 6.7 ppm corresponding to Trp H32 from the cyclic peptide **126** (Figure 4.19), and the doublet at 3.5 ppm from the proton at C7, as well as the *N*-acetyl peak at 2.0 ppm from SA (**125**, Figure 4.10). The peaks corresponding to SA (**125**) were chosen because there were no overlapping

signals at those chemical shifts and therefore any changes could be easily tracked. One peak corresponding to each aromatic amino acid in the cyclic peptide **126** was chosen because it was simple to follow changes in that region, wheareas the rest of the spectrum was obscured by SA, especially at very high concentrations. Additionally, the solution of the cyclic peptide **126** was spiked with neat acetone to use as an internal standard and allow corrections in shift changes due to dilution effect.

It is worth mentioning that the system was in fast exchange on the chemical shift time-scale, and thus single peaks were observed corresponding to the mole fraction weighted average of the free and bound states.[78] In addition, all the shifts observed in the selected protons were downfield and in the magnitude of 0.02 ppm for the highest [SA]/[CP] ratio.

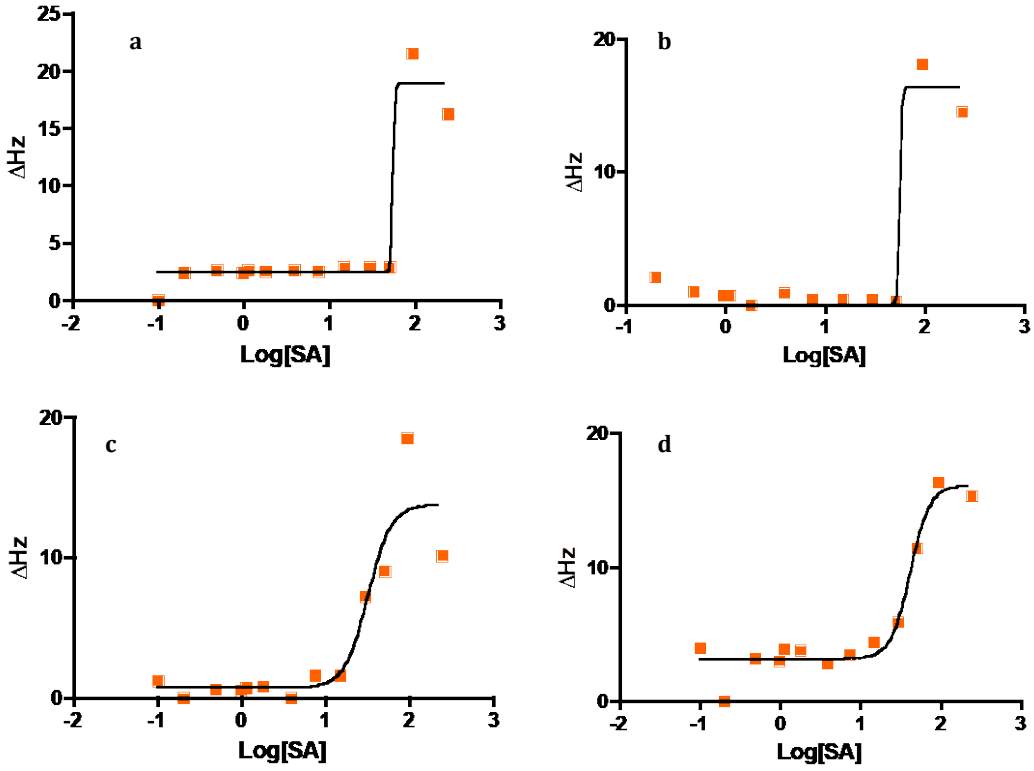

Figure- 4.27 – Titration curves for sialic acid (**125**) to cyclic peptide **126** as determined by chemical shift changes at selected protons. a) SA's *N*-Ac methyl peak at 2.0 ppm; b) SA's proton at C7 at 3.5 ppm; c) cyclic peptide's Trp proton at 6.7 ppm; d) cyclic peptide's Tyr proton at 7.5 ppm. [SA] concentration reported in mM, ΔHz =observed δ-lowest observed δ.

The chemical shifts were plotted as the difference between the observed shifts (mole fraction weighted average of the free and bound states) and the lowest

observed shift (free state for the cyclic peptide **126** and bound state for SA (**125**)) versus the logarithmic concentration of total SA (**125**). A sigmoidal dose-response curve (variable slope) was fitted to the plotted values to obtain a K_D form the EE_{50} of the resulting curve. As can be seen in Figure 4.27, while the lowest and highest observed chemical shifts did not correspond exactly to the free or bound states of the participating molecules, these values can be derived from the resulting curves. It is important to mention that the correction of the ΔHz, when the determined chemical shift for the free or bound states was used, did not affect the K_D values obtained. Furthermore, since the obtained K_D values were within the mM range, there was no need to adjust the line equation to account for the concentration of bound SA (**125**) in the x-axis.

Table 4.3 - Determined K_D constants from observed peaks

	Observed ^{1}H		K_D	Std.Error (LogK_D)
Sialic acid (125)	*N*-Ac	2.0 ppm	55.4 mM	1.74
	C7	3.5 ppm	56.1 mM	1.75
Cyclic peptide 126	Trp	6.7 ppm	31.8 mM	1.50
	Tyr	7.5 ppm	42.0 mM	0.05

Values determined from a sigmoidal dose-response curve (variable slope) fitted to the plotted observed chemical shifts as Log[SA] vs. ΔHz. K_Ds obtained from the EE_{50} of each curve and Standard Error reported form the line fitting equation, from a single measurement.

The design of this experiment, where the concentration of peptide was kept relatively constant, allows for more accurate K_D values determination where the protein protons are observed. The large increases in SA (**125**) concentration throughout the experiment cause a dramatic change between single measurements where the equilibrium shifts from the bound to the free state. Nevertheless, the K_D values determined by the fitted curves (Table 4.3) are consistent for both SA (**125**) and cyclic peptide **126** protons, which further validates the data obtained. All determined K_Ds were within a 32-56 mM range, which corresponds to a low-affinity interaction. A NMR study by Wiley and co-workers[79] titrated a sialic acid methyl ester (α-Me, **139**α, Figure 4.23) to influenza hemagglutinin (strain X-31 from a H3N2 virus) and found a K_D of 2.8±2 mM. The same study titrated the β anomer of the same sialic acid methyl ester

(**139**β) and obtained a K_D higher than 200 mM, thus highlightly the specificity of the active site.[79] Based on these facts, while the designed cyclic peptide **126** showed a low binding affinity to SA, it still showed higher affinity than HA to a SA (**125**) with inverted stereochemistry at the anomeric carbon. Moreover, since the titration curve did not generate a linear dose-response, it is generally accepted that the observed K_D is not generated by non-specific binding.[80] It is worth mentioning that the titration curves seem to fit a model for a single binding conformation, supported by the fact that the K_Ds are similar for different parts of the molecules involved.[81]

Determining the position of the molecules would require an in-depth structural study, however, previous crystallography studies place the *N*-Acetyl group of SA (**125**) interacting with a Trp residue (Figure 4.10).[71] Wiley's work followed the shift in the *N*-Acetyl group of SA (**125**) by NMR, and determined a slight upfield shift in the bound state of SA presumably corresponding to the Trp current.[71] In contrast, this titration study determined a downfield shift in the *N*-Acetyl group of SA (**125**) indicating that is possible the sugar is not oriented in the same manner towards the selected critical residues in the cyclic peptide **126**. Nevertheless, corresponding shifts were obtained for both Trp and Tyr, thus indicating that they are interacting in some way with SA (**125**).

It is important to highlight that the results presented here were obtained from a single experiment with a limited range of concentrations, therefore no statistical error can be determined other than the standard error associated with curve fitting. Errors in the resolution of the NMR spectra and in the concentration of both peptide **126** and SA (**125**) could be adequately treated by experiment repetition.

4. Conclusions

The use of a rationally designed cyclic peptide as means to prevent viral entry is a novel concept and as such the current research provided only the initial stages in its development. Analysis of the binding sites of four different sialic acid enzymes allowed identification of 6 critical residues in their active sites contributing to the binding of sialic acid. Further analysis of the relative distances between these amino acids in the active site of hemaglutinnin provided a general guidance on the number of amino acids required to link them while conserving their relative positions as much as possible. The resulting cyclic peptide was shown to fit in the binding site of HA-NA *in silico,* thus providing a positive confirmation that the designed molecule had the desired size and proportions.

Chemical synthesis of the designed cyclic peptide was successful, as confirmed by NMR data (^{1}H, COSY and ROESY experiments) as well as MS. While the synthesis of a sialic acid fluorescent probe for testing affinity with the cyclic peptide was unsuccessful, a NMR titration of the synthesised peptide with free sialic acid rendered the desired information regarding binding affinity. The obtained K_D values corresponded to a low-affinity interaction between the two molecules. Nevertheless, the obtained data pointed to specific binding with a single binding conformation. These characteristics provide a solid base to hypothesise that further optimisations of the cyclic peptide might allow tighter bindings that could eventually compete with hemagglutin to achieve their goal as prophylactics against viral infections.

5. Future work

The use of a cyclic peptide as means of preventing entry of the influenza virus to a host cell is a novel concept and the research so far is only the initial phase in its development. Among the first experiments that could determine the viability of this approach is the testing of the cyclic peptide in a cellular based model for blocking entry of influenza virus to determine its viability as treatment. Cytotoxicity and entry inhibition kinetics would be the first pieces of information that ought to be collected.

A parallel line of development is the lead optimisation of the cyclic peptide. The seven spacing glycines in the peptide provide a simple avenue for optimisation. Randomising of amino acids in these positions could increase the affinity and selectivity of the peptide. *In silico* binding studies could provide a good indication of which are the most promising sequences for testing. The synthesised cyclic peptides could also be tested for specificity against a glycan array to determine whether their affinity is selective for sialic acid.

Throughout this process, NMR data could be used to obtain information on the structural interactions between the cyclic peptide and its target, which could feed into the lead optimisation cycle for improvement of the cyclic peptide. Furthermore, all experiments (*in silico* studies, specificity determination, structure elucidation) could be done not only to determine information with sialic acid, but also narrowing down specificity by including specific sialic acid-galactose linkages. As mentioned before, this project is still in its initial stages and thus there are multiple areas for exploration if this project were to be continued.

6. Experimental

6.1. Materials and general methods

All solvents used were laboratory or analytical grade and were purchased from Fisher Scientific unless otherwise stated. Anhydrous solvents were purchased from Acros. HPLC grade solvents were from AnalaR and Fisher Scientific. All commercially available reagents were purchased from Sigma or Acros unless otherwise specified, and were used as received without further purification. All amino acids, and reagents required for peptide synthesis were purchased from C S Bio Co (USA). Water was Milli-Q™ grade.

Semi-preparative scale HPLC (Agilent) was performed using a protein and peptide C18 column (Vydec). The chromatography system consisted of Agilent 1100 Degasser, Quat pump and MWP modules. Spectra were collected for λ256 nm, λ214 nm, and λ495 nm absorptions with a UV/Vis detector. Solvent A was 0.1% TFA in Water and solvent B was 0.1% TFA in CH_3CN. Program A (3 mL/min flow) - gradient: t=0 min, 5% B; t=3 min, 5%; t=20 min, 40% B; t=23 min, 95% B; t=25 min, 95% B; t=28 min, 5%B; t=30 min, 5% B – 8.4 % B.

Silica gel column chromatography was done using Merck silica gel (60, particle size 0.040-0.063 mm (as stationary phase). Thin layer chromatography was performed using pre-coated silica gel plates (Merck 0.25mm Kieselgel 60 F_{254}) visualised by UV (254 nm) or by staining with 10% ammonium molybdate in 2 M H_2SO_4, 0.3 M DNPH in 20% H_2SO_4 50% aqueous EtOH or 0.1 M ninhydrin in 3% ethanolic AcOH, followed by heating.

Fluorescence spectra and UV absorbance were recorded on a Spectramax M5 microtiter plate reader (Molecular Devices).

NMR spectra were recorded on a Varian Spectrometer (500 MHz) at 30°C or a Brücker DPX (400 MHz) machine at ambient temperature. The following abbreviations are used to denote multiplicities: br-broad, s-singlet, d-doublet, t-triplet, q-quartet, dd-doublet of doublet, ddd- doublet of doublet of doublets, dt-

doublet of triplets, m-multiplet. Coupling constant values (*J*) are reported to the nearest O.1 Hz. Chemical shifts are reported in parts per million (ppm) and are referenced to the residual solvent peak (^{1}H: $CDCl_3$ – 7.24 ppm, D_2O - 4.80 ppm, Acetone-d_6 – 2.05 ppm, MeOD-d_4 – 4.87 ppm and 3.31 ppm, or DMSO-d_6 – 2.50 ppm; ^{13}C: $CDCl_3$ – 77.23 ppm, Acetone-d_6 – 29.92 ppm and 206.68 ppm, MeOD-d_4 – 49.15 ppm, or DMSO-d_6 – 39.51 ppm).

Mass spectra were recorded on a Micromass LCT electrospray ionisation mass spectrometer with medium-high (7,000) resolution running openlynx. High-resolution mass spectra were recorded on a Brücker MicroTOF electrospray ionisation mass spectrometer with medium-high resolution (10,000).

Melting points were recorded on a Gallenkamp capillary melting point apparatus and are reported uncorrected.

PDB files were manipulated using DS ViewerLite software. Protein and molecule manipulations were done using Maestro Schrodinger Suite 2008 on a Microsoft PC.

All graphs were generated using GraphPrism 4.0a for Macintosh. Calibration curves were fitted with a linear regression curve.

^{1}H NMR and MS data are reported for all synthesised compounds. ^{13}C NMR data, m.p., and high resolution MS are reported when available.

6.2. *In silico* studies

All 3D molecule and protein manipulations were performed using the Maestro Schrodinger Suite 2008. The cyclic peptide minimum energy model was developed using the LigPrep, Protein Preparation Wizard and Prime modules. Initially, a previously prepared 2D structure was imported into the LigPrep module and transformed to 3D using standard parameters for atom and residue properties. Hydrogen treatment was allowed to use hydrogen atoms explicitly (instead of as part of another atom). The resulting 3D structure contained all

atoms linked through correct conformations, with the most energy favourable rotamers. This structure was transferred to the Protein Preparation Wizard and subjected to standard optimisation. While this module usually cleans up crystal structures, detecting missing atoms, or determine bound metals ionisation states, in this case the module was used to predict the most likely ionisation state of the constitutive amino acids and render a PDB structure that could be used in protein modelling experiments such as docking ligands and superimposing on protein active sites. The produced structure was then transferred to the Prime module where it was subjected to an energy minimisation experiment to predict the minimum energy conformation of the cyclic peptide. The only changes made to the standard processing parameters were to allow full flexibility to all bonds and to permit hydration.

The rendered structure was then given to Dr. Balali for further experiments using Gold software.

6.3. Attempted synthesis of a sialic acid probe

Methyl-5-acetamido-3,5-dideoxy-D-*glycero*-D-*galacto*-2-nonulopyranosonate[71]

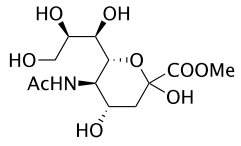

139

Dowex 50WX8 H^+ (3 g) was added to a solution 5-acetyl neuraminic acid (**125**, 1 g, 3.2 mmol) in MeOH (100 mL). The mixture was allowed to stir for 12 h after which the solids were removed by filtration and the solvent was evaporated *in vacuo* to yield the desired methyl ester **139** as a white powder in quantitative yield (1.03 g, 3.2 mmol). The product was used without further purification.

^{1}H NMR (D_2O, 500 MHz) δ 1.97 (ddd, 1 H, *J*=13.0 Hz, 11.5 Hz, 2.5 Hz, H3a), 2.11 (d, 3H, *J*=2.5, Ac), 2.38 (ddd, 1H, *J*=13.0 Hz, 5 Hz, 2.5 Hz, H3b), 3.41 (d, 1H, *J*=2.5 Hz, H5), 3.62 (dq, 1H, *J*=9.4 Hz, 1.3 Hz, H4), 3.68 (ddd, 1H, *J*=12.0 Hz, 6.5 Hz, 2.5 Hz, H9a), 3.79 (m, 1H, H9b), 3.88 (t, 1H, *J*=2.5 Hz, H6), 3.90 (d, 3H, *J*=2.5 Hz, OMe), 3.98 (td, 1H, *J*=10.5 Hz, 2.5 Hz, H7), 4.13 (m, 1H, H8).

^{13}C {^{1}H} NMR ($CDCl_3$, 125 MHz) δ 22.04 (Ac), 38.62 (C3), 52.03 (OMe), 53.46 (C5), 63.14 (C9), 66.64 (C4), 68.16 (C7), 70.08 (C8), 70.32 (C6), 95.28 (C2), 171.38 (C1), 174.81 (Ac CO).

m.p.: 188-191.9°C (lit. m.p. 191-193°C)

LR-MS (ESI): *m/z* 534.4 $[M+H]^+$

Methyl-5-acetamido-2-chloro-4,7,8,9-tetra-*O*-acetyl-3,5-dideoxy-D-*glycero*-β-D-*galacto*-2-nonulopyranosonate[82]

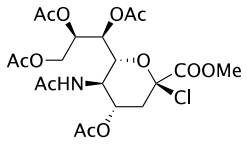

137

HCl gas was bubbled for 10 min through a solution of the methyl ester **139** (50 mg, 0.15 mmol) in a mixture of acetyl chloride and acetic acid (1:1, 3 mL), previously cooled down to 0°C. The solution was then sealed and allowed to stir overnight at RT. The solvents were then evaporated *in vacuo* and the residue was dissolved in a mixture of EtOAc and ether (1:1, 5 mL). The insoluble particles were removed by filtration and the filtrate was evaporated *in vacuo* to give the title compound **137** as a white foam (88% yield, 67 mg, 0.13 mmol).

^{1}H NMR ($CDCl_3$, 500 MHz) δ 1.93 (s, 3H, NAc), 2.07 (s, 3H, C4 Ac), 2.08-2.08 (m, 1H, H3a), 2.09 (s, 3H, C9 Ac), 2.11 (s, 3H, C7 Ac), 2.14 (s, 3H, C8 Ac), 2.29 (t, 1H, *J*=12.5 Hz, H3b), 2.80 (dd, 1H, *J*=13.9 Hz, 4.6 Hz, H5), 3.89 (s, 3H, OMe), 4.08 (dd, 1H, *J*=12.5 Hz, 5.8 Hz, H4), 4.22 (q, 1H, *J*=10.2 Hz, H6), 4.41 (dd, 2H, *J*=37.0 Hz, 11.5 Hz, H9), 5.19 (m, 1H, H7), 5.42 (td, 1H, *J*=10.6 Hz, 4.5 Hz, H8).

^{13}C {^{1}H} NMR ($CDCl_3$, 125 MHz) δ 20.57 (C9 Ac), 40.54 (C7 Ac), 46.42 (C8 Ac), 48.87 (C4 Ac), 52.50 (NAc), 53.78 (C3), 62.11 (OMe), 67.01 (C5), 67.68 (C9), 68.23 (C7), 68.71 (C8), 69.99 (C4), 73.64 (C6), 96.53 (C2), 161.55 (C9 Ac CO), 165.55 (41 Ac CO), 169.97 (C8 Ac CO), 170.62 (C1), 171.67 (C7 Ac CO), 175.24 (NAc CO).

LR-MS (ESI): *m/z* 510.4 $[M+H]^+$

Methyl-5-acetamido-2,4,7,8,9-penta-*O*-acetyl-3,5-dideoxy-D-glycero-D-galacto-2-nonulopyranosonate[74]

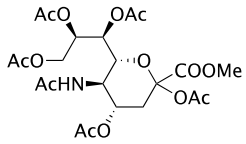

140

Acetic anhydride (23.1 mL, 0.22 mol) was added to a solution of compound **139** (1.96 g, 6.1 mmol) in dry pyridine (50 mL). The reaction mixture was allowed to stir overnight at RT, after which the solvent was evaporated under reduced pressure. The residue was purified by silica gel chromatography (EtOAc) to obtain the fully acetylated SA **140** as a white froth (79% yield, 2.5 g, 4.8 mmol).

R_f 0.80 (1:1 CH_3CN:EtOAc, *p*-anisaldehyde stain).

^1H NMR ($CDCl_3$, 500 MHz) δ 1.27 (t, 1H, *J*=7.1 Hz, H3a), 1.89 (s, 3H, NAc), 2.03-2.14 (m, 15H, C1 Ac, C4 Ac, C7 Ac, C8 Ac, C9 Ac), 2.56 (dd, 1H, *J*=13.5 Hz, 5.0 Hz, H3b), 3.79 (s, 3H, OMe), 4.09-4.14 (m, 2H, H5, H4), 4.51 (dd, 1H, *J*=12.4 Hz, 2.5 Hz, H9a), 5.04-5.08 (m, 1H, H9b), 5.21-5.28 (m, 1H, H6), 5.38 (dd, 1H, *J*=5.0 Hz, 1.7 Hz, H7), 5.47 (d, 1H, *J*=9.5 Hz, H8).

^{13}C {^1H} NMR ($CDCl_3$, 125 MHz) δ 20.71 (C9 Ac), 20.76 (C1 Ac), 20.81 (C7 Ac, C8 Ac, C4 Ac), 23.14 (NAc), 36.85 (C3), 49.02 (OMe), 52.86 (C5), 62.14 (C9), 67.38 (C7), 68.44 (C8), 69.96 (C4), 73.83 (C6), 95.42 (C2), 168.24 (C1), 168.53 (C1 Ac CO), 169.94 (C4 Ac CO), 170.04 (C9 Ac CO), 170.31 (C8 Ac CO), 170.72 (C7 Ac CO), 170.84 (NAc CO).

m.p.: 93.1-93.9°C

LR-MS (ESI): *m/z* 534.2 $[M+H]^+$

Methyl-(methyl-5-acetamido-4,7,8,9-tetra-*O*-acetyl-3,5-dideoxy-2-thio-D-glycero-D-galacto-2-nonylopyranosonate[74,75]

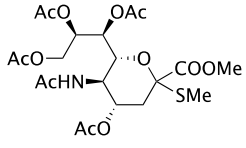

136

Trimethylsilylthiomethyl (1.3 mL, 9.5 mmol) and trymetylsilyltriflate (167 μL, 2.6 mmol) were added to a solution of the fully protected sialic acid **140** (1 g, 1.9 mmol) in DCM (15 mL). The reaction mixture was heated under conditions of

reflux for 6 h, after which it was diluted with DCM (85 mL) and extracted with aqueous Na_2CO_3 (sat., 2 x 100 mL). The combined organic fractions were further washed with brine (2 x 50 mL) and then dried over $MgSO_4$, the desiccant removed by filtration and the solvent evaporated *in vacuo*. The residue was purified by silica gel chromatography (EtOAc) to obtain thioether **136** as a white powder (65% yield, 0.64 g, 1.2 mmol) in a 3:5 α:β anomer mixture.

R_f 0.52 (EtOAc, *p*-anisaldehyde stain).

^{1}H NMR ($CDCl_3$, 500 MHz) δ 1.68 (s, 3H, Nac), 1.89 (s, 3H, SMe), 2.03-2.18 (m, 13H, C4 Ac, C7 Ac, C8 Ac, C9 Ac, H3a), 2.55 (dd, 1H, *J*=13.9 Hz, 5.0 Hz, H3b), 3.82 (s, 3H, OMe), 4.06-4.12 (m, 2H, H5, H4), 4.29-4.33 (m, 1H, H9a), 4.82 (dd, 1H, *J*=12.4 Hz, 2.4 Hz, H9b), 5.15-5.20 (m, 1H, H6), 5.35-5.39 (m, 1H, H8), 5.44 (t, 1H, *J*=2.8 Hz, H7).

^{13}C {^{1}H} NMR ($CDCl_3$, 125 MHz) δ 11.29 (SMe), 20.74 (C4 Ac), 20.83 (C9 Ac), 20.99 (C8 Ac), 21.14 (C7 Ac), 23.09 (NAc), 36.91 (C3), 49.41 (C5), 52.82 (OMe), 60.38 (C9), 62.38 (C7), 68.45 (C8), 69.29 (C4), 72.09 (C6), 84.64 (C2), 167.90 (C1), 170.15 (C4 Ac CO), 170.21 (C9 Ac CO), 170.26 (C8 Ac CO), 170.55 (C7 Ac CO), 170.92 (NAc CO).

m.p.: 79.3-80.5°C

LR-MS (ESI): *m/z* 544.3 $[M+H]^+$

Benzyl (5-hydroxypentyl)carbamate[83]

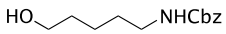

138

A cold (0°C) solution of 5-aminopentanol (6 g, 58 mmol) and $NaHCO_3$ (14.7 g, 175 mmol) in water (32 mL) was added to a solution of benzyloxycarbonylchloride (11.2 mL, 79 mmol) in THF (32 mL). The reaction mixture was allowed to warm up to RT overnight with stirring, after which it was extracted with EtOAc (3 x 100 mL), and washed with brine (100 mL). The combined organic fractions were dried over $MgSO_4$, the desiccant removed by filtration and the solvent evaporated under reduced pressure. The residue was washed with ether (3 x 50 mL) and dried in vacuum to obtain the protected alcohol **138** as a white powder in quantitative yield (13.8 g, 58 mmol). The product was used without further purification.

R_f 0.82 (1:1 CH_3CN:EtOAc, molybdate stain).

^1H NMR ($CDCl_3$, 500 MHz) δ 1.37-1.43 (m, 2H, H3), 1.50-1.60 (m, 4H, H2, H4), 3.22 (t, 2H, *J*=6.8 Hz, H5), 3.65 (t, 2H, *J*=6.4 Hz, H1), 5.10 (s, 2H, CH_2Ph), 7.31-7.38 (m, 5H, Ph).

^{13}C {^1H} NMR ($CDCl_3$, 125 MHz) δ 29.73(C3), 32.19 (C2), 40.90 (C4), 62.62 (C1), 65.32 (C5), 66.60 (*C*H_2Ph), 126.96 (Ph C4), 128.08 (Ph C3), 128.50 (Ph C2), 136.58 (Ph C3), 156.46 (CO).

m.p.: 44.1-46.5°C (lit. m.p. 45.5-47.0°C)

LR-MS (ESI): *m/z* 160.1 $[M+Na]^+$

Penta-*O*-acetyl-α-D-galactopyranose[83]

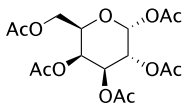

145

Acetic anhydride (42 mL, 0.44 mol) was added to a solution of galactose (**144**) (2 g, 11.1 mmol) in dry pyridine (50 mL). The reaction mixture was allowed to stir overnight at RT, after which the solvent was evaporated under reduced pressure. The residue was purified by silica gel chromatography (DCM) to obtain the acetylated sugar **145** as a white foam (78% yield, 3.4 g, 8.7 mmol).

R_f 0.67 (9:1 DCM: EtOAc, molybdate stain).

^1H NMR ($CDCl_3$, 500 MHz) δ 2.01 (s, 3H, C2 Ac), 2.03 (s, 3H, C3 Ac), 2.05 (s, 3H, C4 Ac), 2.16 (s, 6H, C1 Ac, C6 Ac), 4.09-4.11 (m, 2H, C6), 4.36 (t, 1H, *J*=6.7 Hz, H5), 5.34-5.34 (m, 2H, H2, H3), 5.50-5.51 (m, 1H, H4), 6.39-6.38 (m, 1H, H1).

^{13}C {^1H} NMR ($CDCl_3$, 125 MHz) δ 20.52 (C4 Ac), 20.58 (C6 Ac), 20.61 (C2 Ac), 20.64 (C5 Ac), 20.86 (C1 Ac), 61.25 (C6), 66.45 (C4), 67.36 (C2), 67.41 (C3), 68.72 (C5), 89.70 (C1), 169.00 (C4 Ac CO, C6 Ac CO), 169.96 (C2 Ac CO), 170.23 (C5 Ac CO), 170.50 (C1 Ac CO).

m.p.: 98.9-99.9°C (lit. m.p. 96.0-97.0°C)

LR-MS (ESI): *m/z* 391.2 $[M+H]^+$

2,3,4,6-Tetra-*O*-acetyl-D-galactopyranose[83]

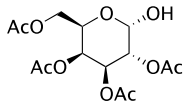

146

Glacial acetic acid (205 µL, 3.6 mL) was added drop wise to a solution of ethylenediamine (205 µL, 3.1 mL) in THF (65 mL). After the addition was complete, the fully acetylated galactose **145** (1 g, 2.6 mmol) was added to the reaction mixture and allowed to stir overnight at RT. Water (25 mL) was then added to the reaction mixture, and extracted with DCM (3 x 100 mL). The combined organic fractions were then washed with aqueous HCl (2 M, 100 mL), aqueous $NaHCO_3$ (sat., 100 mL) and water (100 mL), dried over $MgSO_4$, , the desiccant removed by filtration and the solvent evaporated *in vacuo*. The residue was purified by silica gel chromatography (4:1 DCM:EtOAc) to obtain the tetra-acetylated galactose **146** as a white foam (71% yield, 0.6 g, 1.8 mmol).

R_f 0.48 (9:1 DCM:EtOAc, molybdate stain).

^{1}H NMR ($CDCl_3$, 500 MHz) δ 2.00 (s, 3H, C2 Ac), 2.06 (s, 3H, C6 Ac), 2.10 (s, 3H, C4 Ac), 2.15 (s, 3H, C3 Ac), 4.09-4.16 (m, 2H, H6), 4.49 (t, 1H, *J*=6.6 Hz, H5), 5.18 (dd, 1H, *J*=10.8 Hz, 3.6 Hz, H3), 5.43 (dd, 1H, *J*=10.8 Hz, 3.3 Hz, H2), 5.48 (dd, 1H, *J*=3.1 Hz, 1.0 Hz, H4), 5.53 (d, 1H, *J*=3.6 Hz, H1).

^{13}C {^{1}H} NMR ($CDCl_3$, 125 MHz) δ 20.58 (C6 Ac), 20.60 (C4 Ac), 20.64 (C2 Ac), 20.75 (C3 Ac), 61.75 (C6), 65.99 (C4), 67.13 (C2), 68.17 (C3), 68.36 (C5), 90.50 (C1), 170.18 (C6 Ac CO), 170.34 (C4 Ac CO), 170.52 (C2 Ac CO), 170.69 (C3 Ac CO).

LR-MS (ESI): *m/z* 371.3 $[M+Na]^+$

2,3,4,6-Tetra-*O*-acetyl-α-D-galactopyranose trichloroacetimidate[84]

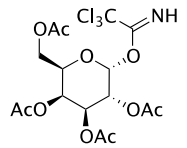

147

K_2CO_3 (0.43 g, 3.1 mmol) was added to a solution of the tetra-acetylated galactose derivative **146** (0.63 g, 1.8 mmol) and Cl_3CCN (529 µL, 5.3 mmol) in dry DCM (5 mL). The reaction mixture was allowed to stir for 2 h at RT, after

which a NaH (0.33 g, 2.3 mmol) and Cl_3CCN (260 µL, 2.6 mmol) were added to drive the formation of the α-anomer. The reaction mixture was further stirred for 2 h at RT, and then the insoluble particles were removed by filtration through a celite path. The solvent was removed under reduced pressure and the residue was purified by silica gel chromatography (17:3 DCM:EtOAc) to isolate the desired product **147** as a white powder (75% yield, 0.66 g, 1.4 mmol).

R_f 0.50 (9:1 DCM:EtOAc, molybdate stain) - α-anomer; β-anomer R_f 0.37.

^{1}H NMR ($CDCl_3$, 500 MHz) δ 2.01 (s, 3H, C2 Ac), 2.02 (s, 3H, C3 Ac), 2.03 (s, 3H, C4 Ac), 2.17 (s, 3H, C6 Ac), 4.06-4.14 (m, 2H, H6), 4.45 (t, 1H, *J*=6.6 Hz, H5), 5.37 (dd, 1H, *J*=10.8 Hz, 3.5 Hz, H3), 5.43 (dd, 1H, *J*=10.9 Hz, 3.1 Hz, H2), 5.56 (d, 1H, *J*=3.0 Hz, H4), 6.60 (d, 1H, *J*=3.4 Hz, H1).

LR-MS (ESI): *m/z* 491.1 $[M+H]^+$

5-(Benzyloxycarbonylamino)pentyl-2,3,4,6-tetra-*O*-acetyl-α-D-galactopyranoside[73]

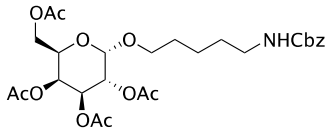

148

Compound **135** (194 mg, 0.8 mmol) and 4Å activated molecular sieves were added to a solution of trichloroacetimidate **147** (200 mg, 0.4 mmol) in dry DCM (5 mL). The solution was allowed to stir for 20 min at RT, after which the reaction mixture was cooled down to 0°C in an ice bath. $BF_3{\cdot}OEt_2$ (100 µL, 0.8 mmol) was added and the reaction mixture was stirred at 0°C during 4 h. The insoluble particles in the resulting suspension were removed by filtration, and the filtrate was diluted with DCM (20 mL). The solution was washed with aqueous $NaHCO_3$ (sat., 20 mL) and water (20 mL), and the combined organic fractions were dried over $MgSO_4$, the desiccant removed by filtration and the solvent evaporated *in vacuo*. The residue was purified by silica gel chromatography (17:3 DCM:EtOAc) to obtain the title compound **148** as a white powder (30% yield, 68 mg, 0.12 mmol).

R_f 0.74 (4:1 DCM:EtOAc, molybdate stain).

^{1}H NMR ($CDCl_3$, 500 MHz) δ 1.33-1.40 (m, 2H, H3), 1.48-1.56 (m, 2H, H4), 1.58-1.65 (m, 2H, H2), 1.99 (s, 3H, Gal C4 Ac), 2.04 (s, 3H, Gal C3 Ac), 2.05 (s, 3H, Gal C4 Ac), 2.15 (s, 3H, Gal C6 Ac), 3.21 (q, 2H, *J*=6.6 Hz, Gal H6), 3.50 (dd, 1H, *J*=16.0 Hz, 6.7 Hz, Gal H5), 3.91 (t, 2H, *J*=6.5 Hz, H5), 4.20 (ddd, 2H, *J*=26 Hz, 11.2 Hz, 6.7 Hz, H1), 4.46 (d, 1H, *J*=7.9 Hz, Gal H2), 5.03 (dd, 1H, *J*=10.5 Hz, 3.4 Hz, Gal H3), 5.09 (s, 2H, CH_2Ph), 5.22 (dd, 1H, *J*=10.4 Hz, 8.0 Hz, Gal H4), 5.39 (d, 1H, *J*=3.4 Hz, Gal H1), 7.31-7.37 (m, 5H, Ph).

^{13}C {^{1}H} NMR ($CDCl_3$, 125 MHz) δ 20.57 (Gal C6 Ac), 20.64 (Gal C4 Ac), 20.72 (Gal C2 Ac), 23.02 (Gal C3 Ac), 28.94 (C3), 29.57 (C4), 29.67 (C2), 40.87 (C5), 61.25 (C1), 66.56 (*C*H_2Ph), 67.03 (Gal C6), 68.88 (Gal C4), 69.85 (Gal C3), 70.58 (Gal C2), 70.89 (Gal C5), 101.28 (Gal C1), 127.91 (Ph H4), 128.07 (Ph H3), 128.49 (Ph H2), 136.59 (Ph H1), 156.37 (CBz CO), 169.43 (Gal C6 Ac CO), 170.17 (Gal C4 Ac CO), 170.28 (Gal C2 Ac CO), 170.40 (Gal C3 Ac CO).

LR-MS (ESI): *m/z* 568.4 $[M+H]^+$

5-(Benzyloxycarbonylamino)-pentyl-α-D-galactopyranoside[84]

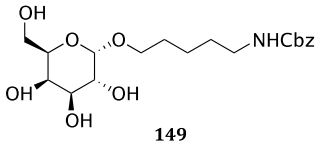

149

Sodium methoxide (16 µL, 71 µmol) was added to a solution of the protected galactose construct **148** (100 mg, 176 µmol) in MeOH (5 mL), previously cooled down to 0°C in an ice bath. The solution was allowed to stir for 1 h, after which Dowex 50 H^+ was added until a neutral pH was reached. The solids were then removed by filtration and the filtrate was evaporated under reduced pressure to obtain the desired galactose ether **149** as a white powder (90%, 63 mg, 158 µmol). The product was used without further purification.

R_f 0.12 (1:1 CH_3CN:EtOAc, molybdate stain).

^{1}H NMR (MeOD-$_{d4}$, 500 MHz) δ 1.41-1.45 (m, 2H, H3), 1.52-1.55 (m, 2H, H4), 1.62-1.67 (m, 2H, H2), 3.15 (t, 2H, *J*=6.9 Hz, H5). 3.45-3.54 (m, 4H, Gal H6, H1), 3.76 (dd, 2H, *J*=6.1 Hz, 3.7 Hz, Gal H2, Gal H5), 3.84 (d, 1H, *J*=2.3 Hz, Gal H3), 3.89-3.95 (m, 1H, Gal H4), 4.23 (d, 1H, *J*=7.4 Hz, Gal H1), 5.08 (s, 2H, CH_2Ph), 7.29-7.37 (m, 5H, Ph).

LR-MS (ESI): *m/z* 422.0 $[M+Na]^+$

5-(Benzyloxycarbonylamino)-pentyl-3-*O*-benzyl-α-D-galactopyranoside

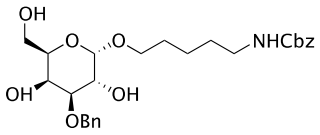

143

Dibutyltinoxide (52 mg, 0.2 mmol) was added to a solution of the galactose derivative **149** (56 mg, 140 μmol) in dry benzene (1.5 mL). The solution was heated to 80°C, and allowed to stir for 5 h, after which tetrabutylammonium bromide (23 mg, 70 μmol) and benzyl bromide (207 μL, 1.7 mmol) were added. The resulting reaction mixture was allowed to cool to 60°C and stirred at that temperature for a further 3 h, after which the solvent was removed *in vacuo*. The residue was purified by silica gel chromatography (19:1 DCM:MeOH) to obtain the benzyl protected galactose derivative **143** (73% yield, 50 mg, 102 μmol).

R_f 0.73 (1:1 CH_3CN:EtOAc, molybdate stain).

^{1}H NMR ($CDCl_3$, 500 MHz) δ 1.36-1.43 (m, 2H, H3), 1.48-1.53 (m, 2H, H4), 1.60-1.66 (m, 2H, H2), 3.13-3.22 (m, 2H, H5), 3.39-3.46 (m, 2H, H1), 3.50-3.56 (m, 1H, Gal H5), 3.76-3.83 (m, 2H, Gal H6), 3.88-3.97 (m, 2H, Gal H3, Gal H2), 4.00 (d, 1H, *J*=2.9 Hz, Gal H4), 4.24 (d, 1H, *J*=7.8 Hz, Gal H1), 4.74 (br d, 2H, *J*=2.3 Hz, Bn CH_2Ph), 5.08 (s, 2H, Cbz CH_2Ph), 7.27-7.39 (m, 10H, 2xPh).

m.p.: 109.9-111.9°C

LR-MS (ESI): *m/z* 512.4 $[M+Na]^+$

6.4. Cyclic peptide synthesis

6.4.1. On resin synthesis

Fmoc-Tyr-OMe[78,80,81]

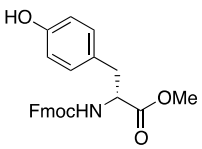

127

$NaHCO_3$ (1.01 g, 12 mmol) was added to a solution of Tyr-OMe (1.39 g, 6 mmol) in water (10 mL) with stirring. The solution was cooled to 0°C in an ice bath, and a solution of Fmoc-*O*Su (3.04 g, 9 mmol) in dioxane (2 mL) was added slowly to the reaction mixture. The resulting solution was stirred at 0°C for 1 h and then allowed to warm up to RT overnight, after which it was diluted with water (40

mL) and extracted with EtOAc (3 x 50 mL). The combined organic fractions were dried over $MgSO_4$, the desiccant removed by filtration and the solvent evaporated under reduced pressure. The residue was purified by silica gel chromatography (DCM) to obtain the fully protected tyrosine **127** as a white froth (80% yield, 1.93 g, 4.8 mmol).

^{1}H NMR ($CDCl_3$, 500 MHz) δ 3.08 (ddd, 2H, *J*=28.9 Hz, 14.0 Hz, 5.8 Hz, βH), 3.75 (s, 3H, OMe), 4.24 (t, 1H, *J*=6.9 Hz, Fmoc C*H*), 4.39 (m, 1H, Fmoc CH_2'), 4.48 (m, 1H, CH_2"), 5.31 (d, 1H, *J*=9.9 Hz, αH), 6.76 (d, 2H, *J*=8.2, Ph H2), 6.97 (d, 2H, *J*=8.2 Hz, Ph H3), 7.34 (t, 2H, *J*=7.4 Hz, Fmoc H3), 7.43 (t, 2H, *J*=7.3 Hz, Fmoc H4), 7.59 (t, 2H, *J*=6.8 Hz, Fmoc H5), 7.79 (d, 2H, *J*=7.6 Hz, Fmoc H2).

m.p.: 125.1-133.5°C (lit. m.p. 120.0-125.0°C)

LR-MS (ESI): *m/z* 418.2 $[M+H]^+$

Wang-like resin

The addition of an HMPA linker (**34**) to an AMS resin (**33**) was conducted by the same method described in Chapter 2.

Resin loading through Tyr side chain[85]

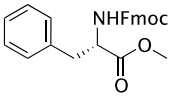

The Wang-like resin (**35**) (3.8 g, 1.5 mmol) was soaked in DCM (50 mL) for 2 h at RT. After draining the solvent, a solution of triphenylphosphine (2.8 g, 10 mmol) and Fmoc-Tyr-OMe (**127**) (3.8 g, 9.0 mmol) in DCM (70 mL) was added to the resin. The resultant mixture was then cooled to 0°C and a solution of DIAD (1.6 mL, 10 mmol) in DCM (7.0 mL) was added drop wise. The reaction mixture was allowed to stir overnight at RT, after which the solvent was removed by filtration and the resin was washed with DCM (3 x 10 mL), DMF (3 x 10 mL), MeOH (2 x 10 mL), DMF (3 x 10 mL) and ether (2 x 10 mL) and dried *in vacuo*. The resin was

then suspended in a solution of acetic anhydride (0.89 mL, 14 mmol) and DIPEA (1.6 mL) in DCM (17 mL) and stirred for 20 min at RT. The solvents were removed by filtration and the resin was again washed with DCM (2 x 10 mL) and DMF (2 x 10 mL), and finally dried in vacuum to give resin **128** (7.4 g).

To determine loading, a sample (10 mg) of resin was treated with 20% piperidine. After 30 min, the absorbance was recorded at 290 nm and compared to a standard curve generated after treatment under the same conditions of a resin with known loading (in this case Fmoc-Ala-Wang resin with 0.74 mmol/g loading). Loading for this resin was determined to be 0.38 mmol/g.

Peptide elongation

Peptide elongation for both peptides was carried out using the same protocol as described in Chapter 2.

C-terminus deprotection (on-resin)

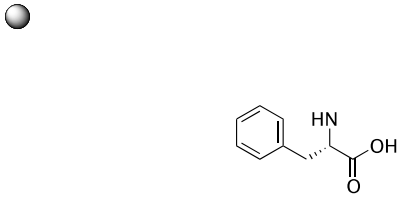

After the synthesis was completed, the methyl ester was saponified by shaking resin **129** (0.38 mmol) for 3 days on a solution of NaOH in MeOH (0.40 M, 20 mL). After this time the resin **130** was separated by filtration and washed with MeOH (3 x 10 mL), DMF (3 x 10 mL), DCM (3 x 10 mL), DMF (3 x 10 mL) MeOH (2 x 10 mL), DMF(2 x 10 mL) and ether (1 x 10 mL).

Cyclisation (on resin)

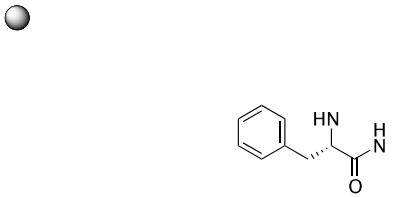

A solution of HOBT (0.25 g, 3.0 mmol), TBTU (0.60 g, 3.0 mmol), and DIPEA (0.57 mL, 3.9 mmol) in DMF (10 mL) was added to resin **130** (0.38 mmol) and the

reaction mixture was stirred for 5 hrs. The solvent was then removed by filtration and the resin washed with DMF (3 x 10 mL), DCM (3 x 10 mL), DMF (3 x 10 mL), MeOH (2 x 10 mL), DMF (2 x 10 mL) and ether (10 mL) to give resin **131**.

Cleavage and deprotection

Cleavage and deprotection for both peptides was conducted in the same method as described in Chapter 2.

6.4.2. Cyclisation from Linear Peptide

Linear Peptide

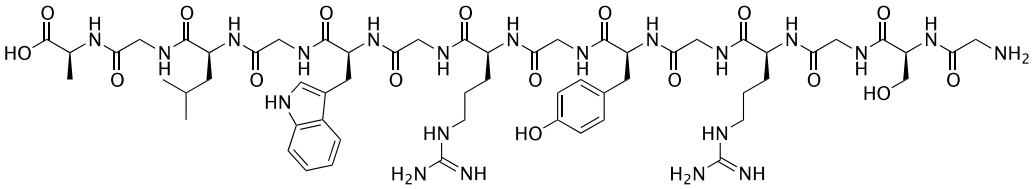

132

Peptide synthesis was completed as described before from Fmoc-Ala-Wang resin (0.74 mmol/g loading, 0.5 g, 0.37 mmol). Purification by preparative scale HPLC led to the isolation of peptide **132** (5% overall yield, 24 mg, 18 μmol).

^{1}H NMR (D_2O, 500 MHz) δ 0.81 (d, 3H, *J*=5.6 Hz, Val Me), 0.85 (d, 3H, *J*=5.7 Hz, Val Me), 1.33 (d, 3H, *J*=7.3 Hz, Ala Me), 1.55 (m, 7H, Arg1 βH, Arg 2 βH, Leu βH, Leu γH), 1.66 (m, 2H, Arg1 γH), 1.77 (m, 2H, Arg2 γH), 2.83 (dd, 1H, *J*=13.9 Hz, 8.6 Hz, Trp βH'), 2.98 (dd, 1H, *J*=14.0 Hz, 6.0 Hz, Trp βH''), 3.10 (q, 4H, *J*=7.3 Hz, Arg1 εH, Arg2 εH), 3.18 (dd, 1H, *J*=14.7 Hz, 7.4 Hz, Tyr βH'), 3.27 (dd, 1H, *J*=14.7 Hz, 6.7 Hz, Tyr βH''), 3.92 (m, 16H, Ser βH, Gly1 αH, Gly2 αH, Gly3 αH, Gly4 αH, Gly5 αH, Gly6 αH, Gly7 αH), 4.23 (m, 2H, Arg1 αH, Arg2 αH), 4.31 (m, 2H, Ala αH, Val αH), 4.48 (m, 2H, Trp αH, Ser αH), 4.60 (t, 1H, *J*=7.1 Hz, Tyr αH), 6.75 (d, 2H, *J*=8.5 Hz, Tyr H2), 6.97 (d, 2H, *J*=8.4 Hz, Tyr H3), 7.10 (t, 1H, *J*=7.5 Hz, Trp H5), 7.13 (s, 1H, Trp H8), 7.19 (t, 1H, *J*=7.6 Hz, Trp H4), 7.43 (d, 1H, *J*=8.2 Hz, Trp H6), 7.54 (d, 1H, *J*=7.9 Hz, Trp H2).

^{13}C {^{1}H} NMR (D_2O, 125 MHz) δ 16.27 (Val Me), 18.75 (Val Me), 20.60 (Arg1 βC), 21.91 (Arg2 βC), 22.18 (Ala Me), 24.16 (Arg1 βC), 24.21 (Arg2 βC), 24.24 (Val γC), 27.01 (Val βC), 27.81 (Arg1 γC), 28.08 (Arg2 γC), 36.15, 39.52, 40.41 (Trp

βC), 40.45 (Tyr βC), 42.17 (Gly1 αC), 42.29 (Gly7 αC), 42.35 (Gly6 αC), 42.36 (Gly4 αC), 42.38 (Gly5 αC), 42.43 (Gly3 αC), 42.45 (Gly2 αC), 48.73 (Ala αC), 52.52 (Val αC), 53.43 (Trp αC), 53.61 (Tyr αC), 54.66 (Arg1 αC), 55.15 (Arg2 αC), 55.49 (Ser αC), 61.22 (Ser βC), 104.82 (Arg1 εC), 108.83 (Arg2 εC), 111.85 (Trp C7), 115.20 (Tyr C1), 115.40 (Trp C6), 117.52 (Trp C5), 118.21 (Trp C4), 119.31 (Trp C3), 121.94 (Trp C2), 124.42 (Tyr C2), 126.87 (Tyr C3), 128.03 (Tyr C4), 130.45 (Trp C1), 136.09 (Trp C8), 154.41 (Arg1 CNH), 156.74 (Arg2 CNH), 167.34 (Gly7 CO), 170.79 (Gly6 CO), 170.84 (Gly5 CO), 171.08 (Gly3 CO), 171.25 (Gly4 CO), 171.28 (Gly2 CO), 172.07 (Gly1 CO), 173.57 (Arg2 CO), 173.87 (Arg1 CO), 173.89 (Ala CO), 173.98 (Val CO), 174.08 (Trp CO), 175.15 (Tyr CO), 176.49 (Ser CO).

HR-MS: ($C_{58}H_{87}N_{21}O_{17}$) theoretical *m/z* 1350.6662 $[M+H]^+$, found *m/z* $[M+H]^+$

HPLC trace (Program A):

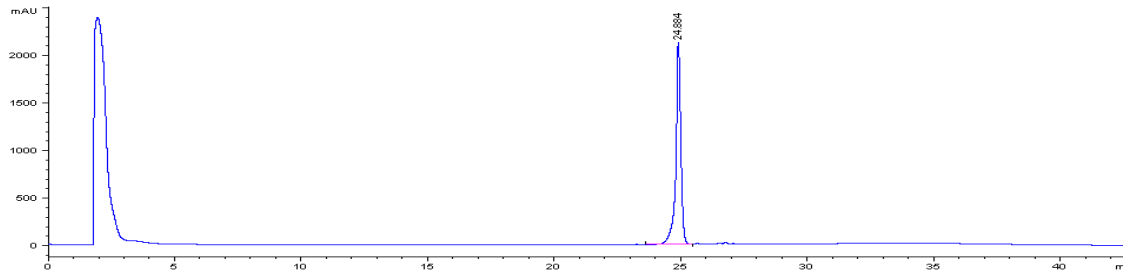

Solution Cyclisation

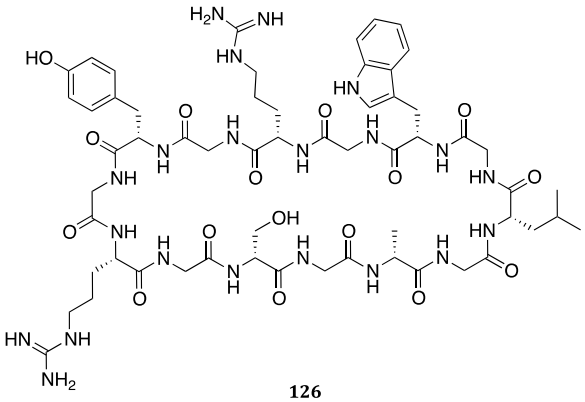

126

HATU (20.3 mg, 53 µmol), HOAt (7.3 mg, 53 µmol) and DIPEA (9.3 µL, 53 µmol) were added to a solution of the linear peptide **132** (18 mg, 13 µmol) in DMF (1 mL). The solution was stirred at RT for 3 h, after which the solvent was removed *in vacuo*. The residue was purified by semi-preparative scale HPLC to obtain the cyclic peptide **126** as a white powder (41% yield, 4 mg, 5.3 µmol).

^{1}H NMR ($CDCl_3$, 500 MHz) δ 0.85 (d, 6H, *J*=22.8 Hz, Val 2xMe), 1.31 (d, 3H, *J*=7.1 Hz, Ala Me), 1.46-1.53 (m, 7H, Arg1 βH, Arg2 βH, Leu γH, Leu βH), 1.59-1.67 (m, 2H, Arg1 γH), 1.70-1.82 (m, 2H, Arg2 γH), 2.79-3.12 (m, 6H, Trp βH, Arg1 εH, Arg2 εH), 3.13-3.18 (m, 1H, Tyr βH'), 3.23-3.27 (m, 1H, Tyr βH"), 3.66-3.92 (m, 16H, Ser βH, Gly1 αH, Gly2 αH, Gly3 αH, Gly4 αH, Gly5 αH, Gly6 αH, Gly7 αH), 4.18-4.28 (m, 4H, Arg1 αH, Arg2 αH, Ala αH, Val αH), 4.33-4.36 (m, 1H, Ser αH), 4.41-4.44 (m, 1H, Trp αH), 4.55-4.61 (m, 1H, Tyr αH), 6.75 (d, 2H, *J*=8.1 Hz, Tyr H2), 6.98 (d, 2H, *J*=7.9 Hz, Tyr H3), 7.09 (t, 1H, *J*=7.7 Hz, Trp H2), 7.13-7.18 (m, 2H, Trp H3, Trp H4), 7.42 (d, 1H, *J*=8.2 Hz, Trp H8), 7.53 (d, 1H, *J*=7.5 Hz, Trp H5).
HR-MS: ($C_{58}H_{85}N_{21}O_{16}$) theoretical *m/z* 1332.6556 $[M+H]^+$, found *m/z* 1332.6569 $[M+H]^+$

HPLC trace (Program A):

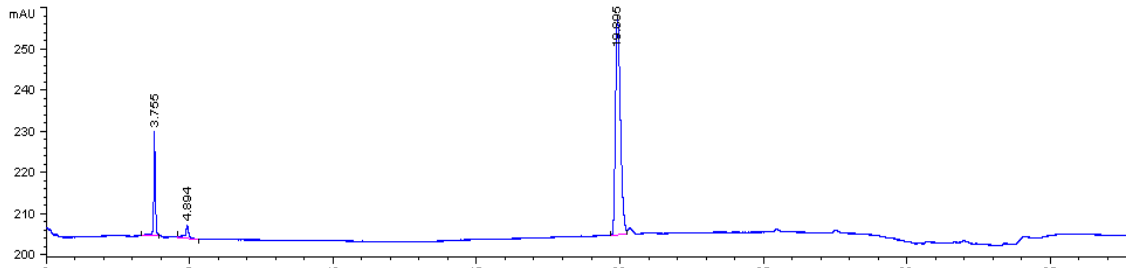

6.5. ^{1}H NMR binding affinity study[78,80,81]

A 10.6 mM solution of the cyclic peptide (**126**) in D_2O (500 µL) was prepared, and the pH adjusted to 7.0 with a solution of NaOD in D_2O (0.1M and 1M). Small aliquots of a solution of SA (**125**) in D_2O (50, 100 and 400 mM solutions) were added according to the table below (Table 4.4), and pH was adjusted to 7.0 ± 0.1 after each addition with solutions of DCl and NaOD in D_2O (1M and 0.1M solutions). Standard ^{1}H NMR spectrum were obtained after each addition at a constant temperature of 30°C.

Table 4.4 - Concentrations used for each data point of NMR titration of cyclic peptide (**126**) with sialic acid.

Data Point	[SA] solution (mM)	Vol. SA solution added (µL)	Vol. added for pH adjustment (µL)	Total vol. (µL)	[SA] (mM)	[CP] (mM)
1	50	1	1	506	0.099	10.534
2	50	1	2	509	0.196	10.472
3	50	3	3	515	0.485	10.350
4	50	5	4	524	0.954	10.172
5	100	1	17	542	1.107	9.834
6	100	4	13	559	1.789	9.535
7	400	3	5	567	3.880	9.400
8	400	5	6	578	7.266	9.221
9	400	12	13	603	14.925	8.839
10	400	25	17	645	29.457	8.264
11	400	40	7	692	50.578	7.702
12	400	100	9	801	93.633	6.654
13	400	800	62	1663	237.523	3.205

7. References

1. Al-Majhdi, F.N. Structure of the sialic acid binding site in influenza A virus hemagglutinin. *Journal of Biological Sciences*. 2007;7(1):113-22.

2. Suarez, D.L. and Schultz-Cherry, S. Immunology of avian influenza virus: a review. *Developmental and Comparative Immunology*. 2000;24(2-3):269-83.

3. Myers, K.P.; Olsen, C.W. and Gray, G.C. Cases of swine influenza in humans: a review of the literature. *Clinical Infectious Diseases : An official publication of the Infectious Diseases Society of America*. 2007;44(8):1084-8.

4. World Health Organization. *Influenza (Seasonal) - Fact sheet No.211*. 2009.

5. Chan, M. *World now at the start of 2009 influenza pandemic*. WHO: 2009.

6. McGeoch, D.; Fellner, P. and Newton, C. Influenza virus genome consists of eight distinct RNA species. *Proceedings of the National Academy of Sciences of the United States of America*. 1976;73(9):3045-9.

7. Klenk, H.D.; Rott, R. and Becht, H. On the structure of the influenza virus envelope. *Virology*. 1972;47(3):579-91.

8. Nayak, D.P.; Ka-Wai, H.E. and Barman, S. Assembly and budding of influenza virus. *Virus Research*. 2004;106:147-65.

9. Schnell, J.R. and Chou, J.J. Structure and mechanism of the M2 proton channel of influenza A virus. *Nature*. 2008;451:591-6.

10. Skehel, J.J. and Wiley, D.C. Receptor binding and membrane fusion in virus entry: the influenza hemagglutinin. *Annual Review of Biochemistry*. 2000;69:531-69.

11. Craik, D.J. Seamless proteins tie up their loose ends. *Science*. 2006;311:1563-4.

12. Samet, J.M. and Cheng, P-W. The role of airway mucus in pulmonary toxicology. *Environmental Health Perspectives*. 1994;102(2):89-103.

13. Chao-Tan, G.; Takahashi, N.; Yagi, H.; Kato, K.; Takahashi, T.; Yi S-Q.; Chen, Y.; Ito, T.; Otsuki, K.; Kida, H.; Kawaoka, Y.; Hidari, K.I-P.J.; Myamoto, D.; Suzuki, T. and Suzuki, Y. The quail and chicken intestine have sialyl-galactose sugar chains

responsible for the binding of influenza A viruses to human type receptors. *Glycobiology*. 2007;17(7):713-24.

14. Bullough, P.A.; Hughson, F.M.; Skehel, J.J. and Wiley, D.C. Structure of influenza haemagglutinin at the pH of membrane fusion. *Nature*. 1994;371:37-42.

15. Antigenic and genetic characteristics of influenza A (H5N1) and influenza A (H9N2) viruses for the development of candidate vaccine viruses for pandemic preparedness Influenza A (H5N1). World Health Organization: 2008.

16. Olofsson, S.; Kumlin, U.; Dimock, K. and Amberg, N. Avian influenza and sialic acid receptors: more than meets the eye? *Lancet Infectious Diseases*. 2005;5:184-8.

17. van Riel, D.; Munster, V.J.; de Wit, E.; Rimmelzwaan, G.F.; Fouchier, R.A.M.; Osterhaus, A.D.M.E. and Kuiken, T. H5N1 virus attachment to lower respiratory tract. *Science*. 2006;312:399.

18. Kumlin, U.; Olofsson, S.; Dimock, K. and Arnberg, N. Sialic acid tissue distribution and influenza virus tropism. *Influenza and Other Respiratory Viruses*. 2008;2:147-54.

19. Kuiken, T.; Rimmelzwaan, G.F.; van Riel, D.; van Amerongen, G.; Baars, M.; Fouchier, R.A.M. and Osterhaus, A. Avian H5N1 influenza in cats. *Science*. 2004;306:241.

20. Samji, T. Influenza A: understanding the viral life cycle. *The Yale journal of Biology and Medicine*. 2009;82(4):153-9.

21. Wilson, I.A.; Skehel, J.J. and Wiley, D.C. Structure of the haemagglutinin membrane glycoprotein of influenza virus at 3A resolution. *Nature*. 1981;289:366-73.

22. Memoli, M.J.; Morens, D.M. and Taubenbenrger, J.K. Pandemic and seasonal influenza: therapeutic challenges. *Drug Discovery Today*. 2008;13(13):590-5.

23. Brown, D. Health experts guess wrong on flu vaccine. *The Seattle Times*. 2008;February 1.

24. Palese, P. Making better influenza virus vaccines? *Emerging infectious Diseases*. 2006;12(1):61-5.

25. Gilbert, S. Human Influenza Programme. 2009.

26. von Itzstein, M. The war against influenza : discovery and development of sialidase inhibitors. *Nature*. 2007;6(December):967-74.

27. Stouffer, A.L.; Acharya, R.; Salom, D.; Levine, A.S.; Di Constanzo, L.; Soto, C.S.; Tereshko, V.; Nanda, V.; Stayrook, S. and DeGrado, W.F. Structural basis for the function and inhibition of an infuenza virus proton channel. *Nature*. 2008;451:596-9.

28. Miller, C. Coughing up flu ' s proton channels. *Nature*. 2008;451 (January).

29. Jing, X.; Ma, C.; Ohigashi, Y.; Oliveira, F.A.; Jardetzky, T.S.; Pinto, L.H.; Lamb, R.A. Functional studies indicate amantadine binds to the pore of the influenza A virus M" proton-selective ion channel. *Proceedings of the National Academy of Science*. 2008;105(31):10967-72.

30. Colman, P. Zanamivir: an influenza virus neuraminidase inhibitor. *Expert Reviews of Anti-infective Therapy*. 2005;3(2):191-9.

31. Miller, C.A.; Wang, P. and Flashner, M. Mechanism of *Arthrobacter sialophilus* neuraminidase: the binding of substrates and transition-state analogs. *Biochemical and Biophysical Research Communications*. 1978;83(4):1479-87.

32. Lew, W.; Chen, X. and Kimm, C.U. Discovery and development of GS 4101 (oseltamivir): an orally active influenza neuraminidase inhibitor. *Current Medical Chemistry*. 2000;7(6):573-662.

33. Gubareva, L.V.; Webster, R.G. and Hayden, F.G. Comparison of the activities of Zanamivir, Oseltamivir, and RWJ-270201 against Clinical Isolates of Influenza Virus and Neuraminidase Inhibitor-Resistant Variants-. *Antimicrobial Agents and Chemotherapy*. 2001;45(12):3403-8.

34. Seaman, M. BioCryst says flu drug candidate failed in trial. *Yahoo! Finance*. 2009;May 8.

35. Fry, A.M.; Pérez, A. and Finelli, L. Use of intravenous neuraminidase inhibitors during the 2009 pandemic: results from population-based surveillance. *JAMA : the Journal of the American Medical Association*. 2011;306(2):160-2.

36. Dyer, O. European agencies find 14% of flu isolates are resistant to oseltamivir. *Biomedical Journal*. 2008;336(7639):298.

37. Le, Q.M.; Someya, K.; Sakai, Y.T.; Nguyen, T.H.; Nguyen, K.H.L.; Pham, N.D.; Ngyen, H.H.; Yamada, S.; Muramoto, Y.; Horimoto, T.; Takada, A.; Goto, H.; Suzuki,

T.; Suzuki, Y. and Kawaoka, Y. Isolation of drug-resistant H5N1 virus. *Nature*. 2005;437:1108.

38. Lagoja, I.M. and Clercq, E.de. Anti-influenza virus agents: synthesis and mode of action. *Medicinal Research Reviews*. 2008;28(1):1-38.

39. Fenton, R.J. and Potter, C.W. Dose-response activity of ribavirin against influenza virus infection in ferrets. *Journal of Antimicrobial Chemotherapy*. 1977;3:263-71.

40. Tsai, C-H.; Lee, P-Y.; Stollar, V. and Li, M-L. Antiviral therapy targeting viral polymerase. *Current Pharmaceutical Design*. 2006;12(11):1339-55.

41. Furuta, Y.; Takahashi, K.; Fukuda, Y.; Kuno, M.; Kamiyama, T.; Kozaki, K.; Nomura, N.; Egawa, H.; Minami, S.; Watanabe, Y.; Narita, H. and Shiraki, K. *In vitro* and *in vivo* activities of anti-influenza virus compound T-705. *Antimicrobial Agents and Chemotherapy*. 2002;46(4):977-81.

42. Furuta, Y.; Takahashi, K.; Kuno-Maekawa, M.; Sangawa, H.; Uehara, S.; Kozaki, K.; Nomura, N. and Egawa, H. Mechanism of action of T-705 against influenza virus. *Antimicrobial Agents and Chemotherapy*. 2005;49(3):981-6.

43. Zhou, H.; Jin, M.; Yu, Z.; Xu, X.; Peng, Y.; Wu, H.; Liu, J.; Liu, H.; Cao, S. and Huanchun, C. Effective small interfering RNAs targeting matrix and nucleocapsid protein gene inhibit influenza A virus replication in cells and mice. *Antiviral Research*. 2007;76:186-93.

44. Watson, K.G.; Cameron, R.; Fenton, R.J.; Gower, D.; Hamilton, S.; Jin, B.; Krippner, G.Y.; Luttick, A.; McConnell, D.; MacDolnald, S.J.F.; Mason, A.M.; Nguyen, V.; Tucker, S.P. and Wu W-Y. Highly potent and long-acting trimeric and tetrameric inhibitors of influenza virus neuraminidase. *Bioorganic & Medicinal Chemistry Letters*. 2004;14:1589-92.

45. Belser, J.A.; Lu, X.; Szretter, K.J.; Jin, X.; Aschenbrenner, L.M.; Lee, A.; Hawley, S.; Kim do, H.; Malakhov, M.P.; Yu, M.; Fang, F. and Katz, J.M. DAS181, a novel sialidase fusion protein, protects mice from lethal avian influenza H5N1 virus infection. *Journal of Infectious Diseases*. 2007;196(10):1493-9.

46. Zhang, H. Concerns of using sialidase fusion protein as an experimental drug to combat seasonal and pandemic influenza. *Journal of Antimicrobial Chemotherapy*. 2008;62:219-23.

47. Jones, J.C.; Turpin, E.A.; Bultmann, H.; Brandt, C.R. and Schultz-Cherry, S. Inhibition of influenza virus infection by a novel antiviral peptide that targets viral attachment to cells. *The Journal of Virology*. 2006;80(24):11960-7.

48. Goodman, M.; Zapf, C. and Rew, Y. New reagents, reactions and peptidomimetics for drug design. *Biopolymers*. 2001;60:229-45.

49. Lambert, J.N.; Mtichell, J.P. and Roberts, K.D. The synthesis of cyclic peptides. *Journal of the Chemical Society, Perkin Transactions 1*. 2001:471-84.

50. Blout, E.R. Cyclic peptides: past, present and future. *Biopolymers*. 1981;20:1901-12.

51. Staiano, M.; Bazzicalupo, P.; Rossi, M. and D'Auria, S. Glucose biosensors as models for the development of advanced protein-based biosensors . *Molecular Biosystems*. 2005;1(5-6):354-62.

52. Costoff, A. Structure, synthesis, and secretion of somatostain. In: *Endocrinology: The Endocrine Pancreas*. Georgia: Medical College of Georgia.

53. Borel, J.F. History of the discovery of cyclosporin and of its early pharmacological development. *Wiener Klinische Wocheschrift*. 2002;114(12):433-7.

54. Cappelletti, S.; Annoni, P.G.D. and Storace, O.M.P. Peptides for the pharmaceutical market: Chemical synthesis and downstream procession on industrial scale. *Chim. Oggi /Chem. Today*. 2002;20:47-50.

55. Valero, M.L.; Giralt, E. and Andreu, D. A comparative study of cyclization strategies applied to the synthesis of head-to-tail cyclic analogs of a viral epitope. *The Journal of Peptide Research : Official journal of the American Peptide Society*. 1999;53(1):56-67.

56. Katsara, M.; Minigo, G.; Plebanski, M. and Apostolopoulos, V. The good, the bad and the ugly: how altered peptide ligands modulate immunity. *Expert Opinion on Biological Therapy*. 2008;8(12):1873-84.

57. Koivunen, E.; Wang, B. and Ruoslahti, E. Phage libraries displaying cyclic peptides with different right sizes: ligand specificities of the RGD-Directed Integrins. *Nature Biotechnology*. 1995;13:265-70.

58. Pinilla, C.; Appel, J.R. and Houghten, R.A. Synthetic peptide libraries for research and drug discovery. In: *Immunological Recognition of Peptides in Medicine and Biology*. CRC Press; 1995:1-14.

59. Davies, J.S. The cyclization of peptides and depsipeptides. *Journal of Peptide Science*. 2003;9(8):471-501.

60. Romanovskis, P. and Spatola, A.F. Preparation of head to tail cyclic peptides via side chain attachment. *Journal of Peptide Ressearch.* 1998;52:356-74.

61. Cavallaro, V.; Thomspon, P. and Hearn, M. Solid phase synthesis of cyclic peptides; model studies involving i-(i+4) side chain-side chain cyclisation. *Journal of Peptide Science.* 1998;4:335-43.

62. Tam, J.P. and Lu, Y.A. Synthesis of large cyclic cysteine-knot peptide by orthogonal coupling strategy using unprotected peptide precursor. *Tetrahedron Letters*. 1997;38:5599-602.

63. Bordusa, F. Enzymes for peptide cyclisation. *ChemBioChem.* 2001;2:405-9.

64. Bertozzi, C.R. Chemical glycobiology. *Science*. 2001;291(5512):2357-64.

65. Attrill, H.; Takazawa, H.; Witt, S.; Klm, S.; Isecke, R.; Brossmenr, R.; Ando, T.; Ishida, H.; Kiso, M.; Crocker, P.R. and van Aalten, D.M.F. The structure of siglec-7 in complex with sialosides: leads for rational structure-based inhibitor design. *Biochemistry Journal*. 2006;397:271-8.

66. Weis, W.; Brown, J.H.; Cusack, S.; Paulson, J.C.; Skehel, J.J. and Wiley, D.C. Structure of the influenza virus haemagglutinin complexed with its receptor, sialic acid. *Nature*. 1988;333(2):426-431.

67. Zaitsev, V.; Itzstein, M.von; Groves, D.; Kiefel, M.; Takimoto, T.; Portner, A.; Taylor, G. Second sialic acid binding site in Newcastle disease virus hemagglutinin-neuramidase: implications for fusion. *Journal of Virology*. 2003;78(7):3733-41.

68. Crocker, P.R. and Varki, A. Siglecs, sialic acids and innate immunity. *Trends in Immunology*. 2001;22(6):337-342.

69. Czrniecki, M.F. and Thornton, E.R. Carbon-13 nuclear magnetic resonance spin-laticce relaxation in the *N*-acetylneuraminic acids. Probes for internal dynamics and conformational analysis. *Journal of the American Chemical Society*. 1977;99(25):8273-9.

70. Malapelle, A.; Coslovi, A.; Doisneau, G. and Beau, J-M. An expeditious synthesis of *N*-acetylneuraminic Aaid alpha-*C*-glycosyl derivatives (idquoalpha-*C*-glycosidesrdquo) from the anomeric acetates. *European Journal of Organic Chemistry*. 2007;2007(19):3145-57.

71. Marra, A. and Sinay, P. Acetylation of *N*-acetylneuraminic acid and its methyl ester. *Carbohydrate Research*. 1989;190(2):317-22.

72. Kabsch, W. and Sander, C. Dictionary of protein secondary structure: pattern recognition of hydrogen-bonded and geometrical features. *Biopolymers*. 1983;22:2577-637.

73. Sinnott, M. *Carbohydrate chemistry and biochemistry: structure and mechanism*. RSC publishing; 2007:703.

74. Bergmann, M. and Zervas, L. Uber ein all-gemeines Verfahren der Peptid-Synthese. *Synthese*. 1932:1192.

75. Okitsu, O.; Suzuki, R. and Kobayashi, S. Efficient synthesis of piperidine derivatives. Development of metal triflate-catalyzed diastereoselective nucleophilic substitution reactions of 2-methoxy- and 2-acyloxypiperidines. *The Journal of Organic Chemistry*. 2001;66(3):809-23.

76. Haque, M.E.; Kikuchi, T.; Yoshimoto, K. and Tsuda, Y. Regioselective monoalkylation of non-protected glycopyranoisde by dibutyltin oxide method. *Chemical & Pharmaceutical Bulletin*. 1985;33(6):2243-55.

77. Ress, D.K. and Linhardt, R.J. Sialic acid donors: chemical synthesis and glycosylation. *Current Organic Synthesis*. 2004;1(1):31-46.

78. Fielding, L. NMR methods for the determination of protein–ligand dissociation constants. *Progress in Nuclear Magnetic Resonance Spectroscopy*. 2007;51(4):219-42.

79. Sauter, N.K.; Bednarski, M.D.; Wurzburg, B.A.; Hanson, J.E.; Whiteside, G.M.; Skehel, J.J. and Wiley, D.C. Hemagglutinins from two influenza virus variants bind to sialic acid derivatives with millimolar dissociation constants: a 500-MHz proton nuclear magnetic resonance study. *Biochemistry*. 1989;28(21):8388-96.

80. Fielding, L.; Rutherford, S. and Fletcher, D. Determination of protein-ligand binding affinity by NMR: observations from serum albumin model systems. *Magnetic Resonance in Chemistry : MRC*. 2005;43(6):463-70.

81. Billo, E.J. Calculation of binding constants. In: *Excel (R) for chemists: A Comprehensive Guide*. Vol 9. John Wiley & Sons, Inc. 2001:349-372.

82. Hasegawa, A.; Ohki, H.; Nagahama, T. and Kiso, M. A facile, large-scale preparation of the methyl 2-thioglyco- side of *N*-acetylneuraminic acid, and its usefulness for the stereoselective synthesis of sialoglycosides. *Cell*. 1991;212:3-7.

83. Lindhorst, T. *Essentials of carbohydrate chemistry and biochemistry*. 2nd ed. WILEY-VCH Verlag; 2003:332.

84. Hanessian, S. *Preparative Carbohydrate Chemistry*. 1st ed. CRC Press; 1997:648.

85. Murase, T.; Kameyama, A.; Kartha, K.P.R. Synthetic studies on sialoglycoconjugates. 5 : a facile, regio and stereoselective synthesis of ganglioside GM 4 and its position isomer. *Journal of Carbohydrate Chemistry*. 2011;(September):37-41.